

Isopeptidic Desferrioxamine Analogues: Solid Phase Synthesis and Evaluation of Zirconium Complexes

Department of Chemistry, Institute of Pharmacy
University of Hamburg

Dissertation

A thesis submitted for the degree of
Dr. rer. nat.

Lasse Outzen

Hamburg 2025

1. **Academic supervisor:** Prof. Dr. Wolfgang Maison
2. **Academic supervisor:** Prof. Dr. Ralph Holl

Date of the oral defense: 24.10.2025

Und dennoch bewegt sich die Erde.

Galileo Galilei

Danksagung

Ich bedanke mich bei Herrn Prof. Dr. Wolfgang Maison für die nette Aufnahme in den Arbeitskreis und das sehr spannende Forschungsthema. Ich danke dir für die wirklich tolle Betreuung und der Philosophie der stets offenen Tür. Die schöne Atmosphäre im Arbeitskreis liegt nicht zuletzt an deinem unkomplizierten und wertschätzenden Umgang. Vielen Dank für die schöne Zeit im Arbeitskreis!

Herrn Prof. Dr. Ralph Holl danke ich für die freundliche Übernahme des Zweitgutachtens. Bei Frau Prof. Dr. Louisa Temme und Herrn Dr. Thomas Hackl bedanke ich mich für die Bereitschaft der Teilnahme an der Prüfungskommission.

Ich möchte mich auch bei den vielen Menschen bedanken, durch die meine Forschung und die Arbeit am Fachbereich zu einer lehrreichen, produktiven und schönen Zeit wurden. Zunächst möchte ich mich bei allen Mitarbeitenden der NMR-Abteilung bedanken, die den steten Fluss an NMR-Proben vermessen haben. Auch der MS-Abteilung möchte ich danken. Dort vor allem Erik, der sich teilweise etwas intensiver mit meinen Proben auseinandersetzen musste. Durch den Freundes- und Förderverein Chemie konnte meine Stelle für ein halbes Jahr verlängert werden. Dafür bin ich in einer familiär aufregenden Zeit sehr dankbar gewesen! Einen besonderen Dank möchte ich an Frau Prof. Dr. Susanne Kossatz, Herrn Prof. Dr. Johannes Notni und die Arbeitsgruppe am TranslaTUM in München richten. Die Kooperation hat mir sehr viel Spaß bereitet und die Arbeit mit radioaktivem Material fand ich sehr spannend. In dem Kontext geht ein besonderer Dank an Maxi, mit dem ich eine sehr angenehme Planungsphase im Vorfeld hatte und der sich vor Ort zwei Wochen Zeit für mich genommen hat. Auch an die Leute im Institut für Pharmazie möchte ich einen Dank richten. Danke in diesem Sinne zunächst an Melanie und Claudia. Euch beiden konnte ich immer bei Problemen und Fragen ansprechen. Immer hilfreich und freundlich! Auch neben der Fachlichkeit habe ich das Zusammensein mit euch aufgrund eurer nahbaren Art und Weise sehr zu schätzen gewusst. Auch bei den Praktikumsleitungen Thomas und Uli möchte ich mich für die kollegiale und angenehme Zusammenarbeit bedanken. Die Grillabende bei Uli zuhause waren immer ein angenehmer Rahmen, um auch mal anders ins Gespräch zu kommen. Vielen Dank auch an Antje, Kathleen und Anette, die immer bei allen Fragen und Anliegen hilfsbereit und freundlich waren! Vielen Dank Antje für das Gegenlesen der Manuskripte.

Meinen PraktikantInnen möchte ich einen Dank aussprechen: Max Münchow & Henri Peters, Elahe Ramandi & Omran Hamo, Darius Ludolfs und Hoang Duc Nguyen. Darius und Duc haben nach Beendigung des Praktikums im späteren Verlauf freudigerweise den Weg als Masterand und Doktorand in den AK zurückgefunden. Duc hat seine Masterarbeit mit mir als Betreuer erkocht. Ihm will ich einen besonderen Dank für seine Arbeiten aussprechen, denn ohne seine gute, motivierte und gründliche Arbeit wäre ein Meilenstein meiner Arbeit evtl. nicht

erreicht worden! Danke dir Duc! Ebenso möchte ich mich bei Michel bedanken, dessen Masterarbeit ich teilweise betreuen durfte und von dem ich wertvolle Verbindungen erben konnte, die ich in meine Arbeit, ohne sie nachziehen zu müssen, einsetzen konnte. Ziemlich zum Start meiner Doktorarbeit hat Marfa ihre Bachelorarbeit mit mir als Betreuer im Arbeitskreis durchgeführt. Mit ihrer Hilfe konnte ich einige Einblicke in die Thematik der Kupplungschemie gewinnen. Für Ihre Mühen und die gewissenhafte Arbeit möchte ich mich ebenfalls bedanken!

Nun zu den Arbeitskreismitgliedern. Im Laufe der Zeit ändert sich ein Arbeitskreis durch das Verlassen und Hinzukommen von Mitgliedern. Besonders schön war daher, dass ich zu jeder Zeit den Arbeitskreis als eine sehr angenehme und harmonische Gruppe wahrgenommen habe, mit der man auch neben dem Arbeitskreisalltag gerne Zeit verbracht hat! Ich denke, das ist keine Selbstverständlichkeit! In meiner Startzeit mit Erik, Tim, Tom, Silke und Sharah wurde ich herzlich aufgenommen und ich lernte das Arbeitskreisleben neben dem Laboralltag in so manch einem lustigen „AK-Abend“ kennen. Danke für die nette Aufnahme euch fünf! Danke an dieser Stelle auch an Moritz, dessen Thema ich geerbt habe und der mir zum Start einige Tipps geben konnte. Leider kam sehr zeitnah nach meinem Start Corona auf, wodurch ich das Labor im zweiten Stock mit Tom und Tim wieder verlassen musste, bevor wir uns dort richtig eingespielt hatten. Schade, dass wir da nicht mehr Zeit zu dritt hatten. Danke Tom für die anschließende entspannte Zeit im Corona-Büro des ersten Stocks mit den lustigen und interessanten Gesprächen! Für die Gans ist nach wie vor Frieden keine Option!!1! Ein großer Dank geht auch an Eili, Nils und Svenja, mit denen ich (ich etwas früher als die drei...) zusammen begonnen habe. Danke Svenja für die vielen netten Abende mit dir zusammen mit einem gemütlichen Bierchen in der Küche. Danke Nils für die Aufnahme in das Labor 510 aus meiner Corona-Exklave im zweiten Stock und die Zeit dort. Die Spotify-Playlist „Lab 510 Outzmeister“ existiert und wird (teilweise) fleißig gehört. Es sind halt geile Lieder drin! Eins davon habe ich in jeder meiner Playlists gefunden Oo lol. Vielen Dank auch dir liebe Eili für deine freundliche Art, deinen Witz und deine ansteckende Fröhlichkeit. Es war richtig cool, dass wir beide aus einer flapsigen Idee heraus zweimal die Dockville-Tage für die Menschen geplant und organisiert haben! Danke euch dreien auch für die entspannte Zeit bei den beiden Tagungen in Marburg und Tübingen :) Vielen Dank auch an meine Buddys Laurens und Lennart. Die Zeit im Büro werde ich nicht vergessen! Grenzwertiger Humor und Nerf-Guns sind eine sehr geile Kombi. Vielen Dank euch aber auch für den oft hilfreichen fachlichen Austausch und die ernsthaften Gespräche. Und natürlich vielen Dank für das Gegenlesen meiner Arbeit! Vielen Dank auch an Timo, Mimi, Hauke und Inga (die dann irgendwie doch oft im AK zugegen war) für das immer nette und herzliche Miteinander und auch teilweise für den angebrachten Gegenpol. Es ist immer witzig mit euch gewesen! Danke euch dafür :) Ich bin froh, am Ende Erica, Darius (da ist er wieder), Shirin, Alek und Leif mitbekommen zu haben.

Besonderen Dank an Erica Sonnenschein für die gemeinsame Zeit im Labor und deine fröhliche Art! Ich habe mich mega über deine Entscheidung gefreut, im AK anzufangen! Richtig coole Truppe zusammen! Vielen Dank an jeden von euch für die schöne und unvergessliche Zeit im AK Maison!

Ich möchte mich bei meiner Tante Martina aus Alaska und bei ihrem Mann Larry ganz herzlich bedanken, die meine Arbeit in Rekordzeit gegengelesen haben. Danke für eure Zeit und Mühe! Vielen Dank auch an meine lieben Freunde! Ich war dann ja doch teilweise so begeistert und/oder frustriert von meiner Arbeit, dass ich es manchmal nicht lassen konnte, euch eine Kartoffel ans Ohr zu labern! Vielen Dank für die gemeinsame Zeit, die immer schöne Abwechslung und dass ihr bei mir seid!

Ein ganz besonderer Dank geht an meine direkte Familie: an meine Eltern, an meine Brüder und an meine Schwägerin und den Kindern! Ihr seid eine starke Konstante für mich und ein großer Ruhepol in meinem Leben! Danke für euer Vertrauen, eure Zusprache und dass ihr bei meiner langen Ausbildung immer an meiner Seite gestanden habt! Danke Mama! Danke Papa!

Zum Schluss will ich mich bei meiner Lisa bedanken! Was soll ich dazu sagen? Meine Arbeit ist beinahe so alt wie unsere erste Tochter! Ein irgendwie witziger Vergleich. Wir haben jetzt unser halbes Leben zusammen verbracht. Hätten wir damals geglaubt, hier zu landen? Erträumt haben wir es uns :) Vielen Dank, für die vielen Abende, an denen du mir Zuhause den Rücken freigehalten hast, damit ich Raum hatte, diese Arbeit zu erstellen! Vielen Dank, dass du diesen Weg mit mir zusammen gegangen bist! Vielen Dank für deine schönen täglichen Eindrücke, für deine Gedanken, für deine Ratschläge, für die Klarheit und den Halt, den du mir gibst und deine liebevolle Art! Ich bin mir nicht sicher, ob ich ohne dich so weit gegangen wäre! Ich freue mich auf die Zukunft mit dir und unserer Rasselbande! Vielen Dank Lisa für alles! For the long run ;)

The following results presented in this work were obtained in the working group of Prof. Dr. Wolfgang Maison's at the Institute of Pharmacy of the University of Hamburg from November 2019 till June 2024.

List of Publications

1) Synthesis of Modular Desferrioxamine Analogues and Evaluation of Zwitterionic Derivatives for Zirconium Complexation

Outzen, L., Münzmay, M., Frangioni J.V., Maison, W.

ChemMedChem, **2023**, 18, e202300112.

Impact Factor: 3.6

2) Mixed Liquid and Solid Phase Synthesis of Isopeptidic Desferrioxamine Analogues for Complexation of Zirconium

Outzen, L., Nguyen, H.D., Ludolfs, D., Maison, W.

Eur. J. Org. Chem., **2024**, 27, e202400266.

Impact Factor: 2.5

3) Isopeptidic Desferrioxamine Analogues: The Role of Hydroxamate Spacing for Chelating of Zr⁴⁺

Outzen, L., Ludolfs, L., Irl, M., Kossatz, S., Maison, W.

ChemMedChem, **2025**, 20, e202400890.

Impact Factor: 3.6

Supplementary Publications and unpublished Work

4) Synthesis and Evaluation of DFO-Derivatives for the Application in immunoPET Diagnostics

Outzen, L., Maison, W.

Poster Presentation

DPhG Conference, Marburg **2022**.

5) Synthesis and Evaluation of octadentate DFO-Derivatives for Application in PET Diagnostics

Outzen, L., Maison, W.

Poster Presentation

DPhG Conference, Tübingen **2023**.

6) Unveiling the Role of StmPr1 in *Stenotrophomonas maltophilia* Virulence: A structural Perspective

Sommer, M., Outzen, L., Negm, A., Windhorst, S., Weber, W., Betzel, C.

Presumably: *Scientific Reports*, **2025**.

Status: in work

Related to this.

a. **StmPr1, *Stenotrophomonas maltophilia* Protease 1, 36 kDa alkine serine protease**

Sommer, M., Outzen, L., Negm, A., Windhorst, S., Betzel, C.

Protein Structure in *Protein Data Bank in Europe (PDBe)*

Status: Hold for Publication

b. **StmPr1, *Stenotrophomonas maltophilia* Protease 1, 36 kDa alkine serine protease in complex with PMSF**

Sommer, M., Outzen, L., Negm, A., Windhorst, S., Betzel, C.

Protein Structure in *Protein Data Bank in Europe (PDBe)*

Status: Hold for Publication

c. **StmPr1, *Stenotrophomonas maltophilia* Protease 1, 36 kDa alkine serine protease in complex with Bortezomib**

Sommer, M., Outzen, L., Negm, A., Windhorst, S., Betzel, C.

Protein Structure in *Protein Data Bank in Europe (PDBe)*

Status: Hold for Publication

Content

1. Zusammenfassung	1
2. Abstract	4
3. Introduction	6
3.1 PET imaging	6
3.1.1 Conventional PET, PET Combinations and Alternatives	6
3.1.2 Principle and physical background of PET imaging	10
3.1.3 Non-targeted PET	11
3.1.4 Targeted PET	14
3.1.4.1 Targeted PET with small molecules	16
3.1.4.2 ImmunoPET	17
3.1.5 Radionuclides for targeted PET and immunoPET	20
3.1.6 Radiochelators for ^{89}Zr	22
3.2 Solid Phase Peptide Synthesis (SPPS)	28
4. Aim of the work	34
5. Results and Discussion (cumulative part)	37
5.1 Solution Phase Synthesis of isopeptidic DFOB and DFO* analogs	37
5.2 Transfer to SPPS and Synthesis of complex DFO* analogs with side chains	54
5.3 Investigations towards an optimal spacing between the hydroxamic acids	61
6. Critical summary and Outlook	72
6.1 Solid Phase Peptide Synthesis	72
6.2 Non-radiocactive Stability Assay	75
6.3 Comparability of stability assays in the literature	77
6.4 Structural and conceptual discussion of discrepancies in stability results	81
6.5 Outlook	83
7. Literature	85
8. Appendix	96
8.1 Supplementary Materials	96

8.1.1 Synthesis of Modular Desferrioxamine Analogues and Evaluation of Zwitterionic Derivatives for Zirconium Complexation	96
8.1.2 Mixed Liquid and Solid Phase Synthesis of Isopeptidic Desferrioxamine Analogues for Complexation of Zirconium	125
8.1.3 Isopeptidic Desferrioxamine Analogues: The Role of Hydroxamate Spacing for Chelation of Zr^{4+}	162
8.2 Hazardous Materials	200
9. Declaration	207

List of Abbreviations

AHX	Aminohexanoic acid
Ala	Alanine
Alloc	Allyloxycarbonyl
BFC	Bifunctional Chelator
BnBr	Benzylbromide
Boc	<i>tert</i> -Butyloxycarbonyl protecting group
BPO	Benzoyl peroxide
BTFFH	1-(Fluoro(pyrrolidin-1-yl)methylene)pyrrolidin-1-ium hexafluorophosphate(V)
Bz	Benzoyl
CD	Cluster of Differentiation
CDI	Carbonyldiimidazol
c-MET	mesenchymal-epithelial transition factor
CT	Computer tomography
CTC	2-Chlorotrityl chloride resin
CuAAC	Copper-catalyzed azide-alkyne cycloaddition
Dab	2,4-Diaminobutyric acid
DAD	Diode Array Detector
DBU	1,8-Diazabicyclo(5.4.0)undec-7-ene
DCC	<i>N,N'</i> -Dicyclohexylcarbodiimide
DFOB	Desferrioxamine B
DIC	<i>N,N'</i> -Diisopropylcarbodiimide
DIPEA	<i>N,N</i> -Diisopropylethylamine
Dmb	2,4-Dimethoxybenzyl
DMF	Dimethylformamide
DMSO	Dimethyl sulfoxide
DOTA	2,2',2'',2'''-(1,4,7,10-Tetraazacyclododecane-1,4,7,10-tetrayl)tetraacetic acid
Dpr	2,3-diaminopropanoic acid
EC	Electron Capturing
EDTA	Ethylenediaminetetraacetic acid
EGFR	epidermal growth factor receptor

EIC	Extracted Ion Chromatogram
ESI	Electrospray Ionization
FAP	Fibroblast Activation Protein
FAPi	Fibroblast Activation Protein Inhibitor
FDG	Fluorodeoxyglucose
Fmoc	Fluorenylmethoxycarbonyl protecting group
FWHM	Full Width at Half Maximum
GABA	γ -Aminobutyric acid
Gly	Glycine
HATU	Hexafluorophosphate Azabenzotriazole Tetramethyl Uronium
HBED-CC	<i>N,N'</i> -Bis-[2-hydroxy-5-(carboxyethyl)benzyl]ethylenediamine- <i>N,N'</i> -diacetic acid
HBTU	Hexafluorophosphate benzotriazole tetramethyl uronium
HCTU	Hexafluorophosphate 6-chloro-1-hydroxybenzotriazole uronium
HEPES	4-(2-hydroxyethyl)-1-piperazineethanesulfonic acid
HER	Human epidermal growth factor receptor
HILIC	Hydrophilic interaction chromatography
HMBA	4-(Hydroxymethyl)benzoyl-aminomethyl
HOAt	1-Hydroxy-7-azabenzotriazole
HOBt	1-Hydroxybenzotriazole
HPLC	High-performance liquid chromatography
HRMS	High resolution mass spectrometry
HSA	human serum albumin
IgG	Immunoglobulin G
ip	isopeptidic
KuE	lysine urea glutamate
LC	Liquid Chromatography
LOR	Line of Response
Lys	Lysine
mAb	monoclonal antibody
MeOH	Methanol
Mmt	Monomethoxytrityl
MRI	Magnetic Resonance Imaging

MS	Mass spectrometry
NAAG	<i>N</i> -acetylaspartylglutamate
NCS	<i>N</i> -Chlorosuccinimide
NHS	<i>N</i> -Hydroxysuccinimide
NMR	Nuclear magnetic resonance
OEG	Oligo(ethylene glycol)
Orn	Ornithine
PEG	Polyethylene glycol
PET	Positron Emission Tomography
PSMA	Prostate-specific membrane antigen
PTSA	<i>p</i> -Toluenesulfonic acid
RGD	Arginine-Glycine-Aspartic acid
RTK	Receptor tyrosine kinase
SPECT	Single-Photon Emission Computed Tomography
SPPS	Solid Phase Peptide Synthesis
TBTA	Tris(benzyltriazolylmethyl)amine
TES	Triethylsilane
TFA	Trifluoroacetic acid
TFFH	<i>N,N,N',N'</i> -Tetramethylfluoroformamidinium hexafluorophosphate
THF	Tetrahydrofuran
TIC	Total Ion Chromatography
TIPS	Triisopropylsilane
TLC	Thin Layer Chromatography
UHPLC	Ultra-high-performance liquid chromatography
UV	Ultraviolet
VEGFR	Vascular endothelial growth factor
Vis	Visible
Zr	Zirconium

1. Zusammenfassung

Diese kumulative Dissertation beinhaltet drei Veröffentlichungen und befasst sich mit dem rationalen Design und der Entwicklung einer neuen Gruppe von Desferrioxamin B (DFOB)-Analoge, die die ^{89}Zr -Chelatisierung für das *targeted* Positronen-Emissions-Tomographie (PET)-Imaging optimieren sollen. Die beschriebenen Einschränkungen von DFOB und seinem oktaedrischen Analogon DFO* - insbesondere die suboptimale *in vivo*-Stabilität und Löslichkeit - bilden die Grundlage für den hier entwickelten synthetischen Ansatz. Ziel ist es, optimierte Chelatoren zu entwickeln, die auf leicht verfügbaren Bausteinen basieren und zu isopeptidischen Strukturen mit einstellbaren Eigenschaften zusammengesetzt werden. Zu den wichtigsten Strukturmerkmalen gehören vier Hydroxamsäuren für eine effiziente Zr^{4+} -Koordination, Funktionalitäten für eine Konjugation der *targeting* Vektoren, variable Abstände zwischen den Hydroxamsäuren für ein *fine tuning* hinsichtlich der Komplexstabilität mit Zr^{4+} und clickbaren Seitenketten für eine verbesserte Löslichkeit und der Beeinflussung der Pharmakokinetik. Anhand dieser Kriterien wurde ein modularer Ansatz entwickelt, der sowohl die synthetischen als auch die funktionellen Einschränkungen der bisher verfügbaren Chelatoren überwinden kann.

In der ersten Veröffentlichung (*ChemMedChem*, **2023**) wurden isopeptidische Analoga von DFOB mit Azidoseitenketten synthetisiert. Diese Chelatoren mit den Bezeichnungen AZA-DFO (hexadentat) und AZA-DFO* (oktaedrisch) wurden durch eine modulare Synthese aus Bausteinen bestehend aus Ornithin- β -Alanin (Orn- β -Ala) und Lysin- β -Alanin (Lys- β -Ala) aufgebaut. Neun Chelatoren wurden durch kupferkatalysierte Azid-Alkin-Cycloaddition (CuAAC) an zwitterionische Moleküle konjugiert. Dies führte zu wasserlöslichen Verbindungen, die Zr^{4+} unter milden Bedingungen (Raumtemperatur, 90 Minuten) komplexierten. Experimente zu Transchelatierung mit Ethylendiamintetraessigsäure (EDTA)- und DFOB-Überschuss zeigten, dass die kürzeren Hydroxamatabstände auf Orn-Basis die Komplexstabilität im Vergleich zu längeren Varianten auf Lys-Basis verbessern. Zusätzlich konnte gezeigt werden, dass die Anordnung der Amidgruppen und das Vorhandensein zwitterionischer Seitenketten die Stabilität der Komplexe nicht beeinträchtigten. Das oktaedrische Orn-basierte AZA-DFO*-Derivat wurde als besonders vielversprechender Chelator identifiziert. Dieser vereint hohe Komplexstabilität und schnelle Komplexierungskinetik mit Modularität für weitere Funktionalisierungen.

Die zweite Veröffentlichung (*European Journal of Organic Chemistry*, **2024**) beinhaltet eine Festphasensynthesestrategie für isopeptidische DFOB und DFO*-Analoge (ipDFOB und ipDFO*), die vier Hydroxamsäuren für eine gute Zr^{4+} -Chelatisierung enthalten. Der Ansatz verwendet leicht herzustellende Fmoc geschützte Vorstufen und ermöglicht die Synthese sowohl von ipDFO* als auch von clickbaren AZA-ipDFO* Derivaten in nur wenigen Stunden.

Im Vergleich zur mehrstufigen *liquid-phase* Synthese reduziert die Festphasenmethode den Syntheseaufwand erheblich und ermöglicht den modularen Aufbau von Chelatoren mit einstellbaren Abständen zwischen Hydroxamaten. Diese Flexibilität ist entscheidend für die Optimierung der Komplexierungsstabilität, da der Abstand zwischen den Hydroxamaten die Stabilität des Komplexes mit harten Metallkationen wie Zr^{4+} beeinflusst. Diese Methode stellt somit einen robusten und skalierbaren Weg zur Entwicklung maßgeschneiderter Chelatoren nicht nur für Zr^{4+} , sondern möglicherweise auch für andere klinisch relevante Radiometalle dar.

Die dritte Veröffentlichung (*ChemMedChem*, **2024**) beschreibt die Festphasensynthese mehrerer oktaedrativer DFO*-Analoga mit unterschiedlichen Hydroxamat-Abständen. Die Komplexstabilität dieser Analoga wurde durch Radiomarkierung mit ^{89}Zr sowohl in Humanserum als auch in kompetitiven Assays mit EDTA und DFOB im Überschuss bewertet. Der radiochemische Assay diente dabei als *Benchmark* für die Validierung einer nicht-radioaktiven LC/MS-basierten Methode. Die Daten zeigten, dass ein längerer Hydroxamat-Abstand (9 Atome) zu einer höheren Stabilität führt, was den Ergebnissen der ersten Veröffentlichung auf den ersten Blick widerspricht. Der stabilste Komplex widerstand der EDTA-Kompetition über 72 Stunden, was sowohl durch *Radio-Thin Layer Chromatography* (TLC) als auch durch *liquid chromatography* gekoppelt an ein Massenspektrometer (LC/MS) bestätigt wurde. Die unkomplizierte Synthese, die hohe Komplexstabilität und der modulare Ansatz dieser ipDFO-Derivate unterstreichen ihr Potenzial als Chelatoren der nächsten Generation für das *targeted* PET-Imaging.

Eine der größten Herausforderungen bei dieser Arbeit war die Synthese von strukturell komplexen, orthogonal geschützten Bausteinen. Der Ansatz umfasst Aminosäurederivate mit Seitenketten wie Ornithin und Lysin. Die γ -ständigen Amine dieser Verbindungen wurden mit Benzoylperoxid oxidiert, um ein geschütztes Hydroxylamin als Aminäquivalent für die *solid phase peptide synthesis* (SPPS) zu erzeugen. Auch nicht-seitenkettentragende Verbindungen wie γ -ständige Bromcarbonsäuren (bspw. 5-Brompentansäure) wurden zur Synthese von Chelatoren ohne Seitenkette verwendet. Hier führten Substitutionsreaktionen mit *O*-Benzylhydroxylamin zu den entsprechenden Intermediaten für die Verwendung in der SPPS. In einem dritten Ansatz wurde Boc-Allylglycin zur Herstellung von Kupplungsintermediaten über Ozonolyse mit anschließender reduktiver Aminierung verwendet. Für die Entwicklung eines belastbaren Festphasenprotokolls wurde der anspruchsvolle Kupplungsschritt von benzylgeschützten Hydroxylaminderivaten mit aktivierten Carbonsäuren im Hinblick auf Kupplungsreagenzien, Äquivalente, Temperatur, Zeit und Festphasenharz optimiert.

Zusammenfassend lässt sich sagen, dass diese Arbeit den Zugang zu einer neuen Gruppe von Molekülen mit erheblichem Potenzial für die klinische Diagnostik ermöglicht hat. Insbesondere für das *targeted* PET-Imaging könnten Verbindungen wie das in der zweiten

Veröffentlichung präsentierte Lysin-Urea-Glutaminsäure (KuE)-ipDFO*-Konstrukt von höchstem Interesse sein, da es in einer Synthese die Herstellung vom *targeting vector* und Chelator in einer Verbindung ermöglicht. Die neu entwickelte Festphasensynthesestrategie reduziert den manuellen Arbeitsaufwand deutlich und erleichtert die Herstellung von klickbaren Derivaten für die gezielte Konjugation. Der in dieser Arbeit vorgestellte Syntheseansatz weist ein hohes Potenzial für eine vollständige Automatisierung auf und erweist sich als robust unter Bedingungen, die ein Scale-up ermöglichen.

2. Abstract

This cumulative thesis contains of three publications and focuses the rational design and development of a new group of desferrioxamine B (DFOB) analogues aimed at improving ^{89}Zr chelation for targeted PET imaging. The described limitations of DFOB and its octadentate analogue DFO* - particularly their suboptimal *in vivo* stability and solubility - form the foundation for the synthetic approaches developed herein. The objective was to create optimized chelators based on readily available building blocks, assembled into isopeptidic structures with tunable properties. Key structural features include four hydroxamic acids for efficient Zr^{4+} coordination, bifunctionalities for targeting vector conjugation, variable spacer lengths for fine-tuning complex stability, and clickable side chains for improved solubility and pharmacokinetic control. These criteria guided the development of a modular platform capable of addressing both the synthetic and functional limitations of previously available chelators.

In the first publication (*ChemMedChem*, **2023**) isopeptidic analogues of DFOB with azido side chains were synthesized. Termed AZA-DFO (hexadentate) and AZA-DFO* (octadentate), these chelators were constructed via modular synthesis from Orn- β -Ala and Lys- β -Ala. Nine chelators were further conjugated to zwitterionic moieties via copper-catalyzed azide-alkyne cycloaddition (CuAAC), resulting in water-soluble compounds capable of complexing Zr^{4+} under mild conditions (room temperature, 90 min). Transchelation studies using 1000-fold excess EDTA and 300-fold DFOB showed that shorter Orn-based hydroxamate spacing improves the complex stability compared to longer Lys-based variants. Notably, the arrangement of amide groups and presence of zwitterionic side chains did not impair complex stability. The octadentate AZA-DFO* derivative was identified as a particularly promising chelator, combining high stability and fast complexation kinetics with modularity for further functionalization.

The second publication (*European Journal of Organic Chemistry*, **2024**) describes a solid-phase synthesis strategy for isopeptidic DFOB and DFO* analogues (ipDFOB and ipDFO*) containing four hydroxamic acids for strong Zr^{4+} chelation. The approach utilizes commercially available or easily prepared Fmoc-protected precursors and enables synthesis of both ipDFO* and its clickable derivative AZA-ipDFO* in only a few hours. Compared to traditional multistep solution synthesis, the solid-phase method significantly reduces synthetic effort and enables modular assembly of chelators with adjustable spacer lengths. This flexibility is crucial for optimizing complexation properties, as the spacing between hydroxamates impacts complex stability with hard metal cations like Zr^{4+} . This method thus represents a robust and scalable route for developing tailored chelators not only for Zr^{4+} , but potentially for other clinically relevant radiometals.

The third publication (*ChemMedChem*, **2024**) reports the solid-phase synthesis of multiple octadentate DFOB analogues with varying hydroxamate spacers. The complex stabilities of these analogues by radiolabeling with ^{89}Zr were evaluated both in human serum and in competitive assays with excess EDTA and DFOB. The radiochemical assay served as the benchmark for validating a non-radioactive LC/MS-based method. The data clearly demonstrated that longer hydroxamate spacing (9 atoms) results in higher stability, contradicting the results of the first publication. The most stable complex resisted EDTA challenge over 72 h, confirmed via both radio-TLC and LC/MS. The straightforward synthesis, high complex stability, and modular nature of these ipDFO derivatives highlight their potential as next-generation chelators for targeted PET imaging.

One of the major challenges in this work was the synthesis of structurally complex, orthogonally protected building blocks. The approach involved side chain bearing amino acid derivatives such as ornithine and lysine. These γ -standing amines of these compounds were oxidized via benzoyl peroxide to create a protected hydroxyl amine as an amine equivalent for the SPPS. As well non-side chain bearing compounds like γ -positioned bromo carbon acids like, 5-bromo pentanoic acid was used to synthesize non-side bearing chelators. Here substitution reactions with O-benzyl hydroxylamine leads to the corresponding intermediates for the usage in SPPS. In a third approach Boc-allylglycine was used to prepare intermediates via ozonolysis with followed reductive amination. For developing a solid-phase protocol the demanding coupling step of benzyl protected hydroxyl amine derivatives was optimized with respect to coupling reagents, equivalents, temperature, time, and resin choice.

In summary, this work has enabled access to a new group of molecules with significant potential for clinical diagnostics, particularly in targeted PET, exemplified by the KuE-ipDFO* construct described in the second publication. The newly developed solid-phase synthesis (SPPS) strategy markedly reduces manual workload and facilitates the generation of clickable derivatives for targeted conjugation. The synthetic approach presented in this thesis demonstrates strong potential for full automation and exhibits robustness under conditions amenable to scale-up. The chelators introduced herein possess high flexibility for adaptation to a variety of novel applications.

3. Introduction

This introduction aims to provide an understanding of the medical imaging procedure of positron emission tomography (PET), as it is important for the intention of this thesis. The first section explains the procedure's physical principles and the strengths and weaknesses and how it is different from or can be combined with other imaging methods. Current relevance to the daily clinical practice is also discussed. Then, the principles of targeted PET and immunoPET and their associated biological background are presented to give the basis, context and motivation of the thesis carried out. From a chemical point of view, the current problems of clinical use with respect to radiochelator and nuclide are also addressed.

In the second part of the introduction, the synthetic background of this thesis is presented. In this section, the principles of solid phase peptide synthesis (SPPS) are explained and the possible influence of the choice of protecting groups, different resins and coupling reagents is discussed.

3.1 PET imaging

3.1.1 Conventional PET, PET Combinations and Alternatives

Conventional PET imaging is an imaging method used in clinical analysis for the diagnosis of cancer, and for various metabolic processes, cardiovascular issues or bone injuries.^[1-3] Depending on the radiotracer used, this non-invasive method can be used to selectively address different targets of the patient's body and display them in an image.

The method is based on the application of a radiotracer. The radioactive β^+ decay of a neutron-deficient radionuclide in the radiotracer emits positrons, which react with the electron as an antiparticle from the surrounding tissue in the physical process of annihilation.^[4] In this process, both particles are extinguished, resulting in the emission of two collinear γ -photons with an energy of 511 keV.^[4-5] These photons are converted into low energy photons in the Vis range by scintillators arranged in a ring around the patient, which are then converted from the visual signal into an electronic signal by photosensors and multipliers.^[4] The detector registers a total of three electronic signals: 1. the energy of the γ -photon, 2. the time at which the γ -photon hit the detector and 3. the position at which the γ -photon hit the detector.^[6] These three signals are used to calculate a line of response (LOR), which can be used to determine the point of origin of the annihilation on the basis of a coincidence-based calculation. A large number of coincidence-based calculations can then be used to create a PET image that shows the distribution of the radiotracer in the patient's body.^[4] Figure 1 shows the principle of a PET measurement.

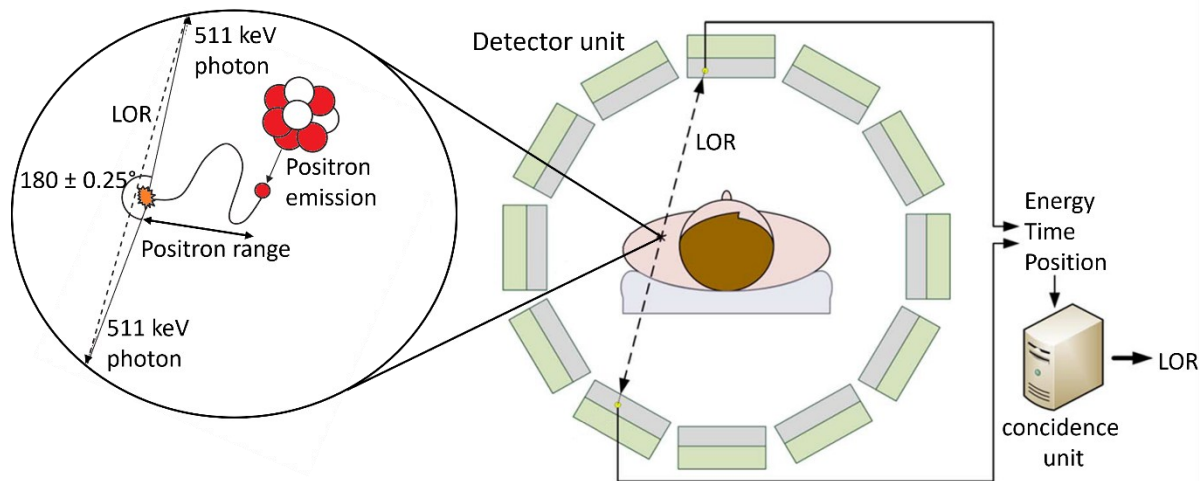


Figure 1: Principle of PET measurements. The decay of the positron emitting radionuclide, which is injected in the patient, leads to an annihilation event between the positron and an electron of the environment resulting in two photons with an angle of nearly 180° to each other. The distance between the place of decay and annihilation depends on the kinetic energy of the released positron. The resulting photons can be detected via a ring of detectors around the patient. After transforming it into a specific electric signal a PET image can be created.^[6-7]

For a better mapping of the PET image in the morphology of the patient, the PET measurement is usually performed in combination with computed tomography (CT) or magnetic resonance imaging (MRI). The CT and MRI methods allow the presentation of the anatomy of a patient. In a CT measurement, the organism is irradiated with X-ray radiation from an X-ray source. Depending on the constitution, structure and composition of different tissues, the absorption of the X-rays varies, allowing production of a contrast image on the emersion side.^[8-9] rotating the X-ray source and detector around the patient's body along the axis from head to toe, a computer can merge the recorded slices into a three-dimensional image.^[8] To improve the spatial resolution of a CT measurement, the patient is usually administered a contrast agent (typically containing iodine) in advance.^[8-9] The morphology of the tissue can also be visualized using the MRI method. In contrast to CT, this avoids radiation exposure for the patient. In MRI, the nuclear spins of an organ's hydrogen atoms align along a magnetic field, creating an overall magnetization.^[10] A short magnetic pulse disturbs this equilibrium, and while the spins return, an electrical signal is recorded. Differences in relaxation and hydrogen distribution allow the differentiation of tissue types. For spatial characterization, layer selection and gradient magnetic fields are used to selectively vary the signal, enabling imaging with spatial resolution.^[10]

Based on the morphological information obtained from the CT or MRI measurement, the PET image can be overlayed on an image of the patient's anatomy, aiding, for example, a prognosis, a characterization of the affected tissue and determination of the treatment's efficacy.^[1, 3, 11] In the daily hospital practice, PET/CT measurements tend to be carried out due

to common availability and well-established protocols. PET/MRI is not yet widely used and is still in the establishment phase, which increases costs. PET/CT, on the other hand, enables faster measurements, but with lower soft tissue resolution and the need for X-rays exposure.^[12] Figure 2 shows a PET/CT with PET/MRI comparison based on ^{18}F -FDG of a patient with lung cancer.^[13] PET/MRI demonstrates a better vertebrae resolution compared to PET/CT. Compared to CT images, bone tissue in MRI images has a signal intensity similar to that of fat tissue due to the high fat content in the bone marrow. This similarity limits the accuracy of MRI-based methods for generating reliable attenuation correction maps, which are essential in positron emission tomography (PET). The attenuation of annihilation photons travelling through the body differs among the tissues encountered, due to their densities and compositions (e.g., bone, fat, air, etc.). If this attenuation is not properly accounted for, it can lead to misinterpretation of the PET signals and ultimately compromise the quantitative accuracy of the resulting images.^[13]

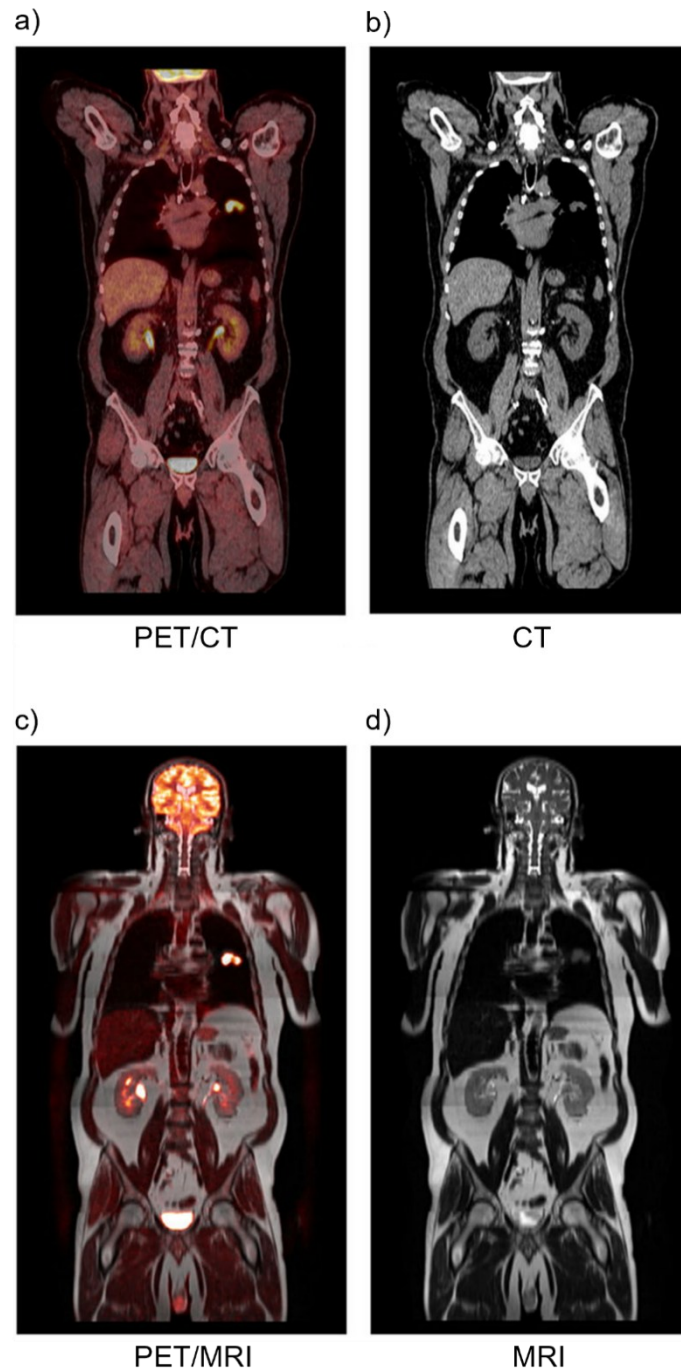


Figure 2: PET/CT vs. PET/MRI image of the same patient with lung cancer. A PET/CT image (a) is based on the morphological image from a corresponding CT scan (b)). A PET/MRI (c) is embedded in a corresponding MRI image (d)).^[13]

An alternative imaging method to PET is the single-photon emission computed tomography (SPECT). A radionuclide introduced into the patient directly emits γ -photons. These are registered by collimators rotating around the patient and translated into an image using gamma cameras, similar to PET.^[7, 14] The use of a collimator is essential, as this is the only way to trace the origin of the photon. At the same time, the linear structure of the collimator leads to a

detecting yield of only around 0.01% of the photons, which significantly reduces the sensitivity compared to PET (around 1%).^[7, 14] The higher sensitivity with PET therefore reduces the individual scan times in relative terms, which increases the feasibility of making multiple scans. This in turn improves temporal resolution, which is an important factor in dynamic biological processes.^[7] The coincidence-based calculation in PET achieves a significantly higher sensitivity compared to collimator-based detection in SPECT. However, because of their inherent characteristics (discussed in the next section) the resolution of PET is significantly reduced, compared to SPECT. Briefly, this is because the positron's kinetic energy and the non-collinearity of the annihilation photons. Thus, the choice between PET and SPECT as a diagnostic method is often a case-by-case decision, depending on the disease and condition of the patient.^[7]

The imaging methods mentioned are summarized with their properties in Table 1.

Table 1: Overview of the mentioned diagnostic methods with their properties.^[8]

Method	Temporal Resolution	Spatial Resolution (clinical) [mm]	Sensitivity [M]	Costs	Signal
PET	s – min	5 – 7	$10^{-11} - 10^{-12}$	€€	β^+
SPECT	min	8 – 10	$10^{-10} - 10^{-11}$	€	γ
CT	min	0.5 – 1	ND	€	γ
MRT	min – h	1	$10^{-3} - 10^{-5}$	€€	T_1

3.1.2 Principle and physical background of PET imaging

Several criteria have major influence on the quality of the measurement. Some of these criteria are the basis of clinical practice and therefore this work, the most important physical influences on the resolution of a PET image are discussed in this section.

First, the emitted positron's kinetic energy influences the spatial resolution of a PET measurement. It is important to keep in mind that not only the type of radioisotope determines the kinetic energy - there is also a certain energy distribution within a radioisotope, that can range from 0 to a value characteristic of the particular radionuclide.^[5] After emission, the positrons kinetic energy decreases through interaction with the surrounding medium until an energy level is reached at which annihilation can take place.^[7] The distance covered up to this point has a negative influence on the resolution of the measurement, as there is a spatial difference in the coincidence-based calculation of the LOR and the actual point of origin of the annihilation (Figure 1, left).^[5, 7] Choosing a suitable and appropriate radionuclide with the lowest

possible maximum kinetic energy can help reduce this measurement error. A second inherent factor that affects spatial resolution occurs during the annihilation process. This is because the two collinear photons do not always have an angle of exactly 180° to each other. A deviation of approximately 0.25° has been observed, which leads to an error in the calculation of the LOR and thus to a deterioration of resolution (Figure 1, left).^[5, 7, 15] For that reason and because a smaller diameter also reduces the error potential due to non-collinear γ -photons, it seems intuitive that they are why modern PET devices tend to have the smallest possible diameter.

In addition to these inherent factors, technical factors also have an influence on the quality of the PET image. One factor is the energy resolution of the detector. This describes which energy range is registered by the detector via the full-width-half-maximum (FWHM) of the photo signal.^[16-17] Today's detectors have a percentage energy resolution of around 10%, which corresponds to an energy window between 400-600 keV.^[4-5, 16-17] This is an important aspect when choosing the radioisotope, because many β^+ -decays occur with simultaneous emission of γ -rays. Although some radionuclides have suitable kinetic energies, good positron yields and interesting half-lives, they emit γ -rays during decay that are located directly in or near the energy window, which dramatically reduces the quality of the image due to interference.^[18] These γ -rays can make the patient's radiation exposure very high. Unfortunately, photons with higher energies can also fall into the energy window due to Compton scattering, which further limits the choice of possible radionuclides with high γ -emission.^[5, 16, 19-20] Other factors that seem counterintuitive are detector-related effects. These include the width of the scintillator crystal, inter-crystal scattering and inter-crystal penetration. However, the influence can be minimized by further development of detector technology and corresponding algorithms in the data processing step.^[7]

3.1.3 Non-targeted PET

Non-targeted PET is commonly used in the field of oncology for the diagnosis and evaluation of tumors,^[2, 21] and also in cardiology for blood flow examinations or coronary heart diseases or in neurology for the characterization of early stages of neurological diseases such as Alzheimer's and Parkinson's.^[21-27] Applying conventional PET is preceded by an understanding of the physiological and biochemical processes in which the small radiolabeled chemical molecules act and which parts are to be visualized. Temporal observation of the distribution and concentration of the labeled molecule in the patient is accomplished through detecting the produced annihilation photons. When labeling with conventional radionuclides, the basic assumption is that the labeled structures' behavior must be chemically and biologically identical to the naturally occurring derivatives. Table 2 provides an overview of clinically common

radioisotopes with their half-lives, the positron fraction during decay, the kinetic energies of the positrons and the associated loss of resolution.^[28]

Table 2: Overview of some positron emitting radioisotopes regarding the half-life, the branching of positrons and values of the kinetic energy and the related loss of resolution.^[28]

Radioisotope	Half-life $t_{1/2}$ [min]	Decay β^+ [%]	kin. E_{\max} [keV]	kin. E_{mean} [keV]	Loss of Resolution R_{\max} [mm]	Loss of Resolution R_{mean} [mm]
^{11}C	20.4	99.8	960	386	4.2	1.2
^{13}N	10	99.8	1199	492	5.5	1.8
^{15}O	2	99.9	1732	735	8.4	3.0
^{18}F	110	96.9	634	250	2.4	0.6

Due to the short half-lives of 2 min to almost 2 h of radioisotopes shown in Table 2, it is necessary to prepare them on the day of use directly before application. This is done with cyclotrons, which are located in the same hospital.^[29] Subsequently, the radioisotopes must be able to be transferred to the radiotracer in clean and fast reactions with high yields. Before using the radiotracers, the following quality standards must be met or determined: physical parameters (osmolarity and pH value), radionuclide purity (γ -spectrum, calculation of half-life), radiochemical purity (radioactive by-products), determination of molar activity, chemical purity, solvent residues and microbial contamination.^[29] Only then can the radiotracers be safely injected into the patient. The choice of radionuclide must always be made in the context of the time scale of the question to be examined. The very short-lived ^{15}O in $[^{15}\text{O}]\text{H}_2\text{O}$, for example, is suitable for investigations of blood flow in the brain.^[21, 27] ^{13}N , which is also very short-lived, is used as $[^{13}\text{N}]\text{NH}_3$ for measuring myocardial blood flow.^[21, 24] The ^{11}C isotope, has a wider range of applications, as it occurs ubiquitously in biological molecules and can be easily inserted into radiotracers via methylation reactions due to its chemical nature. The ^{18}F acts in a similar way as the most widely used radionuclide.^[21] Its use is rather unintuitive as it is not a common atom in biological molecules. However, it has very favorable physical properties. The half-life of 110 min allows multi-step labeling syntheses and the outstanding low kinetic energy leads to the highest resolution in the resulting PET images of all possible positron emitters.^[21] To date, a number of ^{11}C and ^{18}F -based radiotracers have been developed and approved for clinical use.^[30] Figure 3 shows four clinically relevant radiotracers for conventional PET imaging.

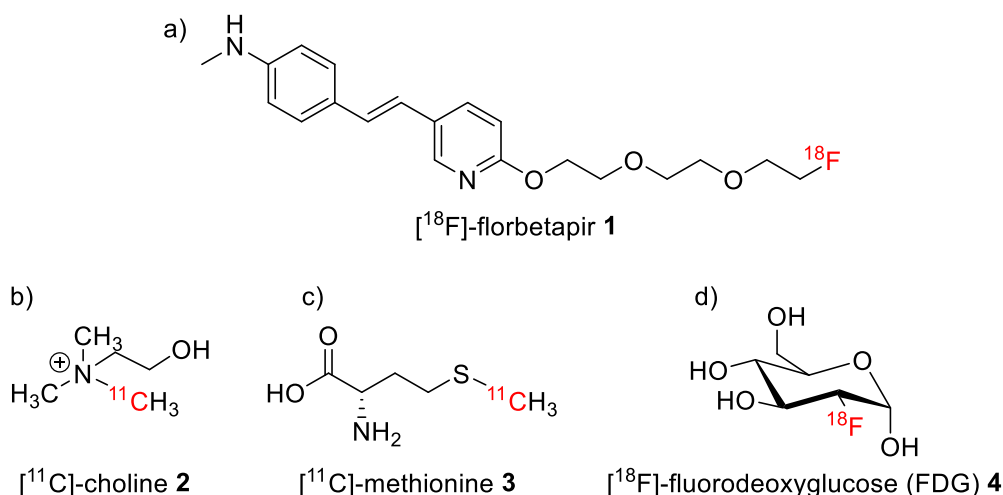


Figure 3: Some clinically relevant PET tracer: [¹⁸F]-florbetapir a), [¹¹C]-choline b), [¹¹C]-methionine c) and [¹⁸F]-fluorodeoxyglucose (FDG) d).^[31-37]

For example, [¹⁸F]-florbetapir **1** (Figure 3 a)) is used for the early detection of Alzheimer's disease. It attaches to the amyloid structures in the brain which are developing at an early stage of Alzheimer's.^[31-32] Similarly, the neurodegenerative disease Parkinson's can now be diagnosed via the accumulating tau proteins using PET.^[25] The [¹¹C]-choline **2** (Figure 3 b)) is used in the early detection of recurrent prostate cancer when other radiotracers give false negative results.^[33-34] Choline acts as a marker for phospholipid synthesis and therefore has an increased requirement as a component of the cell membrane in tumor tissue with an increased cell division rate.^[38] [¹¹C]-choline **2** or [¹¹C]-methionine **3** (Figure 3 c)) can achieve good results in the diagnosis of diffuse bone marrow infiltration or inflammatory lesions of multiple myeloma when other radiotracers such as [¹⁸F]-fluorodeoxyglucose (FDG) **4** (Figure 3 d)) fail in sensitivity or specificity.^[35-37] However, [¹¹C]-methionine **3** is best known for its use in the diagnosis of brain tumors.^[39-41] The increased sensitivity is based on the hypermetabolism of amino acids in tumor tissue.^[37] The most important and by far the most widely used PET radiotracer is the glucose derivative [¹⁸F]-FDG **4**.^[1, 30, 42] Normally differentiated cells generate the energy for their cell processes in the mitochondria via oxidative phosphorylation.^[43] However, it has been observed that most cancer cells switch their energy production to aerobic glycolysis. This phenomenon is known as the Warburg effect and is the reason why [¹⁸F]-FDG **4** has been so successful in PET diagnostics in recent years.^[43] The accumulation of [¹⁸F]-FDG **4** in tumor cells allows the detection of a variety of cancer types and the evaluation of the treatment progress. The glucose derivative shows high sensitivity and specificity in the PET images of many cancers due to excellent resolution of ¹⁸F as a radionuclide.^[44]

The principles and molecules explained so far provide a brief overview of the current medical possibilities in conventional PET diagnostics. One weakness of the principles outlined is that physiological and biochemical events can lead to misinterpretations in the PET image due to the non-targeted nature of the molecules.^[45-46] For example, [^{18}F]-FDG **4** leads to intrinsically increased uptake in the brain and bladder, which significantly reduces its suitability for gliomas and prostate cancer. In addition, uptake in inflammatory tissue is drastically increased, which can lead to false-positive diagnoses.^[46] Furthermore, in all cases (attachment to amyloid structures, synthesis of phospholipids for the cell membrane, hypermetabolism of amino acids and sugars), the principles described are based on ubiquitous processes. This leads to a reduced signal-to-noise ratio, which means that only a spatial resolution of 6 - 10 mm can be achieved in the clinical context.^[47] This is extremely unfavorable, especially for the detection of recurrent cancer and the detection of metastases. The next section will therefore present PET methods in which tissues are marked in a targeted manner. It thus represents a replenishment of conventional PET diagnostics.

3.1.4 Targeted PET

With increasing understanding of the molecular pathogenesis of diseases, especially cancer, and a simultaneous improvement in knowledge of the immune system, more and more targeted radiotracers can be realized today.^[45] This can be fulfilled by conjugating a targeting vector, e.g. a small molecule or antibody, to a chelator that complexes a metallic radioisotope. Figure 4 shows a schematic representation of a typical targeted PET tracer.

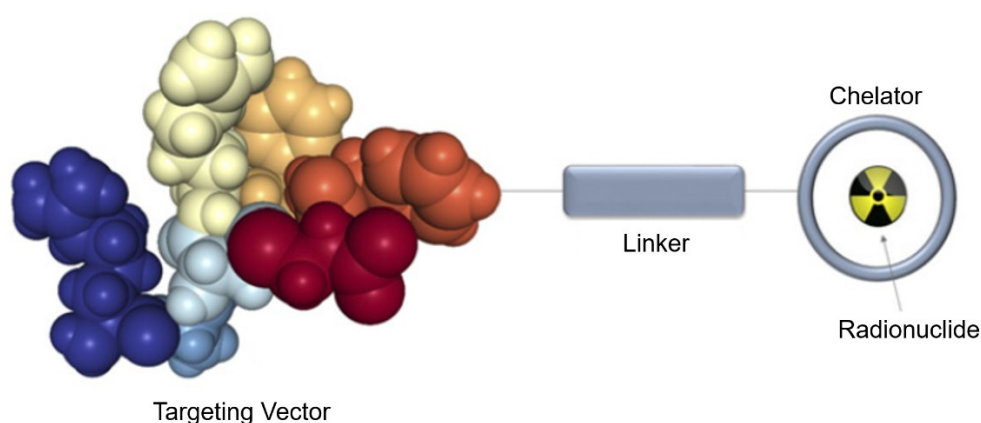


Figure 4: Principle setup of a targeted pet tracer. It consists of a targeting vector, a linker unit which provides a distance between the vector and the last part of the tracer: the chelator which holds a radionuclide.^[48]

The targeting vector is structure-specifically addressed, which enables good image quality, spatial resolution and quantification in targeted PET imaging.^[45] The targeting vector is conjugated via a linker to the chelator, which carries the radionuclide. This method ideally combines the targeted specificity of the vector with the high sensitivity and resolution of PET. A suitable targeted PET tracer must have a high uptake in the desired tissue, leading to rapid saturation, while at the same time eliminating the unbound tracer from the bloodstream as quickly as possible. This reduces the radiation exposure and at the same time optimizes the signal-to-lesion ratio.

So-called bifunctional chelating agents (BFCs) are generally used for the formation of this type of PET tracer. On the one hand, these chelators have the function of coordinating the radionuclide through specific functional groups and, on the other hand, conjugation to the targeting vector is made possible by other functional groups. It is important that conjugation to the targeting vector can take place under reaction conditions (e.g. temperature and pH value) that do not lead to inactivation of a biomolecule as targeting vector through denaturation.^[49] Amines are often used as conjugation sites for the targeting vector part, which can be accessed non-site-specifically via *N*-hydroxysuccinimide esters (NHS) or isothiocyanates (NCS). When using small molecules as shown in the following section, the conjugation site is clearly defined and intrinsically positioned in such a way that no influence on the biological binding properties (when using a biological targeting vector) is to be expected later on. But, when using biological targeting vectors such as antibodies as the bioactive part of the tracer, there is the major drawback that the number and location of the conjugation is not clearly defined.^[49] Thus, for example, the active binding region of the antibody can be affected, which can lead to a reduction in affinity and immunoreactivity to the antigen.^[49] In addition, the number of conjugated chelators can vary (chelator-targeting vector-ratio), which can lead to a problem of homogeneity in the conjugates, as only the average of the conjugated chelators per biomolecule can be determined in a solution.^[49] For this reason, several techniques have been developed that are site-specific. The most used technique is coupling to the thiol group of a cysteine residue.^[45, 49] In the past, this approach was often implemented via binding with maleimide. However, since *in vivo* cleavage of the conjugate occurs via a retro-Michael reaction in plasma, irreversible techniques have also been developed.^[45, 50] Another approach is the click chemistry. These reactions are bioorthogonal, rapid, stereospecific and lead to high yields under suitable conditions for antibodies.^[51] Functional groups are used that do not occur in natural structures and can therefore only bind to the intended positions. Special bi- or tri-specific antibodies with suitable functional groups can be produced for this purpose.^[45, 52-53] The most used click reaction in this context is copper-catalyzed azide-alkyne cycloaddition (CuAAC).^[45] One disadvantage is the use of harmful copper ions, which must be quantitatively separated before using in a medical context.

In addition, the entire PET tracer can be optimized with regard to the pharmacokinetic and pharmacodynamic properties and the tissue-specific requirements in the biological system using various approaches. For example, the log*D* value can be adjusted by PEGylation, which can influence improved penetration into the target tissue and the clearance pathway (renal or hepatic) and the associated clearance rate can be adjusted.^[54-55] The introduction of lipophilic groups such as lipofuscin has been shown to achieve effective cell membrane passage in senescent cells.^[56] In other work, the influence of carbohydrates was investigated. For example, the popular RGD motif, which often binds integrin associated with cancer, was labelled with various carbohydrates. These structures showed high affinities for integrin and high tumor retention with simultaneous favorable *in vivo* biodistribution.^[57] The introduction of galactose into the radiotracer PSMA I&T led to a strong reduction in binding to human serum albumin (HSA), which in turn led to a strong reduction in non-specific uptake in nontarget tissue and thus to a better signal-to-lesion ratio.^[58] In other cases, binding to albumin was specifically focussed in order to enable an extension of the circulation time and thus improved tumor uptake.^[59-60] The introduction of zwitterionic groups has the consequence that the extended hydration shell can reduce the non-specific interactions with serum proteins and cell membranes. The reduced interactions with components of the immune system increase the tolerability of the tracers in patients. In addition, the neutral overall charge promotes rapid excretion via the kidneys, which indirectly increases the signal in the target tissue.^[61-62]

The next two sections deal with the state of the art for the targeting vector part of targeted PET tracers. Firstly, two clinically relevant small molecules are presented, which can be used to produce target-specific images for certain types of cancer. Then immunoPET, which is based on the specific interaction of antibodies, will be presented in more detail. In the course of this, the potential of antibody engineering is discussed and illustrated with examples.

3.1.4.1 Targeted PET with small molecules

Certain tumor markers are present at elevated levels in cancer cells compared to other cells.^[2, 63-64] These tissue markers of cancerous tumors include molecules of various categories such as membrane receptors, oncogenes, tumor suppressor genes, nuclear antigens and growth factors.^[64] Selective tumor markers can define susceptibility risks and help with tumor detection and diagnosis so that therapeutic steps for effective treatment can be initiated rapidly.^[64]

One example of a targeted PET tracer is PSMA-11 (Figure 5 a)).^[65] It addresses the prostate-specific membrane antigen (PSMA), which occurs naturally on the prostate epithelium and cleaves glutamate residues from folic acids or from the neuropeptide *N*-acetylasparylglutamate (NAAG) hydrolytically.^[66-67] In certain types of prostate cancer it is

strongly overexpressed (known as PSMA(+)) cancer cell lines), making it particularly suitable as a biomarker for prostate cancer. With PSMA-11, detection via PET can be ensured by complexing ^{68}Ga as a positron emitter into the *N,N'*-Bis-[2-hydroxy-5-(carboxyethyl)benzyl]ethylendiamin-*N,N'*-diacetic acid (HBED-CC) scaffold (marked in blue) resulting in PET tracer **5**. The urea structure consisting of glutamic acid and lysine (marked in green) mimics the natural substrate of PSMA and is therefore an excellent inhibitor for PSMA with high specificity.^[68-70] Another example is the quinoline-based fibroblast activation protein inhibitor (FAPi-04) conjugated to 1,4,7,10-Tetraazacyclododecane-1,4,7,10-tetraacetic acid (DOTA) (Figure 5 b).^[71] FAPi-04 (marked in green) binds to the fibroblast activation protein (FAP), a type II transmembrane serine protease.^[71] FAP is overexpressed in some cancer-associated fibroblasts, and has been detected in a variety of cancers. This is an example of a tumor marker that is not related to a specific cancer type. The chelator DOTA (marked in blue) binds the radionuclide in this conjugate. In many clinical studies the use of FAP-targeted radiotracers like **6** has been shown to be promising.^[72-74] In the field of PET imaging, both tracers **5** and **6** are mainly used with ^{68}Ga .^[28, 75-76]

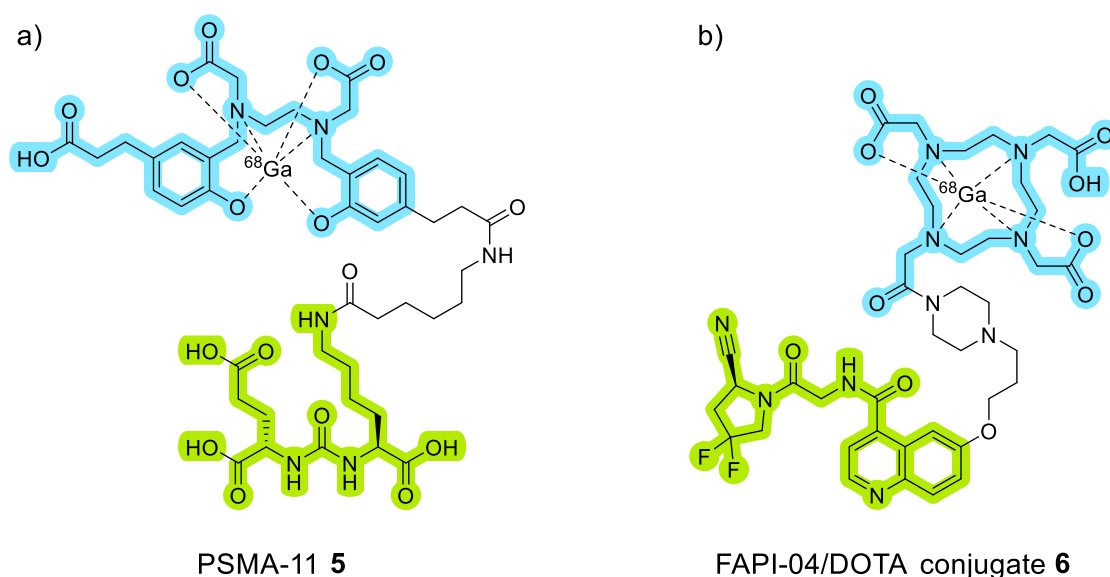


Figure 5: Two examples of targeted PET radio tracers. PSMA-11 with the urea binding motif (marked in green) and the HBED-CC chelator (marked in blue) which is used for the diagnosis of prostate cancer (a). FAPi-04 (marked in green) also with a DOTA complexation motif (marked in blue) which is used to detect fibroblast activation protein (FAP) for the diagnosis of some cancer types.^[65, 71]

3.1.4.2 ImmunoPET

Besides the small molecule-based targeted PET strategy, the high specificity of antibodies in the human organism is used to transport radiotracers to specific tissues in a targeted manner. The basic structure of an immunoPET tracer is depicted in Figure 4. The targeting vector is an antibody or an antibody fragment with high specificity for a tumor marker.

Typical tumor markers are receptor tyrosine kinases (RTKs). The class of RTKs consists of cell membrane proteins that are involved in mediating cell-to-cell communication and thereby control several important and complex biological functions such as cell growth, motility, differentiation and metabolism.^[77] They are overexpressed and mutated in a variety of cancer types and are therefore ideally suited as target structures for the therapy and diagnosis of cancer.^[77] Typical representatives of the RTK class are: epidermal growth factor receptor (EGFR), human epidermal growth factor receptor (HER2 and HER3), vascular endothelial growth factor receptor (VEGFR) or mesenchymal-epithelial transition factor (c-MET).^[45, 78] Another group of interest for targeting in the human organism are the cluster of differentiation (CD) antigens. These include a variety of cell surface molecules that have been grouped by immunophenotyping of cells. A CD antigen always includes one or more CD antibodies that are addressed accordingly.^[79] A frequently used CD is the CD20 on the cell surface of B-cells and is therefore directed against lymphoma.^[80]

A large number of antibodies (e.g. recombinant, chimeric, fragmented, immunoconjugate or bispecific antibodies) have been developed specifically for the targets mentioned above.^[81-83] Figure 6 shows a schematic representation of a typical antibody and antibody fragments.

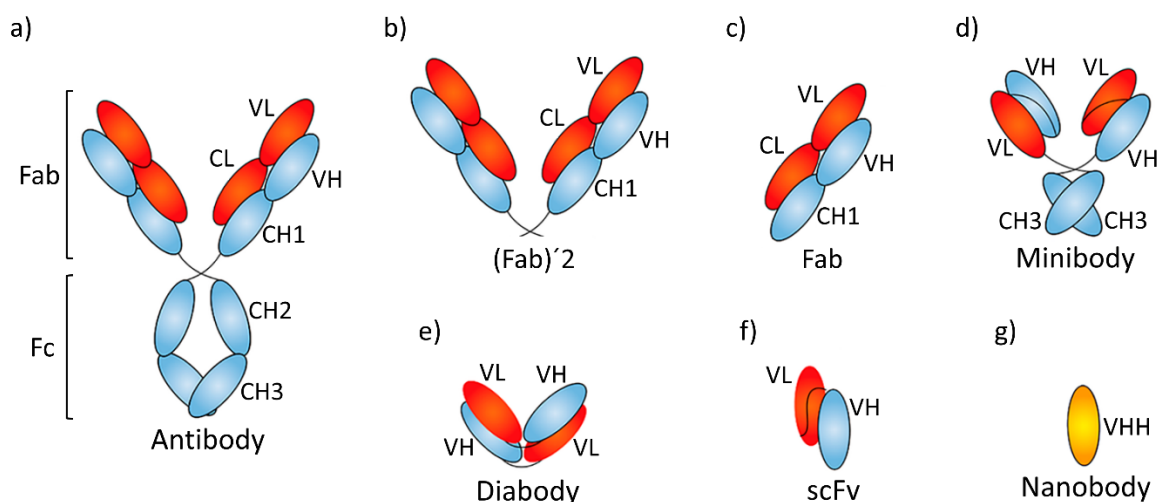


Figure 6: Antibody and antibody fragments produced via antibody engineering. A full antibody with all of its compartment's a), the Fab-region fragment called (Fab)'2 b), the Fab-region but only one of its arms called Fab c), an overall reduced form of a whole antibody called minibody d), diabody e), scFv f) and a nanobody g).^[45, 84]

The molecular size of the targeting vectors has a significant influence on their pharmacokinetics.^[85] ImmunoPET tracers range in size from around 15 kDa (nanobody-conjugate) to around 150 kDa for conjugates of monoclonal antibodies (mAbs), with a variety of smaller mAb-based constructs in between.^[85] Due to their relatively large molecular mass, monoclonal antibodies (mAbs) have only a limited ability to penetrate from the blood into the

tissue by diffusion. Therefore, their tissue distribution is slow and the overall distribution volume remains low. Penetration by mAbs is particularly limited in the tumor center, which means that distribution within the tumor tissue is often heterogeneous. In contrast, smaller, antibody-based constructs can cross the blood-tissue barrier much more easily - an advantage that increases their suitability for efficient tumor targeting.^[85] Smaller molecules are generally cleared faster via the kidneys, while larger structures have longer blood half-lives. Table 3 provides an overview of various mAb-based constructs, their molecular size, pharmacokinetic properties and elimination pathways.^[85]

Table 3: Antibody and antibody based fragments and its estimated sizes, the pharmacokinetic half-life and the way of elimination.^[85]

Name	IgG	(Fab)'2	Minibody	Fab	scFv	Nanobody
Size	150 kDa	110 kDa	75 kDa	50 kDa	25 kDa	15 kDa
Pharmacokinetic $t_{1/2}$	few days to weeks	~ 24 h	few hours	~ 4 h	~ 1 h	~ 1 h
Elimination	hepato biliary	hepato biliary	hepato biliary	Kidney	Kidney	Kidney

IgG-type antibodies (Figure 6 a)) are the most common approach in PET imaging.^[84] consist of an Fc fragment and an antigen-binding Fab fragment with constant and variable regions based on heavy and light chains.^[84] The Fab fragment in particular is relevant due to its antigen recognition via different glycosylation patterns.^[86] To date, numerous therapeutically approved antibodies also have diagnostic potential.^[45, 87-88] Detection of cancer in many organs via ImmunoPET is possible, e.g. intestine,^[89] breast,^[90] lymphatic system,^[80] pancreas,^[91] prostate,^[92] kidney,^[93] brain,^[94] lung,^[95] and solid tumors in general.^[96-99] Despite clinical success, IgG antibodies have disadvantages. Due to their size (approx. 150 kDa), they exceed the renal filtration limit (60 kDa), which leads to slow blood clearance and a low signal-to-background ratio.^[45, 84, 100] Unlabeled antibodies are sometimes necessary to saturate specific binding sites in advance, which makes reproducible protocols due to heterogeneity of antibodies, tumors, patients and individual therapies difficult.^[91, 101-102]

To improve tumor penetration, blood clearance and targeting accuracy, smaller antibody fragments were developed as part of antibody engineering (Figure 6 b - g).^[100, 103-104] molecules penetrate tumors better and are excreted more quickly.^[100] In any case, the Fc region is omitted. Initial approaches used (Fab)'2 and Fab fragments (Figure 6 b and c), but their production is complex^[104]. Alternatively, only variable regions were used (Figure 6 d - f) to optimize specificity and clearance. Minibodies (Figure 6 d) are eliminated after 48 h, diabodies (Figure 6 e) after 24 h.^[100] The scFv fragment (Figure 6 f) with a mass of ~25 kDa offers a good

balance of clearance (<12 h), tumor penetration and ease of production, but suffers from monovalent binding.^[105] Diabodies improve this, but have poorer pharmacokinetics.^[45] VHHs (Figure 6 g), which at ~15 kDa are small, stable and can be functionalized in many ways (e.g. with ¹⁸F, biotin, fluorophores), are also promising.^[106-108] Too rapid clearance can be compensated for by PEGylation or albumin binding.^[109-110] Overall, antibody engineering allows a modular approach for patient-adapted diagnostics and therapy, tailored to biological and physical half-lives.

3.1.5 Radionuclides for targeted PET and immunoPET

As already mentioned in sections 3.1.1 and 3.1.2, the selected radioisotope has a major influence on the quality of the PET measurement. If the conventional PET tracers from section 3.1.3 are compared with the targeted PET tracers from section 3.1.4, it becomes clear that the requirements with regard to the radionuclide properties have changed. Whereas the conventional PET tracers are still dominated by covalently bound radionuclides with short physical half-lives (see Table 2) of up to 110 min for ¹⁸F, the leading requirements with regard to the physical half-life are associated with biological half-lives of up to several hours to several days in relation to the modern targeted PET tracers. This is achieved by the introduction of mostly metallic radionuclides. These metallic radionuclides cannot be covalently bound directly to the tracer but must be fixed via chelators. An overview of typical PET-radionuclides is listed in Table 4.^[28]

Table 4: Overview of some positron emitting radiometals with selected properties.^[28, 111]

Radioisotope	Half-life $t_{1/2}$	Decay β^+ [%]	kin. E_{mean} [keV]	Loss of Resolution R_{mean} [mm]	Possible Gamma-rays γ [keV]
⁶⁴ Cu	12.7 h	17.5	278	0.7	/
⁶⁸ Ga	67.8 min	87.7	836	3.5	1077
⁸⁶ Y	14.7 h	11.9, 5.6	535, 681	1.9, 2.8	1077, 627, 1153
¹²⁴ I	100.2 h	11.7, 10.7	687, 975	2.8, 4.4	602, 1691, 723
⁸⁹ Zr	78.4 h	22.7	396	1.3	909

All radionuclides in Table 4 have longer half-lives and are therefore suitable for use in targeted PET and immunoPET, as they fit well into the time range in which the antibodies or antibody fragments have their biological half-life (see section 3.1.4.2). A further advantage of using radionuclides with longer half-lives is that an increased signal-to-noise ratio can be achieved by increasing the time between injection and acquisition of the diagnostic image, due to the clearance of the tracer that took place meanwhile. The positron fraction during decay is given

in percentage as a dimension of the amount of radiotracer to be used in the clinical measurements. It is noticeable that the metallic radionuclides used here have significantly lower values than the conventional radionuclides in Table 2. The proportion of electron capture (EC) is significantly higher here. In EC, the proton-rich atomic nucleus is not stabilized by the release of a positive charge through the emission of a positron, but by the capture of an electron, whereby a proton is converted into a neutron.^[112] Column 4 shows the mean kinetic energy of the positrons, which determines the loss of spatial resolution (column 5), as explained in more detail in section 3.1.2. The last column shows possible gamma-rays with the corresponding energy. The higher the values, the higher the radiation exposure. In Figure 7 the decay schemes of the five radiometals shown in Table 4 are depicted.

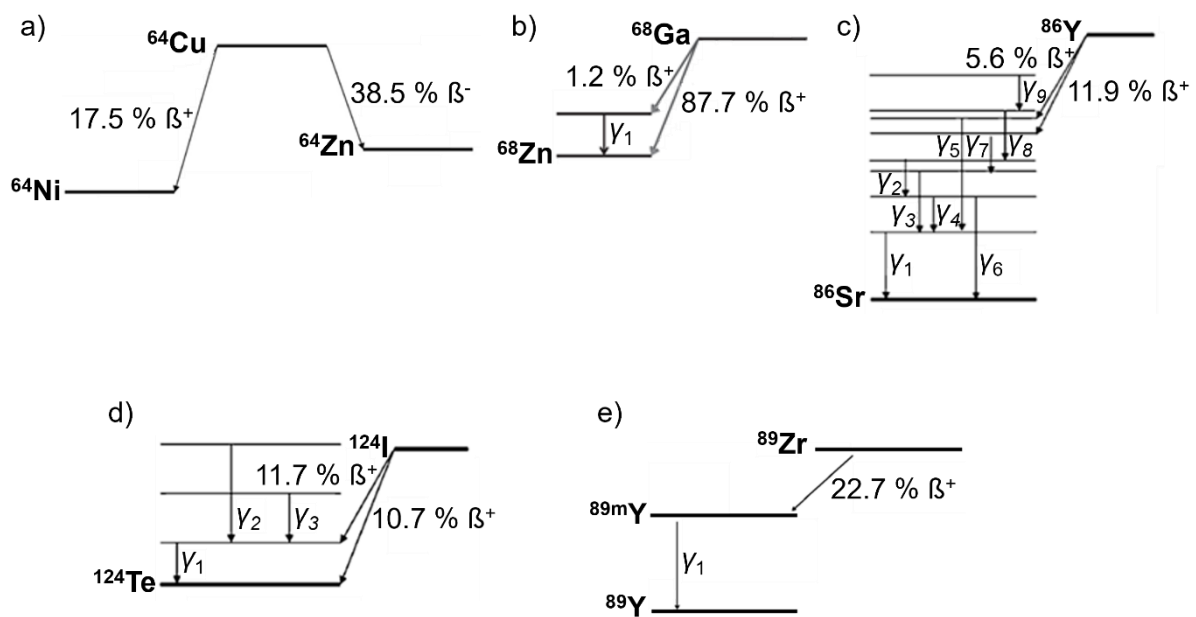


Figure 7: Simplified decay schemes of ^{64}Cu , ^{68}Ga , ^{86}Y , ^{124}I and ^{89}Zr . Only the decay products, β^+ abundance and possible gamma rays are shown.^[111, 113-115]

^{64}Cu has a half-life ($t_{1/2} = 12.7$ h) which only matches the antibody fragments with relatively short biological half-lives. It emits a positron that has a low energy (278 keV), which resulting in a low loss of spatial measurement resolution (only 0.7 mm).^[28] In addition to the positron emission, ^{64}Cu also has a 40% probability of β^- -emission during decay. This can potentially be used for radiotherapy, making it in combination with ^{67}Cu a good candidate for theranostic approaches in the future.^[28, 116] The ^{68}Ga , ^{86}Y and ^{124}I all belong to the group of typically long-range positron emitters (1.9 - 4.4 mm spatial resolution loss), which reduces attractiveness.^[28] In addition, some of them cause additional radiation exposure due to high generation of gamma rays during decay. These can interfere with the annihilation photons through scattering or fall

into the energy window of the PET detector and thus negatively affect the quality of the PET image. The use of ^{86}Y in particular is almost impossible due to the high energy gamma rays.^[28]

A very interesting radionuclide for targeted PET and especially for immunoPET is the radionuclide ^{89}Zr . With a half-life of 78.4 h, it matches the biological half-life of antibodies and is also suitable for immunoPET applications with short detection times, such as the use of small antibody fragments.^[117-118] It is therefore ideally suited for investigating issues relating to pharmacokinetics and biodistribution.^[115, 119] With an average positron energy of 396 keV, it is described as a short-range positron emitter, which leads to a spatial resolution loss of only 1.3 mm.^[28] In Table 4, a gamma ray with 909 keV is listed with a probability of 100%. This is a relatively strong additional radiation exposure.^[119] However, since this gamma ray is not produced during the decay of ^{89}Zr to $^{89\text{m}}\text{Y}$, but during the subsequent decay of $^{89\text{m}}\text{Y}$ to ^{89}Y with a relatively long half-life of 16 s, it is assumed that it has no negative influence on the coincidence of the detection of the annihilation photons and also cannot interfere with them.^[28] The production of ^{89}Zr has been improved in the past to a standard process, which includes automatic production and purification. Thus, ^{89}Zr can be obtained with a purity of >99.99% and a yield of >94%.^[115, 120-121] For these reasons, ^{89}Zr is an optimal candidate for application in immunoPET and is already increasingly used for imaging.^[45]

3.1.6 Radiochelators for ^{89}Zr

The radiolabeling process presents a major challenge in the development of antibody-based PET tracers. It requires mild physiological conditions – typically at temperatures not exceeding 37 °C – to preserve the structural integrity of the antibody. This presents a significant limitation, as many widely used chelators, such as DOTA (see Figure 5 b)), require elevated temperatures (e.g. ~90 °C) to effectively complex metals such as Zr^{4+} . Consequently, a prelabelling strategy followed by conjugation of the metal complex to the antibody would be necessary, which introduces additional synthetic complexity. This includes multiple purification steps that not only increase workload and cost but also raise concerns regarding reproducibility, quality assurance, and radiation exposure during synthesis. Given the growing relevance of ^{89}Zr as a radionuclide for immunoPET applications, the identification of a suitable chelator for its stable complexation becomes a central focus. The chelator is a critical component in the design of targeted PET tracers and must be specifically tailored to meet the demanding coordination chemistry of ^{89}Zr . Therefore, the next section first explains the chemical behavior of Zr^{4+} in more detail. Subsequently, the currently published acyclic Zr^{4+} chelator are presented, its weaknesses are analyzed and several structural alternatives from the literature are presented which promise improved complexation properties.

3.1.6.1 Chemical aspects of Zr^{4+}

^{89}Zr is available in aqueous solution containing Zr^{4+} ions. Due to its high charge compared to the relatively small ionic radius (85 pm), it is a particularly hard ion and a strong Lewis acid. In addition, it tends to form oligomeric zirconates of limited solubility.^[122-123] Figure 8 shows the dominant species in aqueous NaClO_4 (1 M) of Zr^{4+} as a function of concentration and pH.^[123]

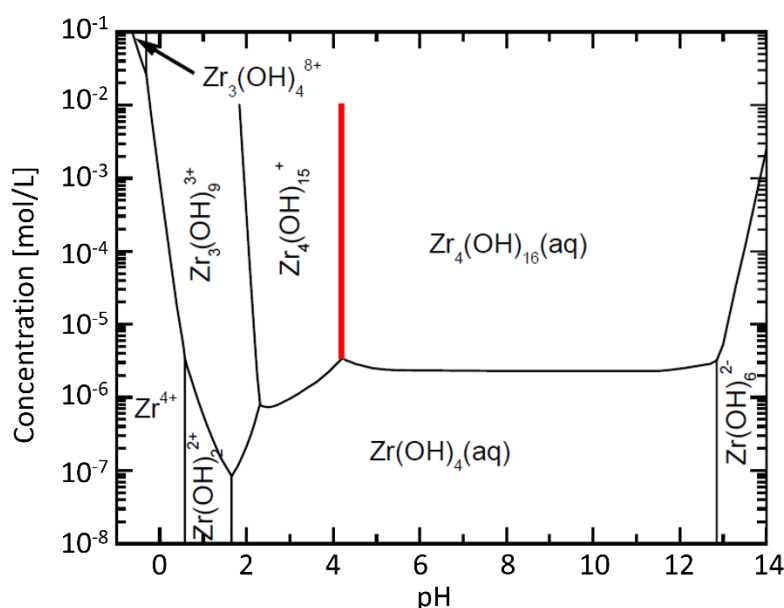


Figure 8: Behavior of Zr^{4+} ion in aqueous conditions depending on Zr^{4+} -concentration and pH value. For a successful complexation it is important that Zr^{4+} is accessible for the chelator and is not precipitated. Precipitation occurs with the trespass of the red line.^[123]

Above a pH of approx. 0.5, Zr^{4+} is present as a hydroxide. At the same time, polynuclear zirconium compounds are formed over the entire pH range above a concentration of 10^{-6} mol/L.^[123] For the complexation of Zr^{4+} with a suitable chelator, it is important that Zr^{4+} is not precipitated as a hydroxide. Studies have shown that precipitation takes place by neutralization from tetrameric $\text{Zr}_4(\text{OH})_{15}^{+}$ at pH 4 to 5 via $\text{Zr}_4(\text{OH})_{16} \times 8\text{H}_2\text{O}$ to $(\text{Zr}_4(\text{OH})_{16})_n$ (transition marked in red in Figure 8).^[123-124] This transition should therefore be avoided. However, other amorphous hydrous oxides and basic salts are also known to precipitate from aqueous solutions. The formation is a complex balance of pH value, total Zr concentration in solution, temperature and the presence of anions such as chloride, acetate, sulphate or nitrate.^[123] When complexing Zr^{4+} , care should therefore be taken to ensure that the solutions are diluted and a pH value is set at which the resulting complex is stable.

3.1.6.2 Coordination Chemistry of Zr^{4+} and Chelators

Zr^{4+} as a hard cation favors complexation by equally hard donor groups.^[125] Thus, hydroxamates have become the focus of complexation for Zr^{4+} .^[126-127] The popular desferrioxamine B (DFOB) **7** (Figure 9 a)) is already a widely used natural product in this context.^[45, 128-130]

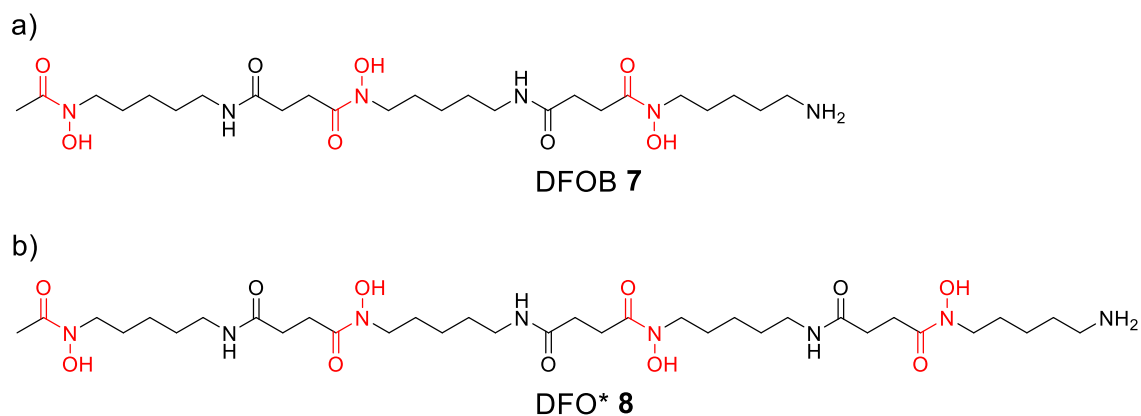


Figure 9: Structures of the natural siderophore DFOB **7** and octadentate derivative DFO* **8**.

DFOB **7** belongs to the group of siderophores and originates from the bacterium *Streptomyces pilosus*, from which it is used to make Fe^{3+} from the environment usable for the bacterium.^[131-133] It forms very stable complexes with Fe^{3+} ($\log K = 32$) and has therefore been used in a clinical context since the 1960s as "desferal" for the treatment of iron overload.^[134] DFOB **7** has a molar mass of 560 g/mol and has a linear, polyamide structure with three hydroxamic acids. Hydroxamates are among the best ligands for hard, oxophilic cations such as Fe^{3+} or Zr^{4+} . In aqueous solutions, hydroxamic acids have a pK_a of 8.5 - 9.3. When a hard cation (M^{n+}) is present in the solution, both Lewis acids (H^+ and M^{n+}) compete for the donor group, resulting in an exchange of the proton for the metal with a pK_a of about 1.^[135-136] DFOB **7** can be complexed with Zr^{4+} under mild conditions at room temperature within 30 – 60 min, can therefore be conjugated to sensitive biomolecules via the free terminal amine and has already been investigated in many studies with regard to its applicability in immunoPET.^[78, 126, 133, 137-147] Unfortunately, a reduced *in vivo* stability of the complexes was observed, which leads to a degradation of the complex and thus to the release of ^{89}Zr into the investigated organism.^[119, 129, 139, 148-151] The released ^{89}Zr was partially not excreted, but was deposited in the bones. In addition to the safety issue, this also has a negative impact on the quality of the PET image due to a higher background signal.

This instability was attributed to a not fully saturated coordination sphere of zirconium. Actually Zr^{4+} prefers a coordination number of eight, DFOB **7**, due to its three hydroxamic acids (marked in red in Figure 9) offers only six donor atoms.^[139] In order to achieve an octadentate

coordination sphere, the coordination sites are saturated by water ligands, which rapidly exchange and in this way kinetically destabilize the complex.^[139] To overcome this shortcoming, DFO* **8** (Figure 9 b)) was developed by Patra et al. in 2014.^[152] The structure of DFOB **7** was simply extended by one repeating unit, thereby introducing a fourth hydroxamic acid and ensuring octadentate complexation. Investigations via transchelation assays against a large excess of competing chelators such as DFOB **7** and EDTA have demonstrated the increased stability in *in vitro* studies and thus fundamentally confirmed the unsaturated coordination sphere hypothesis.^[152-153] Beside DFO* **8**, a large number of other tetrahydroxamic acids bearing Zr chelators have been presented in the literature in recent years: DFOB-PPH **9** and DFOB-PPHNOCO **10**,^[154] Orn4-hx **11**,^[155] DFO-HOPO **12**,^[156-157] DFOcyclo* **13**,^[158] H₃DFOSqOEt **14**,^[159] DFO2 **15**,^[160] DFO2p **16**,^[161] DFO-Em **17**,^[162] DFO-Km **18**,^[163] oxoDFO* **19**,^[164] and the macrocyclic derivatives CTH36 **20**^[165] and PPDFOT₁ **21**.^[166] They are illustrated in Figure 10. Many showed increased stability in *in vitro* experiments. Unfortunately, only a few of them (Orn4-hx **11**, DFOcyclo* **13**, DFO-Km **18**, H₃DFOSqOEt **14**, 3,4,3-(LI-1,2-HOPO) and DFO-HOPO **12**) have been labeled with ⁸⁹Zr and compared to DFOB **7** in *in vivo* immunoPET measurements.^[150, 155, 158-159, 163, 167-168]

Unfortunately, none of the chelators could show outstanding results that correspond to the *in vitro* results. Even DFO* **8**, one of the best chelators investigated in this regard, showed little to no improvement in a direct comparison with DFOB **7** as an ⁸⁹Zr complex conjugated to trastuzumab, an antibody addressed to HER2.^[158, 169-171]

3. Introduction

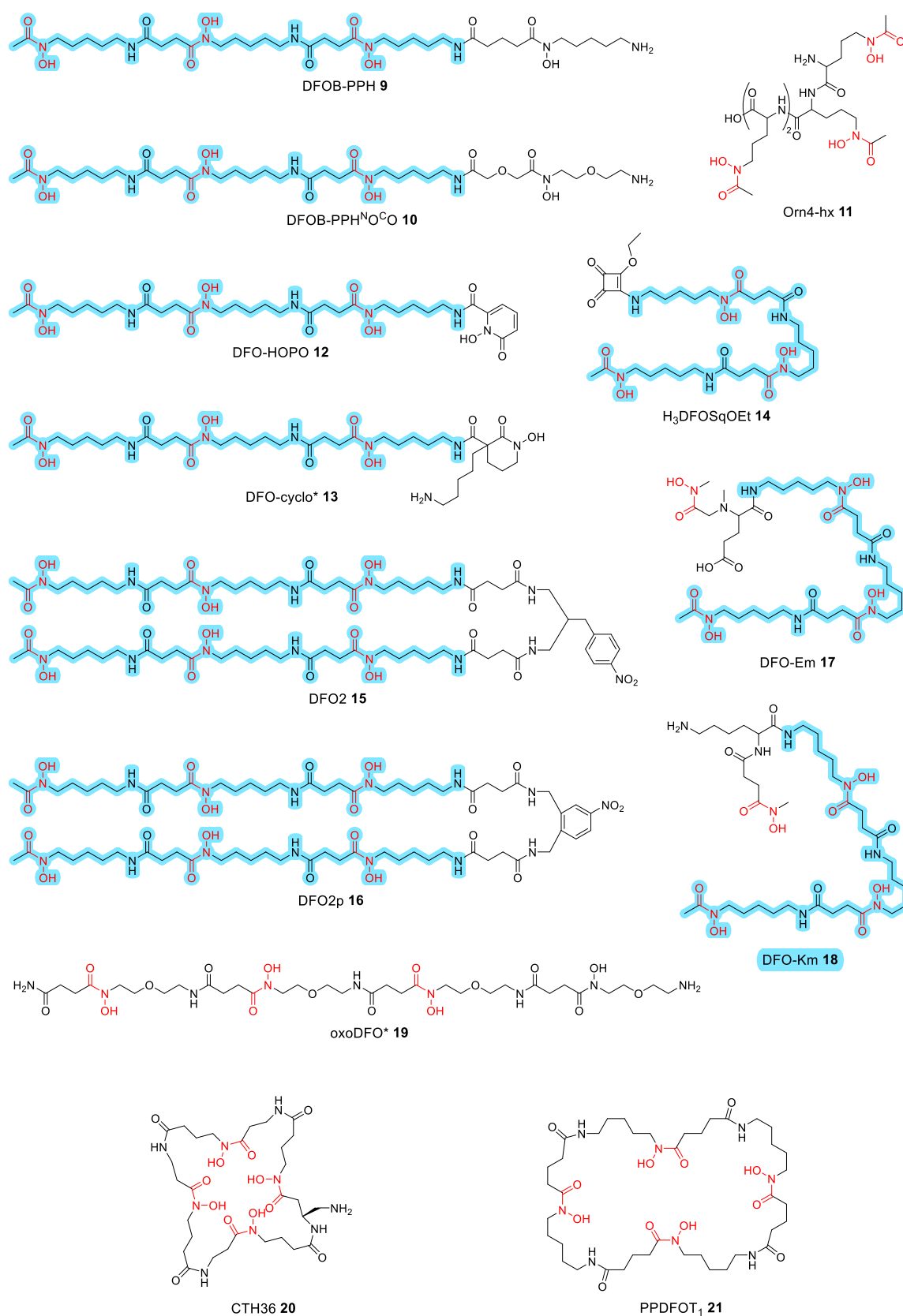


Figure 10: Published hydroxamate based Zr-chelators. Most of them used DFOB 7 as starting material (marked in blue). DFOB-PPH **9** and DFOB-PPHNOCO **10**,^[154] Orn4-hx **11**,^[155] DFO-HOPO **12**,^[156-157] DFOcyclo* **13**,^[158] H₃DFOSqOEt **14**,^[159] DFO2 **15**,^[160] DFO2p **16**,^[161] DFO-Em **17**,^[162] DFO-Km **18**,^[163] oxoDFO* **19**,^[164] and the macrocyclic derivatives CTH36 **20**^[165] and PPDFOT₁ **21**.^[166]

Since the synthesis of most of the mentioned chelators uses DFOB **7** as a starting material (marked in blue in Figure 10) for derivatization, this raises the question of whether, in addition to the positive effect of the fourth hydroxamic acid, the spacing between the hydroxamic acids could have an influence on complex stability. Considering the bacterial origin of DFOB **7**, it seems intuitive that DFOB **7** spacing is optimal for Fe^{3+} but not for Zr^{4+} . When complexing Zr^{4+} , with its different radius, the DFOB **7** spacing could lead to tensions in the complex geometry due to rigidity, which could destabilize the complex. A schematic representation of this hypothesis is shown in Figure 11.

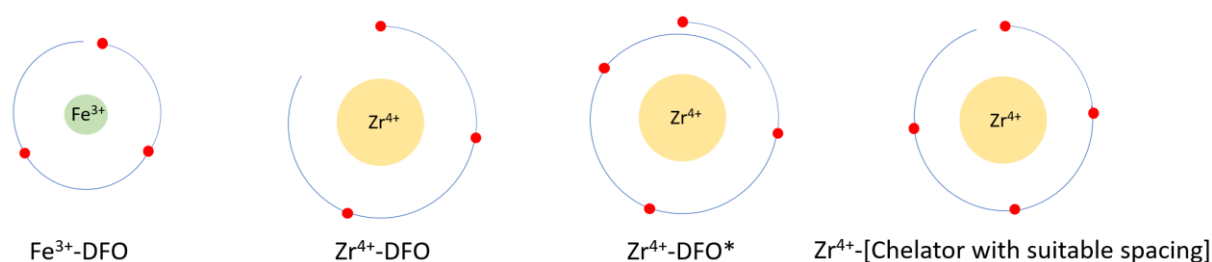


Figure 11: Schematic drawing of chelators for the coordination of Zr^{4+} and Fe^{3+} .

Iron, with the atomic number 26, is present as Fe^{3+} with an outer electron configuration of $[\text{Ar}]3d^5$ in the DFOB **7** complex as a distorted octahedral high spin complex and has an ionic radius of 66 pm.^[122, 172] Zirconium, on the other hand, with the atomic number 40, has the noble gas configuration $[\text{Kr}]$ and thus a d^0 configuration. As an octadentate complex with four hydroxamates, a square antiprismatic geometry is favored in which only 16 electrons are involved.^[173] Therefore, there is a free d_{π} orbital, which can accept the electrons from the lone electron pair of the oxygens and thus strengthens the bond between Zr^{4+} and the hydroxamates.^[125] For this reason, the elements in the first few groups of transition metals are also referred as oxophilic.^[125] Zr^{4+} has an ion radius of 85 pm, which is around 29% larger than of Fe^{3+} .^[122] With the additional introduction of a fourth repeating unit from DFOB **7** to DFO* **8**, this could result in a chelator which is too long overall and the flexibility of the alkyl chains is not sufficient to compensate. It must also be considered that in the practical application of ^{89}Zr in the clinical context, the corresponding ^{89}Y is formed during the process of radioactive decay.^[28] Although ^{89}Y also favors octadentate chelation, it has a less contracted ion radius of 102 pm due to the single reduced charge of $3+$.^[122, 124] The question of stable DFOB **7** analogue complexes with Y^{3+} has not yet been discussed in the literature.

Another weakness of the chelators presented in the literature to date is difficulty in making them functional. All derivatives based on DFOB **7** have so far only one conjugation site that can be used for functionalization. This limits their use with regard to multimerization platforms or for bi or even multispecificity. DFOB **7** and its derivatives are known for the poor water

solubility, which is particularly bad for conjugation to sensitive biomolecules that are only stable in aqueous media and poorly tolerate other solvents.^[164]

Previous work has shown that a minimum distance of seven atoms between the hydroxamic acids is necessary to enable complexation with Zr.^[174] In comparison, DFOB **7** and DFO* **8** (see Figure 9) have a distance of nine atoms. Seibold et al. published the Zr chelator CTH36 **20** in 2017, which structure was based on semiempirical calculations.^[165] CTH36 **20** is a circular DFOB **7** analog with a distance of seven atoms between the hydroxamic acids and has shown very good stability in *in vitro* experiments. In a comparative study with many published Zr chelators, thermodynamic complex constants were estimated and compared.^[175] CTH36 **20** was even rated above DFO* **8**, which strengthens the assumption of a non-optimal spacing of DFO* **8** as a chelator for Zr⁴⁺.

3.2 Solid Phase Peptide Synthesis (SPPS)

In the past, efforts have been made to prepare DFOB **7** and its analogues via solid-phase synthesis. However, the attempts were not successful so far.^[164-165] Nevertheless, the approach is highly promising. Its sequential design enables a high degree of modularity and significantly reduces the need for purification steps. Moreover, the process is readily amenable to automation, which facilitates standardization, increases reproducibility, and renders the method highly suitable for repetitive or high-throughput synthesis. For these reasons, establishing a solid-phase peptide synthesis (SPPS) route for DFOB **7** and its analogues would represent a valuable advancement in the development of novel zirconium-based PET chelators.

Sequential peptide synthesis on an insoluble resin matrix goes back to Bruce Merrifield in the 1960s.^[176] In this process, a protected amino acid is immobilized on a resin bead, whereupon the next amino acid is selectively coupled by targeted (orthogonal) cleavage of a protective group. This enables a controlled monomer sequence, simplifies multi-stage reactions and increases the efficiency and speed of synthesis.^[177] Today, there is a wide range of resins, protective groups and specialized synthesis equipment for solid-phase synthesis.

Solid-phase peptide synthesis is often supported by microwave radiation at 2.45 GHz.^[178] This radiation has an energy below the threshold required to break chemical bonds directly but generates heat through dielectric heating: polarized molecules and ions align themselves in the alternating electric field, which leads to molecular friction. The heat is thus generated directly in the solution in contrast to an oil bath. There the heat is transferred via the reaction vessel. Materials such as borosilicate absorb hardly any microwaves, which means that the energy is transferred directly to the reactants. This results in reversed temperature gradients

compared to the classic oil bath (Figure 12), which enables significantly shorter reaction times of often only a few minutes.^[178]

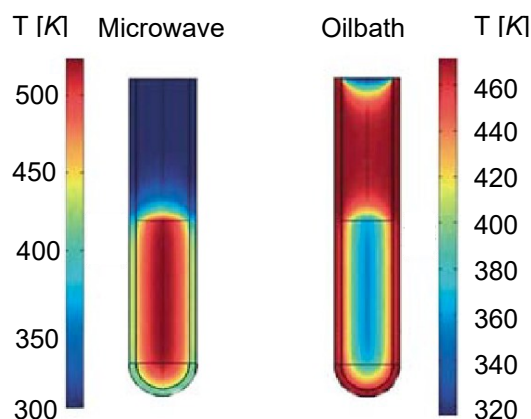


Figure 12: Depicturing of the Inverted temperature gradient when using microwave heating (left) and conventional heating with an oil bath (right).^[178]

The resin usually consists of small polystyrene beads (35 - 150 μm) that are crosslinked with 1 – 2 % divinylbenzene.^[177] Before synthesis, the beads must swell in a suitable solvent in order to increase reactivity through better diffusion and accessibility. The extent of swelling depends on the solvent: THF, toluene, CH_2Cl_2 and dioxane lead to a 5 to 6-fold increase in volume, DMF about 4-fold, while MeOH and water hardly show any swelling effects.^[176-177] However, stronger swelling does not necessarily mean higher conversions: Although CH_2Cl_2 lead to high swelling, it hinders the reaction by salt formation with piperidine during Fmoc deprotection. CH_2Cl_2 is therefore usually only used for initial swelling, while DMF is used for the actual synthesis steps.^[177]

A linker connects the resin with the first amino acid and plays a central role in the synthesis.^[177] It must be cleavable at the end of the synthesis and this determines the reaction conditions. It also determines whether the C- or N-terminus is bound to the resin and influences the chemical structure of the sequence start.^[177] Figure 13 shows four common linkers that illustrate the influence of the linker.

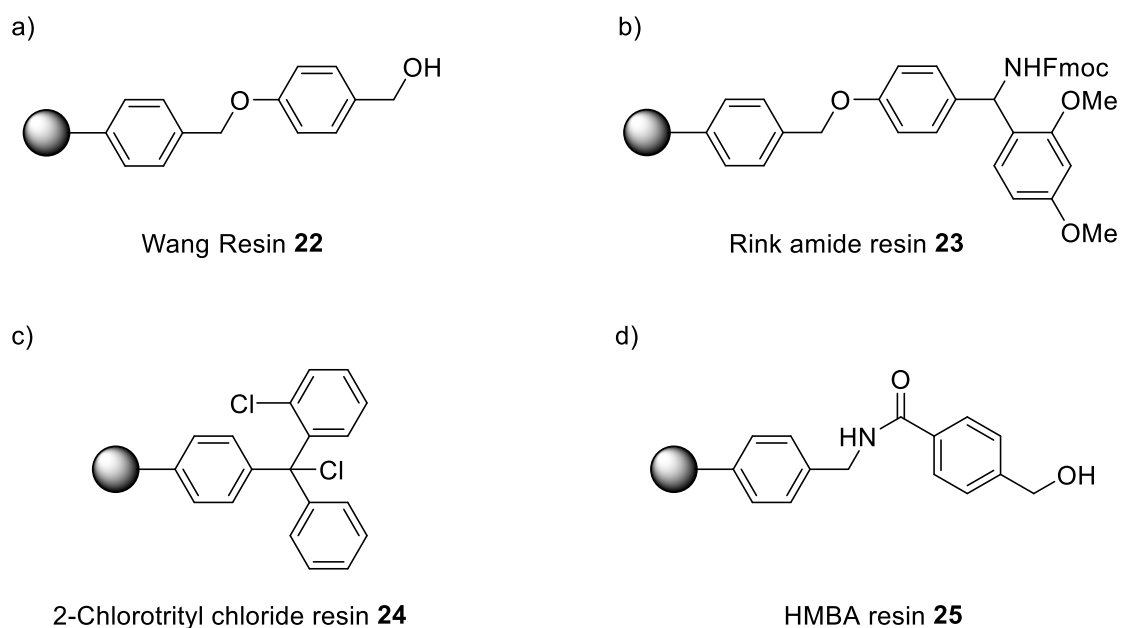


Figure 13: Common types of linker which forms the connecting unit between the PS beads of the solid phase and the first attached amino acid.^[177]

After cleavage with 90 – 95 % TFA in CH_2Cl_2 (1 – 2 h), the Wang resin **22** yields a carboxylic acid, as the first amino acid is esterified.^[177, 179] The Rink amide resin **23** yields an amide under similar conditions (50 % TFA in CH_2Cl_2 , 1 h).^[177, 180] For acid-labile products, 2-chlorotrityl resin **24** is suitable, which can already be cleaved with 1 – 5 % TFA in CH_2Cl_2 within 1 min.^[177, 181] If acidic conditions are not possible, the HMBA resin **25** can be used. Here the cleavage takes place with NaOH, N_2H_4 or NH_3 in MeOH over 24 h.^[177, 182]

The most frequently used protecting group strategy in peptide synthesis is the *tert*-butyl/Fmoc strategy.^[183] Fmoc can be removed under mild conditions with piperidine, producing 9-methylene fluorene.^[183-184] Numerous groups are available for orthogonal protection: e.g. 4-methyltrityl (cleavable with 1 % TFA in CH_2Cl_2), Alloc (removable by palladium catalysis), *tert*-butyl (90 % TFA or 4 M HCl), Dmb (extremely acid-labile and selectively removable), trityl (95 % TFA with scavenger) and Mmt (1 % TFA, also cleavable by oxidation).^[185] collection represents only a selection of established protecting groups.

Amide synthesis takes place by coupling a carboxylic acid with an amine with the elimination of water.^[186] This only takes place efficiently above approx. 200 °C. Many temperature-sensitive molecules cannot tolerate these temperatures. To increase reactivity, the OH group is usually replaced by a better leaving group to form, for example, an active ester.^[187] this can lead to racemization, particularly through enolization (red box in Figure 14) or oxazolone formation (blue box in Figure 14).^[187]

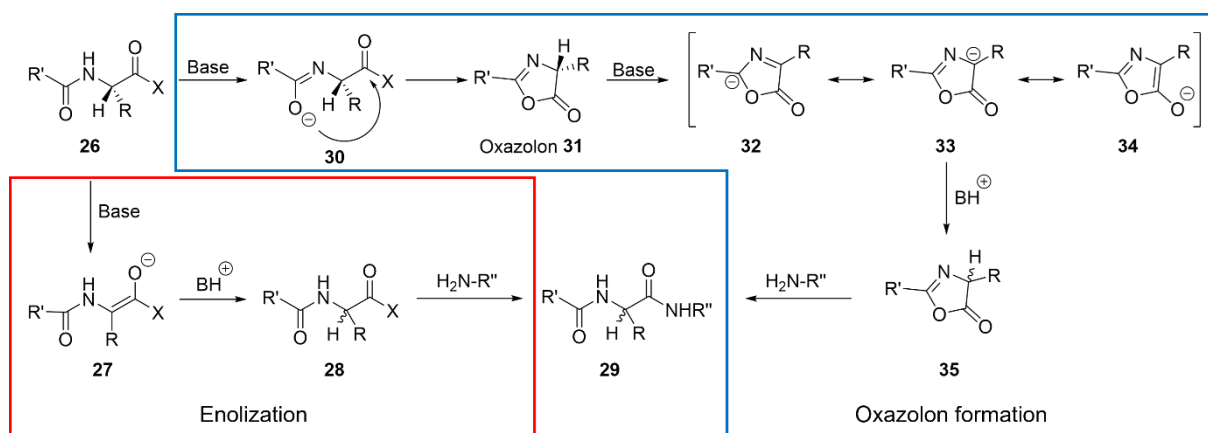


Figure 14: Two known mechanism of how the loss of chiral integrity in β -position of an active ester can take place via basic conditions: enolization (red box) and via a formation of an oxazolone (blue box).^[187]

The enolization of compound **26** leads to a loss of stereochemistry via proton abstraction and addition in the β -position (compounds **27** and **28**). Alternatively, an oxazolone ring is formed by intramolecular attack (compound **31**), whereby the configuration is lost via compound **35**. If the ring is finally opened by an amine, product **29** is formed, but as a racemate.^[187]

In this work, DFO* analogues with β -standing chiral centers are investigated. Their influence on complexation is as yet unknown. Therefore, specific coupling reagents were used which avoids racemization through enolization or oxazolone formation as far as possible and at the same time meet the special requirements of the coupling discussed in this work. The preferred coupling reagents of this work are presented in Figure 15.

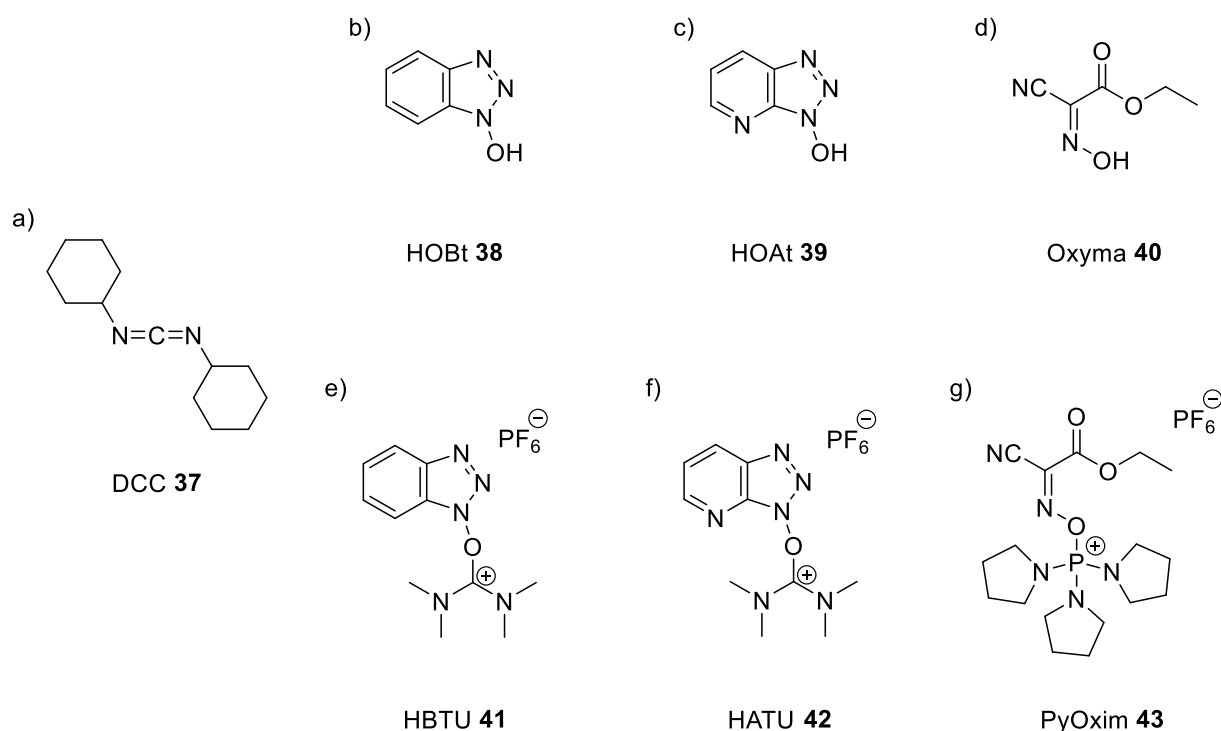


Figure 15: Coupling agents DCC, HOBT, HOAt, Oxyma®, HBTU, HATU and PyOxim®.

A classic approach is the use of carbodiimides such as *N,N'*-Dicyclohexylcarbodiimide (DCC) **37**, which forms reactive *O*-acylureas **46**. However, these can rapidly rearrange to *N*-acylureas **47**, which leads especially in DMF to chain termination. DCC **37** is therefore unsuitable for DMF-based SPPS.^[187]

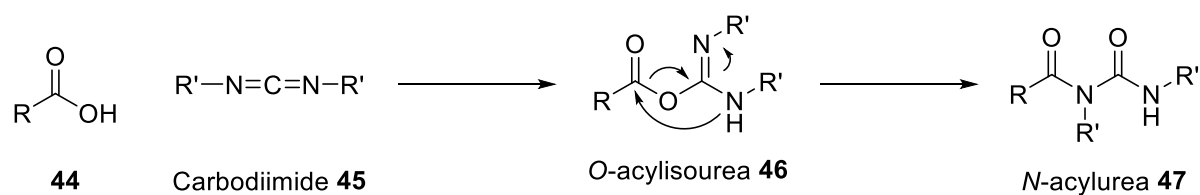


Figure 16: Formation of *N*-acylurea within the activation of a carboxylic acid via a carbodiimide.^[187]

The addition of benzotriazole derivatives such as Hydroxybenzotriazole (HOBT) **38** or 1-Hydroxy-7-azabenzotriazole (HOAt) **39** produces more stable, less reactive active esters. These prevent rearrangements through protonation and conversion into reactive esters, which simultaneously reduces racemization.^[188-189] HOAt has an additional nitrogen atom, which improves the leaving behavior through its electron-withdrawing effect and increases both reactivity and stereointegrity through the so-called *Neighboring Effect*.^[189]

Oxyma[®] **40**, introduced in 2009, offers a safe alternative without explosion risk and with comparable reactivity to HOAt as well as lower racemization compared to HOBt.^[190]

The combination of additives like uronium or phosphonium components led to the development of highly reactive coupling reagents such as HBTU **41**, HATU **42** and PyOxim[®] **43**, which are characterized by high efficiency and improved control of racemization.^[187] PyOxim[®] **43** in particular, an Oxyma[®]-based phosphonium salt, showed outstanding results in the coupling of sterically hindered peptides in this study and was therefore favored.

4. Aim of the work

The described limitations of DFOB **7** and DFO* **8** as chelators for immunoPET tracers form the basis for a new synthesis to develop an optimized chelator for zirconium. The approach should be based on easy-to-produce building blocks, which are to be constructed into isopeptidic chelators via modular synthesis (Figure 17). Some requirements are given as basic prerequisites: the chelator should have four hydroxamic acids for Zr-binding (Figure 17, marked in turquoise), possess bifunctionality to enable conjugation to targeting vector (Figure 17, marked in rose), variable distance between the hydroxamic acid units for investigations regarding sufficient complex stabilities (Figure 17, marked in blue) and clickable sidechain groups for fine tuning of pharmacokinetic properties and solubility (Figure 17, marked in red).

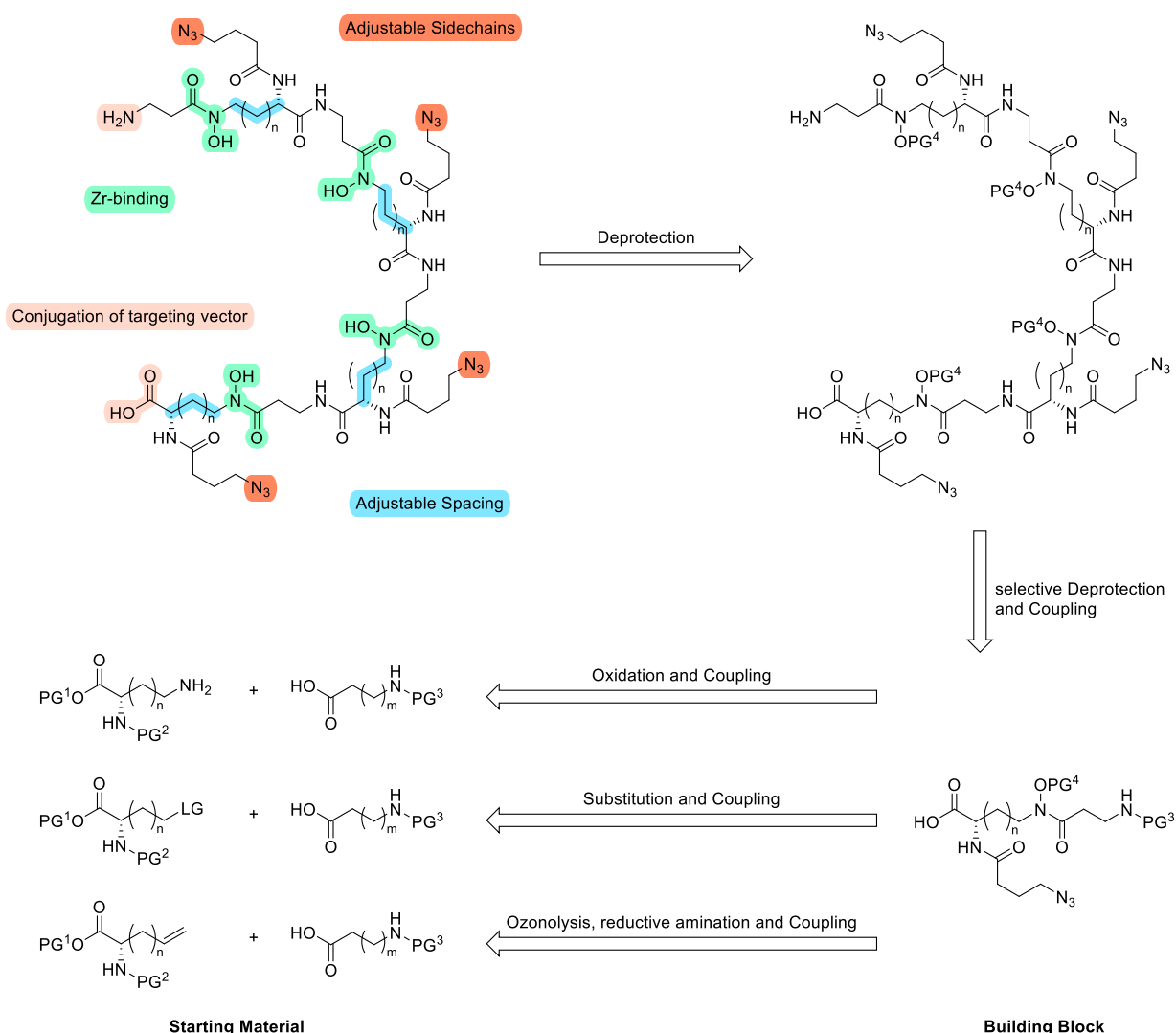


Figure 17: Retrosynthesis for the synthesis of complex Zr chelators. Requirements are the use of cheap, readily available and easy-to-modify starting materials, which are converted to basic building blocks with different chain lengths in the backbone. By selective deprotection of protective groups, the building blocks are to be converted to the protected hydroxamic acid chelators in a liquid-phase and a solid-phase approach. After deprotection of the hydroxamic acids, the multifunctional Zr chelator is synthesized successfully.

One of the main challenges lies in the synthesis of the highly complex building blocks, which requires a demanding protecting group strategy. For studies focused on determining the optimal spacing for Zr^{4+} complexation, the selected building blocks should be derived from inexpensive and readily available starting materials bearing side chains, such as 2,3-diaminopropanoic acid (Dpr), 2,4-diaminobutyric acid (Dab), ornithine and lysine, as well as from non-side chain bearing precursors like β -alanine and 4-aminobutyric acid (GABA). Glycine is unsuitable as a starting material, as glycine-derived DFOB analogues have been shown to exhibit limited chemical stability.^[191] The oxidation of the γ -standing amines to form protected hydroxylamines in side chain-bearing starting materials must proceed under conditions compatible with existing protective groups. If this proves infeasible, an alternative approach involves using structural analogues containing a leaving group at the γ -position, enabling substitution with protected hydroxylamine. Another strategy includes the introduction of a γ -positioned double bond, which can be transformed into the desired modified precursor via ozonolysis followed by reductive amination.

In an initial step, the building blocks should be converted into the corresponding protected tetrahydroxamic acids via liquid-phase synthesis, followed by solid-phase synthesis. Given literature-reported challenges and failed syntheses,^[164-165] it is essential to optimize the reaction conditions regarding coupling reagents, equivalents, reaction time, temperature and resin choice. These parameters should be systematically investigated through targeted experiments. Additionally, the feasibility of scaling up the reaction to a gram scale should be assessed.

With the isopeptidic DFOB and DFO* analogues on hand, a protocol for cleaving the protective groups of the hydroxamic acids must be created. One challenge here could be that the integrity of the additional functional groups in the compounds must be ensured. Furthermore, a protocol for the functionalization of the azide groups via click chemistry should be developed. This approach allows fine-tuning of the compounds by introducing prosthetic groups, such as zwitterionic side chains, to enhance aqueous solubility. Improved solubility is critical for ensuring reliable conjugation to the targeting vector.

The functionalized isopeptidic DFOB and DFO* analogues should then be evaluated for their relative stability using a radioactive assay in competition with EDTA and DFOB **7**. The aim is to identify an optimal spacing between the hydroxamic acid groups for efficient coordination of Zr^{4+} . Based on these findings, a corresponding non-radioactive assay will be developed using the same competing chelators. The radioactive assay data should serve as a benchmark to validate the non-radioactive method. Additional assays will investigate the serum stability of the Zr^{4+} complexes and determine the optimal conditions for the complexation reaction. Parameters to be assessed include the Zr^{4+} -to-chelator ratio, temperature, and reaction time.

This is particularly relevant for radiochemical applications, where reactions are performed at very low concentrations.

Based on these insights, a new synthetic approach should be developed in which both the targeting vector and the chelator are assembled on the solid phase in a single approach. As an initial model, the fundamental urea-based structures of PSMA should be employed, necessitating the development of a urea synthesis protocol suitable for solid-phase application. Furthermore, the deprotection of the hydroxamic acids under metal catalysis, as well as the metal-catalyzed click reaction, should be performed in a final step on the solid phase. This strategy offers the advantage of immediate and quantitative removal of potentially toxic metal cations, thus enabling a GMP-compliant synthesis.

5. Results and Discussion (cumulative part)

5.1 Solution Phase Synthesis of isopeptidic DFOB and DFO* analogs

As previously discussed, DFOB **7** exhibits limited *in vivo* stability, which can result in the release and subsequent accumulation of free ^{89}Zr in bones and organs. This not only compromises image quality but also raises safety concerns. To address this issue, novel DFOB and DFO* analogues were developed in this work, designed to form highly stable complexes with Zr^{4+} while maintaining water solubility and allowing for modular structural customization.

A total of nine isopeptidic desferrioxamine analogues were synthesized and categorized into two groups: AZA-DFOB (hexadentate chelators with three hydroxamate moieties) and AZA-DFO* (octadentate chelators with four hydroxamate moieties). These were prepared through a modular synthetic approach based on ornithine- β -alanine (Orn- β -Ala) and lysine- β -alanine (Lys- β -Ala) building blocks. All nine chelators were further functionalized via copper(I)-catalyzed azide-alkyne cycloaddition (CuAAC) to introduce zwitterionic side chains, thereby enhancing aqueous solubility.

To evaluate their suitability for radiolabeling with ^{89}Zr , a newly developed HPLC-MS-based assay was applied to monitor complex formation under physiologically relevant conditions. The experiments demonstrated rapid and complete complexation of Zr^{4+} by the new chelators. Notably, the zwitterionic, octadentate chelator composed exclusively of Orn- β -Ala units achieved full complexation within 90 min at 37 °C, performing comparably to the established Zr-chelator DFO* **8**.

For stability assessment, a non-radioactive, HPLC-MS-based transchelation assay was established. In this method, Zr-complexes were incubated with large excesses of competing chelators such as EDTA and DFOB **7** at pH 7, and aliquots were analyzed over time. The results revealed that hexadentate chelators - particularly those with extended alkyl chains derived from Lys- β -Ala - exhibited lower complex stability. In contrast, the octadentate analogues showed markedly enhanced stability. The Zr-complex of the pure Orn- β -Ala-based chelator remained stable for over 24 hours, even in the presence of a 1000-fold excess of EDTA and a 300-fold excess of DFOB **7**.

These findings confirm that the spacing between hydroxamate groups significantly influences Zr^{4+} complex stability. Shorter distances, as found in ornithine-derived monomers with eight atoms between hydroxamates, resulted in more stable complexes than longer spacings from lysine-based monomers (nine atoms). This supports the hypothesis that the distance plays a role in complexation and possibly also that its flexibility and the orientation of the amides in the isopeptidic structure could have an influence on the stability of Zr complexes.

Title: Synthesis of Modular Desferrioxamine Analogues and Evaluation of Zwitterionic Derivatives for Zirconium Complexation

Authors: Outzen, L., Münzmay M., Frangioni, J. V., Maison, W.

Type: Research Article

Journal: ChemMedChem

Year: 2023

Volume: 18

Issue: 13

Pages: e202300112

DOI: 10.1002/cmdc.202300112

Number of Pages: 15

Submitted: 24.02.2023

Accepted: 14.04.2023

VIP Very Important Paper

Synthesis of Modular Desferrioxamine Analogues and Evaluation of Zwitterionic Derivatives for Zirconium Complexation

Lasse Outzen,^[a] Moritz Münzmay,^[a] John V. Frangioni,^[b] and Wolfgang Maison^{*,[a]}

The natural siderophore desferrioxamine B (DFOB) has been used for targeted PET imaging with ⁸⁹Zr before. However, Zr-DFOB has a limited stability and a number of derivatives have been developed with improved chelation properties for zirconium. We describe the synthesis of pseudopeptidic analogues of DFOB with azido side chains. These are termed AZA-DFO (hexadentate) and AZA-DFO* (octadentate) and are assembled via a modular synthesis from Orn-β-Ala and Lys-β-Ala. Nine different chelators have been conjugated to zwitterionic moieties by copper-catalyzed azide-alkyne cycloaddition (CuAAC). The resulting water-soluble chelators form Zr complexes under mild conditions (room temperature for 90 min).

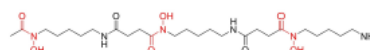
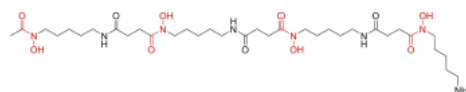
Transchelation assays with 1000-fold excess of EDTA and 300-fold excess of DFOB revealed that a short spacing of hydroxamate groups in (Orn-β-Ala)₃₋₄ leads to improved complex stability compared to a longer spacing in (Lys-β-Ala)₃₋₄. We found that the alignment of amide groups in the pseudopeptide backbone and the presence of zwitterionic sidechains did not compromise the stability of the Zr-complexes with our chelators. We believe that the octadentate derivative AZA-DFO* is particularly valuable for the preparation of new Zr-chelators for targeted imaging which combine tunable pharmacokinetic properties with high complex stability and fast Zr-complexation kinetics.

Introduction

Hydroxamic acids (*N*-hydroxy-amides) are among the best complex ligands for the hard Fe(III) cation and are thus abundant motifs in siderophores.^[1] Many of these siderophores are based on peptide and pseudopeptide structures and are produced and used by microorganisms for the uptake of iron as an important but barely water-soluble growth factor. The non-ribosomal biosynthesis of these peptides starts usually from ornithine and lysine derivatives.^[2] Hydroxamic acids have a pK_a of 8.5–9.3 in aqueous solutions.^[3] If Fe(III) is present in solution, competition occurs between the two hard Lewis acids (H⁺ and Fe³⁺), resulting in an exchange of protons with the Fe(III) cation with a pK_a of about 1.^[4] In addition to Fe³⁺ other hard and oxophilic metal cations also form stable chelate complexes with hydroxamic acids making them attractive chelators for a number of applications in metal-based imaging.^[5]

A prominent hydroxamate-based siderophore is desferrioxamine B (DFOB, Figure 1),^[6] first isolated by Prelog and co-workers from *Streptomyces pilosus*.^[7] DFOB has a molar mass of

Natural siderophore DFOB

Patra et al.^[10] DFO*

This work: 2,n-AZA-DFO*

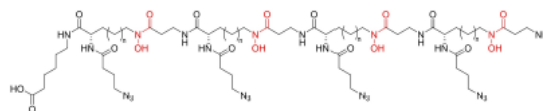


Figure 1. Structural comparison of the hexadentate natural siderophore DFOB, octadentate analogue DFO* and AZA-DFO*.

560 g/mol and a linear pseudopeptidic structure with three hydroxamic acid groups and a free terminal amine. It forms stable octahedral complexes with Fe³⁺ (logK=32) and is thus clinically used since the late 1960s as "Desferal" for the treatment of iron overload.^[8] In addition, DFOB forms stable complexes with a number of other hard metal cations with high relevance in disease imaging.^[9] DFOB is modular due to its free amine functionality and can easily be conjugated to targeting vectors such as peptides and antibodies. It is thus suitable for the construction of conjugates for targeted disease imaging.^[10] In addition, DFOB and other siderophores are themselves targeting moieties for microorganisms.^[11]

DFOB has attracted considerable interest as a bifunctional chelator for ⁸⁹Zr-PET-imaging. ⁸⁹Zr has favourable decay characteristics (particularly a relatively low positron emission energy)

[a] L. Outzen, Dr. M. Münzmay, Prof. Dr. W. Maison
Department of Chemistry, University of Hamburg
Bundesstrasse 45, 20146 Hamburg (Germany)
E-mail: wolfgang.maison@uni-hamburg.de

[b] Dr. J. V. Frangioni
The Curadel Companies
11 Erie Drive, Natick, MA 01760 (USA)

Supporting information for this article is available on the WWW under
https://doi.org/10.1002/cmdc.202300112

© 2023 The Authors. ChemMedChem published by Wiley-VCH GmbH. This is an open access article under the terms of the Creative Commons Attribution Non-Commercial NoDerivs License, which permits use and distribution in any medium, provided the original work is properly cited, the use is non-commercial and no modifications or adaptations are made.

and a half-life of 3.3 days, matching perfectly with the typical time required for extravasation and binding of antibodies used as targeting vectors in immunoPET diagnostics.^[12] In addition, the production and purification of ⁸⁹Zr has been optimized and partially automated in recent years.^[13] DFOB is characterized by fast complex formation with Zr(IV) (within 30–60 minutes) under mild conditions at room temperature making it an attractive chelator for immunoPET with ⁸⁹Zr.^[14] However, a shortcoming of DFOB is its hexadentate chelation which does not saturate the octadentate coordination sphere preferred by Zr(IV). The saturation of the coordination sphere to an octadentate complex is achieved by two water molecules, which are kinetically unstable and therefore exchange quickly.^[15] The *in vivo* stability of Zr-DFOB complexes is thus limited leading to the uptake of radioactive zirconium in bones during PET-imaging. This phenomenon is a possible safety issue and might deteriorate the signal to noise ratio.^[15–16]

Various other Zr(IV)-chelators have been developed to overcome the shortcomings of DFOB and to increase the complex stability.^[17] In this context, hexadentate macrocyclic hydroxamates of the fusarinine and the desferrichrome family,^[18] octadentate desferrichrome-derivatives like Orn4-hx,^[18b] DFO-HOPO,^[19] DFO*,^[20] DFOcyclo*,^[21] DFO2,^[22] DFO-Em,^[23] H₂DFOsqOEt^[24] and macrocyclic octadentate analogues are notable examples.^[25] However, many *in vivo* experiments with the corresponding targeted analogues showed comparable radioactive bone-uptake to DFOB despite improved complex stability as measured *in vitro*.^[18b,26] A notable exception is ⁸⁹Zr-complexation with DFO* (Figure 1): radiochemical yields were shown to be excellent for targeted (antibody conjugated) derivatives using standard labelling protocols at neutral pH and ambient temperature within 90 min.^[20,27] A transchelation assay showed that Zr-DFO* complexes remained stable *in vitro* even when challenged with large excess of competing chelators such as DFOB and EDTA, confirming the predicted higher stability of octadentate Zr-complexes.^[20] In addition, Zr-DFO*-antibody conjugates have the same blood clearance and tumor uptake but reduced zirconium uptake in bones, liver and spleen compared to corresponding DFOB conjugates.^[27a,28] However, a disadvantage when working with DFO* and other octadentate chelators is their poor water solubility, due to the hydrophobic backbone structures and the formation of net-neutral Zr-complexes. The low water solubility is often approached with DMSO addition which can lead to the degradation or aggregation of biomolecules upon conjugation.^[25b,27a,29] The water soluble analogue oxoDFO* has thus been developed and shown to have favorable properties for Zr-complexation.^[30]

A truly modular Zr-chelator should combine high complex stability with fast and efficient radiochemical labelling and should allow molecular finetuning with respect to pharmacokinetic properties, solubility and conjugation of additional effector molecules for theranostic applications or multimodal imaging. We describe herein the synthesis of peptidic octadentate DFO analogues termed AZA-DFO* bearing azide chain functionalities for easy derivatization *via* copper-catalyzed azide-alkyne cycloaddition (CuAAC).^[31] Furthermore, we have evaluated the complexation of Zr(IV) and the stability of the

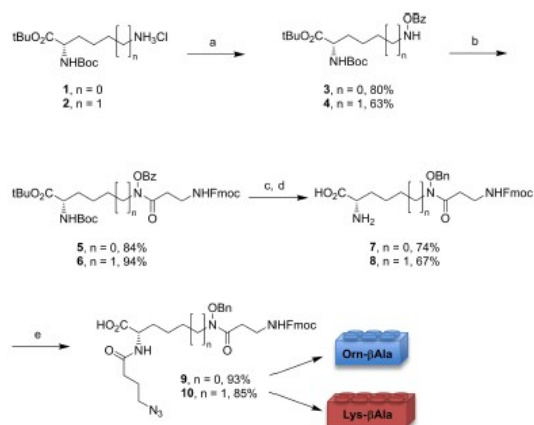
resulting complexes *in vitro*. With this work we extend the concept of clickable chelators from cyclic derivatives like DOTAZA^[32] and TRAP(azide)₃^[33] to acyclic chelators with presumably faster complexation kinetics.

Results and Discussion

Synthesis of chelators

Adapting the general concept of Wängler for the assembly of cyclic DFOB-analogues,^[25a] we used amino acids to build up the pseudopeptide backbone structure. This strategy allows a modular assembly for variation of intramolecular hydroxamate distances and the introduction of sidechains. A recent theoretical study of Holland revealed that backbone flexibility might be a key factor for efficient Zr-chelators.^[34] Pioneering work by Brechbiel and coworkers suggested that the spacer between two complexing hydroxamic acids should contain at least 7 atoms to allow the stable complexation of Zr.^[25b] The same spacing of 7 atoms was also used by Wängler for cyclic DFOB-analogues.^[25a] However, in DFO* a larger spacing of 9 atoms was used retaining the spacing of hydroxamic acids found in DFOB.^[20] As mentioned above, this spacing led to excellent chelation properties of DFO* and motivated us to target backbone structures with 8–9 atoms in spacing. In addition, the position of connecting amide bonds in the spacer can have an influence on the stability of corresponding metal complexes. This factor has not been studied for Zr complexation so far, but has been evaluated by Farkas for a number of other metal cations with dihydroxamates as a model system.^[25a,35] We chose to fix the amide to a central spacer position and used β-alanine (β-Ala, adding 3 atoms to the spacer) as a constant building block for all of our derivatives. Gly and GABA would be obvious alternative non-functionalized amino acids. However, peptidic DFOB-analogues derived from glycine have been found to have only limited chemical stability.^[36] Also, GABA caused problems in our synthetic approach due to unwanted formation of γ-butyrolactame during peptide coupling under forcing conditions. We used either L-ornithine (Orn, adding 5 atoms to the spacer) or L-lysine (Lys, adding 6 atoms to the spacer) as additional building blocks to β-Ala. Orn and Lys allow the introduction of sidechains to the spacer *via* their respective α-amino function.

The assembly of the pseudopeptidic repeat motifs 9 and 10 including β-Ala-Orn or β-Ala-Lys respectively is shown in Scheme 1 and starts from commercially available building blocks 1 and 2. Conversion with BPO gave the protected hydroxylamines 3 and 4 in good yield. The subsequent coupling of these relatively unreactive hydroxylamines with β-Ala to 5 and 6 was realized successfully with the acid chloride of β-Ala. We have tested a number of alternative coupling procedures involving activators like HBTU, BOP, HATU and TFFH, but none of these protocols gave satisfying results. As mentioned above, the use of an acid chloride intermediate for coupling limited our approach to β-Ala as a spacer, because GABA acid chloride led to rapid formation of the corresponding γ-butyrolactame.



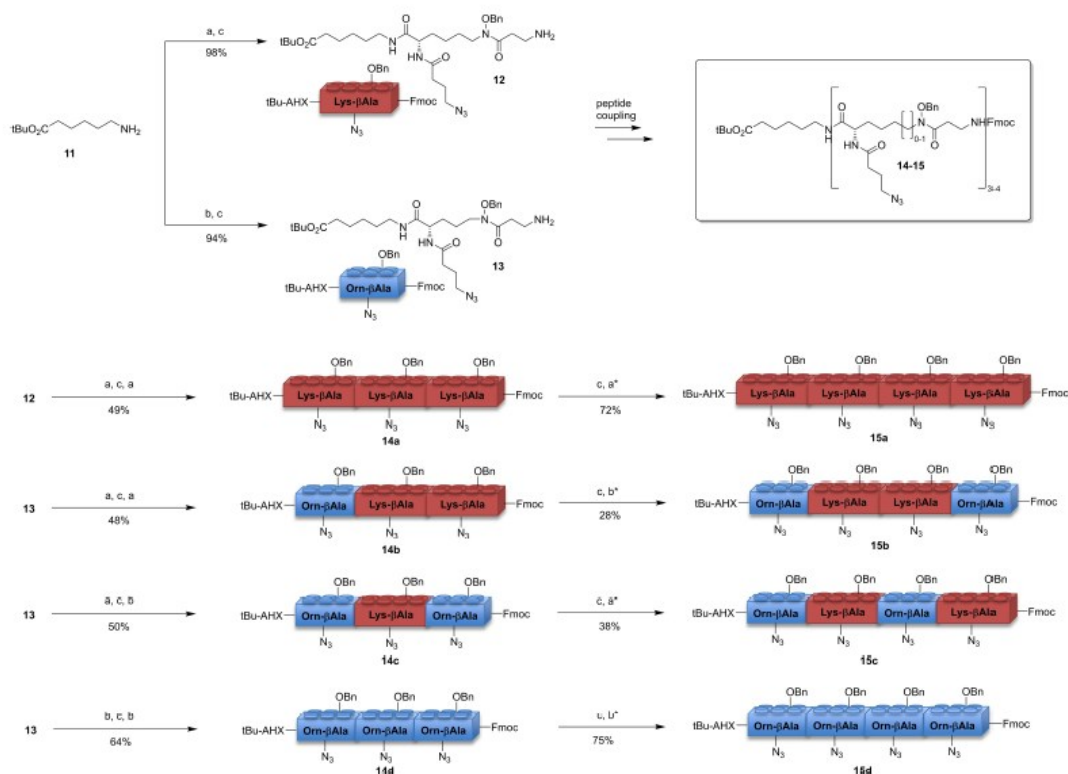
Scheme 1. Synthesis of pseudopeptide repeat units **9** (blue) and **10** (red) with different spacing. a) BOP, H_2O , CH_2Cl_2 , pH = 10.5, rt, 18 h; b) Fmoc- β -Ala-COCl, pyridine, THF, rt, 24 h; c) BnBr, DIEA, MeOH, rt, 22 h; d) TFA/ CH_2Cl_2 , TES, rt, 35 min; e) 2,5-dioxopyrrolidin-1-yl 4-azidobutanoate, DIEA, DMF, rt, 72 h.

We exchanged the Bz-protecting groups for Bn and cleaved Boc and *tert*-butyl protecting groups with TFA to obtain the free

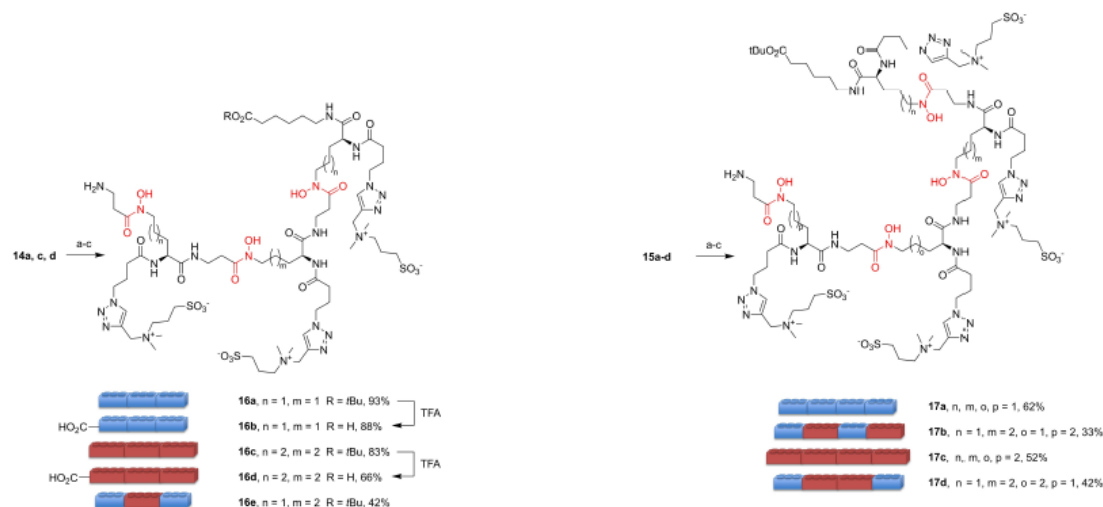
amino acids **7** and **8**. These intermediates were coupled to azido butyric acid *via* its NHS ester to install a “clickable” azide functionality in the side chain. The resulting acids **9** and **10** were now ready for the assembly of AZA-DFOB (including three hydroxamic acids) and AZA-DFO* (including four hydroxamic acids) derivatives. For easier identification in the following schemes, we have assigned the repeat units two different bricks (in blue and red).

The assembly of pseudopeptide analogues **14** and **15** including three or four hydroxamic acids is depicted in Scheme 2. We started with *tert*-butyl protected aminohexanoic acid (AHX *tert*-butylester, **11**) and used standard coupling conditions with HBTU/HOBt, DIEA at room temperature for 3–5 h to assemble protected AZA-DFOB derivatives **14a–d** stepwise. For the last coupling step to AZA-DFO* derivatives **15a–d**, a longer coupling time of 7 h was necessary to achieve reasonable yields.

Protected AZA-DFOB-derivatives **14** and AZA-DFO*-derivatives **15** may be functionalized *via* copper-catalyzed azide-alkyne cycloaddition (CuAAC). We performed this reaction in a proof of concept experiment with addition of a zwitterionic alkyne (3-(dimethyl(prop-2-yn-1-yl)ammonio)propane-1-sulfonate) (Scheme 3). It was important to perform these reactions without addition of additives such as TBTA and in



Scheme 2. Synthesis of protected AZA-DFOB (**14a–d**, including three hydroxamic acids) and AZA-DFO* (**15a–d**, including four hydroxamic acids) derivatives. a) peptide coupling with **10**, HBTU, HOBt, DIEA, rt, 3 h (7 h)*; b) peptide coupling with **9**, HBTU, HOBt, DIEA, rt, 3 h (7 h)*; c) piperidine, MeCN, rt, 20 min.



Scheme 3. Copper-catalyzed azide-alkyne cycloaddition (CuAAC) and subsequent deprotection to AZA-DFOB (**16a–e**) and AZA-DFO* derivatives **17a–d**. a) CuI, NaAsc, MeCN, H₂O, 3-(dimethyl(prop-2-yn-1-yl)ammonio)propane-1-sulfonate; b) Pd/C, H₂, 60 bar, 18 h; c) piperidine H₂O, rt, 20 min.

solvent mixtures with low water content (CH₃CN/H₂O, 98:2) to avoid side reactions. The resulting protected zwitterionic DFOB and DFO*-analogues were deprotected in final steps to give nine chelators **16** and **17** with three and four free hydroxamic acids respectively (highlighted in red). Complete debenzoylation required 60 bar hydrogen pressure in 20% AcOH to avoid catalyst deactivation. These conditions led to partial Fmoc-deprotection, which was completed by additional treatment with piperidine in a final step. Zwitterionic groups were installed to increase the water solubility of the chelators and might prove useful as stealth chelators in upcoming studies to create targeted imaging reagents with low non-specific tissue retention.^[37] The resulting set of zwitterionic DFOB and DFO*-derivatives **16** and **17** allowed us to study the influence of denticity and spacing of hydroxamic acids on the stability of corresponding Zr complexes.

Zr complexation and transchelation

To assess the complexation of Zr with our chelators, we used natural abundance ZrCl₄ in low μ M concentration and followed a standard protocol developed for radioactive labelling.^[20,25a] A first complexation was performed with the octadentate zwitterionic chelator **17a** at 24 °C and 37 °C at pH 8.5. The reaction was monitored for six hours by LC/MS. As depicted in Figure 2, full labelling of **17a** was achieved within approximately 90 min at 37 °C and 3 h at 24 °C. Complexation of Zr(IV) with our new chelator **17a** is thus slightly slower than complexation with hexadentate DFOB, but matches the complexation time measured for other octadentate chelators such as DFO*.^[20] We assume therefore that new chelators like **17a** are suitable for radioactive ⁸⁹Zr labelling under mild conditions, compatible

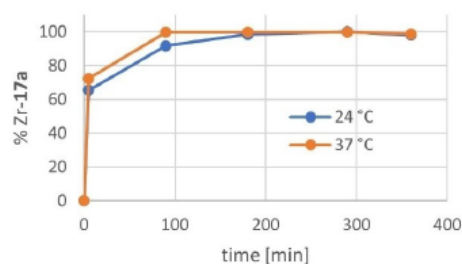


Figure 2. Monitoring of Zr-complexation with octadentate chelator **17a** at 24 °C and 37 °C. Complexation was performed at pH 8.5 at low μ M concentration and monitored by LC/MS-analysis.

with sensitive targeting vectors such as cyclic peptides or antibodies.

For the following evaluation of complex stability, a transchelation assay with excess EDTA as competing chelator was performed for each Zr-complex of the new chelators **16** and **17**.^[18a,21,25a,38] For this purpose, the appropriate chelator was incubated with ZrCl₄ at pH=8.5 for 90 min to form the Zr-complex. After pH adjustment to pH=7, a 1000-fold excess of EDTA was added and transchelation was followed by LC/MS for 24 h. After 0 h, 2 h, 8 h and 24 h, aliquots were taken from the solutions and analyzed by LC/MS. Peaks were nicely separated, because EDTA and EDTA–Zr complexes showed no retention on a C18 column with a MeCN/H₂O (0.1% HCO₂H) gradient, whereas all of our new complexes did. The extracted ion chromatogram for the most abundant Zr-isotopes, clearly confirmed the presence of the intact Zr-complexes. Zr-DFOB was used as a reference compound with very limited stability under these challenging conditions. Figure 3 shows the trans-

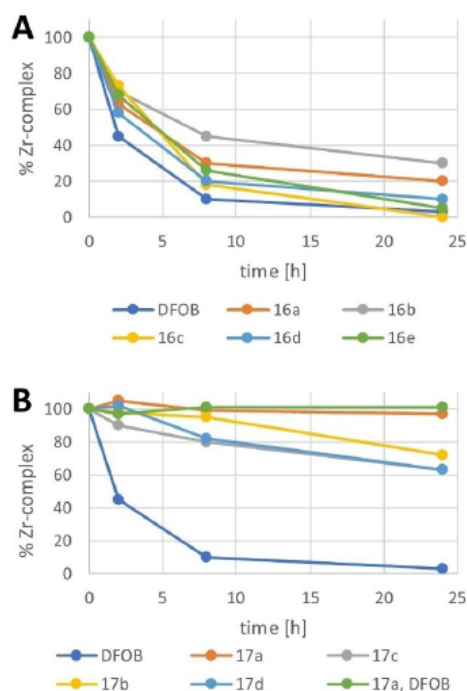


Figure 3. Transchelation assay of A) Zr-DFOB and Zr-16a–e challenged with a 1000-fold excess of EDTA at pH 7; B) Zr-DFOB and Zr-17a–d challenged with a 1000-fold excess of EDTA at pH 7. The green dots show the values of Zr-17a in competition to 300-fold excess DFOB.

chelation of Zr-DFOB in relation to five different analogues Zr-16a–e (Figure 3A) including three hydroxamic acid groups and in relation to four analogues Zr-17a–d (Figure 3B) including four hydroxamic acid groups. All of the tested Zr-complexes with only three hydroxamic acids showed relatively low stability in this assay with only 2–35% intact Zr-complexes after 24 hours. However, some trends are notable. Derivatives Zr-16a and Zr-16b including the shorter (8 atoms) β -Ala-Orn spacer were slightly more stable than DFOB (9 atoms) and the corresponding derivatives Zr-16c–e including the longer β -Ala-Lys (9 atoms) spacer. The most stable analogue with three hydroxamic acids was derivative Zr-16b with an additional free carboxylate group, which contributed significantly to complex stability. It is also notable, that the different positioning of the connecting amide bonds and the presence of the highly hydrophilic zwitterionic groups in all of our new chelators did not compromise complex stability compared to DFOB. A similar trend was observed for chelators 17a–d with four hydroxamic acids. However, in this case the complexes were significantly more stable. The most stable analogue was Zr-17a with the short β -Ala-Orn (8 atoms) spacer. This derivative showed no transchelation even under these challenging assay conditions. Both mixed sequences Zr-17b and Zr-17d as well as complex Zr-17b including a chelator with the longer β -Ala-Lys (9 atoms) spacer showed a lower complex stability than Zr-17a. The

remarkably high stability of complex Zr-17a was confirmed in an additional competition experiment against a 300-fold excess DFOB as depicted in Figure 3B with the green line.

Conclusion

We have described the synthesis of various clickable analogues of the natural siderophore DFOB (termed AZA-DFOB) and its octadentate homologue DFO* (termed AZA-DFO*). These new analogues were prepared by modular assembly of two building blocks differing in spacer length *via* peptide coupling. Two orthogonally protected β -Ala-Orn 9 and β -Ala-Lys 10 fragments allowed the assembly of AZA-DFOB 14 and AZA-DFO* 15 with a spacing of either 8 or 9 connecting atoms between hydroxamic acid moieties. In addition, the α -amino group of Orn and Lys allowed the introduction of sidechain functionalities *via* CuAAC. The chelators can thus be optimized for improved solubility and pharmacokinetic properties or for use as a multimerization platform for targeted imaging. The *N*- and the *C*-terminus of the chelators may be used to conjugate further functional molecules or targeting vectors, which might be useful for applications in multimodal imaging. Complexation of chelator 17a bearing zwitterionic sidechains and four hydroxamic acids with ^{nat}Zr was evaluated using protocols previously established for ^{89}Zr radio labelling. These experiments confirmed the rapid formation of Zr-17a within approximately 90 min at 37 °C and 3 h at room temperature. Zr-complexes of various new chelators with zwitterionic sidechains and either three or four hydroxamic acids for complexation were evaluated for complex stability by transchelation with 1000-fold excess of EDTA. We found that the alignment of amide groups in the pseudopeptide backbone and the presence of zwitterionic sidechains did not compromise the stability of the Zr-complexes 16 and 17. The spacer length in turn had an influence on complex stability with derivatives of β -Ala-Orn (8 atoms spacer length) having the highest stability. Chelator 17a with four hydroxamic acids for Zr-complexation was found to form the most stable Zr-complex and showed no transchelation over 24 h when challenged with 1000-fold excess EDTA and 300-fold excess DFOB as competing chelators. We believe that 17a is a valuable new Zr-chelator for targeted imaging which combines good solubility with high complex stability and fast Zr-complexation kinetics. However, it should be noted that both AZA-DFOB 14 and AZA-DFO* 15 might also be useful chelators for other oxophilic metal cations than zirconium.

Experimental Section

General Methods

All reagents and solvents were obtained commercially in required grades and used without further purification. Reactions sensitive to atmospheric oxygen or moisture were performed under a protective gas atmosphere (N_2 or Ar). The progress of reactions was monitored by TLC performed on silica gel ALUGRAM Xtra SIL G (normal phase) or Nano-SIL C₁₈ TLC plates (reverse phase) from

Macherey-Nagel. The detection was achieved by UV ($\lambda = 254$ nm) or by dipping in cerium(IV)-sulfate/ H_2SO_4 , ninhydrin/EtOH, vanillin/EtOH/ H_2SO_4 or Hanessian's stain followed by heating. Silica gel for column chromatography was of 60–200 μm size (POLYGOPREP 60–80 from Macherey-Nagel) for normal phase and 40–63 μm size (POLYGOPREP 100–50 C_{18} from Macherey-Nagel) for reverse phase. Automated column chromatography was performed on a puri-Flash450 from the manufacturer Interchim with POLYGOPREP 60–80 silica gel from Macherey-Nagel for normal phase and CHROMABOND Flash RS 15, CHROMABOND Flash RS 25 or CHROMABOND Flash RS 80 cartridges from Macherey-Nagel for reverse phase. For the purification by preparative HPLC a VWR Hitachi LaChrom Elite with a L-2130 pump and a UV-2400 UV-Detector or a VWR Hitachi LaChrom Elite with a L-7150 pump, L-700 interface and UV-2400 UV-Detector with the columns NUCLEODUR C_{18} HTEC EC, 250 \times 10 mm ID, 5 μm and NUCLEODUR C_8 HTEC EC, 250 \times 10 mm ID, 5 μm was used. Elemental analysis was performed by the device vario EL III from Elementar Analysensysteme GmbH or by EuroEA Elemental Analyzer from EuroVector with a HEKAtech HT oxygen analyzer from HEKAtech. IR-spectra were obtained on a FT/IR-4100-Spectrometer from Jasco with an ATR-unit. ^1H and ^{13}C spectra were recorded on an Avance III 600 MHz, Avance I 500 MHz, DRX 500 MHz, Avance III HD 400 MHz, Avance II 400 MHz, Avance I 400 MHz or FourierHD 300 MHz from Bruker Daltonics. ESI-MS spectra were obtained by MicroTOF-Q or amaZon SL from Bruker Daltonics or by 6224-ESI-TOF from Agilent Technologies. For the recording of LC/MS-spectra the MicroTOF-Q-mass spectrometer and a VWR Hitachi LaChrom Elite HPLC with L-2130 pump, a L-2400 Diode Array Detector and a L-2200 autosampler with the columns NUCLEODUR C_{18} HTEC EC, 250 \times 10 mm ID, 5 μm and NUCLEODUR C_8 HTEC EC, 250 \times 10 mm ID, 5 μm were used. Specific rotations were obtained on a M550 from A. Krüss Optotronic with a 1 mL capillary tube (0.5 dm length). UV-Vis analysis was achieved by Genesys 10uv from Thermo Scientific. Reactions with microwave conditions were performed by Initiator+ from Biotage with a Robot Sixty autosampler from Biotage or by Initiator Classic from Biotage.

Following molecules were synthesized according to literature procedures: Fmoc- β -Ala-COCl;^[39] 2,5-dioxopyrrolidin-1-yl-4-azidobutanoate;^[40] 6-aminohexanoic acid *tert*-butylester 11;^[41] 3-(dimethyl(prop-2-yn-1-yl)ammonio)propane-1-sulfonate;^[42] (N_α -Boc)-Orn *tert*-butylester 1;^[43] (N_α -Boc)-Lys *tert*-butylester 2.^[44]

General procedures

General procedure for O-Bz protection reaction (A). (N_α -Boc)-amino acid *tert*-butylester (1.00 eq.) was dissolved in CH_2Cl_2 and a $\text{NaHCO}_3/\text{NaOH}$ buffer solution (pH = 10.5, 3:1 (NaHCO_3 (0.05 mol/L)/ NaOH (0.1 mol/L)) was added. Benzoyl peroxide with 25% H_2O (1.15 eq.) was added in portions with vigorous stirring and the reaction was stirred at room temperature for 18 h. The phases were separated and the organic phase was concentrated to dryness and the residue was dissolved in EtOAc, washed with aqueous $\text{Na}_2\text{S}_2\text{O}_3$ (2 M) solution and sat. NaCl solution, dried over Na_2SO_4 and filtered. The crude product obtained after evaporation of solvent in vacuo was purified by column chromatography on SiO_2 (*n*-pentane/EtOAc 7:1 \rightarrow 3:1 v/v).

General procedure for amide couplings with Fmoc- β -Ala-COCl (B). (N_α -Boc)-amino acid (N_ω -OBz) *tert*-butylester (1.00 eq.) was dissolved in abs. THF and abs. pyridine (3.00 eq.) was added. Then Fmoc- β -Ala-COCl (1.00 eq.) dissolved in abs. THF was added dropwise and the reaction solution was stirred at room temperature. The solvent was removed under reduced pressure and the residue was dissolved in EtOAc and washed with HCl(aq) (1 M), sat. NaHCO_3 and sat. NaCl. After drying over Na_2SO_4 , filtration and removal of the solvent under reduced pressure, the crude product

obtained was purified by column chromatography on SiO_2 (*n*-pentane/EtOAc 10:1 \rightarrow 1:4 v/v).

General procedure for OBz to OBn exchange (C). (N_α -Boc)-amino acid- (N_ω -OBz)- N_ω - β -Ala-Fmoc *tert*-butylester (1.00 eq.) was dissolved in CH_3OH and DIPEA (4.00 eq.) was added. The solution was stirred at room temperature for 20 min and then benzylbromide (2.00 eq.) was added dropwise. The reaction solution was stirred at room temperature for 20 h. After complete conversion (TLC), the solvent was removed under reduced pressure and the residue was dissolved in EtOAc and washed with HCl(aq) (1 M), sat. NaHCO_3 , H_2O and sat. NaCl. The organic phase was dried over Na_2SO_4 and, after filtering, the solvent was removed under reduced pressure and the crude product obtained was purified by column chromatography on SiO_2 .

General procedure for *tert*-butyl deprotection (D). (N_α -Boc)-amino acid- (N_ω -OBn)- N_ω - β -Ala-Fmoc *tert*-butylester (1.00 eq.) was dissolved with triethylsilane (5.00 eq.) in 66% TFA in CH_2Cl_2 and stirred at room temperature. All volatile components were removed under reduced pressure and the residue obtained was purified by column chromatography on SiO_2 -RP18 (Column: NUCLEODUR C_{18} HTEC EC, 250 \times 10 mm ID, 5 μm , $\text{H}_2\text{O}/\text{CH}_3\text{CN}$ 95:5 + 0.1% HCO_2H \rightarrow 5:95 + 0.1% HCO_2H v/v). Due to the treatment with TFA a simultaneously deprotection of Boc occurred for compounds 76 and 78.

General procedure for peptide coupling with HBTU/HOBt (E). Carboxylic acid (1.00 eq.) was dissolved with HBTU (1.05 eq.), HOBt (2.00 eq.) and DIPEA (3.00 eq.) in abs. DMF followed by stirring at room temperature. Amine (1.00 eq.) in abs. DMF was added and the reaction solution was stirred further at room temperature. The solvent was removed under reduced pressure and the solid obtained was purified by column chromatographic purification on SiO_2 . In some cases, further purification on SiO_2 -RP18 (Column: NUCLEODUR C_{18} HTEC EC, 250 \times 10 mm ID, 5 μm) was necessary.

General procedure for Fmoc deprotection (F). Fmoc protected amine (1.00 eq.) was dissolved in 20% piperidine in acetonitrile and stirred for 20 min at room temperature. The solvent was removed under reduced pressure and the crude product was purified by column chromatography on SiO_2 .

General procedure for Cu-catalyzed click reaction (G). The appropriate azide (1.00 eq.), 3-(dimethyl(prop-2-yn-1-yl)ammonio)propane-1-sulfonate (1.50 eq. per azide), CuI (0.13 eq. per azide) and sodium ascorbate (0.67 eq. per azide) were dissolved in CH_3CN . Demineralized H_2O was added until a clear solution resulted. The solution was stirred at 70 $^\circ\text{C}$ under microwave heating for 2 h. The solvent was removed under reduced pressure and the crude product obtained was purified by column chromatography on SiO_2 -RP18 (Column: NUCLEODUR C_{18} HTEC EC, 250 \times 10 mm ID, 5 μm , $\text{H}_2\text{O}/\text{CH}_3\text{CN}$ 95:5 + 0.1% HCO_2H \rightarrow 5:95 + 0.1% HCO_2H v/v).

General procedure for OBn and Fmoc deprotection (H). The appropriate OBn protected hydroxamate (1.00 eq.) was dissolved in $\text{H}_2\text{O}/\text{AcOH}$ (2:1 by volume). Pd/C (10% on activated carbon) was added and the suspension was stirred under a H_2 atmosphere for 18 h at room temperature. The catalyst was removed by filtration through a celite pad and the solvent was removed under reduced pressure. Demineralized H_2O (4 mL) and piperidine (1 mL) were added. The resulting Fmoc-piperidine adduct precipitated as a white, voluminous solid. After stirring for 15 min, the suspension obtained was filtered and the solvent was removed under reduced pressure. The purified product was obtained by preparative HPLC (Column: NUCLEODUR C_{18} HTEC EC, 250 \times 10 mm ID, 5 μm , $\text{H}_2\text{O}/\text{CH}_3\text{CN}$ 98:2 + 0.1% HCO_2H \rightarrow 2:98 + 0.1% HCO_2H v/v, 5 mL/min). Products were characterized by HPLC-HRMS ($\text{H}_2\text{O}/\text{CH}_3\text{CN}$ 98:2 + 0.05% HCO_2H \rightarrow 5:95 + 0.05% HCO_2H v/v, 0.2 mL/min).

(*N_ε*-Boc)-Orn(*N_ε*-OBz) *tert*-butylester (3): Preparation according to method A, scale: (*N_ε*-Boc)-Orn *tert*-butylester 1^[43] (12.7 g, 38.6 mmol, 1.00 eq.), CH₂Cl₂ (300 mL), NaHCO₃/NaOH buffer (300 mL), benzoyl peroxide with 25% H₂O (10.8 g, 44.4 mmol, 1.15 eq.), EtOAc (350 mL), Na₂S₂O₃ solution (2 M, 2×250 mL) and sat. NaCl (300 mL). Colorless solid; yield: 80%. *R_f*=0.56 (SiO₂, *n*-pentane/EtOAc 3:1 v/v, UV₂₅₄, Ammonium cerium(IV) sulfate). The analytical data were identical to those reported in the literature.^[45]

(*N_ε*-Boc)-Orn(*N_ε*-OBz)-*N_ε*-β-Ala-Fmoc *tert*-butylester (5): Preparation according to method C, scale: 3 (2.99 g, 7.32 mmol, 1.00 eq.) in THF (20 mL), abs. pyridine (1.77 mL, 22.0 mmol, 3.00 Eq.), Fmoc-β-Ala-COCl (2.41 g, 7.32 mmol, 1.00 Eq.) in THF (10 mL), reaction time (24 h), EtOAc (200 mL), HCl(aq) (1 M, 2×250 mL), sat. NaHCO₃ (2×150 mL), sat. NaCl (100 mL). Colorless solid; yield: 4.26 g (84%). *Mp.*=68.2–69.7 °C. ¹H NMR (600 MHz, CDCl₃) δ 8.07 (d, ³*J*=8.2 Hz, 2H, H-21), 7.75 (d, ³*J*=7.4 Hz, 2H, H-14), 7.68 (t, ³*J*=7.4 Hz, 1H, H-23), 7.60 (d, ³*J*=7.4 Hz, 2H, H-17), 7.51 (t, ³*J*=7.8 Hz, 2H, H-22), 7.39 (t, ³*J*=7.4 Hz, 2H, H-15), 7.31 (t, ³*J*=7.4 Hz, 2H, H-16), 5.54 (sbr, 1H, H-9), 5.08 (d, ³*J*=7.7 Hz, 1H, H-24), 4.34 (d, ³*J*=7.1 Hz, 2H, H-11), 4.21 (t, ³*J*=7.1 Hz, 1H, H-12), 4.20 (sbr, 1H, H-2), 3.87 (sbr, 2H, H-5), 3.51 (sbr, 2H, H-8), 2.54 (sbr, 2H, H-7), 1.92–1.84 (m, 1H, H-3), 1.77–1.66 (m, 3H, H-3, H-4), 1.43 (s, 9H, H-29), 1.41 (s, 9H, H-27). ¹³C NMR (151 MHz, CDCl₃) δ 164.6 (C-20), 156.5 (C-10), 155.5 (C-25), 144.1 (C-13), 141.4 (C-18), 134.9 (C-23), 130.2 (C-21), 129.1 (C-22), 127.8 (C-15), 127.2 (C-16), 125.3 (C-17), 120.1 (C-14), 82.2 (C-28), 79.8 (C-26), 67.0 (C-11), 53.7 (C-2), 47.8 (C-5), 47.4 (C-12), 36.2 (C-8), 32.7 (C-7), 30.4 (C-3), 28.4 (C-29), 28.1 (C-27), 23.1 (C-4). IR: $\tilde{\nu}_{\text{max}}$ (cm⁻¹)=3351.7, 2971.8, 2935.1, 2022.0, 1763.6, 1707.7, 1514.8, 1452.1, 1367.3, 1242.9, 1155.2, 1040.4, 1007.6, 850.5, 761.7, 742.5, 705.8, 621.0, 562.2. HRMS (ESI, pos.): calc. for C₃₉H₄₇N₃NaO₉⁺ [*M*+Na]⁺ 724.3205; found 724.3209. CHNO-Analysis: calc. for C₃₉H₄₇N₃O₉: C, 66.75%; H, 6.75%; N, 5.99%; O, 20.52%; found: C, 66.66%; H, 6.75%; N, 5.85%; O, 20.43%.

Orn(*N_ε*-OBn)-*N_ε*-β-Ala-Fmoc (7): The title compound 7 was obtained in two steps via intermediate (*N_ε*-Boc)-Orn(*N_ε*-OBn)-*N_ε*-β-Ala-Fmoc *tert*-butylester. The latter compound was obtained from 5 employing method C, scale: 5 (390 mg, 0.56 mmol, 1.00 eq.), CH₂OH (10 mL), DIPEA (0.26 mL, 2.22 mmol, 4.00 eq.), benzylbromide (0.19 mL, 1.12 mmol, 2.00 Eq.), EtOAc (20 mL), HCl(aq) (1 M, 2×15 mL), sat. NaHCO₃ 2×15 mL, H₂O (2×15 mL) and sat. NaCl (3×15 mL), column chromatography on SiO₂: *n*-pentane/EtOAc 3:2 v/v. Pale yellow solid; yield of the intermediate *tert*-butylester: 314 mg (80%). *Mp.*=60.2–61.2 °C. ¹H NMR (600 MHz, CDCl₃) δ 7.75 (d, ³*J*=7.3 Hz, 2H, H-17), 7.60 (d, ³*J*=7.3 Hz, 2H, H-14), 7.39 (t, ³*J*=7.5 Hz, 2H, H-15), 7.37–7.34 (m, 5H, H-21, H-22, H-23), 7.30 (t, ³*J*=7.5 Hz, 2H, H-16), 5.56–5.53 (m, 1H, H-9), 5.07 (d, ³*J*=7.2 Hz, 1H, H-24), 4.78 (s, 2H, H-19), 4.35 (d, ³*J*=7.2 Hz, 2H, H-11), 4.22–4.19 (m, 2H, H-2, H-12), 3.70 (sbr, 2H, H-5), 3.49–3.46 (m, 2H, H-8), 2.65–2.62 (m, 2H, H-7), 1.82–1.77 (m, 1H, H-3), 1.73–1.66 (m, 2H, H-4), 1.64–1.60 (m, 1H, H-3), 1.43 (s, 9H, H-29), 1.43 (s, 9H, H-27). ¹³C NMR (151 MHz, CDCl₃) δ 171.8 (C-1), 156.5 (C-6), 155.5 (C-25), 144.2 (C-13), 141.4 (C-18), 134.2 (C-20), 129.4 (C-23), 129.2 (C-21), 128.9 (C-22), 127.8 (C-15), 127.2 (C-16), 125.3 (C-14), 120.1 (C-17), 82.2 (C-28), 79.8 (C-26), 76.5 (C-19), 66.9 (C-11), 53.6 (C-2), 47.4 (C-12), 45.0 (C-5), 36.5 (C-8), 32.8 (C-7), 30.3 (C-3), 28.5 (C-29), 28.1 (C-27), 22.9 (C-4). IR: $\tilde{\nu}_{\text{max}}$ (cm⁻¹)=2981.4, 2889.8, 1704.8, 1655.6, 1505.2, 1449.2, 1390.4, 1364.4, 1246.8, 1148.4, 1069.3, 1003.8, 965.2, 850.5, 758.9, 735.7, 696.2. HRMS (ESI, pos.): calc. for C₃₉H₄₉N₃NaO₉⁺ [*M*+Na]⁺ 710.3412; found 710.3417. CHNO-Analysis: calc. for C₃₉H₄₉N₃O₉: C, 68.10%; H, 7.18%; N, 6.11%; O, 18.61%; found: C, 67.88%; H, 7.23%; N, 6.04%; O, 18.67%.

This intermediate *tert*-butylester was converted to the title compound 7 via method D. Scale: intermediate *tert*-butylester mentioned above (3.07 g, 4.46 mmol, 1.00 eq.), triethylsilane (3.56 mL, 22.3 mmol, 5.00 eq.), 66% TFA in CH₂Cl₂ (24 mL), reaction time

(35 min). Colorless solid; yield of 7: 871 mg (30%). *R_f*=0.69 (CH₂Cl₂/CH₃OH 9:1 v/v, UV₂₅₄, Ninhydrin). *Mp.*=136.1–136.8 °C. ¹H NMR (500 MHz, CDCl₃) δ 8.31 (sbr, 2H, H-25), 7.69–7.57 (m, 2H, H-18), 7.52–7.39 (m, 2H, H-15), 7.32–7.24 (m, 2H, H-16), 7.22–7.06 (m, 7H, H-17, H-22, H-23, H-24), 6.06 (sbr, 1H, H-10), 4.57 (s, 2H, H-20), 4.24–4.11 (m, 2H, H-12), 4.10–3.99 (m, 1H, H-13), 3.90–3.75 (m, 1H, H-3), 3.74–3.61 (m, 1H, H-6), 3.57–3.43 (m, 1H, H-6), 3.38–3.22 (m, 2H, H-9), 2.64–2.31 (m, 2H, H-8), 1.95–1.68 (m, 4H, C-4, C-5). ¹³C NMR (126 MHz, CDCl₃) δ 171.9 (C-2), 144.2 (C-14), 141.3 (C-19), 134.0 (C-21), 129.4 (C-24), 129.0 (C-22), 128.7 (C-23), 127.7 (C-16), 127.1 (C-17), 125.4 (C-15), 120.0 (C-18), 76.3 (C-20), 66.8 (C-12), 47.3 (C-13), 32.7 (C-8). ¹³C-NMR (151 MHz, CDCl₃): δ 54.2 (C-3), 44.6 (C-6), 36.7 (C-9), 28.0 (C-4), 23.0 (C-5). IR: $\tilde{\nu}_{\text{max}}$ (cm⁻¹)=3318.9, 2980.5, 2883.1, 1709.6, 1651.7, 1510.0, 1450.2, 1392.4, 1384.7, 1366.3, 1247.7, 1150.3, 1076.1, 1007.6, 843.7, 758.9, 751.1, 740.5, 699.1. HRMS (ESI, pos.): calc. for C₃₀H₃₄N₃O₆⁺ [*M*+H-TFA]⁺ 532.2442; found 532.2441.

Protected (Orn-β-Ala) monomer (80): 76 (1.23 g, 2.32 mmol, 1.00 eq.) was dissolved in abs. DMF (20 mL) and DIPEA (1.21 mL, 6.97 mmol, 3.00 eq.) was added. 2,5-dioxopyrrolidin-1-yl 4-azidobutanoate 36 (523 mg, 2.32 mmol, 1.00 eq.) was added and the reaction solution was stirred for 3 h at room temperature. The solvent was removed under reduced pressure and the residue was dissolved in CH₂Cl₂ (10 mL) to co-evaporate residues of DMF and DIPEA. This process was repeated twice. The brown crude product obtained was purified by column chromatography on SiO₂ (CH₂Cl₂/CH₃OH 15:1+1% AcOH→10:1+1% AcOH v/v). Colorless solid; yield: 1.39 g (93%). *R_f*=0.39 (CH₂Cl₂/CH₃OH 15:1+1% AcOH v/v, UV₂₅₄, Ninhydrin). ¹H NMR (500 MHz, CDCl₃) δ 7.74 (d, 2H, ³*J*=7.6 Hz, H-18), 7.57 (d, 2H, ³*J*=7.6 Hz, H-15), 7.38 (t, 2H, ³*J*=7.6 Hz, H-17), 7.35–7.33 (m, 5H, H-22, H-23, H-24), 7.29 (t, 2H, ³*J*=7.6 Hz, H-16), 6.87–6.70 (m, 1H, H-10), 5.65 (sbr, 1H, H-25), 4.76 (s, 2H, H-20), 4.59–4.56 (m, 1H, H-3), 4.34 (d, 2H, ³*J*=6.9 Hz, H-12), 4.18 (t, 1H, ³*J*=6.9 Hz, H-13), 3.76–3.64 (m, 2H, H-6), 3.45–3.37 (m, 2H, H-9), 3.27 (t, 2H, ³*J*=6.4 Hz, H-29), 2.63–2.50 (m, 2H, H-8), 2.27 (t, 2H, ³*J*=6.9 Hz, H-27), 1.90–1.83 (m, 3H, H-4, H-28), 1.75–1.65 (m, 3H, H-4, H-5). ¹³C NMR (126 MHz, CDCl₃) δ 174.1 (C-2), 172.8 (C-26), 156.7 (C-11), 144.1 (C-14), 141.4 (C-19), 133.9 (C-21), 129.4 (C-24), 129.3 (C-22), 128.9 (C-23), 127.8 (C-17), 127.2 (C-16), 125.2 (C-15), 120.1 (C-18), 76.6 (C-20), 66.9 (C-12), 52.1 (C-3), 50.7 (C-29), 47.3 (C-13), 44.8 (C-6), 36.5 (C-9), 33.0 (C-27), 32.8 (C-8), 28.9 (C-4), 24.8 (C-28), 23.2 (C-5). IR: $\tilde{\nu}_{\text{max}}$ (cm⁻¹)=2980.5, 2892.7, 2093.4, 1716.3, 1648.9, 1539.9, 1449.2, 1246.8, 1148.4, 1072.2, 1007.6, 968.1, 758.9, 699.1. HRMS (ESI, pos.): calc. for C₃₄H₃₈N₆O₇⁺ [*M*+H]⁺ 643.2875; found 643.2877. CHNO-Analysis: calc. for C₃₄H₃₈N₆O₇: C, 63.54%; H, 5.96%; N, 13.08%; O, 17.43%; found: C, 63.59%; H, 6.07%; N, 12.95%; O, 17.37%.

(*N_ε*-Boc)-Lys(*N_ε*-OBz) *tert*-butylester (69): Preparation according to method A, scale: (*N_ε*-Boc)-Lys *tert*-butylester 98^[44] (15.9 g, 46.9 mmol, 1.00 eq.), CH₂Cl₂ (300 mL), NaHCO₃/NaOH buffer (300 mL), benzoyl peroxide with 25% H₂O (16.7 g, 51.7 mmol, 1.10 eq.), EtOAc (350 mL), Na₂S₂O₃ solution (2 M, 2×250 mL) and sat. NaCl (300 mL). Colorless solid; yield: 12.4 g (63%). *R_f*=0.60 (SiO₂, *n*-pentane/EtOAc 3:1 v/v, UV₂₅₄, Ammonium cerium(IV) sulfate). ¹H NMR (500 MHz, CDCl₃) δ 8.02–7.98 (m, 2H, H-10), 7.89 (sbr, 1H, H-7), 7.58–7.55 (m, 1H, H-12), 7.46–7.42 (m, 2H, H-11), 5.07–5.03 (m, 1H, H-13), 4.20–4.15 (m, 1H, H-2), 3.12 (t, 2H, ³*J*=7.1 Hz, H-6), 1.83–1.76 (m, 1H, H-3), 1.68–1.59 (m, 3H, H-3, H-4), 1.51–1.48 (m, 2H, H-5), 1.46 (s, 9H, H-18), 1.42 (s, 9H, H-16). ¹³C NMR (126 MHz, CDCl₃) δ 172.0 (C-1), 167.0 (C-14), 155.5 (C-14), 133.4 (C-12), 129.4 (C-10), 128.6 (C-11), 128.5 (C-9), 81.9 (C-17), 79.7 (C-15), 53.9 (C-2), 52.4 (C-6), 32.9 (C-3), 28.4 (C-18), 28.1 (C-16), 27.1 (C-4), 22.8 (C-5). HRMS (ESI, pos.): calc. for C₂₂H₃₄N₂O₆Na⁺ [*M*+Na]⁺ 445.2309; found 445.2301.

(*N_ε*-Boc)-Lys(*N_ε*-OBz)-*N_ε*-β-Ala-Fmoc *tert*-butylester (74): Preparation according to method B, scale: 69 (12.1 g, 28.5 mmol, 1.00 eq.) in THF (40 mL), abs. pyridine (4.60 mL, 57.0 mmol, 2.00 eq.), Fmoc-

β -Ala-COCl (10.1 g, 30.5 mmol, 1.05 eq.) in THF (20 mL), reaction time (19 h), EtOAc (400 mL), HCl(aq) (1 M, 2 \times 250 mL), sat. NaCl (150 mL). Colorless solid; yield: 19.2 g (94%). R_f = 0.42 (SiO₂, *n*-pentane/EtOAc 2:1 v/v, UV₂₅₄, Phosphomolybdic acid). Mp. = 67.4–68.6 °C. ¹H NMR (600 MHz, CDCl₃) δ 8.08 (d, 2H, ³*J* = 7.5 Hz, H-22), 7.75 (d, 2H, ³*J* = 7.5 Hz, H-18), 7.68 (t, 2H, ³*J* = 7.5 Hz, H-24), 7.60 (d, 2H, ³*J* = 7.5 Hz, H-15), 7.51 (t, 2H, ³*J* = 7.5 Hz, H-23), 7.39 (t, 2H, ³*J* = 7.5 Hz, H-16), 7.31 (t, 2H, ³*J* = 7.5 Hz, H-17), 5.59 (sbr, 1H, H-10), 5.10–5.07 (m, 1H, H-25), 4.34 (d, 2H, ³*J* = 7.4 Hz, H-12), 4.21 (t, 1H, ³*J* = 7.4 Hz, H-13), 4.18–4.15 (m, 1H, H-2), 3.83–3.74 (m, 2H, H-6), 3.51–3.45 (m, 2H, H-9), 2.58–2.47 (m, 2H, H-8), 1.83–1.70 (m, 2H, H-3), 1.68–1.61 (m, 2H, H-5), 1.46–1.40 (m, 20H, H-4, H-28, H-30). ¹³C NMR (151 MHz, CDCl₃) δ 171.9 (C-1), 156.6 (C-11), 155.5 (C-26), 144.2 (C-14), 141.4 (C-19), 134.8 (C-24), 133.7 (C-21), 130.2 (C-22), 129.1 (C-23), 127.8 (C-17), 127.2 (C-16), 125.3 (C-15), 120.1 (C-18), 82.0 (C-29), 79.8 (C-27), 67.0 (C-12), 53.9 (C-2), 47.9 (C-6), 47.3 (C-13), 36.2 (C-9), 32.7 (C-8), 28.5 (C-30), 28.1 (C-28), 26.7 (C-3), 22.5 (C-4). IR: $\tilde{\nu}_{\text{max}}$ (cm⁻¹) = 3341.1, 2978.5, 1763.6, 1711.5, 1508.1, 1452.1, 1390.4, 1364.4, 1240.0, 1151.3, 1036.6, 1010.5, 843.7, 758.9, 742.5, 709.7, 571.8. HRMS (ESI, pos.): calc. for C₄₀H₄₉N₃O₉⁺ [M + Na]⁺ 738.3361; found 738.3369. CHNO-Analysis: calc. for C₄₀H₄₉N₃O₉: C, 67.12%; H, 6.90%; N, 5.87%; O, 20.11%; found: C, 66.84%; H, 6.84%; N, 5.85%; O, 20.17%.

Lys(N_ε-OBn)-N_ε-β-Ala-Fmoc (78): The title compound 78 was obtained in two steps via intermediate (N_ε-Boc)-Lys(N_ε-OBn)-N_ε-β-Ala-Fmoc *tert*-butylester. The latter compound was obtained from 74 employing method C, scale: 74 (19.1 g, 26.7 mmol, 1.00 eq.), CH₃OH (100 mL), DIPEA (13.9 mL, 80.1 mmol, 3.00 eq.), benzylbromide (6.34 mL, 53.4 mmol, 2.00 eq.), EtOAc (400 mL), HCl(aq) (1 M, 2 \times 150 mL), sat. NaHCO₃ (2 \times 150 mL), H₂O (150 mL) and sat. NaCl (150 mL), column chromatography on SiO₂: *n*-pentane/EtOAc 10:1–1:4 v/v. Pale yellow solid; yield of the intermediate *tert*-butylester: 14.4 g (77%). R_f = 0.37 (SiO₂, *n*-pentane/EtOAc 2:1 v/v, UV₂₅₄, phosphomolybdic acid). Mp. = 52.6–53.9 °C. ¹H NMR (600 MHz, CDCl₃) δ 7.75 (d, 2H, ³*J* = 7.5 Hz, H-18), 7.60 (d, 2H, ³*J* = 7.5 Hz, H-15), 7.39 (t, 2H, ³*J* = 7.5 Hz, H-17), 7.37–7.34 (m, 5H, H-22, H-23, H-24), 7.30 (t, 2H, ³*J* = 7.5 Hz, H-16), 5.58 (sbr, 1H, H-10), 5.09–5.07 (m, 1H, H-25), 4.78 (s, 2H, H-20), 4.35 (d, 2H, ³*J* = 7.2 Hz, H-12), 4.20 (t, 1H, ³*J* = 7.2 Hz, H-13), 4.17–4.14 (m, 1H, H-2), 3.70–3.60 (m, 2H, H-6), 3.52–3.44 (m, 2H, H-9), 2.71–2.58 (m, 2H, H-8), 1.81–1.75 (m, 1H, H-3), 1.72–1.67 (m, 1H, H-5), 1.66–1.58 (m, 2H, H-3, H-5), 1.44 (s, 18H, H-28, H-30), 1.40–1.29 (m, 2H, H-4). ¹³C NMR (151 MHz, CDCl₃) δ 172.0 (C-1), 156.6 (C-11), 155.5 (C-7), 144.2 (C-14), 141.4 (C-19), 134.3 (C-21), 129.4 (C-24), 129.2 (C-22), 128.9 (C-23), 127.8 (C-16), 127.2 (C-17), 125.3 (C-15), 120.1 (C-18), 81.9 (C-29), 79.8 (C-27), 76.5 (C-20), 66.9 (C-12), 54.0 (C-2), 47.4 (C-13), 45.2 (C-6), 36.5 (C-9), 32.8 (C-8), 32.6 (C-3), 28.5 (C-30), 28.1 (C-28), 26.6 (C-5), 22.6 (C-4). IR: $\tilde{\nu}_{\text{max}}$ (cm⁻¹) = 2980.5, 2886.0, 1709.6, 1650.8, 1508.1, 1450.2, 1390.4, 1366.3, 1247.7, 1197.6, 1150.3, 1094.4, 1071.3, 1010.5, 953.6, 843.7, 758.9, 751.1, 739.6, 699.1. HRMS (ESI, pos.): calc. for C₄₀H₅₁N₃O₈⁺ [M + H]⁺ 702.3749; found 702.3746. CHNO-Analysis: calc. for C₄₀H₅₁N₃O₈: C, 68.45%; H, 7.32%; N, 5.99%; O, 18.24%; found: C, 68.28%; H, 7.35%; N, 5.92%; O, 18.31%.

This intermediate *tert*-butylester was converted to the title compound 78 via method D. Scale: intermediate *tert*-butylester mentioned above (10.0 g, 14.3 mmol, 1.00 eq.), triethylsilane (11.4 mL, 71.2 mmol, 5.00 eq.), 50% TFA in CH₂Cl₂ (50 mL), reaction time (2 h). Colorless solid; yield: 6.84 g (88%). R_f = 0.72 (CH₂Cl₂/CH₃OH 9:1 v/v, UV₂₅₄, Ninhydrin). Mp. = 139.3–139.7 °C. ¹H NMR (500 MHz, CDCl₃) δ 8.33 (sbr, 2H, H-26), 7.69–7.63 (m, 2H, H-16), 7.31–7.28 (m, 2H, H-18), 7.25–7.12 (m, 7H, H-17, H-23, H-24, H-25), 5.93 (sbr, 1H, H-11), 4.59 (s, 2H, H-21), 4.29–4.18 (m, 2H, H-13), 4.10–4.04 (m, 1H, H-14), 3.75–3.64 (m, 1H, H-3), 3.61–3.49 (m, 2H, H-7), 3.37–3.23 (m, 2H, H-10), 2.55–2.38 (m, 2H, H-9), 1.96–1.74 (m, 2H, H-4), 1.64–1.53 (m, 2H, H-6), 1.47–1.36 (m, 2H, H-5). ¹³C NMR (151 MHz,

CDCl₃) δ 156.6 (C-12), 144.1 (C-15), 141.3 (C-20), 134.1 (C-22), 129.4 (C-24), 129.1 (C-25), 128.8 (C-23), 127.7 (C-18), 127.1 (C-17), 125.3 (C-16), 120.0 (C-19), 76.3 (C-21), 66.8 (C-13), 54.9 (C-3), 47.3 (C-14), 45.1 (C-7), 36.7 (C-10), 32.7 (C-9), 30.7 (C-4), 27.3 (C-6), 22.8 (C-5). IR: $\tilde{\nu}_{\text{max}}$ (cm⁻¹) = 2980.5, 2974.7, 2971.8, 2920.7, 2886.9, 1692.2, 1641.1, 1544.7, 1537.0, 1461.8, 1457.9, 1451.2, 1390.4, 1387.5, 1381.8, 1251.6, 1150.3, 1073.2, 965.2, 962.3, 953.6, 757.9, 740.5, 700.0. HRMS (ESI, pos.): calc. for C₃₁H₃₆N₃O₆⁺ [M + H]⁺ 546.2599; found 546.2581.

Protected (Lys-β-Ala) monomer (82): 78 (391 mg, 717 μmol, 1.00 eq.) was dissolved in abs. CH₂Cl₂ (15 mL) and mixed with *N*-methylmorpholine (158 μL, 1.43 mmol, 2.00 eq.), 2,5-Dioxopyrrolidin-1-yl 4-azidobutanoate 36 (195 mg, 860 μmol, 1.20 eq.) was added and the reaction solution was stirred at room temperature for 4 h. The solvent was removed under reduced pressure and the brown crude product obtained was purified by column chromatography on SiO₂ (CH₂Cl₂/CH₃OH 15:1 + 1% AcOH → 10:1 + 1% AcOH v/v). The product was obtained as a colorless solid (405 mg, 617 μmol, 86%). R_f = 0.43 (SiO₂, CH₂Cl₂/CH₃OH 10:1 + 1% HAc v/v, UV₂₅₄, Ninhydrin). ¹H NMR (600 MHz, CDCl₃) δ 7.76–7.71 (m, 2H, H-19), 7.60–7.52 (m, 2H, H-16), 7.40–7.27 (m, 9H, H-17, H-18, H-23, H-24, H-25), 6.62–6.52 (m, 1H, H-26), 5.62 (sbr, 1H, H-11), 4.79–4.69 (m, 2H, H-21), 4.61–4.53 (m, 1H, H-3), 4.47–4.33 (m, 2H, H-13), 4.23–4.16 (m, 1H, H-14), 3.85–3.59 (m, 2H, H-7), 3.49–3.38 (m, 2H, H-10), 3.34–3.28 (m, 2H, H-30), 2.69–2.54 (m, 2H, H-9), 2.29 (t, 2H, ³*J* = 7.4 Hz, H-28), 1.92–1.86 (m, 2H, H-29), 1.85–1.72 (m, 2H, H-4), 1.71–1.58 (m, 2H, H-6), 1.38–1.16 (m, 2H, H-5). ¹³C NMR (151 MHz, CDCl₃) δ 174.7 (C-2), 174.3 (C-27), 172.6 (C-8), 156.7 (C-12), 144.0 (C-15), 141.4 (C-20), 134.0 (C-22), 129.4 (C-25), 128.9 (C-23), 127.9 (C-24), 127.8 (C-17), 127.2 (C-18), 125.2 (C-16), 120.1 (C-19), 76.5 (C-21), 67.0 (C-13), 52.3 (C-3), 50.8 (C-30), 47.3 (C-14), 44.6 (C-7), 36.6 (C-10), 33.0 (C-28), 32.8 (C-8), 31.2 (C-4), 26.3 (C-6), 24.8 (C-29), 22.1 (C-5). IR: $\tilde{\nu}_{\text{max}}$ (cm⁻¹) = 3315.0, 2951.5, 2101.1, 2031.6, 1714.4, 1647.9, 1522.5, 1449.2, 1244.8, 1144.6, 1003.8, 700.0, 650.9. HRMS (ESI, pos.): calc. for C₃₅H₄₁N₆O₇⁺ [M + H]⁺ 657.3031; found 657.3028. CHNO-Analysis: calc. for C₃₅H₄₀N₆O₇: C, 64.01%; H, 6.14%; N, 12.80%; O, 17.05%; found: C, 63.93%; H, 6.14%; N, 12.66%; O, 17.01%.

Protected AHX-(Orn-β-Ala) monomer (157): The title compound 157 was obtained in two steps via its intermediate Fmoc-protected analogue. The latter compound was obtained from 80 and 107 employing method E. Scale: 80 (1.00 g, 1.56 mmol, 1.00 eq.), HBTU (620 mg, 1.63 mmol, 1.05 eq.), HOBt (421 mg, 3.11 mmol, 2.00 eq.), DIPEA (603 mg, 813 μL, 4.67 mmol, 3.00 eq.) in abs. DMF (12 mL), reaction time (15 min), 107 (306 mg, 1.63 mmol, 1.05 eq.) in abs. DMF (3 mL), reaction time (3 h), column chromatography on SiO₂ (CH₂Cl₂/CH₃OH, 40:1 + 0.1% NEt₃ → 25:1 + 0.1% NEt₃). Colorless solid; yield: 1.19 g (94%). R_f = 0.18 (CH₂Cl₂/CH₃OH 24:1 v/v, UV₂₅₄, Ammonium cerium(IV) sulfate). ¹H NMR (600 MHz, CDCl₃) δ 7.76 (d, 2H, ³*J* = 7.4 Hz, H-24), 7.59 (d, 2H, ³*J* = 7.4 Hz, H-21), 7.39 (t, 2H, ³*J* = 7.4 Hz, H-23), 7.38–7.32 (m, 5H, H-28, H-29, H-30), 7.30 (t, 2H, ³*J* = 7.4 Hz, H-22), 6.50 (sbr, 1H, H-31), 6.42 (sbr, 1H, H-7), 5.56 (sbr, 1H, H-16), 4.80 (s, 2H, H-26), 4.57–4.51 (m, 1H, H-9), 4.36 (d, 2H, ³*J* = 6.9 Hz, H-18), 4.20 (t, 1H, ³*J* = 6.9 Hz, H-19), 4.04–3.99 (m, 1H, H-12), 3.63–3.60 (m, 1H, H-12), 3.53–3.43 (m, 2H, H-15), 3.31 (t, 2H, ³*J* = 7.3 Hz, H-35), 3.18–3.13 (m, 2H, H-6), 2.72–2.64 (m, 2H, H-14), 2.29 (t, 2H, ³*J* = 7.3 Hz, H-33), 2.18 (t, 2H, ³*J* = 7.4 Hz, H-2), 1.90 (quin, 2H, ³*J* = 7.3 Hz, H-34), 1.73–1.65 (m, 3H, H-10, H-11), 1.61–1.58 (m, 1H, H-10), 1.57–1.53 (m, 2H, H-3), 1.40 (s, 9H, H-37), 1.39 (t, 2H, ³*J* = 7.4 Hz, H-4), 1.31–1.26 (m, 2H, H-5). ¹³C NMR (151 MHz, CDCl₃) δ 173.1 (C-1), 172.3 (C-32), 171.8 (C-8), 156.6 (C-17), 144.1 (C-20), 141.4 (C-25), 134.0 (C-27), 129.5 (C-30), 129.4 (C-28), 129.0 (C-29), 127.8 (C-23), 127.2 (C-22), 125.2 (C-21), 120.1 (C-24), 80.3 (C-36), 76.6 (C-26), 66.9 (C-18), 51.7 (C-9), 50.9 (C-35), 47.4 (C-19), 44.1 (C-12), 39.6 (C-6), 36.7 (C-15), 35.5 (C-2), 33.2 (C-33), 32.8 (C-14), 30.2 (C-10), 29.2 (C-4), 28.3 (C-37), 26.4 (C-5), 24.8 (C-34), 24.7 (C-3), 23.2 (C-11). HRMS (ESI, pos.): calc. for C₄₄H₅₈N₇O₈⁺ [M + H]⁺ 812.4341; found 812.4344. This

intermediate Fmoc-protected analogue was converted to the title compound 157 via method F. Scale: intermediate Fmoc-derivative mentioned above (1.10 g, 1.35 mmol, 1.00 eq.), 20% Piperidine in CH_3CN (10 mL), reaction time (20 min), column chromatography on SiO_2 ($\text{CH}_2\text{Cl}_2/\text{CH}_3\text{OH}$, 15:1 + 0.1% NEt_3 →9:1 + 1% NEt_3 v/v). Yellow oil; yield: 797 mg (99%). ^1H NMR (500 MHz, CDCl_3) δ 8.49 (sbr, 1H, H-29), 7.68 (sbr, 3H, H-16), 7.57 (t, 2H, $^3J=5.7$ Hz, H-7), 7.46 (d, 1H, $^3J=7.6$ Hz, H-22), 7.39–7.32 (m, 5H, H-19, H-20, H-21), 4.82–4.77 (m, 2H, H-17), 4.43–4.40 (m, 1H, H-9), 3.78–3.62 (m, 2H, H-12), 3.26 (t, 2H, $^3J=7.1$ Hz, H-26), 3.17–3.13 (m, 2H, H-6), 3.13–3.09 (m, 2H, H-14), 2.92–2.77 (m, 2H, H-15), 2.30–2.27 (m, 2H, H-24), 2.16 (t, 2H, $^3J=7.6$ Hz, H-2), 1.84 (quin, 2H, $^3J=7.1$ Hz, H-25), 1.74–1.65 (m, 1H, H-10), 1.65–1.59 (m, 3H, H-10, H-11), 1.54 (quin, 2H, $^3J=7.6$ Hz, H-3), 1.51–1.46 (m, 2H, H-5), 1.42 (s, 9H, H-28), 1.30–1.24 (m, 2H, H-4). ^{13}C NMR (126 MHz, CDCl_3) δ 173.2 (C-1), 172.5 (C-23), 171.8 (C-8), 168.5 (C-29), 134.0 (C-18), 129.4 (C-21), 129.3 (C-19), 128.9 (C-20), 80.2 (C-27), 76.4 (C-17), 52.6 (C-9), 50.9 (C-26), 44.7 (C-12), 39.5 (C-6), 35.5 (C-2), 35.3 (C-14), 33.1 (C-24), 29.7 (C-15), 29.6 (C-11), 29.2 (C-5), 28.2 (C-28), 26.5 (C-4), 24.9 (C-25), 24.8 (C-3), 22.9 (C-10). HRMS (ESI, pos.): calc. for $\text{C}_{29}\text{H}_{48}\text{N}_7\text{O}_6$ $^+ [M-\text{HCOOH}+\text{H}]^+$ 590.3661; found 590.3666.

Protected (Orn- β -Ala)-(Orn- β -Ala)-(Orn- β -Ala) trimer (110): The title compound 110 was obtained in three steps. The first intermediate (protected Orn-Orn dimer) was obtained from 80 and 107 employing method E. Scale: 80 (871 mg, 1.35 mmol, 1.00 eq.), HBTU (540 mg, 1.42 mmol, 1.05 eq.), HOBT (366 mg, 2.71 mmol, 2.00 eq.), DIPEA (708 μL , 4.06 mmol, 3.00 eq.) in abs. DMF (25 mL), reaction time (30 min), 157 (766 mg, 1.35 mmol, 1.00 eq.) in abs. DMF (5 mL), reaction time (3 h), column chromatography on SiO_2 ($\text{CH}_2\text{Cl}_2/\text{CH}_3\text{OH}$, 25:2 v/v). Yellow oil; yield: 1.49 (91%). ^1H NMR (300 MHz, $\text{DMSO}-d_6$) δ 8.05–7.91 (m, 3H, H-16, H-40, H-50), 7.90–7.83 (m, 3H, H-7, H-33), 7.67 (d, 2H, $^3J=7.4$ Hz, H-30), 7.44–7.34 (m, 12H, H-32, H-37, H-38, H-39, H-47, H-48, H-49), 7.33–7.27 (m, 3H, H-25, H-31), 4.84–4.78 (m, 4H, H-35, H-45), 4.28 (d, 2H, $^3J=6.9$ Hz, H-27), 4.25–4.16 (m, 3H, H-9, H-18, H-28), 3.65–3.51 (m, 4H, H-12, H-21), 3.31–3.16 (m, 8H, H-15, H-24, H-44, H-54), 3.04–2.95 (m, 2H, H-6), 2.64–2.53 (m, 4H, H-14, H-23), 2.23–2.09 (m, 6H, H-2, H-42, H-52), 1.77–1.65 (m, 4H, H-43, H-53), 1.63–1.41 (m, 10H, H-3, H-10, H-11, H-19, H-20), 1.38 (s, 9H, H-56), 1.36–1.29 (m, 2H, H-5), 1.25–1.17 (m, 2H, H-4). ^{13}C NMR (75 MHz, $\text{DMSO}-d_6$) δ 172.2, 171.6, 171.2, 156.0, 143.9, 140.7, 134.6, 129.3, 128.7, 128.4, 127.6, 127.0, 125.1, 120.1, 75.5, 65.3, 52.1, 50.3, 46.7, 44.1, 38.2, 36.3, 34.7, 32.0, 29.4, 28.7, 27.7, 25.7, 24.5, 24.3, 23.2, 23.1. IR: $\tilde{\nu}_{\text{max}}$ (cm^{-1}) = 2327.6, 2154.1, 2092.4, 2023.0, 1969.0, 1714.4, 1702.8, 1652.7, 1540.9, 1517.7, 1452.1, 1243.9, 1143.6, 1074.2, 977.7, 912.2, 877.5, 742.5, 696.2. HRMS (ESI, pos.): calc. for $\text{C}_{63}\text{H}_{84}\text{N}_{13}\text{O}_{12}$ $^+ [M+\text{H}]^+$ 1214.6357; found 1214.6380. The second intermediate (Fmoc-deprotected Orn-Orn dimer) was obtained from the above mentioned Fmoc-protected Orn-Orn dimer via Fmoc-deprotection employing method F. Scale: Fmoc-protected Orn-Orn dimer (1.35 g, 1.11 mmol, 1.00 eq.), 20% Piperidine in CH_3CN (20 mL), reaction time (30 min), column chromatography on SiO_2 ($\text{CH}_2\text{Cl}_2/\text{CH}_3\text{OH}$, 20:1 + 0.1% NEt_3 →10:1 + 1% NEt_3). Colorless oil; yield: 841 mg (76%). $R_f=0.48$ ($\text{CH}_2\text{Cl}_2/\text{CH}_3\text{OH}$ 12:1 + 0.1% NEt_3 v/v, UV_{254} , Ninhydrin). Anal. HPLC (Nucleodur RP8, 150×2 mm ID, 5 μm , $\text{H}_2\text{O}/\text{CH}_3\text{CN}$ 90:10 + 0.05% HCO_2H →5:95 + 0.05% HCO_2H , 15 min, 0.2 mL/min): $t_R=19.0$ min. HRMS (ESI, pos.): calc. for $\text{C}_{48}\text{H}_{73}\text{N}_{13}\text{O}_{10}$ $^+ [M+\text{H}]^+$ 992.5676; found 992.5651. This intermediate Fmoc-deprotected Orn-Orn dimer was coupled to 80 and converted to the title compound 110 employing method E. Scale: 80 (518 mg, 806 μmol , 1.00 eq.), HBTU (336 mg, 887 μmol , 1.05 eq.), HOBT (272 mg, 2.02 mmol, 2.50 eq.), DIPEA (421 μL , 2.42 mmol, 3.00 eq.) in abs. DMF (15 mL), reaction time (30 min), Fmoc-deprotected Orn-Orn dimer (800 mg, 806 μmol , 1.00 eq.) in abs. DMF (5 mL), reaction time (3 h), column chromatography on SiO_2 ($\text{CH}_2\text{Cl}_2/\text{CH}_3\text{OH}$, 25:1 + 0.1% NEt_3 →8:1 + 1% NEt_3 v/v). Colorless solid; yield: 94%. Anal. HPLC (Nucleodur RP8, 150×2 mm ID, 5 μm , $\text{H}_2\text{O}/\text{CH}_3\text{CN}$ 30:70 +

0.05% HCO_2H →5:95 + 0.05% HCO_2H , 15 min, 0.2 mL/min): $t_R=10.5$ min. $[\alpha]_{\text{D}}^{25}$ $D=-3.8$ ($c=1.6$ mg/mL, CH_2Cl_2). ^1H NMR (500 MHz, CDCl_3) δ 7.75 (d, 2H), 7.58 (d, 2H), 7.57–7.47 (sbr, 1H), 7.41–7.30 (m, 17H), 7.30–7.27 (m, 2H), 7.17–6.74 (m, 4H), 6.14–5.95 (m, 1H), 4.88–4.68 (m, 6H), 4.64–4.47 (m, 2H), 4.44–4.38 (m, 1H), 4.39–4.28 (m, 2H), 4.24–4.15 (m, 1H), 4.09–3.67 (m, 3H), 3.65–3.39 (m, 8H), 3.31–3.21 (m, 6H), 3.20–3.06 (m, 2H), 2.79–2.70 (m, 1H), 2.68–2.56 (m, 3H), 2.51–2.36 (m, 2H), 2.32–2.24 (m, 4H), 2.23–2.13 (m, 4H), 1.91–1.78 (m, 6H), 1.76–1.60 (m, 8H), 1.58–1.51 (m, 4H), 1.49–1.38 (m, 11H), 1.31–1.24 (m, 2H). ^{13}C NMR (126 MHz, CDCl_3) δ 172.3, 156.7, 144.2, 141.4, 134.1, 129.4, 128.9, 127.8, 127.1, 125.3, 120.1, 80.2, 76.5, 66.8, 52.6, 52.1, 50.9, 50.9, 47.4, 44.5, 39.5, 36.7, 35.3, 33.2, 32.8, 29.2, 28.2, 26.5, 24.9, 24.8, 23.1. HRMS (ESI, pos.): calc. for $\text{C}_{82}\text{H}_{111}\text{N}_{19}\text{O}_{16}$ $^+ [M+\text{H}]^+$ 808.9223; found 808.9226. CHNO-Analysis: calc. for $\text{C}_{82}\text{H}_{108}\text{N}_{19}\text{O}_{16}$: C, 60.19%; H, 6.80%; N, 16.46%; O, 15.83%; found: C, 60.75%; H, 6.83%; N, 16.30%; O, 15.66%.

Protected (Orn- β -Ala)-(Orn- β -Ala)-(Orn- β -Ala)-(Orn- β -Ala) tetramer (111): The title compound 111 was obtained in two steps via an intermediate Fmoc-deprotected analogue. The latter compound was obtained from 110 employing method F. Scale: 110 (200 mg, 124 μmol , 1.00 eq.), 20% piperidine in CH_3CN (8 mL), reaction time (30 min), column chromatography on SiO_2 ($\text{CH}_2\text{Cl}_2/\text{CH}_3\text{OH}$, 20:1 + 0.1% NEt_3 →8:1 + 1% NEt_3 v/v). Colorless liquid; yield: 142 mg (82%). Anal. HPLC (Nucleodur RP8, 150×2 mm ID, 5 μm , $\text{H}_2\text{O}/\text{CH}_3\text{CN}$ 98:2 + 0.05% HCO_2H →5:95 + 0.05% HCO_2H , 15 min, 0.2 mL/min): $t_R=21.1$ min. IR: $\tilde{\nu}_{\text{max}}$ (cm^{-1}) = 3294.8, 2970.8, 2939.0, 2098.2, 1718.3, 1636.3, 1540.9, 1450.2, 1366.3, 1246.8, 1150.3, 1004.7, 948.8, 741.5, 699.1, 544.8. HRMS (ESI, pos.): calc. for $\text{C}_{95}\text{H}_{100}\text{N}_{19}\text{O}_{14}$ $^+ [M+\text{H}]^+$ 1394.7692; found 1394.7721. This intermediate Fmoc-deprotected analogue was converted to the title compound 111 via coupling to 80 using method E. Scale: 80 (65.4 mg, 102 μmol , 1.00 eq.), HBTU (40.5 mg, 107 μmol , 1.05 eq.), HOBT (34.4 mg, 255 μmol , 2.50 eq.), DIPEA (53.0 μL , 306 μmol , 3.00 eq.) in abs. DMF (6 mL), reaction time (30 min), intermediate Fmoc-deprotected derivative mentioned above (142 mg, 102 μmol , 1.00 eq.) in abs. DMF (2 mL), reaction time (7.5 h), column chromatography on SiO_2 ($\text{CH}_2\text{Cl}_2/\text{CH}_3\text{OH}$, 25:1 + 0.5% NEt_3 →9:1 + 0.5% NEt_3 v/v), column chromatography on SiO_2 -RP18 ($\text{H}_2\text{O}/\text{CH}_3\text{CN}$, 95:5 + 0.1% HCO_2H →5:95 + 0.1% HCO_2H v/v). Colorless solid; yield: 188 mg (91%). Anal. HPLC (Nucleodur RP8, 150×2 mm ID, 5 μm , $\text{H}_2\text{O}/\text{CH}_3\text{CN}$ 30:70 + 0.05% HCO_2H →5:95 + 0.05% HCO_2H , 15 min, 0.2 mL/min): $t_R=11.6$ min. $[\alpha]_{\text{D}}^{25}$ $D=-9.0$ ($c=1.0$ mg/mL, CH_2Cl_2). ^1H NMR (600 MHz, CDCl_3) δ 7.75 (d, 2H), 7.58 (d, 2H), 7.54–7.48 (m, 1H), 7.38–7.27 (m, 25H), 7.21–7.04 (m, 3H), 7.00–6.74 (m, 2H), 5.97 (sbr, 1H), 4.88–4.65 (m, 9H), 4.59–4.38 (m, 4H), 4.37–4.31 (m, 2H), 4.22–4.14 (m, 1H), 3.92–3.71 (m, 4H), 3.66–3.33 (m, 14H), 3.30–3.20 (m, 9H), 3.19–3.06 (m, 3H), 2.77–2.39 (m, 9H), 2.34–2.21 (m, 8H), 2.20–2.09 (m, 6H), 1.94–1.79 (m, 9H), 1.77–1.58 (m, 14H), 1.57–1.49 (m, 6H), 1.47–1.40 (m, 13H), 1.32–1.24 (m, 4H). ^{13}C NMR (125 MHz, CDCl_3) δ 173.4, 173.1, 172.3, 172.0, 171.6, 156.7, 144.1, 141.4, 134.1, 129.4, 129.4, 129.2, 128.9, 127.8, 127.1, 125.3, 120.1, 80.2, 76.5, 76.4, 66.8, 52.6, 52.3, 52.3, 52.1, 50.9, 50.9, 47.3, 44.8, 44.4, 39.5, 36.6, 35.5, 35.4, 35.1, 33.1, 33.1, 33.0, 32.7, 32.2, 30.3, 29.8, 29.3, 28.2, 26.5, 24.9, 24.9, 24.8, 23.2. IR: $\tilde{\nu}_{\text{max}}$ (cm^{-1}) = 3291.9, 2980.5, 2886.0, 2096.2, 1717.3, 1673.5, 1540.9, 1484.0, 1449.2, 1413.6, 1367.3, 1248.7, 1150.3, 1036.2, 1007.6, 876.5, 740.5, 698.1, 539.0. HRMS (ESI, pos.): calc. for $\text{C}_{101}\text{H}_{137}\text{N}_{25}\text{O}_{21}$ $^+ [M+2\text{H}]^{2+}$ 1010.0230; found 1010.0199.

Protected AHX-(Lys- β -Ala) monomer (160): The title compound 160 was obtained in two steps via its intermediate Fmoc-protected analogue. The latter compound was obtained from 82 and 107 employing method E. Scale: 82 (1.50 g, 2.28 mmol, 1.00 eq.), HBTU (1.04 g, 2.74 mmol, 1.20 eq.), HOBT (463 mg, 3.43 mmol, 1.50 eq.), DIPEA (1.19 mL, 6.85 mmol, 3.00 eq.) in abs. DMF (30 mL), reaction time (30 min), 107 (449 mg, 2.40 mmol, 1.05 eq.) in abs. DMF (3 mL), reaction time (3 h), column chromatography on SiO_2

(CH₂Cl₂/CH₃OH, 40:1 + 0.1% NEt₃→25:1 + 0.1% NEt₃). Colorless semiliquid; yield: 1.85 (98%). *R*_f = 0.46 (CH₂Cl₂/CH₃OH 40:1 v/v, UV₂₅₄, Ninhydrin). Anal. HPLC (Nucleodur RP8, 150×2 mm ID, 5 μm, H₂O/CH₃CN 30:70 + 0.05% HCO₂H→5:95 + 0.05% HCO₂H, 15 min, 0.2 mL/min): *t*_R = 11.0 min. ¹H NMR (500 MHz, CDCl₃) δ 7.75 (d, 2H, ³*J* = 7.6 Hz, H-25), 7.58 (d, 2H, ³*J* = 7.6 Hz, H-22), 7.38 (t, 2H, ³*J* = 7.6 Hz, H-24), 7.36–7.32 (m, 5H, H-29, H-30, H-31), 7.28 (t, 2H, ³*J* = 7.6 Hz, H-23), 6.50 (sbr, 2H, H-7, H-32), 5.68 (sbr, 1H, H-17), 4.77 (s, 2H, H-27), 4.38–4.30 (m, 3H, H-9, H-19), 4.22–4.17 (m, 1H, H-20), 3.74–3.59 (m, 2H, H-13), 3.51–3.40 (m, 2H, H-16), 3.30 (t, 2H, ³*J* = 7.1 Hz, H-36), 3.22–3.17 (m, 2H, H-6), 2.71–2.54 (m, 2H, H-15), 2.27 (t, 2H, ³*J* = 7.1 Hz, H-34), 2.18 (t, 2H, ³*J* = 7.6 Hz, H-2), 1.88 (quin, 2H, ³*J* = 7.6 Hz, H-35), 1.84–1.76 (m, 1H, H-10), 1.71–1.60 (m, 3H, H-10, H-11), 1.55 (quin, 2H, ³*J* = 7.6 Hz, H-3), 1.50–1.45 (m, 2H, H-5), 1.42 (s, 9H, H-38), 1.35–1.25 (m, 4H, H-4, H-12). ¹³C NMR (151 MHz, CDCl₃) δ 173.1 (C-1), 172.1 (C-33), 171.6 (C-8), 156.6 (C-18), 144.1 (C-21), 141.4 (C-26), 134.1 (C-28), 129.3 (C-31), 129.2 (C-29), 128.9 (C-30), 127.8 (C-24), 127.1 (C-23), 125.2 (C-22), 120.1 (C-25), 80.2 (C-37), 76.5 (C-27), 66.8 (C-19), 53.1 (C-9), 50.9 (C-36), 47.3 (C-20), 46.7, 44.7 (C-13), 39.4 (C-6), 36.7 (C-16), 35.4 (C-21), 33.1 (C-34), 32.8 (C-15), 31.8 (C-10), 29.1 (C-5), 28.2 (C-38), 26.4 (C-11), 26.4 (C-4), 24.8 (C-3), 24.6 (C-35), 22.6 (C-12). IR: $\tilde{\nu}_{\text{max}}$ (cm⁻¹) = 2925.5, 2154.1, 2100.1, 1984.4, 1718.3, 1645.0, 1544.7, 1521.6, 1444.4, 1367.3, 1243.9, 1147.4, 946.9, 869.7, 757.9, 738.6, 703.9. HRMS (ESI, pos.): calc. for C₄₅H₆₀N₃O₈⁺ [*M* + *H*]⁺ 826.4498; found 826.4555. This intermediate Fmoc-protected analogue was converted to the title compound 160 via method F. Scale: intermediate Fmoc-derivative mentioned above (1.79 g, 2.17 mmol, 1.00 eq.), 20% Piperidine in CH₃CN (40 mL), reaction time (2 h), column chromatography on SiO₂ (CH₂Cl₂/CH₃OH, 15:1 + 0.1% NEt₃→9:1 + 1% NEt₃ v/v). Yellow brown oil; yield: 1.28 g (98%). *R*_f = (CH₂Cl₂/CH₃OH 40:1 v/v, UV₂₅₄, Ninhydrin). Anal. HPLC (Nucleodur RP8, 150×2 mm ID, 5 μm, H₂O/CH₃CN 90:10 + 0.05% HCO₂H→5:95 + 0.05% HCO₂H, 15 min, 0.2 mL/min): *t*_R = 17.1 min. ¹H NMR (600 MHz, CDCl₃) δ 7.41–7.33 (m, 5H, H-20, H-21, H-22), 6.76–6.74 (m, 1H, H-7), 6.67–6.64 (m, 1H, H-23), 4.80 (s, 2H, H-18), 4.34–4.31 (m, 1H, H-9), 3.75–3.60 (m, 2H, H-13), 3.31 (t, 2H, ³*J* = 6.8 Hz, H-27), 3.21–3.17 (m, 2H, H-6), 3.04–2.95 (m, 2H, H-16), 2.68–2.53 (m, 2H, H-15), 2.31 (sbr, 2H, H-17), 2.28 (t, 2H, ³*J* = 6.8 Hz, H-25), 2.19 (t, 2H, ³*J* = 7.4 Hz, H-2), 1.89 (quin, 2H, ³*J* = 6.8 Hz, H-26), 1.80–1.73 (m, 1H, H-10), 1.72–1.68 (m, 1H, H-12), 1.66–1.59 (m, 2H, H-10, H-12), 1.58–1.55 (m, 2H, H-3), 1.50–1.44 (m, 2H, H-5), 1.42 (s, 9H, H-29), 1.33–1.27 (m, 4H, H-4, H-11). ¹³C NMR (151 MHz, CDCl₃) δ 173.2 (C-1, C-14), 172.1 (C-24), 171.7 (C-8), 134.5 (C-19), 129.3 (C-22), 129.2 (C-20), 128.9 (C-21), 80.3 (C-28), 76.4 (C-18), 53.2 (C-9), 50.9 (C-27), 44.3 (C-13), 39.4 (C-6), 37.3 (C-16), 35.5 (C-2), 34.9 (C-15), 33.1 (C-25), 31.8 (C-10), 29.2 (C-5), 28.2 (C-29), 26.4 (C-4), 26.2 (C-12), 24.9 (C-3), 24.7 (C-26), 22.5 (C-11). IR: $\tilde{\nu}_{\text{max}}$ (cm⁻¹) = 2979.5, 2088.5, 1714.4, 1591.0, 1367.3, 1344.1, 1267.0, 1147.4, 962.3, 846.6, 730.9, 696.2, 650.9. HRMS (ESI, pos.): calc. for C₃₀H₅₀N₃O₆⁺ [*M* + *H*]⁺ 604.3817; found 604.3827.

Protected (Lys-β-Ala)-(Lys-β-Ala)-(Lys-β-Ala) trimer (114): The title compound 114 was obtained in three steps. The first intermediate (protected Lys-Lys dimer) was obtained from 82 and 160 employing method E. Scale: 82 (751 mg, 1.14 mmol, 1.00 eq.), HBTU (455 mg, 1.20 mmol, 1.05 eq.), HOBT (309 mg, 2.29 mmol, 2.00 eq.), DIPEA (597 μL, 3.43 mmol, 3.00 eq.) in abs. DMF (20 mL), reaction time (30 min), 160 (630 mg, 1.14 mmol, 1.00 eq.) in abs. DMF (5 mL), reaction time (4 h), column chromatography on SiO₂ (CH₂Cl₂/CH₃OH, 15:1 + 0.1% NEt₃ v/v). Brown solid; yield: 950 mg (67%). *R*_f = 0.23 (CH₂Cl₂/CH₃OH 24:1 v/v, UV₂₅₄, ammonium cerium(IV) sulfate). HRMS (ESI, pos.): calc. for C₆₅H₈₈N₁₃O₁₂⁺ [*M* + *H*]⁺ 1242.6670; found 1242.6683. The second intermediate (Fmoc-protected Lys-Lys dimer) was obtained from the above mentioned Fmoc-protected Lys-Lys dimer via Fmoc-deprotection employing method F. Scale: Fmoc-protected Lys-Lys dimer (1.14 g, 918 μmol, 1.00 eq.), 20% Piperidine in CH₃CN (24 mL), reaction time

(35 min), column chromatography on SiO₂ (CH₂Cl₂/CH₃OH, 25:2 + 0.1% NEt₃ v/v). pale yellow semiliquid; yield: 821 mg (88%). Anal. HPLC (Nucleodur RP8, 150×2 mm ID, 5 μm, H₂O/CH₃CN 90:10 + 0.05% HCO₂H→5:95 + 0.05% HCO₂H, 15 min, 0.2 mL/min): *t*_R = 17.6 min. HRMS (ESI, pos.): calc. for C₅₀H₇₈N₁₃O₁₀²⁺ [*M* + 2H]²⁺ 510.8031; found 510.8010. This intermediate Fmoc-deprotected Lys-Lys dimer was coupled to 82 and converted to the title compound 114 employing method E. Scale: 82 (515 mg, 784 μmol, 1.00 eq.), HBTU (312 mg, 823 μmol, 1.05 eq.), HOBT (212 mg, 1.57 mmol, 2.00 eq.), DIPEA (410 μL, 2.35 mmol, 3.00 eq.) in abs. DMF (15 mL), reaction time (30 min), Fmoc-deprotected Lys-Lys dimer (800 mg, 784 μmol, 1.00 eq.) in abs. DMF (6 mL), reaction time (5 h), column chromatography on SiO₂ (CH₂Cl₂/CH₃OH, 25:1 + 0.1% NEt₃ v/v), column chromatography on SiO₂-RP18 (H₂O/CH₃CN + 0.1% HCO₂H 50:50→10:90 v/v). Colorless solid; yield: 915 mg (70%). Anal. HPLC (Nucleodur RP8, 150×2 mm ID, 5 μm, H₂O/CH₃CN 30:70 + 0.05% HCO₂H→5:95 + 0.05% HCO₂H, 15 min, 0.2 mL/min): *t*_R = 11.4 min. [α]_D²⁵ = 3.6 (c = 1.4 mg/mL, CH₂Cl₂). ¹H NMR (500 MHz, CDCl₃) δ 7.76 (d, 2H), 7.59 (d, 2H), 7.52 (sbr, 1H), 7.40–7.31 (m, 17H), 7.28 (t, 2H), 7.24–6.29 (m, 4H), 6.04–5.66 (m, 1H), 4.84–4.69 (m, 6H), 4.71–4.43 (m, 3H), 4.27–4.13 (m, 1H), 4.01–3.72 (m, 1H), 3.70–3.52 (m, 5H), 3.50–3.36 (m, 5H), 3.36–3.10 (m, 9H), 2.74–2.46 (m, 5H), 2.34–2.14 (m, 9H), 1.92–1.72 (m, 8H), 1.73–1.53 (m, 12H), 1.52–1.46 (m, 2H), 1.44–1.38 (m, 10H), 1.34–1.19 (m, 8H). ¹³C NMR (126 MHz, CDCl₃) δ 171.9, 156.6, 144.2, 141.4, 134.2, 129.5, 129.4, 129.2, 128.9, 127.8, 127.1, 125.3, 120.1, 81.0, 76.5, 76.4, 76.3, 66.8, 53.1, 50.9, 47.4, 39.5, 36.7, 35.5, 35.2, 33.1, 32.8, 29.2, 28.3, 26.5, 24.9, 24.7, 22.7. IR: $\tilde{\nu}_{\text{max}}$ (cm⁻¹) = 3301.5, 2980.5, 2098.2, 1717.3, 1639.2, 1540.9, 1450.2, 1246.8, 1149.4, 968.1, 739.6, 698.1, 506.2. HRMS (ESI, pos.): calc. for C₈₅H₁₁₆N₁₉O₁₆⁺ [*M* + *H*]⁺ 1658.8842; found 1658.8847.

Protected (Lys-β-Ala)-(Lys-β-Ala)-(Lys-β-Ala)-(Lys-β-Ala) tetramer (115): The title compound 115 was obtained in two steps via an intermediate Fmoc-deprotected analogue. The latter compound was obtained from 114 employing method F. Scale: 114 (200 mg, 121 μmol, 1.00 eq.), 20% Piperidine in CH₃CN (10 mL), reaction time (2 h), column chromatography on SiO₂ (CH₂Cl₂/CH₃OH, 24:1 + 0.1% NEt₃→8:1 + 0.1% NEt₃ v/v). Colorless oil; yield: 157 mg (91%). Anal. HPLC (Nucleodur RP8, 150×2 mm ID, 5 μm, H₂O/CH₃CN 90:10 + 0.05% HCO₂H→5:95 + 0.05% HCO₂H, 15 min, 0.2 mL/min): *t*_R = 19.5 min. HRMS (ESI, pos.): calc. for C₁₀₅H₁₄₅N₂₅O₂₀²⁺ [*M* + 2H]²⁺ 1038.0543; found 1038.0512. This intermediate Fmoc-deprotected analogue was converted to the title compound 115 via coupling to 82 using method E. Scale: 82 (35.7 mg, 54.3 μmol, 1.00 eq.), HBTU (21.6 mg, 57.0 μmol, 1.05 eq.), HOBT (14.7 mg, 109 μmol, 2.00 eq.), DIPEA (28.4 μL, 163 μmol, 3.00 eq.) in abs. DMF (3 mL), reaction time (30 min), 162 (78.0 mg, 54.3 μmol, 1.00 eq.) in abs. DMF (1 mL), reaction time (7.5 h), column chromatography on SiO₂ (CH₂Cl₂/CH₃OH, 25:1 + 0.5% NEt₃→9:1 + 0.5% NEt₃ v/v), column chromatography on SiO₂-RP18 (H₂O/CH₃CN + 0.1% HCO₂H 95:5 + 0.1% HCO₂H→5:95 + 0.1% HCO₂H v/v). Colorless solid; yield: 89.1 mg (79%). Anal. HPLC (Nucleodur RP8, 150×2 mm ID, 5 μm, H₂O/CH₃CN 30:70 + 0.05% HCO₂H→5:95 + 0.05% HCO₂H, 15 min, 0.2 mL/min): *t*_R = 12.2 min. [α]_D²⁵ = -8.0 (c = 1.0 mg/mL, CH₂Cl₂). ¹H NMR (600 MHz, CDCl₃) δ 7.93–7.64 (m, 3H), 7.64–7.54 (m, 3H), 7.53–7.46 (m, 1H), 7.39–7.31 (m, 25H), 7.30–7.26 (m, 2H), 7.18–6.57 (m, 5H), 6.08–5.66 (m, 1H), 4.79–4.68 (m, 9H), 4.66–4.34 (m, 5H), 4.35–4.29 (m, 2H), 4.24–4.14 (m, 1H), 4.00–3.79 (m, 1H), 3.71–3.53 (m, 8H), 3.51–3.36 (m, 8H), 3.35–3.25 (m, 8H), 3.24–3.08 (m, 5H), 3.01–2.72 (m, 2H), 2.70–2.51 (m, 8H), 2.33–2.11 (m, 13H), 1.92–1.72 (m, 12H), 1.70–1.53 (m, 17H), 1.52–1.44 (m, 4H), 1.43–1.37 (m, 12H), 1.33–1.27 (m, 6H), 1.26–1.17 (m, 6H). ¹³C NMR (125 MHz, CDCl₃) δ 173.0, 173.0, 171.9, 171.9, 171.8, 156.5, 144.0, 141.3, 134.2, 134.1, 129.4, 129.2, 129.2, 129.1, 128.8, 127.6, 127.0, 125.2, 119.9, 80.1, 76.3, 76.2, 66.7, 53.0, 52.9, 52.7, 52.5, 50.8, 50.7, 50.6, 47.2, 44.4, 43.6, 39.3, 36.5, 35.4, 34.9, 33.0, 32.6, 32.3, 32.2, 31.9, 31.8, 31.6, 29.1, 28.1, 26.4, 26.3, 26.2,

24.8, 24.7, 24.6, 23.0, 22.6, 22.5. IR: $\tilde{\nu}_{\text{max}}$ (cm^{-1}) = 3301.5, 2970.8, 2098.2, 1718.3, 1637.3, 1540.9, 1450.2, 1366.3, 1246.8, 1150.3, 1007.6, 954.6, 740.5, 698.1. HRMS (ESI, pos.): calc. for $\text{C}_{105}\text{H}_{145}\text{N}_{25}\text{O}_{20}^{2+}$ $[M+2\text{H}]^{2+}$ 1038.0543; found 1038.0512.

Protected (Orn- β -Ala)-(Lys- β -Ala)-(Orn- β -Ala) trimer (118): The title compound 118 was obtained in three steps. The first intermediate (protected Orn-Lys dimer) was obtained from 82 and 157 employing method E. Scale: 82 (250 mg, 424 μmol , 1.00 eq.), HBTU (169 mg, 445 μmol , 1.05 eq.), HOBT (143 mg, 1.06 mmol, 2.50 eq.), DIPEA (222 μL , 1.27 mmol, 3.00 eq.) in abs. DMF (5 mL), reaction time (30 min), 157 (250 mg, 424 μmol , 1.00 eq.) in abs. DMF (5 mL), reaction time (3 h), column chromatography on SiO_2 -RP18 ($\text{H}_2\text{O}/\text{CH}_3\text{CN}$ 95:5 + 0.1 % HCO_2H \rightarrow 5:95 + 0.1 % HCO_2H v/v). Colorless solid; yield: 273 mg (52 %). Anal. HPLC (Nucleodur RP8, 150×2 mm ID, 5 μm , $\text{H}_2\text{O}/\text{CH}_3\text{CN}$ 30:70 + 0.05 % HCO_2H \rightarrow 5:95 + 0.05 % HCO_2H , 15 min, 0.2 mL/min): t_R = 8.7 min. HRMS (ESI, pos.): calc. for $\text{C}_{64}\text{H}_{86}\text{N}_{13}\text{O}_{12}^+$ $[M+H]^+$ 1228.6513; found 1228.6489. The second intermediate (Fmoc-deprotected Orn-Lys dimer) was obtained from the above mentioned Fmoc-protected Orn-Lys dimer via Fmoc-deprotection employing method F. Scale: Fmoc-protected Orn-Lys dimer (247 mg, 201 μmol , 1.00 eq.), 20 % Piperidine in CH_3CN (9 mL), reaction time (30 min), column chromatography on SiO_2 ($\text{CH}_2\text{Cl}_2/\text{CH}_3\text{OH}$, 15:1 + 0.1 % NET_3 \rightarrow 9:1 + 0.1 % NET_3 v/v). Colorless oil; yield: 200 mg (99 %). R_f = 0.48 ($\text{CH}_2\text{Cl}_2/\text{CH}_3\text{OH}$ 12:1 + 0.1 % NET_3 v/v, UV_{254} , Ninhydrin). Anal. HPLC (Nucleodur RP8, 150×2 mm ID, 5 μm , $\text{H}_2\text{O}/\text{CH}_3\text{CN}$ 90:10 + 0.05 % HCO_2H \rightarrow 5:95 + 0.05 % HCO_2H , 15 min, 0.2 mL/min): t_R = 18.6 min. HRMS (ESI, pos.): calc. for $\text{C}_{60}\text{H}_{76}\text{N}_{13}\text{O}_{10}^+$ $[M+H]^+$ 1006.5833; found 1006.5863. This intermediate Fmoc-deprotected Orn-Lys dimer was coupled to 80 and converted to the title compound 118 employing method E. Scale: 80 (63.2 mg, 98.4 μmol , 1.10 eq.), HBTU (37.3 mg, 98.4 μmol , 1.10 eq.), HOBT (30.2 mg, 224 μmol , 2.50 eq.), DIPEA (46.7 μL , 268 μmol , 3.00 eq.) in abs. DMF (2 mL), reaction time (30 min), Fmoc-deprotected Orn-Lys dimer (90.0 mg, 89.4 μmol , 1.00 eq.) in abs. DMF (2 mL), reaction time (5 h), column chromatography on SiO_2 ($\text{CH}_2\text{Cl}_2/\text{CH}_3\text{OH}$, 25:1 + 0.1 % NET_3 \rightarrow 9:1 + 0.1 % NET_3 v/v). Colorless oil; yield: 96 %. R_f = 0.52 ($\text{CH}_2\text{Cl}_2/\text{CH}_3\text{OH}$ 25:2 + 0.1 % NET_3 v/v, UV_{254} , Ninhydrin). Anal. HPLC (Nucleodur RP8, 150×2 mm ID, 5 μm , $\text{H}_2\text{O}/\text{CH}_3\text{CN}$ 30:70 + 0.05 % HCO_2H \rightarrow 5:95 + 0.05 % HCO_2H , 15 min, 0.2 mL/min): t_R = 8.7 min. $[\alpha]_{25}^D$ = 8.2 (c = 1.1 mg/mL, CH_2Cl_2). ^1H NMR (600 MHz, CDCl_3) δ 9.80 (sbr, 1H), 7.75 (d, 2H), 7.58 (d, 2H), 7.40–7.31 (m, 17H), 7.28–7.26 (m, 2H), 7.15–7.04 (m, 1H), 7.00–6.76 (m, 2H), 6.09–6.02 (m, 1H), 4.80–4.72 (m, 6H), 4.66–4.58 (m, 1H), 4.52–4.39 (m, 2H), 4.37–4.30 (m, 2H), 4.20–4.16 (m, 1H), 3.91–3.77 (m, 2H), 3.71–3.58 (m, 3H), 3.56–3.42 (m, 5H), 3.39–3.32 (m, 1H), 3.31–3.23 (m, 6H), 3.21–3.11 (m, 6H), 2.84–2.51 (m, 5H), 2.49–2.38 (m, 1H), 2.34–2.27 (m, 4H), 2.26–2.21 (m, 2H), 2.17 (t, 2H), 1.90–1.80 (m, 6H), 1.75–1.52 (m, 13H), 1.48–1.41 (m, 11H), 1.37 (t, 6H), 1.31–1.24 (m, 4H). ^{13}C NMR (126 MHz, CDCl_3) δ 173.1, 172.8, 172.2, 156.7, 144.2, 141.4, 134.1, 129.5, 129.5, 129.4, 129.4, 129.4, 129.4, 129.3, 129.3, 128.9, 128.9, 127.8, 127.2, 125.3, 120.1, 80.2, 76.5, 76.4, 66.8, 52.7, 52.7, 52.6, 52.1, 50.9, 50.9, 50.9, 50.8, 50.8, 50.8, 47.4, 46.7, 44.7, 44.4, 44.3, 39.7, 36.7, 35.9, 35.5, 35.3, 35.1, 33.1, 33.0, 32.9, 32.8, 32.4, 32.2, 30.2, 29.3, 29.1, 28.3, 26.4, 26.4, 26.3, 24.9, 24.9, 24.7, 23.2, 23.1, 23.0, 22.9, 22.6, 22.6, 8.8. IR: $\tilde{\nu}_{\text{max}}$ (cm^{-1}) = 3302.5, 3075.9, 2941.9, 2869.6, 2094.3, 1730.8, 1636.3, 1539.9, 1529.3, 1525.4, 1449.2, 1367.3, 1295.9, 1268.9, 1242.9, 1203.4, 1146.5, 1062.6, 1000.9, 912.2, 853.4, 757.9, 754.0, 741.5, 698.1, 650.9, 557.3. HRMS (ESI, pos.): calc. for $\text{C}_{83}\text{H}_{112}\text{N}_{19}\text{O}_{16}^+$ $[M+H]^+$ 1630.8529; found 1630.8571.

Protected (Orn- β -Ala)-(Lys- β -Ala)-(Orn- β -Ala)-(Lys- β -Ala) tetramer (119): The title compound 119 was obtained in two steps via an intermediate Fmoc-deprotected analogue. The latter compound was obtained from 118 employing method F. Scale: 118 (50.0 mg, 30.7 μmol , 1.00 eq.), 20 % Piperidine in CH_3CN (5 mL), reaction time

(30 min), column chromatography on SiO_2 ($\text{CH}_2\text{Cl}_2/\text{CH}_3\text{OH}$, 25:1 + 0.5 % NET_3 \rightarrow 10:1 + 0.5 % NET_3 v/v). Colorless oil; yield: 41.8 mg (97 %). Anal. HPLC (Nucleodur RP8, 150×2 mm ID, 5 μm , $\text{H}_2\text{O}/\text{CH}_3\text{CN}$ 90:10 + 0.05 % HCO_2H \rightarrow 5:95 + 0.05 % HCO_2H , 15 min, 0.2 mL/min): t_R = 19.4 min. HRMS (ESI, pos.): calc. for $\text{C}_{98}\text{H}_{103}\text{N}_{19}\text{O}_{14}^{2+}$ $[M+2\text{H}]^{2+}$ 704.8960; found 704.8945. This intermediate Fmoc-deprotected analogue was converted to the title compound 119 via coupling to 82 using method E. Scale: 82 (14.8 mg, 22.6 μmol , 1.00 eq.), HBTU (8.99 mg, 23.7 μmol , 1.05 eq.), HOBT (7.63 mg, 56.4 μmol , 2.50 eq.), DIPEA (11.8 μL , 67.7 μmol , 3.00 eq.) in abs. DMF (0.5 mL), reaction time (30 min), Fmoc-deprotected analogue mentioned above (31.8 mg, 22.6 μmol , 1.00 eq.) in abs. DMF (2.3 mL), reaction time (7 h), column chromatography on SiO_2 ($\text{CH}_2\text{Cl}_2/\text{CH}_3\text{OH}$, 25:1 + 0.1 % NET_3 \rightarrow 9:1 + 0.1 % NET_3 v/v). Colorless oil; yield: 17.4 mg (38 %). R_f = 0.44 ($\text{CH}_2\text{Cl}_2/\text{CH}_3\text{OH}$ 15:1 + 0.1 % NET_3 v/v, UV_{254} , Ninhydrin). Anal. HPLC (Nucleodur RP8, 150×2 mm ID, 5 μm , $\text{H}_2\text{O}/\text{CH}_3\text{CN}$ 30:70 + 0.05 % HCO_2H \rightarrow 5:95 + 0.05 % HCO_2H , 15 min, 0.2 mL/min): t_R = 16.4 min. ^1H NMR (500 MHz, CDCl_3) δ 7.74 (d, 2H), 7.58 (d, 2H), 7.55–7.43 (m, 1H), 7.40 (m, 22H), 7.28 (t, 2H), 7.23–6.98 (m, 3H), 6.97–6.68 (m, 2H), 6.07–5.73 (m, 1H), 4.84–4.68 (m, 8H), 4.61–4.51 (m, 1H), 4.50–4.45 (m, 1H), 4.44–4.37 (m, 2H), 4.36–4.27 (m, 2H), 4.24–4.13 (m, 1H), 3.96–3.72 (m, 2H), 3.70–3.51 (m, 7H), 3.50–3.35 (m, 6H), 3.31–3.22 (m, 8H), 3.21–3.11 (m, 2H), 2.84–2.41 (m, 8H), 2.32–2.23 (m, 6H), 2.20–1.95 (m, 6H), 1.89–1.79 (m, 8H), 1.75–1.69 (m, 2H), 1.67–1.60 (m, 7H), 1.58–1.52 (m, 5H), 1.49–1.44 (m, 2H), 1.43 (s, 9H), 1.37–1.17 (m, 10H). ^{13}C NMR (126 MHz, CDCl_3) δ 172.0, 156.6, 144.2, 141.4, 134.2, 129.5, 129.4, 129.3, 129.2, 128.9, 127.8, 127.1, 125.3, 120.1, 80.2, 76.6, 76.4, 66.8, 52.5, 50.9, 47.4, 44.5, 39.5, 36.6, 35.5, 35.1, 33.1, 32.4, 29.3, 28.3, 26.5, 24.9, 24.8, 22.7. HRMS (ESI, pos.): calc. for $\text{C}_{103}\text{H}_{141}\text{N}_{25}\text{O}_{20}^{2+}$ $[M+2\text{H}]^{2+}$ 1024.0387; found 1024.0381.

Protected (Orn- β -Ala)-(Lys- β -Ala)-(Lys- β -Ala) trimer (117): This compound was obtained from Fmoc-deprotected Orn-Lys (see preparation of 118) and 82 employing method E. After removing the solvent under reduced pressure, it was co-evaporated with CH_2Cl_2 (3 \times 5 mL). Scale: 82 (64.6 mg, 98.4 μmol , 1.10 eq.), HBTU (37.3 mg, 98.4 μmol , 1.10 eq.), HOBT (30.2 mg, 224 μmol , 2.50 eq.), DIPEA (46.7 μL , 268 μmol , 3.00 eq.) in abs. DMF (2 mL), reaction time (30 min), Fmoc-deprotected Orn-Lys (90.0 mg, 89.4 μmol , 1.00 eq.) in abs. DMF (2 mL), reaction time (5 h), column chromatography on SiO_2 ($\text{CH}_2\text{Cl}_2/\text{CH}_3\text{OH}$, 25:1 + 0.1 % NET_3 \rightarrow 9:1 + 0.1 % NET_3 v/v). Colorless oil; yield: 135 mg (92 %). R_f = 0.52 ($\text{CH}_2\text{Cl}_2/\text{CH}_3\text{OH}$ 25:2 + 0.1 % NET_3 v/v, UV_{254} , Ninhydrin). Anal. HPLC (Nucleodur RP8, 150×2 mm ID, 5 μm , $\text{H}_2\text{O}/\text{CH}_3\text{CN}$ 30:70 + 0.05 % HCO_2H \rightarrow 5:95 + 0.05 % HCO_2H , 15 min, 0.2 mL/min): t_R = 6.4 min. $[\alpha]_{25}^D$ = -2.0 (c = 1.0 mg/mL, CH_2Cl_2). ^1H NMR (600 MHz, CDCl_3) δ 7.75 (d, 2H), 7.58 (d, 2H), 7.39–7.27 (m, 19H), 7.11–6.99 (m, 2H), 6.89–6.65 (m, 1H), 5.73 (sbr, 1H), 4.77–4.73 (m, 6H), 4.53–4.38 (m, 3H), 4.34 (d, 2H), 4.20–4.17 (m, 1H), 3.94–3.74 (m, 6H), 3.54–3.35 (m, 6H), 3.32–3.24 (m, 6H), 3.18–3.09 (m, 4H), 2.84–2.60 (m, 4H), 2.58–2.40 (m, 2H), 2.34–2.27 (m, 4H), 2.19–2.16 (m, 4H), 1.91–1.85 (m, 4H), 1.84–1.80 (m, 2H), 1.78–1.70 (m, 2H), 1.67–1.58 (m, 7H), 1.57–1.52 (m, 3H), 1.49–1.44 (m, 2H), 1.43 (s, 9H), 1.37 (t, 4H), 1.33–1.24 (m, 6H). ^{13}C NMR (126 MHz, CDCl_3) δ 173.2, 172.6, 172.0, 156.6, 144.1, 141.4, 134.2, 129.5, 129.5, 129.4, 129.4, 129.3, 128.9, 128.9, 127.8, 127.2, 125.3, 120.1, 100.1, 80.2, 76.5, 76.4, 66.9, 53.3, 52.7, 52.7, 52.6, 52.5, 50.9, 50.9, 50.8, 47.4, 46.7, 44.7, 44.3, 44.0, 39.6, 39.6, 36.6, 35.8, 35.8, 35.5, 35.2, 33.1, 33.1, 33.0, 32.9, 32.9, 32.8, 32.5, 32.4, 32.2, 29.1, 28.3, 26.5, 26.4, 25.0, 24.9, 24.9, 24.8, 24.7, 22.7, 22.6, 8.8. IR: $\tilde{\nu}_{\text{max}}$ (cm^{-1}) = 3298.6, 3070.1, 2939.0, 2863.8, 2094.3, 1636.3, 1538.0, 1449.2, 1423.2, 1409.7, 1367.3, 1295.9, 1269.0, 1240.0, 1203.4, 1148.4, 1059.7, 998.0, 912.2, 840.8, 742.5, 696.2, 653.8, 627.7, 555.4. HRMS (ESI, pos.): calc. for $\text{C}_{84}\text{H}_{114}\text{N}_{19}\text{O}_{16}^+$ $[M+H]^+$ 1644.8685; found 1644.8678.

Protected (Orn- β -Ala)-(Lys- β -Ala)-(Lys- β -Ala)-(Orn- β -Ala) tetramer (120): The title compound 120 was obtained in two steps via an

intermediate Fmoc-deprotected analogue. The latter compound was obtained from 117 employing method F. Scale: 117 (50.0 mg, 30.4 μmol , 1.00 eq.), 20% Piperidine in CH_3CN (5 mL), reaction time (30 min), column chromatography on SiO_2 ($\text{CH}_2\text{Cl}_2/\text{CH}_3\text{OH}$, 20:1 + 0.2% $\text{NEt}_3 \rightarrow 10:1 + 1\%$ NEt_3 v/v). Colorless solid; yield: 42 mg (97%). Anal. HPLC (Nucleodur RP8, 150×2 mm ID, 5 μm , $\text{H}_2\text{O}/\text{CH}_3\text{CN}$ 90:10 + 0.05% $\text{HCO}_2\text{H} \rightarrow 5:95 + 0.05\%$ HCO_2H , 15 min, 0.2 mL/min): $t_R = 19.5$ min. HRMS (ESI, pos.): calc. for $\text{C}_{69}\text{H}_{105}\text{N}_{19}\text{O}_{14}^{2+}$ $[M + 2\text{H}]^{2+}$ 711.9039; found 711.9023. This intermediate Fmoc-deprotected analogue was converted to the title compound 120 via coupling to 80 using method E. Scale: 80 (15.5 mg, 22.5 μmol , 1.00 eq.), HBTU (8.96 mg, 23.6 μmol , 1.05 eq.), HOBt (7.60 mg, 56.2 μmol , 2.50 eq.), DIPEA (11.8 μL , 67.5 μmol , 3.00 eq.) in abs. DMF (0.5 mL), reaction time (30 min), Fmoc-deprotected analogue mentioned above (32.0 mg, 22.5 μmol , 1.00 eq.) in abs. DMF (2.3 mL), reaction time (7 h), column chromatography on SiO_2 ($\text{CH}_2\text{Cl}_2/\text{CH}_3\text{OH}$, 25:1 + 0.1% $\text{NEt}_3 \rightarrow 25:2 + 0.5\%$ NEt_3 v/v). Colorless solid; yield: 13.0 mg (28%). $R_f = 0.42$ ($\text{CH}_2\text{Cl}_2/\text{CH}_3\text{OH}$ 15:1 + 0.1% NEt_3 v/v, UV_{254} , Ninhydrin). Anal. HPLC (Nucleodur RP8, 150×2 mm ID, 5 μm , $\text{H}_2\text{O}/\text{CH}_3\text{CN}$ 30:70 + 0.05% $\text{HCO}_2\text{H} \rightarrow 5:95 + 0.05\%$ HCO_2H , 15 min, 0.2 mL/min): $t_R = 16.2$ min. ^1H NMR (500 MHz, CDCl_3) δ 7.75 (d, 2H), 7.58 (d, 2H), 7.39–7.32 (m, 22H), 7.30–7.27 (m, 2H), 7.22–6.85 (m, 4H), 6.80–6.60 (m, 1H), 6.24–5.89 (m, 1H), 4.79–4.70 (m, 8H), 4.68–4.57 (m, 1H), 4.56–4.37 (m, 3H), 4.36–4.25 (m, 2H), 4.24–4.12 (m, 1H), 3.94–3.77 (m, 2H), 3.74–3.67 (m, 1H), 3.65–3.55 (m, 4H), 3.52–3.40 (m, 6H), 3.38–3.33 (m, 1H), 3.31–3.21 (m, 9H), 3.18–3.07 (m, 2H), 2.87–2.68 (m, 2H), 2.65–2.54 (m, 4H), 2.50–2.42 (m, 1H), 2.31–2.24 (m, 5H), 2.23–2.12 (m, 5H), 1.90–1.80 (m, 9H), 1.76–1.66 (m, 5H), 1.65–1.51 (m, 13H), 1.49–1.44 (m, 2H), 1.43 (s, 9H), 1.32–1.19 (m, 10H). ^{13}C NMR (126 MHz, CDCl_3) δ 172.1, 144.2, 141.4, 129.5, 129.2, 128.9, 127.8, 127.2, 125.3, 120.1, 81.3, 77.4, 77.2, 76.9, 76.4, 66.8, 50.9, 47.4, 44.5, 44.4, 39.5, 36.7, 35.5, 33.1, 32.4, 29.8, 29.3, 28.3, 26.5, 24.9, 24.8, 23.2, 22.7. HRMS (ESI, pos.): calc. for $\text{C}_{103}\text{H}_{141}\text{N}_{25}\text{O}_{20}^{2+}$ $[M + 2\text{H}]^{2+}$ 1024.0387; found 1024.0374.

Zwitterionic (Orn- β -Ala)₃(tert-butylester) trimer (133): This compound was prepared in three steps involving CuAAC, debenzoylation and Fmoc-deprotection. CuAAC was performed according to method G. Scale: 110 (200 mg, 124 μmol , 1.00 eq.), 3-(dimethyl(prop-2-yn-1-yl)ammonio)propane-1-sulfonate (114 mg, 557 μmol , 1.50 eq. per azide), CuI (8.83 mg, 46.4 μmol , 0.13 eq. per azide), sodium ascorbate (48.9 mg, 247 μmol , 0.68 eq. per azide), CH_3CN (8 mL). Colorless solid; yield: 239 mg (87%). Anal. HPLC (Nucleodur C₁₈ HTec EC, 150×10 mm ID, 5 μm , $\text{H}_2\text{O}/\text{CH}_3\text{CN}$ 95:5 + 0.05% $\text{HCO}_2\text{H} \rightarrow 5:95 + 0.05\%$ HCO_2H , 10 min, 0.6 mL/min): $t_R = 8.2$ min. ^1H NMR (600 MHz, $\text{DMSO}-d_6$) δ 8.48 (s, 1H), 8.47 (s, 2H), 8.06 (d, 2H, $^3J = 8.0$ Hz), 8.02 (d, 1H, $^3J = 8.0$ Hz), 7.96–7.92 (m, 2H), 7.88 (d, 2H, $^3J = 7.6$ Hz), 7.86 (t, 1H, $^3J = 5.8$ Hz), 7.67 (d, 2H, $^3J = 7.5$ Hz), 7.43–7.35 (m, 17H), 7.33–7.28 (m, 3H), 4.85–4.77 (m, 6H), 4.65–4.61 (m, 6H), 4.42–4.34 (m, 6H), 4.28 (d, 2H, $^3J = 7.4$ Hz), 4.23–4.16 (m, 4H), 3.64–3.55 (m, 6H). ^{13}C NMR (151 MHz, $\text{DMSO}-d_6$) δ 172.2, 171.7, 163.8, 143.9, 140.7, 135.1, 129.4, 128.7, 128.4, 128.2, 127.6, 127.0, 120.1, 115.1, 79.3, 61.8, 57.0, 52.3, 49.7, 49.3, 47.6, 46.7, 40.1, 39.9, 39.8, 39.7, 39.5, 39.4, 39.2, 39.1, 34.7, 31.6, 28.7, 27.8, 25.7, 25.6, 25.5, 24.2, 18.9, 17.0, 66.8, 50.9, 47.4, 44.5, 44.4, 39.5, 36.7, 35.5, 33.1, 32.4, 29.8, 29.3, 28.3, 26.5, 24.9, 24.8, 23.2, 22.7. HRMS (ESI, pos.): calc. for $\text{C}_{106}\text{H}_{156}\text{N}_{22}\text{O}_{25}\text{S}_3^{2+}$ $[M + 2\text{H}]^{2+}$ 1116.5382; found 1116.5409. Debenzylation of this intermediate to 133 was done according to method H. Scale: intermediate benzylhydroxamate (15.2 mg, 6.81 μmol , 1.00 eq.), Pd/C (1.00 mg). After removing the solvent under reduced pressure, the residue was dissolved in demineralized H_2O (4 mL) and piperidine (1 mL), whereupon the Fmoc-piperidine adduct precipitated as a white, voluminous solid. After stirring for 15 min, the suspension obtained was filtered and the solvent was removed under reduced pressure and the product was purified by HPLC. Colorless solid; yield: 11.0 mg (93%). Prep. HPLC: $t_R = 13.4$ min. Anal. HPLC (NUCLEODUR C₁₈ HTec EC, 150×10 mm ID, 5 μm): $t_R =$

14.3 min. HRMS (ESI, pos.): calc. for $\text{C}_{70}\text{H}_{128}\text{N}_{22}\text{O}_{23}\text{S}_3^{2+}$ $[M + 2\text{H}]^{2+}$ 870.4337; found 870.4301.

Zwitterionic (Orn- β -Ala)₃ trimer (135): This compound was obtained from 133 (11.0 mg, 6.73 μmol , 1.00 eq.) which was treated with TFA/ H_2O /triethylsilane (20:20:1, 1 mL) and stirred for 2 h at rt. After removing the solvent under reduced pressure, the residue was dissolved in demineralized H_2O (4 mL) and piperidine (1 mL), whereupon the Fmoc-piperidine adduct precipitated as a white, voluminous solid. After stirring for 15 min, the suspension obtained was filtered and the solvent was removed under reduced pressure. The purified product was obtained by preparative HPLC. Colorless solid; yield: 9.90 mg (88%). Prep. HPLC (NUCLEODUR C₁₈ HTec EC, 250×10 mm ID, 5 μm , $\text{H}_2\text{O}/\text{CH}_3\text{CN}$ 98:2 + 0.1% FA \rightarrow 2:98 + 0.1% FA v/v, 5 mL/min): $t_R = 10.3$ min. The analyses were performed by HPLC-HRMS (NUCLEODUR C₈ HTec EC, 150×10 mm ID, 5 μm , $\text{H}_2\text{O}/\text{CH}_3\text{CN}$ 98:2 + 0.05% FA \rightarrow 5:95 + 0.05% FA v/v, 0.2 mL/min): $t_R = 17.1$ min. HRMS (ESI, pos.): calc. for $\text{C}_{66}\text{H}_{120}\text{N}_{22}\text{O}_{23}\text{S}_3^{2+}$ $[M + 2\text{H}]^{2+}$ 842.4024; found 842.4027.

Zwitterionic (Lys- β -Ala)₃(tert-butylester) trimer (132): This compound was prepared in three steps involving CuAAC, debenzoylation and Fmoc-deprotection. CuAAC was performed according to method G. Scale: 114 (100 mg, 60.3 μmol , 1.00 eq.), 3-(dimethyl(prop-2-yn-1-yl)ammonio)propane-1-sulfonate (55.7 mg, 271 μmol , 1.50 eq. per azide), CuI (4.36 mg, 22.9 μmol , 0.13 eq. per azide), sodium ascorbate (23.9 mg, 121 μmol , 0.68 eq. per azide), CH_3CN (5 mL). Colorless solid; yield: 126 mg (92%). Anal. HPLC (Nucleodur C₁₈ HTec EC, 150×10 mm ID, 5 μm , $\text{H}_2\text{O}/\text{CH}_3\text{CN}$ 98:2 + 0.05% $\text{HCO}_2\text{H} \rightarrow 5:95 + 0.05\%$ HCO_2H , 15 min, 0.2 mL/min): $t_R = 20.1$ min. ^1H NMR (300 MHz, $\text{DMSO}-d_6$) δ 8.49 (s, 1H), 8.47 (s, 2H), 8.04–7.84 (m, 9H), 7.69–7.64 (m, 2H), 7.43–7.27 (m, 21H), 4.84–4.77 (m, 6H), 4.63 (s, 6H), 4.44–4.25 (m, 9H), 4.24–4.07 (m, 5H), 3.61–3.50 (m, 6H), 3.41–3.35 (m, 6H), 3.28–3.15 (m, 7H), 3.00 (s, 20H), 2.64–2.53 (m, 6H), 2.19–1.99 (m, 21H), 1.64–1.39 (m, 16H), 1.39–1.33 (s, 11H), 1.30–1.12 (m, 10H). ^{13}C NMR (75 MHz, $\text{DMSO}-d_6$) δ 171.9, 171.1, 155.4, 143.9, 140.7, 137.4, 135.1, 129.4, 128.7, 128.5, 128.3, 127.6, 127.5, 127.0, 125.1, 120.1, 75.5, 61.8, 57.0, 52.6, 51.0, 49.7, 49.3, 47.6, 36.4, 34.7, 31.6, 28.7, 27.8, 26.7, 25.6, 24.3, 22.7, 18.9. HRMS (ESI, pos.): calc. for $\text{C}_{109}\text{H}_{162}\text{N}_{22}\text{O}_{25}\text{S}_3^{2+}$ $[M + 2\text{H}]^{2+}$ 1137.5616; found 1137.5610. Debenzylation of this intermediate to 132 was done according to method H. Scale: intermediate benzylhydroxamate (15.6 mg, 6.86 μmol , 1.00 eq.), Pd/C (1.00 mg). After removing the solvent under reduced pressure, the residue was dissolved in demineralized H_2O (4 mL) and piperidine (1 mL), whereupon the Fmoc-piperidine adduct precipitated as a white, voluminous solid. After stirring for 15 min, the suspension obtained was filtered and the solvent was removed under reduced pressure and the product was purified by HPLC. Colorless solid; yield: 10.2 mg (93%). Prep. HPLC: $t_R = 14.2$ min. Anal. HPLC (NUCLEODUR C₁₈ HTec EC, 150×10 mm ID, 5 μm): $t_R = 14.6$ min. HRMS (ESI, pos.): calc. for $\text{C}_{73}\text{H}_{134}\text{N}_{22}\text{O}_{23}\text{S}_3^{2+}$ $[M + 2\text{H}]^{2+}$ 891.4572; found 891.4561.

Zwitterionic (Lys- β -Ala)₃ trimer (136): This compound was obtained from 132 (20.0 mg, 8.79 μmol , 1.00 eq.) which was treated with TFA/ H_2O /triethylsilane (20:20:1, 1 mL) and stirred for 2 h at rt. The solvent was removed under reduced pressure. The purified product was obtained by preparative HPLC. Colorless solid; yield: 10.0 mg (66%). Prep. HPLC (NUCLEODUR C₁₈ HTec EC, 250×10 mm ID, 5 μm , $\text{H}_2\text{O}/\text{CH}_3\text{CN}$ 98:2 + 0.1% FA \rightarrow 2:98 + 0.1% FA v/v, 5 mL/min): $t_R = 11.2$ min. The analyses were performed by HPLC-HRMS (NUCLEODUR C₈ HTec EC, 150×10 mm ID, 5 μm , $\text{H}_2\text{O}/\text{CH}_3\text{CN}$ 98:2 + 0.05% FA \rightarrow 5:95 + 0.05% FA v/v, 0.2 mL/min): $t_R = 12.9$ min. HRMS (ESI, pos.): calc. for $\text{C}_{69}\text{H}_{126}\text{N}_{22}\text{O}_{23}\text{S}_3^{2+}$ $[M + 2\text{H}]^{2+}$ 863.4252; found 863.4252.

Zwitterionic (Orn- β -Ala)-(Lys- β -Ala)-(Orn- β -Ala) (tert-butylester) trimer (134): This compound was prepared in three steps involving

CuAAC, debenzoylation and Fmoc-deprotection. CuAAC was performed according to method G. Scale: 118 (50.0 mg, 30.7 μmol , 1.00 eq.), 3-(dimethyl(prop-2-yn-1-yl)ammonio)propane-1-sulfonate (28.3 mg, 138 μmol , 1.50 eq. per azide), CuI (2.22 mg, 11.7 μmol , 0.13 eq. per azide), sodium ascorbate (12.2 mg, 61.3 μmol , 0.68 eq. per azide), CH_3CN (3.5 mL). Colorless solid; yield: 31.3 mg (45%). Anal. HPLC (Nucleodur C_{18} HTec EC, 150×10 mm ID, 5 μm , $\text{H}_2\text{O}/\text{CH}_3\text{CN}$ 98:2+0.05% HCO_2H →5:95+0.05% HCO_2H , 15 min, 0.2 mL/min): t_{R} =20.3 min (product), t_{R} =16.6 min (product – Fmoc). HRMS (ESI, pos.): calc. for $\text{C}_{107}\text{H}_{158}\text{N}_{22}\text{O}_{25}\text{S}_3^{2+}$ $[M+2\text{H}]^{2+}$ 1123.5460; found 1123.5423; calc. for $\text{C}_{92}\text{H}_{148}\text{N}_{22}\text{O}_{23}\text{S}_3^{2+}$ $[M+2\text{H}-\text{Fmoc}]^{2+}$ 1012.5119; found 1012.5121. Debenzoylation and Fmoc-deprotection of this intermediate to title compound 134 was done according to method H. Scale: intermediate benzylhydroxamate (10.0 mg, 4.45 μmol , 1.00 eq.), Pd/C (1.00 mg). After removing the solvent under reduced pressure, the residue was dissolved in demineralized H_2O (4 mL) and piperidine (1 mL), whereupon the Fmoc-piperidine adduct precipitated as a white, voluminous solid. After stirring for 15 min, the suspension obtained was filtered and the solvent was removed under reduced pressure and the product was purified by HPLC. Colorless solid; yield: 3.30 mg (42%). Prep. HPLC: t_{R} =13.7 min. Anal. HPLC (NUCLEODUR C_{18} HTec EC, 150×10 mm ID, 5 μm): t_{R} =14.6 min. HRMS (ESI, pos.): calc. for $\text{C}_{71}\text{H}_{130}\text{N}_{22}\text{O}_{23}\text{S}_3^{2+}$ $[M+2\text{H}]^{2+}$ 877.4415; found 877.4440.

Zwitterionic (Orn- β -Ala) $_4$ (*tert*-butylester) tetramer (137): This compound was prepared in three steps involving CuAAC, debenzoylation and Fmoc-deprotection. CuAAC was performed according to method G. Scale: 111 (100 mg, 49.5 μmol , 1.00 eq.), 3-(dimethyl(prop-2-yn-1-yl)ammonio)propane-1-sulfonate (61.0 mg, 297 μmol , 1.50 eq. per azide), CuI (4.72 mg, 24.8 μmol , 0.13 eq. per azide), sodium ascorbate (26.2 mg, 132 μmol , 0.68 eq. per azide), CH_3CN (5 mL). Colorless solid; yield: 122 mg (87%). Anal. HPLC (Nucleodur C_{18} HTec EC, 150×10 mm ID, 5 μm , $\text{H}_2\text{O}/\text{CH}_3\text{CN}$ 98:2+0.05% HCO_2H →5:95+0.05% HCO_2H , 15 min, 0.2 mL/min): t_{R} =19.9 min. ^1H NMR (300 MHz, DMSO- d_6) δ 8.48 (s, 1H), 8.46 (s, 3H), 8.08–8.00 (m, 4H), 7.98–7.91 (m, 3H), 7.90–7.84 (m, 3H), 7.71–7.64 (m, 2H), 7.43–7.27 (m, 25H), 4.84–4.75 (m, 8H), 4.62 (s, 8H), 4.42–4.32 (m, 8H), 4.30–4.13 (m, 8H), 3.64–3.55 (m, 8H), 3.29–3.14 (m, 9H), 2.99 (s, 24H), 2.63–2.54 (m, 8H), 2.19–1.95 (m, 27H), 1.64–1.41 (m, 19H), 1.37–1.31 (m, 11H), 1.28–1.14 (m, 4H). ^{13}C NMR (75 MHz, DMSO- d_6) δ 176.4, 174.2, 171.2, 153.2, 135.1, 129.4, 128.7, 128.4, 128.3, 127.6, 127.0, 125.1, 120.1, 99.5, 75.4, 61.8, 57.0, 52.3, 49.7, 49.3, 47.6, 43.7, 38.3, 36.3, 34.7, 31.6, 27.8, 25.7, 25.6, 24.9, 24.3, 18.9. HRMS (ESI, pos.): calc. for $\text{C}_{133}\text{H}_{199}\text{N}_{29}\text{O}_{32}\text{S}_4^{3+}$ $[M+3\text{H}]^{3+}$ 1420.1776; found 1420.1751. Debenzoylation and Fmoc-deprotection of this intermediate to title compound 137 was done according to method H. Scale: intermediate benzylhydroxamate (15.5 mg, 5.46 μmol , 1.00 eq.), Pd/C (1.00 mg). After removing the solvent under reduced pressure, the residue was dissolved in demineralized H_2O (4 mL) and piperidine (1 mL), whereupon the Fmoc-piperidine adduct precipitated as a white, voluminous solid. After stirring for 15 min, the suspension obtained was filtered and the solvent was removed under reduced pressure and the product was purified by HPLC. Colorless solid; yield: 7.60 mg (62%). Prep. HPLC: t_{R} =13.5 min. Anal. HPLC (NUCLEODUR C_{18} HTec EC, 150×10 mm ID, 5 μm): t_{R} =14.1 min. HRMS (ESI, pos.): calc. for $\text{C}_{90}\text{H}_{163}\text{N}_{29}\text{O}_{30}\text{S}_4^{3+}$ $[M+2\text{H}]^{2+}$ 1129.0496; found 1129.0484.

Zwitterionic (Orn- β -Ala)-(Lys- β -Ala)-(Orn- β -Ala)-(Lys- β -Ala) (*tert*-butylester) tetramer (139): This compound was prepared in three steps involving CuAAC, debenzoylation and Fmoc-deprotection. CuAAC was performed according to method G. Scale: 119 (15.3 mg, 7.47 μmol , 1.00 eq.), 3-(dimethyl(prop-2-yn-1-yl)ammonio)propane-1-sulfonate (9.20 mg, 44.8 μmol , 1.50 eq. per azide), CuI (740 μg , 3.89 μmol , 0.13 eq. per azide), sodium ascorbate (3.97 mg, 20.0 μmol , 0.68 eq. per azide), CH_3CN (2.0 mL). Colorless solid; yield:

18.6 mg (87%). Anal. HPLC (Nucleodur C_{18} HTec EC, 150×10 mm ID, 5 μm , $\text{H}_2\text{O}/\text{CH}_3\text{CN}$ 98:2+0.05% HCO_2H →5:95+0.05% HCO_2H , 15 min, 0.2 mL/min): t_{R} =20.4 min (product), t_{R} =16.7 min (product – Fmoc). HRMS (ESI, pos.): calc. for $\text{C}_{120}\text{H}_{192}\text{N}_{29}\text{O}_{30}\text{S}_4^{3+}$ $[M+3\text{H}-\text{Fmoc}]^{3+}$ 882.7763; found 882.7703. Debenzoylation and Fmoc-deprotection of this intermediate to title compound 139 was done according to method H. Scale: intermediate benzylhydroxamate (8.00 mg, 2.79 μmol , 1.00 eq.), Pd/C (1.00 mg). After removing the solvent under reduced pressure, the residue was dissolved in demineralized H_2O (4 mL) and piperidine (1 mL), whereupon the Fmoc-piperidine adduct precipitated as a white, voluminous solid. After stirring for 15 min, the suspension obtained was filtered and the solvent was removed under reduced pressure and the product was purified by HPLC. Colorless solid; yield: 2.10 mg (33%). Prep. HPLC: t_{R} =13.6 min. Anal. HPLC (NUCLEODUR C_{18} HTec EC, 150×10 mm ID, 5 μm): t_{R} =14.9 min. HRMS (ESI, pos.): calc. for $\text{C}_{92}\text{H}_{168}\text{N}_{29}\text{O}_{30}\text{S}_4^{3+}$ $[M+3\text{H}]^{3+}$ 762.3793; found 762.3814.

Zwitterionic (Lys- β -Ala) $_4$ (*tert*-butylester) tetramer (138): This compound was prepared in three steps involving CuAAC, debenzoylation and Fmoc-deprotection. CuAAC was performed according to method G. Scale: 115 (57.8 mg, 27.9 μmol , 1.00 eq.), 3-(dimethyl(prop-2-yn-1-yl)ammonio)propane-1-sulfonate (34.3 mg, 167 μmol , 1.50 eq. per azide), CuI (2.65 mg, 13.9 μmol , 0.13 eq. per azide), sodium ascorbate (14.7 mg, 74.4 μmol , 0.68 eq. per azide), CH_3CN (3.5 mL). Colorless solid; yield: 26.3 mg (34%). Anal. HPLC (Nucleodur C_{18} HTec EC, 150×10 mm ID, 5 μm , $\text{H}_2\text{O}/\text{CH}_3\text{CN}$ 98:2+0.05% HCO_2H →5:95+0.05% HCO_2H , 15 min, 0.2 mL/min): t_{R} =20.3 min. ^1H NMR (300 MHz, DMSO- d_6) δ 8.49 (s, 1H), 8.47 (s, 3H), 8.04–7.85 (m, 9H), 7.69–7.65 (m, 2H), 7.43–7.27 (m, 25H), 4.86–4.75 (m, 8H), 4.63 (s, 8H), 4.44–4.32 (m, 8H), 4.30–4.24 (m, 2H), 4.23–4.09 (m, 5H), 3.63–3.48 (m, 8H), 3.42–3.36 (m, 4H), 3.30–3.16 (m, 9H), 3.00 (s, 24H), 2.62–2.54 (m, 6H), 2.19–1.99 (m, 25H), 1.65–1.40 (m, 18H), 1.37 (s, 9H), 1.35–1.29 (m, 2H), 1.28–1.12 (m, 10H). ^{13}C NMR (75 MHz, DMSO- d_6) δ 171.9, 171.5, 171.1, 154.7, 154.3, 143.9, 140.7, 135.1, 129.4, 128.7, 128.5, 128.3, 127.6, 127.1, 125.1, 120.1, 75.6, 61.8, 57.0, 52.6, 49.7, 49.3, 47.6, 44.2, 36.6, 34.7, 31.6, 28.7, 27.8, 26.2, 25.6, 24.3, 22.8, 18.9. HRMS (ESI, pos.): calc. for $\text{C}_{137}\text{H}_{206}\text{N}_{29}\text{O}_{32}\text{S}_4^{3+}$ $[M+3\text{H}]^{3+}$ 965.8083; found 965.8063. Debenzoylation and Fmoc-deprotection of this intermediate to title compound 138 was done according to method H. Scale: intermediate benzylhydroxamate (9.60 mg, 3.31 μmol , 1.00 eq.), Pd/C (1.00 mg). After removing the solvent under reduced pressure, the residue was dissolved in demineralized H_2O (4 mL) and piperidine (1 mL), whereupon the Fmoc-piperidine adduct precipitated as a white, voluminous solid. After stirring for 15 min, the suspension obtained was filtered and the solvent was removed under reduced pressure and the product was purified by HPLC. Colorless solid; yield: 4.00 mg (52%). Prep. HPLC: t_{R} =13.7 min. Anal. HPLC (NUCLEODUR C_{18} HTec EC, 150×10 mm ID, 5 μm): t_{R} =14.9 min. HRMS (ESI, pos.): calc. for $\text{C}_{94}\text{H}_{172}\text{N}_{29}\text{O}_{30}\text{S}_4^{3+}$ $[M+3\text{H}]^{3+}$ 771.7230; found 771.7240.

Zwitterionic (Orn- β -Ala)-(Lys- β -Ala)-(Lys- β -Ala)-(Orn- β -Ala) (*tert*-butylester) tetramer (140): This compound was prepared in three steps involving CuAAC, debenzoylation and Fmoc-deprotection. CuAAC was performed according to method G. Scale: 120 (27.5 mg, 13.4 μmol , 1.00 eq.), 3-(dimethyl(prop-2-yn-1-yl)ammonio)propane-1-sulfonate (16.5 mg, 80.6 μmol , 1.50 eq. per azide), CuI (1.33 μg , 6.98 μmol , 0.13 eq. per azide), sodium ascorbate (7.13 mg, 36.0 μmol , 0.68 eq. per azide), CH_3CN (2.0 mL). Colorless solid; yield: 25.7 mg (67%). Anal. HPLC (Nucleodur C_{18} HTec EC, 150×10 mm ID, 5 μm , $\text{H}_2\text{O}/\text{CH}_3\text{CN}$ 98:2+0.05% HCO_2H →5:95+0.05% HCO_2H , 15 min, 0.2 mL/min): t_{R} =20.3 min (product), t_{R} =16.6 min (product – Fmoc). HRMS (ESI, pos.): calc. for $\text{C}_{120}\text{H}_{192}\text{N}_{29}\text{O}_{30}\text{S}_4^{3+}$ $[M+3\text{H}-\text{Fmoc}]^{3+}$ 882.7763; found 882.7704. Debenzoylation and Fmoc-deprotection of this intermediate to title compound 140 was done according to method H. Scale: intermediate benzylhydroxamate

(7.80 mg, 2.72 μmol , 1.00 eq.), Pd/C (1.00 mg). After removing the solvent under reduced pressure, the residue was dissolved in demineralized H_2O (4 mL) and piperidine (1 mL), whereupon the Fmoc-piperidine adduct precipitated as a white, voluminous solid. After stirring for 15 min, the suspension obtained was filtered and the solvent was removed under reduced pressure and the product was purified by HPLC. Colorless solid; yield: 2.60 mg (42 %). Prep. HPLC: $t_{\text{R}} = 13.6$ min. Anal. HPLC (NUCLEODUR C_{18} HTec EC, 150×10 mm ID, $5 \mu\text{m}$): $t_{\text{R}} = 15.0$ min. HRMS (ESI, pos.): calc. for $\text{C}_{92}\text{H}_{168}\text{N}_{29}\text{O}_{30}\text{S}_4^{3+}$ $[\text{M} + 3\text{H}]^{3+}$ 762.3793; found 762.3804.

Complexation with Zr(IV): For the complexation of DFOB and the ligands 16 and 17 with zirconium, a solution of the chelator (600 μL , 0.0072 mM) in HCl(aq) (0.05 M) was added to a solution of ZrCl_4 (200 μL , 0.0216 mM) in HCl(aq) (0.05 M). While stirring at room temperature, the pH of the solution was adjusted to a value of 8.5–9.0 by adding a solution of Na_2CO_3 (0.05 M) followed by stirring for 90 min. Subsequent freeze-drying yielded a voluminous, colorless solid. The complexes obtained were identified by HPLC-MS (ESI, pos.). HPLC (NUCLEODUR C_{18} HTec EC, 150×10 mm ID, $5 \mu\text{m}$ particles, $\text{H}_2\text{O}/\text{CH}_3\text{CN}$ 98:2 + 0.05 % $\text{HCO}_2\text{H} \rightarrow 5:95$ + 0.05 % HCO_2H , 15 min, 0.2 mL/min).

Transchelation assay with 1000-fold excess of EDTA: The Zr complexes were dissolved in Milli-Q water (500 μL) and EDTA solution (100 μL , 1000-fold excess, 0.0432 mM) were added. The pH of the solution was adjusted to pH = 7 by adding HCl(aq) (0.05 M) and the solution was stored at room temperature. After 0 h, 2 h, 8 h and 24 h, 15 μL of the solution were analyzed by HPLC-MS (ESI, pos.). The amount of intact Zr complex was determined by integrating the EIC for the $[\text{M} + 3\text{H}]^{3+}$, $[\text{M} + 2\text{H} + \text{Na}]^{3+}$ and $[\text{M} + 2\text{H}]^{3+}$. HPLC (NUCLEODUR C_{18} HTec EC, 150×10 mm ID, $5 \mu\text{m}$ particles, $\text{H}_2\text{O}/\text{CH}_3\text{CN}$ 98:2 + 0.05 % $\text{HCO}_2\text{H} \rightarrow 5:95$ + 0.05 % HCO_2H , 15 min, 0.2 mL/min).

Transchelation assay of Zr-17a with 300-fold excess of DFO: A solution of Zr-17a (600 μL , 0.0072 mM) in HCl(aq) (0.05 M) was added to a solution of ZrCl_4 (200 μL , 0.0216 mM) in HCl(aq) (0.05 M). The pH of the solution was adjusted to 8.5–9.0 by adding Na_2CO_3 solution (0.05 M). The solution was incubated for 90 min at 37 °C. Subsequent freeze-drying yielded a voluminous, colorless solid. After dissolving in Milli-Q water (500 μL) DFO solution (100 μL , 300-fold excess, 0.0130 mM) was added. The pH of the solution was adjusted to pH = 7 by adding HCl(aq) (0.05 M) and the solution was stored at room temperature. After 0 h, 2 h, 8 h and 24 h, 15 μL of the solution were analyzed by HPLC-MS (ESI, pos.). The amount of intact Zr complex was determined by integrating the EIC for the $[\text{M} + 3\text{H}]^{3+}$, $[\text{M} + 2\text{H} + \text{Na}]^{3+}$ and $[\text{M} + 2\text{H}]^{3+}$. The value of the intact Zr complex measured after 0 h apply as reference. HPLC (NUCLEODUR C_{18} HTec EC, 150×10 mm ID, $5 \mu\text{m}$ particles, $\text{H}_2\text{O}/\text{CH}_3\text{CN}$ 98:2 + 0.05 % $\text{HCO}_2\text{H} \rightarrow 5:95$ + 0.05 % HCO_2H , 15 min, 0.2 mL/min).

Monitoring of Zr-complexation with chelator 17a: A solution of chelator 17a (600 μL , 0.0072 mM) in HCl(aq) (0.05 M) was added to a solution of ZrCl_4 (200 μL , 0.0216 mM) in HCl(aq) (0.05 M). The pH of the solution was adjusted to 8.5–9.0 by adding Na_2CO_3 solution (0.05 M) and the solution was incubated at 24 °C or 37 °C. After 0.0 h, 1.5 h, 3.0 h, 4.5 h and 6.0 h, 15 μL of the solution were analyzed by HPLC-MS (ESI, pos.). The amount of Zr complex formed was determined by integrating the EIC for the $[\text{M} + 3\text{H}]^{3+}$, $[\text{M} + 2\text{H} + \text{Na}]^{3+}$ and $[\text{M} + 2\text{H}]^{3+}$. HPLC (NUCLEODUR C_{18} HTec EC, 150×10 mm ID, $5 \mu\text{m}$ particles, $\text{H}_2\text{O}/\text{CH}_3\text{CN}$ 98:2 + 0.05 % $\text{HCO}_2\text{H} \rightarrow 5:95$ + 0.05 % HCO_2H , 15 min, 0.2 mL/min).

Acknowledgements

Open Access funding enabled and organized by Projekt DEAL.

Conflict of Interests

The authors declare no conflict of interest.

Data Availability Statement

The data that support the findings of this study are available from the corresponding author upon reasonable request.

Keywords: siderophores · Zr-complexes · DFOB · PET-imaging · zwitterions

- [1] D. Al Shaer, O. Al Musalmi, B. G. de la Torre, F. Albericio, *Eur. J. Med. Chem.* **2020**, *208*, 112791.
- [2] A. Khan, P. Singh, A. Srivastava, *Microbiol. Res.* **2018**, *212–213*, 103–111.
- [3] A. E. Fazary, *J. Chem. Eng. Data* **2005**, *50*, 888–895.
- [4] S. Dhungana, C. Ratledge, A. L. Crumbliss, *Inorg. Chem.* **2004**, *43*, 6274–6283.
- [5] R. Codd, *Coord. Chem. Rev.* **2008**, *252*, 1387–1408.
- [6] R. Codd, T. Richardson-Sanchez, T. J. Telfer, M. P. Gotsbacher, *ACS Chem. Biol.* **2018**, *13*, 11–25.
- [7] H. Bickel, G. E. Hall, W. Keller-Schierlein, V. Prelog, E. Vischer, A. Wettstein, *Helv. Chim. Acta* **1960**, *43*, 2129–2138.
- [8] Z. D. Liu, R. C. Hider, *Coord. Chem. Rev.* **2002**, *232*, 151–171.
- [9] M. Hofmann, G. Retamal-Morales, D. Tischler, *Nat. Prod. Rep.* **2020**, *37*, 1262–1283.
- [10] M. Petrik, C. Zhai, H. Haas, C. Decristoforo, *Clin. Transl. Imaging* **2017**, *5*, 15–27.
- [11] P. Klahn, M. Bronstrup, *Nat. Prod. Rep.* **2017**, *34*, 832–885.
- [12] a) M. Pagani, S. Stone-Elander, S. A. Larsson, *Eur. J. Nucl. Med.* **1997**, *24*, 1301–1327; b) J. L. Klein, M. N. Ling, P. K. Lechner, K. A. Kopher, R. A. Rostock, S. E. Order, *Int. J. Radiat. Oncol. Biol. Phys.* **1985**, *11*, 1489–1494.
- [13] a) J. P. Holland, Y. Sheh, J. S. Lewis, *Nucl. Med. Biol.* **2009**, *36*, 729–739; b) A. L. Wooten, E. Madrid, G. D. Schweitzer, L. A. Lawrence, E. Mebrahtu, B. C. Lewis, S. E. Lapi, *Appl. Sci.* **2013**, *3*, 593–613.
- [14] G. Fischer, U. Seibold, R. Schirmacher, B. Wängler, C. Wängler, *Molecules* **2013**, *18*, 6469–6490.
- [15] J. P. Holland, V. Divilov, N. H. Bander, P. M. Smith-Jones, S. M. Larson, J. S. Lewis, *J. Nucl. Med.* **2010**, *51*, 1293–1300.
- [16] a) D. S. Abou, T. Ku, P. M. Smith-Jones, *Nucl. Med. Biol.* **2011**, *38*, 675–681; b) T. K. Nayak, K. Garmestani, D. E. Milenic, M. W. Brechbiel, *J. Nucl. Med.* **2012**, *53*, 113–120; c) M. A. Deri, B. M. Zeglis, L. C. Francesconi, J. S. Lewis, *Nucl. Med. Biol.* **2013**, *40*, 3–14; d) M. A. Deri, S. Ponnala, P. Kozlowski, B. P. Burton-Pye, H. T. Cicek, C. Hu, J. S. Lewis, L. C. Francesconi, *Bioconjugate Chem.* **2015**, *26*, 2579–2591; e) P. Laverman, T. van der Geest, S. Y. Terry, D. Gerrits, B. Walgreen, M. M. Helsen, T. K. Nayak, A. Freimoser-Grundschober, I. Waldhauer, R. J. Hosse, E. Moessner, P. Umana, C. Klein, W. J. Oyen, M. I. Koenders, O. C. Boerman, *J. Nucl. Med.* **2015**, *56*, 778–783; f) W. E. Meijs, H. J. Haisma, R. P. Klok, F. B. van Gog, E. Kievit, H. M. Pinedo, J. D. Herscheid, *J. Nucl. Med.* **1997**, *38*, 112–118.
- [17] a) N. B. Bhatt, D. N. Pandya, T. J. Wadas, *Molecules* **2018**, *23*, 638–661; b) I. V. J. Feiner, M. Brandt, J. Cowell, T. Demuth, D. Vugts, G. Gasser, T. L. Mindt, *Cancers (Basel)* **2021**, *13*, 4466–4488.
- [18] a) C. Zhai, D. Summer, C. Rangger, G. M. Franssen, P. Laverman, H. Haas, M. Petrik, R. Haubner, C. Decristoforo, *Mol. Pharm.* **2015**, *12*, 2142–2150; b) C. J. Adams, J. J. Wilson, E. Boros, *Mol. Pharm.* **2017**, *14*, 2831–2842.
- [19] a) L. Allott, C. Da Pieve, J. Meyers, T. Spinks, D. M. Ciobota, G. Kramer-Marek, G. Smith, *Chem. Commun.* **2017**, *53*, 8529–8532; b) D. L. White, P. W. Durbin, N. Jeung, K. N. Raymond, *J. Med. Chem.* **1988**, *31*, 11–18.
- [20] M. Patra, A. Bauman, C. Mari, C. A. Fischer, O. Blacque, D. Haussinger, G. Gasser, T. L. Mindt, *Chem. Commun.* **2014**, *50*, 11523–11525.

- [21] R. Raavé, G. Sandker, P. Adumeau, C. B. Jacobsen, F. Mangin, M. Meyer, M. Moreau, C. Bernhard, L. Da Costa, A. Dubois, V. Goncalves, M. Gustafsson, M. Rijpkema, O. Boerman, J.-C. Chambron, S. Heskamp, F. Denat, *Eur. J. Nucl. Med. Mol. Imaging* **2019**, *46*, 1966–1977.
- [22] E. K. Sarbisheh, A. K. Salih, S. J. Raheem, J. S. Lewis, E. W. Price, *Inorg. Chem.* **2020**, *59*, 11715–11727.
- [23] A. K. Salih, S. J. Raheem, M. D. Garcia, W. K. Ahliahonu, E. W. Price, *Inorg. Chem.* **2022**, *61*, 20964–20976.
- [24] S. E. Rudd, P. Roselt, C. Cullinane, R. J. Hicks, P. S. Donnelly, *Chem. Commun.* **2016**, *52*, 11889–11892.
- [25] a) U. Seibold, B. Wängler, C. Wängler, *ChemMedChem* **2017**, *12*, 1555–1571; b) F. Guerard, Y. S. Lee, M. W. Brechbiel, *Chem. Eur. J.* **2014**, *20*, 5584–5591; c) W. Tieu, T. Lifa, A. Katsifis, R. Codd, *Inorg. Chem.* **2017**, *56*, 3719–3728.
- [26] D. Summer, J. Garousi, M. Oroujeni, B. Mitran, K. G. Andersson, A. Vorobyeva, J. Löfblom, A. Orlova, V. Tolmachev, C. Decristoforo, *Mol. Pharm.* **2018**, *15*, 175–185.
- [27] a) D. J. Vugts, C. Klaver, C. Sewing, A. J. Poot, K. Adamzek, S. Huegli, C. Mari, G. W. M. Visser, I. E. Valverde, G. Gasser, T. L. Mindt, G. van Dongen, *Eur. J. Nucl. Med. Mol. Imaging* **2017**, *44*, 286–295; b) H. Damerow, R. Hubner, B. Judmann, R. Schirmacher, B. Wängler, G. Fricker, C. Wängler, *Cancers (Basel)* **2021**, *13*, 6349–6376.
- [28] H. Damerow, X. Cheng, V. von Kiedrowski, R. Schirmacher, B. Wängler, G. Fricker, C. Wängler, *Pharmaceutica* **2022**, *14*, 2114–2129.
- [29] S. Heskamp, R. Raavé, O. Boerman, M. Rijpkema, V. Goncalves, F. Denat, *Bioconjugate Chem.* **2017**, *28*, 2211–2223.
- [30] a) C. J. M. Brown, M. P. Gotsbacher, R. Codd, *Aust. J. Chem.* **2020**, *73*, 969–978; b) M. Brandt, J. Cowell, M. L. Aulsebrook, G. Gasser, T. L. Mindt, *JBIC J. Biol. Inorg. Chem.* **2020**, *25*, 789–796; c) T. Richardson-Sanchez, W. Tieu, M. P. Gotsbacher, T. J. Telfer, R. Codd, *Org. Biomol. Chem.* **2017**, *15*, 5719–5730.
- [31] J. Notni, H. J. Wester, *Chemistry (Easton)* **2016**, *22*, 11500–11508.
- [32] a) E. Kriemen, M. Holzapfel, E. Ruf, J. Rehbein, W. Maisson, *Eur. J. Inorg. Chem.* **2015**, *2015*, 5368–5378; b) E. Kriemen, E. Ruf, U. Behrens, W. Maisson, *Chem. Asian J.* **2014**, *9*, 2197–2204; c) M. Holzapfel, T. Baldau, S. Kerpa, G. Guadalupe, B. Qi, Y. Liu, W. J. Parak, W. Maisson, *Eur. J. Inorg. Chem.* **2022**, *2022*, e202200432.
- [33] Z. Baranyai, D. Reich, A. Vagner, M. Weisenstein, I. Toth, H. J. Wester, J. Notni, *Dalton Trans.* **2015**, *44*, 11137–11146.
- [34] J. P. Holland, *Inorg. Chem.* **2020**, *59*, 2070–2082.
- [35] a) E. Farkas, P. Buglyó, É. A. Enyedy, V. A. Gerlei, A. M. Santos, *Inorg. Chim. Acta* **2002**, *339*, 215–223; b) E. Farkas, D. Batka, Z. Pataki, P. Buglyó, M. A. Santos, *Dalton Trans.* **2004**, 1248–1253.
- [36] A. R. Poreddy, O. F. Schall, T. A. Osiek, J. R. Wheatley, D. D. Beusen, G. R. Marshall, U. Slomczynska, *J. Comb. Chem.* **2004**, *6*, 239–254.
- [37] a) H. S. Choi, K. Nasr, S. Alyabyev, D. Felth, J. H. Lee, S. H. Kim, Y. Ashitate, H. Hyun, G. Patonay, L. Strekowski, M. Henary, J. V. Frangioni, *Angew. Chem. Int. Ed. Engl.* **2011**, *50*, 6258–6263; b) H. S. Choi, S. L. Gibbs, J. H. Lee, S. H. Kim, Y. Ashitate, F. Liu, H. Hyun, G. Park, Y. Xie, S. Bae, M. Henary, J. V. Frangioni, *Nat. Biotechnol.* **2013**, *31*, 148–153.
- [38] a) C. Zhai, S. He, Y. Ye, C. Rangger, P. Kaeopookum, D. Summer, H. Haas, L. Kremser, H. Lindner, J. Foster, J. Sosabowski, C. Decristoforo, *Biomol. Eng.* **2019**, *9*; b) D. N. Pandya, N. Bhatt, H. Yuan, C. S. Day, B. M. Ehrmann, M. Wright, U. Bierbach, T. J. Wadas, *Chem. Sci.* **2017**, *8*, 2309–2314; c) M. A. Deri, S. Ponnala, B. M. Zeglis, G. Pohl, J. J. Dannenberg, J. S. Lewis, L. C. Francesconi, *J. Med. Chem.* **2014**, *57*, 4849–4860.
- [39] J. L. Suh, B. Watts, J. I. Stuckey, J. L. Norris-Drouin, S. H. Cholensky, B. M. Dickson, Y. An, S. Mathea, E. Salah, S. Knapp, A. Khan, A. T. Adams, B. D. Strahl, C. A. Sagum, M. T. Bedford, L. I. James, D. B. Kireev, S. V. Frye, *Biochemistry* **2018**, *57*, 2140–2149.
- [40] a) C. A. DeForest, D. A. Tirrell, *Nat. Mater.* **2015**, *14*, 523–531; b) H. Sun, X. Peng, *Bioconjugate Chem.* **2013**, *24*, 1226–1234.
- [41] a) Y. Kira, Y. Okazaki, T. Sawada, M. Takafuji, H. Ihara, *Amino Acids* **2010**, *39*, 587–597; b) C. De Cola, A. Manicardi, R. Corradini, I. Izzo, F. De Riccardis, *Tetrahedron* **2012**, *68*, 499–506.
- [42] S.-L. Niu, G. Ulrich, P. Retailleau, J. Harrowfield, R. Ziessel, *Tetrahedron Lett.* **2009**, *50*, 3840–3844.
- [43] A. J. Rosenberg, D. A. Clark, *Org. Lett.* **2012**, *14*, 4678–4681.
- [44] T. Usuki, T. Sugimura, A. Komatsu, Y. Koseki, *Org. Lett.* **2014**, *16*, 1672–1675.
- [45] J. R. Heemstra, C. T. Walsh, E. S. Sattely, *J. Am. Chem. Soc.* **2009**, *131*, 15317–15329.

Manuscript received: February 24, 2023
 Revised manuscript received: April 12, 2023
 Accepted manuscript online: April 14, 2023
 Version of record online: April 27, 2023

5.2 Transfer to SPPS and Synthesis of complex DFO* analogs with side chains

The promising results obtained with the structures described in Section 5.1 provided the impetus to transfer the synthesis to a solid-phase peptide synthesis (SPPS) approach. The solution-phase synthesis presented in that section is associated with considerable purification effort, resulting in a high workload, substantial time consumption, and extensive use of solvents and reagents. As previously discussed in Section 3.2, the advantages of SPPS - particularly in terms of efficiency and scalability - become even more apparent when considering the complexity of the nine AZA-DFOB and AZA-DFO* chelators synthesized.

Accordingly, the key innovation of the study presented in this section is the implementation of a microwave-assisted solid-phase synthesis protocol, which markedly reduces the overall synthetic burden compared to the previously employed multi-step liquid-phase approach. Whereas traditional methods required up to 14 synthetic steps, each followed by individual purification, the strategy outlined here allows the efficient preparation of isopeptidic DFO* analogues (referred to as ipDFO* in this work) within a matter of hours. The modular nature of SPPS inherently supports structural variation and customization.

The monomers required for this SPPS were synthesized in short 3 - 4 step sequences from inexpensive starting materials such as *tert*-butyl 4-bromobutanoate, affording high yields. The initial synthetic approach involved the coupling of *O*-benzyl protected hydroxylamine with carboxylic acids to form *O*-benzyl hydroxamic acid derivatives, analogous to conventional peptide bond formation. Although the crude product obtained after resin cleavage exhibited the expected mass by HPLC-MS, its purity was insufficient for further applications. This coupling step had already been identified as a critical point in earlier work. After extensive screening of various coupling reagents, PyOxim® was determined to be the optimal reagent, delivering the highest product purity and yield.

In addition, AZA-ipDFO* analogues bearing azide-containing side chains - structurally analogous to those described in Section 5.1 - were successfully synthesized. For this purpose, a novel monomer synthesis was developed based on Boc-allylglycine as the starting material.

In conclusion, the results demonstrate that solid-phase synthesis constitutes an efficient and scalable method for the preparation of octadentate ipDFO* analogues, offering significant advantages in terms of speed, purity, and synthetic flexibility.

Title: Mixed Liquid and Solid Phase Synthesis of Isopeptidic Desferrioxamine Analogues for Complexation of Zirconium

Authors: Outzen, L., Nguyen, H. D., Ludolfs, D., Maison, W.

Type: Research Article

Journal: European Journal of Organic Chemistry

Year: 2024

Volume: 27

Issue: 29

Pages: e202400266

DOI: 10.1002/ejoc.202400266

Number of Pages: 5

Submitted: 11.03.2024

Accepted: 10.06.2024

Mixed Liquid and Solid Phase Synthesis of Isopeptidic Desferrioxamine Analogues for Complexation of Zirconium

Lasse Outzen,^[a] Hoang Duc Nguyen,^[a] Darius Ludolfs,^[a] and Wolfgang Maison^{*,[a]}

⁸⁹Zr has a number of advantageous properties for PET-imaging, but optimal chelators for its widespread clinical application still need to be found. Tetrahydroxamates derived from the natural siderophore DFOB are promising candidates in this context. This study describes a solid-phase approach to isopeptide analogs of DFOB (termed ipDFO*) with four hydroxamate groups for stable Zr(IV)-chelation. The route uses either commercial or easily available Fmoc-protected precursors and allows the synthesis of ipDFO* and clickable AZA-ipDFO* derivatives in only a few hours. The solid-phase synthesis

reduces the workload for the synthesis of ipDFO* and AZA-ipDFO* derivatives thus significantly compared to a previous multistep solution synthesis. The route is also modular and allows the synthesis of various ipDFO* derivatives with variation in the spacer length between the hydroxamate groups. This spacing is a critical parameter for finding the optimal chelator for hard metal cations like Zr(IV). It might thus help to speed up the search for an ideal Zr-chelator for PET-imaging and might also allow the extension to other metal cations of different size.

Introduction

The radioisotope ⁸⁹Zr has gained interest as a tracer for medical imaging via PET in recent years.^[1] The half-life of 78.4 h or 3.27 d fits well to the biological half-lives of antibodies and is advantageous with respect to reagent processing and also for background reduction *in vivo* due to complete elimination of non-targeted tracer.^[2] Another attractive feature of ⁸⁹Zr is its clean decay to ⁸⁹Y. Initially, ⁸⁹Zr decays to a metastable ^{89m}Y species, emitting β⁺ particles with 22.3% and an EC fraction of 76.6%.^[2b] Further decay of ^{89m}Y to the stable ⁸⁹Y proceeds with the emission of a gamma photon with an energy of 909.9 keV. The wavelength of the gamma photon is thus clearly separated from the two photons produced during the annihilation process of positrons and electrons during a PET measurement. The relatively high gamma energy is also a disadvantage of ⁸⁹Zr. However, the favorable half-life and the relatively low average positron energy of 395.5 keV, which has a positive influence on the spatial resolution in PET measurements typically compensate this disadvantage.^[2b] The supply of ⁸⁹Zr has become reliable in a clinical context and in research due to automated production and cleaning protocols.^[3] The ⁸⁹Zr isotope can be obtained from naturally occurring ⁸⁹Y by bombarding it with protons via a (p,n) reaction. After further work-up and purification via a hydroxamate column, ⁸⁹Zr can then be obtained with a purity of > 99.99% and a yield of > 94%.^[3b] In

consequence, ⁸⁹Zr is increasingly used for imaging particularly in immunoPET tracers.^[4]

A major drawback of Zr for imaging is its complicated complex chemistry. Most Zr-chelators are hydroxamate derivatives which are preferentially binding to hard Lewis acids such as Zr(IV).^[5] A good example is desferrioxamine B (DFOB) (Figure 1),^[6] a natural siderophore, which is used by bacteria, fungi and graminaceous plants to sequester Fe(III) from the environment.^[7] DFOB has a molar mass of 560 g/mol, a linear polyamide backbone structure with three hydroxamic acids and a free terminal amine.^[8] It allows the formation of ⁸⁹Zr-complexes in 30–60 min at room temperature and is therefore suitable for application with proteins or other sensitive targeting vectors.^[5a,9] With three hydroxamic acids in the backbone structure, DFOB is a hexadentate chelator and does

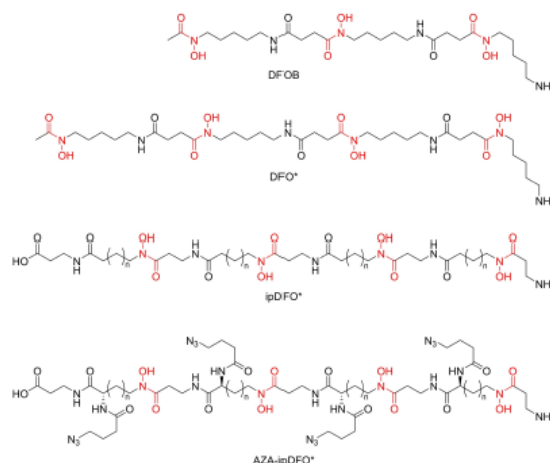


Figure 1. Structure of the natural siderophore DFOB and octadentate derivatives ipDFO*, AZA-ipDFO* developed for Zr-chelation.

[a] L. Outzen, H. Duc Nguyen, D. Ludolfs, W. Maison
Department of Chemistry, University of Hamburg, Bundesstrasse 45, 20146 Hamburg, Germany
E-mail: wolfgang.maison@uni-hamburg.de

Supporting information for this article is available on the WWW under <https://doi.org/10.1002/ejoc.202400266>

© 2024 The Authors. European Journal of Organic Chemistry published by Wiley-VCH GmbH. This is an open access article under the terms of the Creative Commons Attribution License, which permits use, distribution and reproduction in any medium, provided the original work is properly cited.

thus not fully saturate the coordination sphere of Zr(IV), which leads to transmetallation and release of ^{89}Zr *in vivo*.^[2a,10] A number of octadentate Zr-chelators have been introduced in the last years to address this lack of complex stability.^[11] Examples include DFO*,^[12] DFOB-PPH and DFOB-PPH⁶O⁶.^[13] Orn4-hx,^[14] DFO-HOPO,^[15] DFOcyclo*,^[16] DFO₂,^[17] DFO₂p,^[18] DFO-Em,^[19] DFO-Km,^[20] oxoDFO*,^[21] DFOB-O₍₁₋₃₎,^[22] H3DFOSqOEt^[23] and macrocyclic octadentate DFO-analogs.^[24] Many of these chelators are derived from the DFOB-scaffold. This strategy keeps the synthetic effort low, but it also limits the introduction of additional functionality or the variation in hydroxamate spacing. The 9-atom spacer in DFOB is optimized to bind Fe(III) but it might be suboptimal for Zr(IV) binding.^[24a,b]

Isopeptide DFO-analogs like ipDFO* and AZA-ipDFO* were therefore recently introduced.^[25] They allow variation in hydroxamate spacing and thus a finetuning of binding properties for various hard metal cations. In addition, AZA-ipDFO* can be conjugated to further groups *via* copper(I)-catalyzed azide-alkyne cycloaddition (CuAAC) or strain-promoted copper-free variants.^[25-26] These “clickable” chelators^[27] can be used as a multimerization platform or for conjugation of various functionalities such as zwitterions to improve water solubility and the stealth properties of the reagents.^[25,28] Moreover, AZA-ipDFO* derivatives have been shown to form stable Zr-complexes. In total nine different AZA-ipDFO and AZA-ipDFO* analogs with different hydroxamate spacing were synthesized *via* multistep solution phase syntheses.^[25] The synthetic effort undertaken to prepare these structures was considerable and included up to 14 steps for each derivative. A transfer of the synthesis to a solid phase would be advantageous to unfold the potential of the isopeptide backbone structure and, on the long term, would also be good for GMP production of the chelators for use in the clinic. However, the transfer of the solution strategy to a

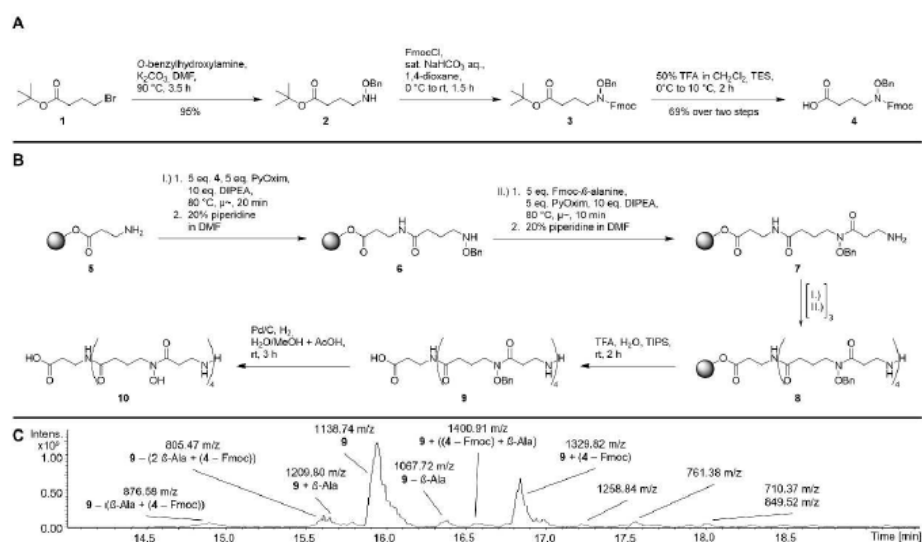
solid phase is not trivial due to notoriously difficult coupling steps involved and the high density of functional groups, which require a sophisticated protection scheme.

In this report we present a microwave-assisted solid phase synthesis (SPS) of isopeptide DFO* analogs ipDFO* and their clickable AZA-derivatives AZA-ipDFO*. The solid phase protocol allows the fast preparation of the chelators in good purity. It might thus help to develop tailored chelators for radiochemical application of hard metal cations like Zr(IV).

Results and Discussion

The target structures 3 and 4 have a regular isopeptide backbone structure and can therefore be prepared from two ω -amino acid precursors. One of them is commercially available Fmoc- β -alanine. Alternatives would be glycine and γ -amino butyric acid (GABA). However, glycine-based DFOB-analogs are known to be unstable.^[29] GABA, on the other hand, tends to form the corresponding butyrolactam and might therefore also complicate the synthesis.

The second precursor is a hydroxylamine derivative of a ω -amino acid which is not commercially available. In our previous solution phase protocol, this motif was prepared *via* oxidation of an appropriate amino acid precursor with benzoylperoxide. This approach generates a benzoyl-protected hydroxylamine, which needs to be transferred to a benzyl-protected hydroxylamine at a later stage of the synthesis. An alternative and more efficient synthetic strategy to the required benzyl- and Fmoc-protected hydroxylamine 4 involved the conversion of the bromide 1 with *O*-benzylhydroxylamine as outlined in Scheme 1A. Subsequent Fmoc-protection and cleavage of the *tert*-butyl ester with TFA gave 4 in excellent yield. We focused in



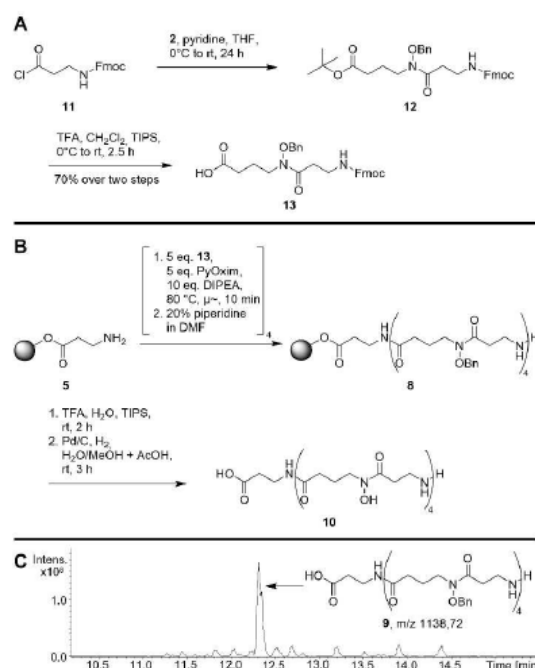
Scheme 1. A: Synthetic scheme for the preparation of the Bn- and Fmoc-protected coupling precursor 4 for solid phase synthesis. B: Solid phase protocol of the immobilized ipDFO* 8 and final cleavage/deprotection to 10. C: LC-MS analysis of the crude reaction product 9.

this study on the butyric acid precursor **1**, but the same protocol would be easily adaptable to other bromo acid esters with different chain length. The combination of β -alanine and aminobutyric acid leads to a short hydroxamate spacing of 7 atoms in the ipDFO* target compound **10**. In a previous study, the ornithine based AZA-ipDFO* (spacing of eight atoms between two hydroxamic acids) had led to better complexation properties with Zr(IV) than a lysine-based AZA-ipDFO* derivative (spacing of nine atoms between two hydroxamic acids).^[25] An even shorter spacing of hydroxamates by seven atoms in AZA-ipDFO* was chosen in this study to expand this series.^[25] Earlier work of Guerard *et al.* suggested that a spacing of at least seven atoms between neighboring hydroxamates must be present in DFO derivatives for a good complexation of Zr(IV).^[24b] In addition, CTH36, a cyclic DFO* derivative prepared by Seibold *et al.* had a spacing of seven atoms between the hydroxamates and showed very promising *in vitro* stability of its Zr-complex.^[9b,24a]

In our earlier solution phase protocol, we had identified the coupling reaction to the hydroxylamine motif to be the most problematic step. Therefore, several different coupling reagents such as EDC/HOBt, HBTU/HOBt, HATU/HOAt, PyBOP, BTFPH, PyOxim and preactivation as acid chloride and different coupling conditions were tested on the solid phase to optimize this step (for further Information see Table S1 and the preceding paragraph in the SI). The best results were obtained with PyOxim as a coupling reagent, a microwave assisted double coupling and 5 eq. acid.

The solid phase synthesis of **10** started with Wang resin preloaded with Fmoc- β -alanine **5** (Scheme 1B). Wang resin was chosen in the first experiments, because it is relatively cheap and has a high chemical stability, which can be advantageous for later conversion of the chelators on the solid phase. Sequential coupling of hydroxylamine **4** or Fmoc- β -alanine gave finally tetrahydroxamate **8** bound to the Wang resin. Cleavage with TFA gave the benzyl-protected chelator **9**, which was debenzylated to ipDFO* **10** in a final step. The chromatogram of the crude chelator ipDFO* **9** is shown in Scheme 1C and reveals that **9** is the major product, which was finally purified by HPLC. However, a number of impurities were also identified by LC-MS. The majority are deletion and insertion sequences next to some unknown side-products. The problematic couplings to the hydroxylamines lead to a relatively complex mixture of products which are challenging to separate by HPLC. An alternative approach was therefore developed avoiding these couplings on the solid phase. We hoped this would lead to cleaner solid-phase conversions and thus an easier purification of the final product. The coupling of hydroxylamine **2** to Fmoc- β -alanine was therefore performed in solution with the acid chloride **11** to give the fully orthogonally protected precursor **12** (Scheme 2A). Cleavage of the *tert*-butyl ester by TFA produced the final coupling precursor **13** for the solid phase synthesis with an overall yield of 67% over three steps.

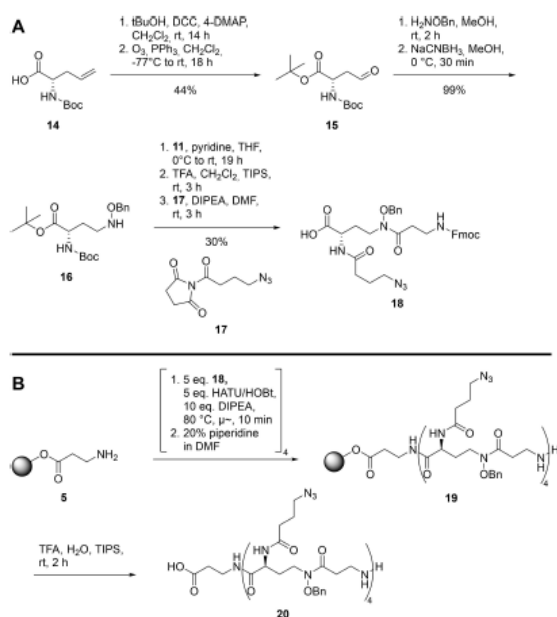
The solid-phase synthesis with Wang resin preloaded with Fmoc- β -alanine and acid **13** gave target compound **8** attached to the solid phase (Scheme 2B). All couplings were performed



Scheme 2. A: Synthetic scheme for the preparation of the Bn- and Fmoc-protected coupling precursor for solid phase synthesis **13**. **B:** Solid phase protocol of the immobilized ipDFO* **8** and final cleavage/deprotection to **10**. **C:** LC-MS analysis of the crude reaction product **9**.

as double couplings for 10 min at 80 °C with 5 eq. acid **13**, 5 eq. PyOxim and 10 eq. DIPEA under microwave heating. Cleavage and deprotection gave chelator **10** with very good purity as indicated by a single major product peak in the LC/MS chromatogram of the crude product (Scheme 2C). The precoupling of the hydroxylamine **2** in solution led thus to a significantly cleaner solid-phase syntheses. It is notable, that chelator **10** is reasonably soluble in water due to the terminal amino group and the carboxylic acid.

The successful solid-phase synthesis was applied to the clickable AZA-ipDFO* analogs **18**. A new monomer synthesis was developed for this purpose (Scheme 3A). The synthesis started with commercially available Boc-allylglycine **14**, which was converted to the corresponding *tert*-butyl ester and oxidized to aldehyde **15** by ozonolysis. A reductive amination with *O*-benzyl hydroxylamine and sodium cyanoborohydride gave **16**. Adjustment of the pH value to 2–3 was crucial in this step to achieve complete conversion. After coupling with **11** the *tert*-butyl and the Boc protecting group were removed under acidic conditions with TFA and the NHS ester **17** was then coupled to give the coupling precursor **18** for solid phase synthesis. The solid phase synthesis was then carried out with monomer **18** according to Scheme 3B. A Wang resin preloaded with Fmoc- β -alanine **5** was used and repeated couplings of **18** led to the tetrahydroxamate **19** bound to the solid phase. Each coupling step was performed at 80 °C for 10 min with 5 eq. acid



Scheme 3. A: Synthetic scheme for the preparation of the Bn- and Fmoc-protected coupling precursor **18** for solid phase synthesis. **B:** Solid phase protocol of the immobilized chelator **19** and cleavage to benzyl protected AZA–ipDFO* **20**.

18, 5 eq. HATU/HOBt and 10 eq. DIPEA with microwave heating. After cleavage with TFA the benzyl protected final AZA–ipDFO* **20** was obtained in good purity.

In a previous study, AZA–ipDFO* derivatives like **20** were prepared over 14 steps in a tedious solution phase synthesis, which required extensive chromatographic purification steps.^[25] It is notable, that this previous work contains a protocol for the debenzoylation of the protected chelators. The solid phase approach presented here allows the rapid synthesis of AZA–ipDFO* analogs in only a few hours from precursors like **18**.

Conclusions

Derivatives of the natural siderophore DFOB with four hydroxamate groups allow the stable complexation of ⁸⁹Zr(IV) and are thus attractive for application in PET-imaging. In this study, a solid-phase approach to the synthesis of isopeptide DFO derivatives (ipDFO*) was developed. The backbone of these chelators is composed of commercially available β -alanine and a hydroxylamine derivative. Fmoc- β -alanine and a Fmoc-protected hydroxylamine **4** was therefore used for the solid-phase synthesis. The latter was synthesized in three steps from 4-bromobutyric acid. The solid-phase synthesis was performed on Wang resin preloaded with Fmoc- β -alanine. Key steps are the repeated couplings of Fmoc- β -alanine to the terminal hydroxylamines. This step is best performed as a double

coupling with PyOxim as a coupling reagent. It was found to be advantageous to perform the problematic coupling of Fmoc- β -alanine to hydroxylamine **4** in solution with Fmoc- β -alanine acid chloride and to use the resulting coupling precursor **13** for solid-phase synthesis. With this improved protocol, ipDFO* **10** and also the clickable derivative AZA–ipDFO* **20** was prepared in good purity.

With the development of a solid-phase synthesis the workload for the synthesis of ipDFO* and AZA–ipDFO* derivatives was significantly reduced to only a few hours for each chelator. The route is also modular and allows the synthesis of various ipDFO* derivatives with variation in the spacer length between the hydroxamate groups. This spacing is a critical parameter to find the optimal chelator for hard metal cations like Zr(IV). It might thus help to speed up the search for an ideal Zr-chelator for PET-imaging and might also allow the extension to other metal cations of different size.

Supporting Information Summary

The authors have cited additional references in the Supporting Information.^[30–33]

Acknowledgements

We acknowledge proofreading of the manuscript by Antje Wagner. Open Access funding enabled and organized by Projekt DEAL.

Conflict of Interests

The authors declare no conflict of interest.

Data Availability Statement

The data that support the findings of this study are available in the supplementary material of this article.

Keywords: Siderophores · Zr-complexes · DFOB · Solid phase synthesis

- [1] Y. W. Jauw, C. W. Menke-van der Houven van Oordt, O. S. Hoekstra, N. H. Hendrikse, D. J. Vugts, J. M. Zijlstra, M. C. Huisman, G. A. van Dongen, *Front Pharmacol* **2016**, *7*, 131.
- [2] a) J. P. Holland, V. Divilov, N. H. Bander, P. M. Smith-Jones, S. M. Larson, J. S. Lewis, *J. Nucl. Med.* **2010**, *51*, 1293–1300; b) M. Pagani, S. Stone-Elander, S. A. Larsson, *Eur. J. Nucl. Med.* **1997**, *24*, 1301–1327.
- [3] a) E. T. Sarcan, M. Silindir-Gunay, A. Y. Ozer, N. Hartman, *J. Radioanal. Nucl. Chem.* **2021**, *330*, 15–28; b) I. Verel, G. W. M. Visser, R. Boellaard, M. Stigter-van Walsum, G. B. Snow, G. A. M. S. van Dongen, *J. Nucl. Med.* **2003**, *44*, 1271; c) A. L. Wooten, E. Madrid, G. D. Schweitzer, L. A. Lawrence, E. Mebrahtu, B. C. Lewis, S. E. Lapi, *Appl. Sci.* **2013**, *3*, 593–613; d) J. P. Holland, Y. Sheh, J. S. Lewis, *Nucl. Med. Biol.* **2009**, *36*, 729–739.
- [4] W. Wei, Z. T. Rosenkrans, J. Liu, G. Huang, Q. Y. Luo, W. Cai, *Chem Rev* **2020**, *120*, 3787–3851.

- [5] a) M. Hofmann, G. Retamal-Morales, D. Tischler, *Nat. Prod. Rep.* **2020**, *37*, 1262–1283; b) R. Codd, *Coord. Chem. Rev.* **2008**, *252*, 1387–1408.
- [6] a) R. Codd, T. Richardson-Sanchez, T. J. Telfer, M. P. Gotsbacher, *ACS Chem. Biol.* **2018**, *13*, 11–25; b) W. E. Meijs, J. D. Herscheid, H. J. Haisma, H. M. Pinedo, *Int. J. Rad. Appl. Instrum. A* **1992**, *43*, 1443–1447.
- [7] R. C. Hider, X. Kong, *Nat. Prod. Rep.* **2010**, *27*, 637–657.
- [8] D. Bellotti, M. Remelli, *Molecules* **2021**, *26*.
- [9] a) G. Fischer, U. Seibold, R. Schirrmacher, B. Wängler, C. Wängler, *Molecules* **2013**, *18*, 6469–6490; b) J. P. Holland, *Inorg. Chem.* **2020**, *59*, 2070–2082; c) P. J. Blower, R. Cusnir, A. Darwesh, N. J. Long, M. T. Ma, B. E. Osborne, T. W. Price, J. Pellico, G. Reid, R. Southworth, G. J. Stasiuk, S. Y. A. Terry, R. T. M. de Rosales, in *Advances in Inorganic Chemistry* (Eds: C. D. Hubbard, R. van Eldik), Vol. 78, Academic Press, **2021**, 1–35.
- [10] a) D. S. Abou, T. Ku, P. M. Smith-Jones, *Nucl. Med. Biol.* **2011**, *38*, 675–681; b) T. K. Nayak, K. Garmestani, D. E. Milenic, M. W. Brechbiel, *J. Nucl. Med.* **2012**, *53*, 113–120; c) M. A. Deri, B. M. Zeglis, L. C. Francesconi, J. S. Lewis, *Nucl. Med. Biol.* **2013**, *40*, 3–14; d) M. A. Deri, S. Ponnala, P. Kozlowski, B. P. Burton-Pye, H. T. Cicek, C. Hu, J. S. Lewis, L. C. Francesconi, *Bioconjug. Chem.* **2015**, *26*, 2579–2591; e) P. Laverman, T. van der Geest, S. Y. Terry, D. Gerrits, B. Walgreen, M. M. Helsen, T. K. Nayak, A. Freimoser-Grundschober, I. Waldhauer, R. J. Hosse, E. Moessner, P. Umana, C. Klein, W. J. Oyen, M. I. Koenders, O. C. Boerman, *J. Nucl. Med.* **2015**, *56*, 778–783; f) W. E. Meijs, H. J. Haisma, R. P. Klok, F. B. van Gog, E. Kievit, H. M. Pinedo, J. D. Herscheid, *J. Nucl. Med.* **1997**, *38*, 112–118; g) G. Sormani, A. Korde, A. Rodriguez, M. Denecke, A. Hassanali, *ACS Omega* **2023**, *8*, 36032–36042.
- [11] V. B. Bubenshchikov, A. A. Larenkov, *Russ. J. Coord. Chem.* **2022**, *48*, 675–695.
- [12] M. Patra, A. Bauman, C. Mari, C. A. Fischer, O. Blacque, D. Haussinger, G. Gasser, T. L. Mindt, *Chem. Commun.* **2014**, *50*, 11523–11525.
- [13] C. J. M. Brown, M. P. Gotsbacher, R. Codd, *Aust. J. Chem.* **2020**, *73*, 969–978.
- [14] C. J. Adams, J. J. Wilson, E. Boros, *Mol. Pharm.* **2017**, *14*, 2831–2842.
- [15] a) L. Allott, C. Da Pieve, J. Meyers, T. Spinks, D. M. Ciobota, G. Kramer-Marek, G. Smith, *Chem. Commun.* **2017**, *53*, 8529–8532; b) D. L. White, P. W. Durbin, N. Jeung, K. N. Raymond, *J. Med. Chem.* **1988**, *31*, 11–18.
- [16] R. Raavé, G. Sandker, P. Adumeau, C. B. Jacobsen, F. Mangin, M. Meyer, M. Moreau, C. Bernhard, L. Da Costa, A. Dubois, V. Goncalves, M. Gustafsson, M. Rijpkema, O. Boerman, J.-C. Chambon, S. Heskamp, F. Denat, *Eur. J. Nucl. Med. Mol. Imaging* **2019**, *46*, 1966–1977.
- [17] E. K. Sarbisheh, A. K. Salih, S. J. Raheem, J. S. Lewis, E. W. Price, *Inorg. Chem.* **2020**, *59*, 11715–11727.
- [18] E. Khozeimeh Sarbisheh, K. L. Summers, A. K. Salih, J. J. H. Cotelesage, A. Zimmerling, I. J. Pickering, G. N. George, E. W. Price, *Inorg. Chem.* **2023**, *62*, 2637–2651.
- [19] A. K. Salih, S. J. Raheem, M. D. Garcia, W. K. Ahiahonu, E. W. Price, *Inorg. Chem.* **2022**, *61*, 20964–20976.
- [20] A. K. Salih, M. Dominguez Garcia, S. J. Raheem, W. K. Ahiahonu, E. W. Price, *Inorg. Chem.* **2023**, *62*, 20806–20819.
- [21] M. Briand, M. L. Aulsebrook, T. L. Mindt, G. Gasser, *Dalton Trans.* **2017**, *46*, 16387–16389.
- [22] T. Richardson-Sanchez, W. Tieu, M. P. Gotsbacher, T. J. Telfer, R. Codd, *Org. Biomol. Chem.* **2017**, *15*, 5719–5730.
- [23] S. E. Rudd, P. Roselt, C. Cullinane, R. J. Hicks, P. S. Donnelly, *Chem. Commun.* **2016**, *52*, 11889–11892.
- [24] a) U. Seibold, B. Wängler, C. Wängler, *ChemMedChem* **2017**, *12*, 1555–1571; b) F. Guerard, Y. S. Lee, M. W. Brechbiel, *Chem. Eur. J.* **2014**, *20*, 5584–5591; c) W. Tieu, T. Lifa, A. Katsifis, R. Codd, *Inorg. Chem.* **2017**, *56*, 3719–3728.
- [25] L. Outzen, M. Munzmay, J. V. Frangioni, W. Maison, *ChemMedChem* **2023**, *18*, e202300112.
- [26] J. Notni, H. J. Wester, *Chemistry* **2016**, *22*, 11500–11508.
- [27] a) E. Kriemen, M. Holzapfel, E. Ruf, J. Rehbein, W. Maison, *Eur. J. Inorg. Chem.* **2015**, *2015*, 5368–5378; b) E. Kriemen, E. Ruf, U. Behrens, W. Maison, *Chem. Asian J.* **2014**, *9*, 2197–2204.
- [28] a) P. Kaeopookum, M. Petrik, D. Summer, M. Klinger, C. Zhai, C. Rangger, R. Haubner, H. Haas, M. Hajdich, C. Decristoforo, *Nucl. Med. Biol.* **2019**, *78–79*, 1–10; b) G. Carlucci, H. J. K. Ananias, Z. Yu, C. Van de Wiele, R. A. Dierckx, I. J. de Jong, P. H. Elsinga, *Curr. Pharm. Des.* **2012**, *18*, 2501–2516; c) S. Kerpa, V. R. Schulze, M. Holzapfel, L. Cvancar, M. Fischer, W. Maison, *ChemistryOpen* **2024**, *13*, e202300298; d) M. Holzapfel, T. Baldauf, S. Kerpa, G. Guadalupe, B. Qi, Y. Liu, W. J. Parak, W. Maison, *Eur. J. Inorg. Chem.* **2022**, *2022*, e202200432; e) Z. Baranyai, D. Reich, A. Vagner, M. Weineisen, I. Toth, H. J. Wester, J. Notni, *Dalton Trans.* **2015**, *44*, 11137–11146.
- [29] A. R. Poreddy, O. F. Schall, T. A. Osiek, J. R. Wheatley, D. D. Beusen, G. R. Marshall, U. Slomczynska, *J. Comb. Chem.* **2004**, *6*, 239–254.
- [30] H. Sun, X. Peng, *Bioconjug. Chem.* **2013**, *24*, 1226–1234.
- [31] C. A. DeForest, D. A. Tirrell, *Nat. Mater.* **2015**, *14*, 523–531.
- [32] J. L. Suh, B. Watts, J. I. Stuckey, J. L. Norris-Drouin, S. H. Cholensky, B. M. Dickson, Y. An, S. Mathea, E. Salah, S. Knapp, A. Khan, A. T. Adams, B. D. Strahl, C. A. Sagum, M. T. Bedford, L. I. James, D. B. Kireev, S. V. Frye, *Biochemistry* **2018**, *57*, 2140–2149.
- [33] M. Gude, J. Ryf, P. D. White, *Lett. Pept. Sci.* **2002**, *9*, 203–206.

Manuscript received: March 11, 2024

Revised manuscript received: June 5, 2024

Accepted manuscript online: June 10, 2024

Version of record online: July 19, 2024

5.3 Investigations towards an optimal spacing between the hydroxamic acids

In this study, the SPPS approach described in the previous section was employed to synthesize three pure backbone variants of isopeptidic DFO* (ipDFO*) without side chains, incorporating seven, eight, and nine atoms between the hydroxamic acid moieties. These DFO* analogues were designed to complete the investigation into optimal spacing for Zr⁴⁺ coordination. For this purpose, the corresponding O-benzyl-protected hydroxamic acid monomers were synthesized following the same procedure as in the previous work. Using SPPS, these monomers were assembled into the desired octadentate chelators, followed by resin cleavage and deprotection of the protective groups. In addition to the previously reported DFO* analogues, a novel oligoethylene glycol-based analogue (OEGDFO*) was designed and synthesized. In this molecule, the peptide backbone was replaced by ether linkages instead of amides, inspired by the oxoDFO* structure introduced by Briand, which was shown to exhibit improved water solubility due to the presence of ether functionalities.^[164] The OEGDFO* structure also features a seven-atom spacing between the hydroxamic acid units.

With the four chelators in hand (the three ipDFO* analogues with different spacings and the OEGDFO*), radiochemical stability studies with ⁸⁹Zr were performed in collaboration with Prof. Dr. Susanne Kossatz's laboratory at TranslaTUM, Munich. Surprisingly, the analogue with nine atoms between the hydroxamic acids exhibited the highest stability, maintaining approximately 73 % intact complexes after seven days in 1000-fold excess EDTA at 37 °C. In contrast, the other three analogues showed only 50 – 55 % intact complexes under the same conditions. This observation initially appears to contradict the findings reported in Section 5.1. However, considering the differences in molecular structure, this discrepancy suggests that factors other than spacing may influence complex stability. Further experiments will be necessary to investigate the underlying causes of this behavior.

To further demonstrate the potential of SPPS for the synthesis of complex radiopharmaceuticals, a complete PET tracer was assembled on the solid phase. For this purpose, the core urea motif of PSMA-617, known as KuE (lysine–urea–glutamic acid), was selected. It was introduced using a solid-phase carbonyldiimidazole (CDI)-mediated urea coupling, whereby the carbonyl group was linked to two amino acids via CDI activation, with both imidazole groups serving as leaving groups. The chelator portion was synthesized subsequently, as described above. After cleavage from the resin and deprotection of the benzyl groups to liberate the hydroxamic acids, a fully functional immunoPET tracer could be obtained within a few hours.

Title: Isopeptidic Desferrioxamine Analogues: The Role of Hydroxamate Spacing for Chelation of Zr⁴⁺

Authors: Outzen, L., Ludolfs, L., Irl, M., Kossatz, S., Maison, W.

Type: Research Article

Journal: ChemMedChem

Year: 2025

Volume: 20

Issue: 6

Pages: e202400890

DOI: 10.1002/cmdc.202400890

Number of Pages: 9

Submitted: 07.11.2024

Accepted: 10.12.2024

Isopeptidic Desferrioxamine Analogues: The Role of Hydroxamate Spacing for Chelation of Zr^{4+}

Lasse Outzen,^[a] Darius Ludolfs,^[a] Maximilian Irl,^[b] Susanne Kossatz,^[b] and Wolfgang Maison^{*,[a]}

$^{89}\text{Zr}^{4+}$ is a radionuclide of increasing clinical relevance for PET (positron emission tomography). However, an ideal chelator for stable Zr-chelation remains to be discovered. This study describes the solid-phase synthesis of octadentate Zr-chelators based on an isopeptidic (ip) scaffold derived from the natural siderophore desferrioxamine (DFOB). Several analogues with different spacers separating the chelating hydroxamates have been prepared and converted to ^{89}Zr -complexes. The stability of these complexes was evaluated in human serum and

in competition to excess of competing chelators. The assays revealed a beneficial effect of long hydroxamate spacing (9 atoms). Shorter spacing led to a decrease in complex stability. The most stable ^{89}Zr -ipDFO complex had a high stability in challenging competition experiments with a large excess of EDTA for 72 h as determined by radio TLC and LC/MS. The straightforward synthesis, high complex stability and a modular character make ipDFO derivatives promising chelators for applications in targeted PET.

Introduction

Imaging via positron emission tomography (PET) is a standard diagnostic method in clinical oncology.^[1] Common radio-nuclides in use are fluorine-18 ($t_{1/2} = 110$ min), oxygen-15 ($t_{1/2} = 2$ min) and gallium-68 ($t_{1/2} = 68$ min). All are rather short-lived nuclides.^[2] The half-life of radionuclides is one of many important radiochemical properties with an impact on PET-imaging. A short half-life has drawbacks for the processing of tracers and restricts the chemistry used for their preparation.^[2] It limits also the delay time between tracer injection and PET-imaging, which can have a positive influence on the signal-to-noise ratio.^[3] PET-nuclides with longer half-lives are copper-64 ($t_{1/2} = 12.7$ h), terbium-152 ($t_{1/2} = 17.5$ h), manganese-52 ($t_{1/2} = 5.6$ d) and zirconium-89 ($t_{1/2} = 3.3$ d).^[4,5] Particularly zirconium-89 has come into focus in recent years, as it has a very attractive half-life for immunoPET applications (well aligned with the biological half-lives of many antibodies) and has other favorable radiochemical properties such as emission of positrons with a relatively low kinetic energy of 396 keV.^[3] Besides immunoPET, the half life of zirconium-89 can also have a positive impact on

imaging with small molecule PET-tracers.^[6] In recent years, standard protocols have been developed for the production and purification of $^{89}\text{Zr}^{4+}$ for clinical and research use.^[7–11] Starting from naturally occurring Y^{3+} , $^{89}\text{Zr}^{4+}$ can be obtained with a purity of >99.99% and a yield of >94%.^[7] In consequence, zirconium-89 is an increasingly used radionuclide for PET-imaging.^[4]

However, the coordination chemistry of the hard oxophilic Zr^{4+} is complex. The gold standard for chelation of Zr^{4+} is desferrioxamine B (DFOB, Figure 1).^[3,12] DFOB is a linear polyamide chelator and a natural siderophore.^[13] It contains three hydroxamates for metal coordination, which bind preferentially hard, oxophilic cations such as Fe^{3+} and Zr^{4+} .^[14,15] Due to the free terminal amine, DFOB can be conjugated to targeting vectors for use in targeted PET-imaging. The linear structure enables a rapid coordination of radioisotopes, which is typically complete in minutes at room temperature. DFO can thus be used to conjugate proteins or other sensitive targeting vectors.^[3,14,16–26] Unfortunately, ^{89}Zr -DFOB has a limited stability *in vivo*. $^{89}\text{Zr}^{4+}$ can thus be released and subse-

[a] L. Outzen, D. Ludolfs, W. Maison
Department of Chemistry, University of Hamburg, Bundesstrasse 45, 20146 Hamburg, Germany
E-mail: wolfgang.maison@uni-hamburg.de

[b] M. Irl, S. Kossatz
Department of Nuclear Medicine, School of Medicine, TUM University Hospital and Central Institute for Translational Cancer Research (Trans-laTUM), Technical University Munich, Ismaninger Straße 22, 81675 Munich, Germany

Supporting Information for this article is available on the WWW under <https://doi.org/10.1002/cmdc.202400890>

© 2024 The Author(s). ChemMedChem published by Wiley-VCH GmbH. This is an open access article under the terms of the Creative Commons Attribution Non-Commercial License, which permits use, distribution and reproduction in any medium, provided the original work is properly cited and is not used for commercial purposes.

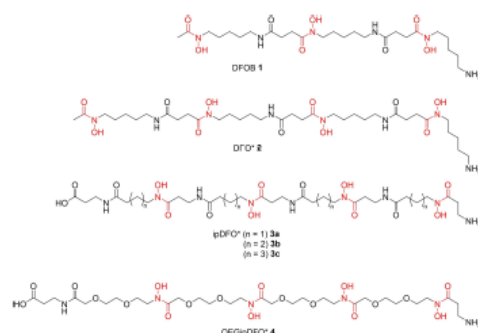


Figure 1. Structures of the natural siderophore DFOB 1 and octadentate derivatives ipDFO* 2, different ipDFO* 3 a-c analogues and OEGipDFO* 4.

quently deposited for example in the bones of test animals or patients.^[3,27–34] This limited stability has been associated to the non-saturated coordination sphere of Zr^{4+} when complexed with DFOB.^[27] Zr^{4+} prefers octadentate coordination, but DFOB offers only three hydroxamates leading to a hexadentate coordination of the metal. The remaining two free coordination sites are saturated with H_2O , which quickly exchanges and thus kinetically destabilizes the complex.^[27] To overcome this lack of complex stability a number of new DFOB analogs with four hydroxamates have been introduced in the last years.^[35–51] The closest structural analogue of DFOB in this series is DFO*, which is an extended analogue of DFOB with an additional hydroxamic acid.^[52] DFO* shows a significantly higher complex stability *in vitro* compared to DFOB. However, some studies with $[^{89}Zr]Zr\text{-DFO}^*$ still revealed an uptake of $[^{89}Zr]Zr^{4+}$ into bone.^[41,53] The search for an ideal Zr-chelator is thus ongoing. Besides the denticity of the chelator, the spacing between the hydroxamic acid has also an influence on complex stability.^[49,54] Being of bacterial origin, DFOB is optimized for chelation of Fe^{3+} . Zr^{4+} however, is slightly larger and prefers higher coordination numbers compared to Fe^{3+} . An ideal Zr^{4+} -chelator should address these points.

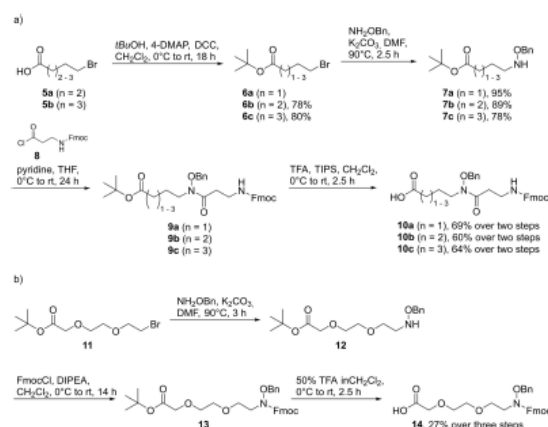
Brechbiel *et al.* proposed that a distance of at least seven atoms between the hydroxamic acids is necessary for good complexation of Zr^{4+} in DFOB-like chelators.^[50] For comparison, DFO* has a distance of nine atoms between the hydroxamic acids. Seibold developed the chelator CTH36, which is a cyclic DFOB analog with a distance of seven atoms between the hydroxamic acids and showed good stability *in vitro*.^[17,49] Recently, clickable DFO* analogues termed AZA-ipDFO* were reported. In these derivatives, the polyamide backbone of DFO* was replaced with an isopeptidic backbone amenable to solid-phase peptide synthesis.^[54,55]

In this study, we report the solid phase synthesis (SPS) of ipDFO* derivatives 3a–c with different spacing of the chelating hydroxamates and the radiochemical evaluation of the corresponding complexes with zirconium-89.

Results and Discussion

Synthesis of Chelators

The ipDFO*-derivatives 3 were synthesized by SPS starting from Fmoc-protected building blocks 10. The latter were prepared according to Scheme 1a from appropriate ω -bromoacids 5. Protection as *tert*-butyl esters 6 was followed by substitution of the bromide with *O*-benzylhydroxylamine to give the protected hydroxylamines 7. The *O*-benzylhydroxylamine motif was finally coupled to Fmoc- β -alanine acid chloride 8 to give the orthogonally protected precursors 9. Final deprotection of *tert*-butyl esters gave the Fmoc-protected building blocks 10 with 40–67% over four steps. Fmoc- β -alanine is a constant structural motif in all building blocks 10. Potential other amino acids such as Gly or GABA are known to be problematic for the synthesis of DFO-derivatives.^[56] Variability in spacing was thus realized via different ω -bromoesters 6 ($n = 1–3$).



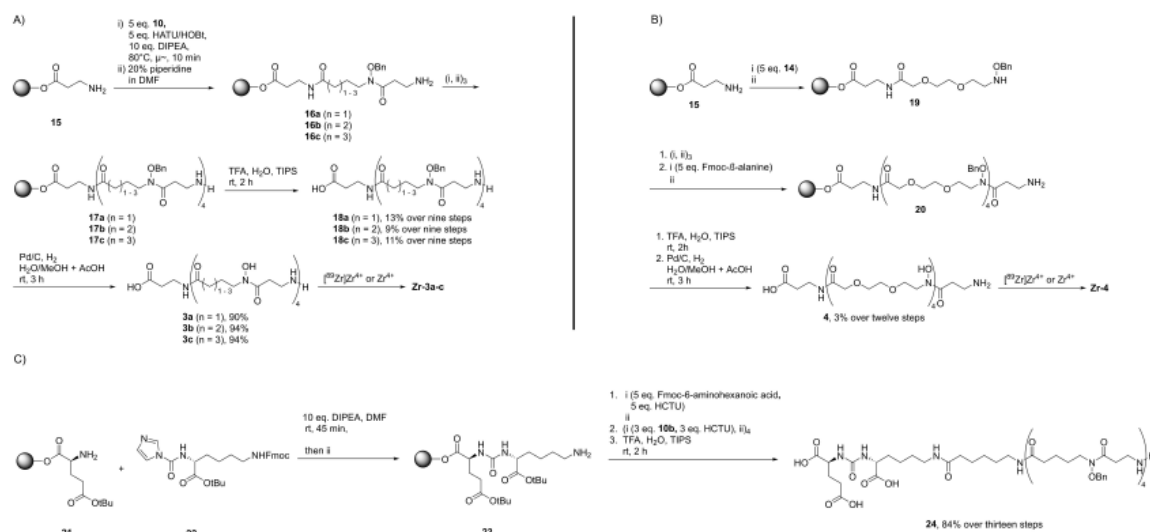
Scheme 1. Synthesis of Fmoc-protected building blocks 10a–c and 14.

An additional building block 14 for the synthesis of an OEG-based analogue of OEGDFO*^[46,47] was prepared *via* a similar route according to Scheme 1b from a commercially available OEG-bromide 11. All four building blocks 10a–c and 14 were converted *via* SPS on Wang-Resin preloaded with Fmoc- β -alanine (15) according to Scheme 2a and b. After acidic cleavage, the benzyl-protected tetrahydroxamates 18a–c and 20 were obtained. Final debenzylation gave the target chelators 3a–c and 4.

The SPS using Wang resin led to reasonably pure crude products 3a–c and 4 after acidic cleavage. However, relatively poor yields of the final products were obtained after chromatography. A switch to the slightly more expensive CTC resin allowed a milder cleavage of products from the resin with 1% TFA. These milder cleavage conditions lead to lower amounts of side products and thus easier purification of the protected chelators 18 (see SI, page 27 for a crude chromatogram). For 18b, for example, this protocol was scaled to 1 mmol and gave the target compound 18b on gram scale in 64% yield after purification. The same protocol was used to prepare the KUE-conjugate 24 in 84% overall yield (Scheme 2C). This example highlights the potential of the solid phase approach for the assembly of vector-chelator conjugates. Both, the targeting urea motif (KUE) and the chelator, were synthesized using one solid phase protocol. This linear assembly of targeting vector and chelator is particularly attractive for targeting vectors of low molecular weight, which are typically accessible by solid phase synthesis. KUE is a well-known targeting vector for prostate cancer and was picked as a representative example.^[57]

Zr^{4+} Chelation and Stability Tests

All chelators 3 and 4 have quite good water solubility (> 10 mM at pH 7). Chelation of ipDFO* derivatives 3a–c and 4 with $[^{89}Zr]Zr^{4+}$ was performed in HEPES buffer (1 M, pH 7) with a chelator concentration of 100 μ M. After the addition of 2.0 MBq $[^{89}Zr]Zr^{4+}$, the solution was heated to 40 $^{\circ}C$ and the progress of



Scheme 2. Synthesis of the target chelators. A) SPS of ipDFO* derivatives **3a–c** and of the corresponding Zr-complexes. B) SPS of ipDFO* derivative **4** and of the corresponding Zr-complex. C) SPS of the KUE-conjugate **24**.

the reaction was monitored by iTLC. This procedure was performed with different chelator concentrations between 100 μM and 1.35 mM. In each case, full conversion was achieved after 20 min. ^{89}Zr Zr-DFO **1** was used as a reference and was synthesized and analyzed in the same way.

The stability in human serum is an important parameter for the characterization of complexes with potential medical applications.

For this, ^{89}Zr Zr-**3a-c**, ^{89}Zr Zr-**4** and ^{89}Zr Zr-**1** (as a reference) were prepared and 0.1 MBq was added to human serum (100 μL). No release of ^{89}Zr Zr $^{4+}$ was detected in any of the complexes confirming complete stability under these conditions (Supporting Information, Figure S39). Therefore, the ipDFO* derivatives ^{89}Zr Zr-**3a-c** and ^{89}Zr Zr-**4** have a high stability in serum, comparable to other complexes of octadentate Zr-chelators.^[39,41–44,50] Thus, changing the spacing between the hydroxamate groups in ipDFO* derivatives ^{89}Zr Zr-**3a-c** and ^{89}Zr Zr-**4** had no impact on complex stability in human serum over a period of seven days. A more challenging assay was therefore needed to reveal the influence of spacing on complex stability of ipDFO* derivatives ^{89}Zr Zr-**3a-c** and ^{89}Zr Zr-**4**. For a more detailed evaluation, a transchelation assay was performed with a large excess of EDTA as competing chelator for the complexes ^{89}Zr Zr-**3a-c** and ^{89}Zr Zr-**4**. ^{89}Zr Zr-**1** was used as a benchmark for comparison. Solutions of the zirconium complexes were prepared as before with the chelators **3a–c**, **4** and DFO **1** (5 μM) and a ^{89}Zr Zr $^{4+}$ activity of 0.1 MBq per test tube before treatment with an EDTA solution (5 mM, pH 7). The samples were heated to 37 $^{\circ}\text{C}$, the identity of ^{89}Zr Zr-species and the ligand exchange process was monitored over seven days by iTLC (Figure 2). The pH value of the test solutions remained stable (pH 7) during this time.

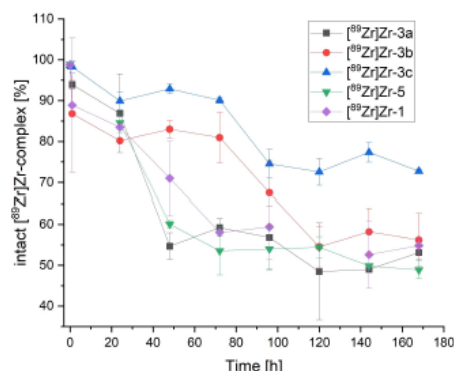


Figure 2. Stability of ^{89}Zr Zr $^{4+}$ -complexes against excess of EDTA. Conditions: chelators **3**, **4** or DFO **1** (5 μM), ^{89}Zr Zr $^{4+}$ activity of 0.1 MBq per test tube, treatment with an EDTA solution (5 mM, pH 7) at 37 $^{\circ}\text{C}$. ^{89}Zr Zr-species and the ligand exchange process was monitored over seven days by iTLC.

Clear differences in complex stabilities were observed for the tested compounds. Almost all of the tested complexes showed limited stability under these challenging test conditions with remaining intact complexes at 49–56% after seven days. With about 73% of intact ^{89}Zr Zr-complex after seven days, only ipDFO* complex ^{89}Zr Zr-**3c** had a significantly increased stability compared to the reference ^{89}Zr Zr-**1** (Figure 2). It should be noted that the values for the time dependent transchelation of ^{89}Zr Zr-**1** are comparable with those obtained in other studies performed under similar conditions (pH 7, 37 $^{\circ}\text{C}$, large excess of EDTA or DFOB).^[41,44]

It is also notable that the stability of ^{89}Zr Zr-**1** (55% intact complex after seven days) was comparable to that of ipDFO* derivative ^{89}Zr Zr-**3a** (53% intact complex after seven days).

The corresponding OEG analog [^{89}Zr]Zr-4 also showed a similar value of 49%. Both compounds are octadentate chelators and have a spacing of 7 atoms between the hydroxamate groups, which is two atoms shorter than the spacing in the hexadentate natural product DFOB 1. The stability of [^{89}Zr]Zr-complexes increased with increasing spacer length in ipDFO* derivative [^{89}Zr]Zr-3b (8 atoms spacing, 56% intact complex after seven days) and ipDFO* derivative [^{89}Zr]Zr-3c (9 atoms spacing, 73% intact complex after seven days). Accordingly, more stable complexes appear to be formed with a "native" DFOB hydroxamate spacing of nine atoms compared to a reduced spacing of eight or seven atoms. This finding is in contrast to some thermodynamically estimated and semi-empirically calculated stabilities of other DFOB-analogues.^[17,49] It is, however, in line with the expected stability trend of DFO-analogues considering the larger ionic radius of Zr^{4+} compared to Fe^{3+} . The results of this radiochemical evaluation were also complemented with results from a non-radioactive LC/MS-assay according to a previously reported protocol.^[54] Test solutions of complexes with Zr were prepared in HEPES at pH 7 and were analyzed for intact complexes via LC/MS using a C_{18} column with a $\text{H}_2\text{O}/\text{CH}_3\text{CN} + 0.1\%$ formic acid gradient (2–98% CH_3CN). Figure 3 shows the complex stability of ipDFO* derivative Zr-3c against 1000fold EDTA and against 300fold DFOB. Zr-1 against 1000fold EDTA was also included here for comparison.

Zr-1 showed a very limited stability in this assay, which is in good agreement with previous observations in our and also other laboratories.^[37,51,54] The Zr-ipDFO* derivative Zr-3c, in contrast, showed a very good stability with 100% intact Zr-complex after 72 h upon treatment with 1000fold excess EDTA. In the competition assay of Zr-3c against 300fold DFOB, 40% of intact complexes were detected after 72 h. The results of the radiochemical evaluation are not strictly comparable to the LC/MS-assay, because the concentrations of metal complexes were significantly higher in the LC/MS assay. It should also be noted that the excess of the challenging chelator EDTA was much

higher in the radiochemical assay. However, both assays revealed a high stability of Zr-3c in a competitive experiment with EDTA excess after 72 h.

Conclusions

The aim of this study was the comparison of different ipDFO* derivatives to decipher the impact of hydroxamate spacing on the stability of Zr complexes. The chelators 3a–c and 4 have been synthesized by a solid-phase protocol from precursors 10 or 14. The protocol was easily scalable (up to gram quantity) and gave particularly pure crude products when CTC resin was employed. The resulting chelators formed stable [^{89}Zr]Zr-complexes within 20 min. All complexes were completely stable in human serum at 37 °C over seven days. A more challenging competition assay with large excess of EDTA as a competing chelator revealed a beneficial effect of long spacing units (9 atoms) separating the hydroxamate groups in isopeptidic DFO derivatives. Shorter spacers with 7 or 8 atoms led to a decrease in complex stability. This is in line with the expected stability trend of DFO-analogues considering the larger ionic radius of Zr^{4+} compared to Fe^{3+} . If longer spacings of more than 9 atoms in isopeptidic DFO analogs have an even higher complex stability remains to be determined in further studies. The most stable Zr-complex in this study was formed by ipDFO* 3c. The corresponding Zr-complex remained completely intact in competition assays with large excess of EDTA for 72 h as determined by a radiochemical and a non-radioactive method.

Experimental Section

General Information

All reagents and solvents were obtained commercially in required grades and used without further purification. Dem. H_2O was obtained through purification by PURELAB Classic from ELGA LabWater. Atmospheric oxygen or moisture sensitive reactions were performed under a protective gas atmosphere (N_2 or Ar). The progress of reactions were monitored by TLC performed on silica gel ALUGRAM Xtra SIL G/UV254 (normal phase) from Macherey-Nagel. The detection was achieved by UV ($\lambda = 254$ nm and 364 nm) or by dipping in ninhydrin solution (1.5 wt% ninhydrin and 3% v/v glacial acetic acid in *n*-butanol) and potassium permanganate solution (KMnO_4 (3 g), K_2CO_3 (20 g), aq. NaOH (5%, 5 mL) in dem. H_2O (300 mL)) followed by heating. Reactions with microwave conditions were performed by Initiator+ from Biotage with a Robot Sixty autosampler from Biotage. Silicagel for column chromatography carried out by hand was POLYGOPREP 60–80 from Macherey-Nagel for normal phase. Purifications with automated column chromatography were performed on the Isolera Prime from the company Biotage with self-packed cartridges from Macherey-Nagel filled with POLYGOPREP 60–80 silicagel. Separation on reversed-phase were performed on the puriFlash450 from Interchim with the cartridges CHROMABOND Flash RS 15, CHROMABOND Flash RS 25 or CHROMABOND Flash RS 80 from the company Macherey-Nagel. Compound were freeze dried in $\text{H}_2\text{O}/\text{CH}_3\text{CN}$ using the ALPHA 2–4 LDplus system from Martin Christ. The purification via preparative HPLC was performed on the Pure C-850 FlashPrep system from the company Büchi with Nucleodur C18 H Tec, 5 μm , 250x10 mm from

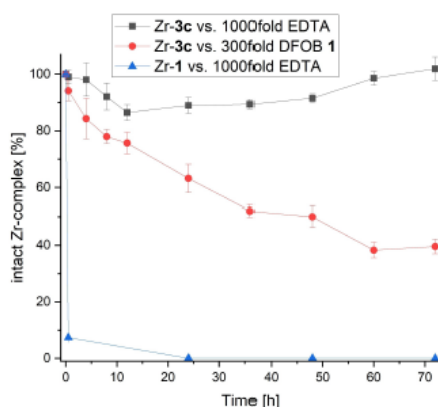


Figure 3. Evaluation of complex stability via LC/MS for complex Zr-3c and Zr-1 (Zr-DFOB). Conditions: HEPES buffered solution of complexes at pH 7. The fate of intact complex was analyzed via LC/MS using a C_{18} column with a $\text{H}_2\text{O}/\text{CH}_3\text{CN} + 0.1\%$ formic acid gradient (2–98% CH_3CN) after addition of excess EDTA or DFOB.

Macherey-Nagel. HRMS-ESI-MS measurements were performed using 6224 ESI-TOF spectrometer coupled with HPLC 1200 series from Agilent Technologies with a Agilent Zorbax Extend C18, 2.1x50 mm. Non-HRMS-ESI-MS measurements were performed using a Agilent HPLC coupled to the ion trap amaZon SL from Bruker Daltonics with Macherey-Nagel EC Nucleodur C18 Gravity-SB, 5 μ m, 150x4 mm and Macherey-Nagel Nucleodur C18 HTec, 3 μ m, 150x4,6 mm. NMR spectra were measured with Avance III 600 MHz, an Avance I 500 MHz, a DRX 500 MHz, an Avance III HD 400 MHz, an Avance II 400 MHz, an Avance I 400 MHz or a FourierHD 300 MHz from Bruker Daltonics. The radionuclide (^{89}Zr) Zr^{4+} was purchased from PerkinElmer, solved in oxalic acid (1 mol/L). The radioTLC plates were purchased from Agilent Technology, iTLC – SG – Glass microfiber chromatography paper impregnated with silica gel. To analyze the radioTLCs a Bioscan, Inc. B-MS-1000 Plate Reader and a Bioscan, Inc. B-FC-1000 Detector was used.

Following Molecules Were Synthesized According to Literature Procedures

tert-butyl 4-(benzyloxy)aminobutanoate **7a**,^[55] *tert*-butyl 4-(benzyloxy)(3-(Fmoc)- β -alanine)aminobutanoate **9a**,^[55] 4-(benzyloxy)(3-(Fmoc)- β -alanine)aminobutanoate **10a**,^[55] *O*-benzyl protected ipDFO* **18a**,^[55] ipDFO* **3a**,^[55] *tert*-butyl N6-(((9H-fluoren-9-yl)methoxy)carbonyl)-N2-(1H-imidazole-1-carbonyl) lysinate **22**.^[58] Protocols for the synthesis of **6b–14** are available in the supporting information.

Initial Loading of the Resin for the Subsequent Solid Phase Synthesis and Determination of the Loading Level

Wang resin (2.00 g, maximum loading density according to the manufacturer: 1.00 mmol/g) was allowed to swell in CH_2Cl_2 (12 mL) on a shaker for 30 min. It was then rinsed three times with DMF (3x6 mL). Fmoc- β -alanine (4 eq., 2.50 g, 8.00 mmol) was dissolved in DMF (10 mL), mixed with 1-hydroxybenzotriazole (HOBt, 4 eq., 1.23 g, 8.00 mmol) and cooled to 0 °C. DCC (4 eq., 1.60 g, 8.00 mmol) was added and the solution was stirred for 15 min at room temperature. The solution with the HOBt-activated Fmoc- β -alanine was transferred to the resin and allowed to react overnight at room temperature with gentle shaking. The reaction solution was then separated from the Wang resin by filtration and the latter was washed three times with CH_2Cl_2 (3x6 mL), three times with 2-propanol (3x6 mL), three times with CH_2Cl_2 (3x6 mL), three times with 2-propanol (3x6 mL) and three times with MeOH (3x6 mL). The resin was stored in a desiccator until constant mass was reached.

The loading density of the initial Fmoc- β -alanine on the resin was determined with a few milligrams of the dry resin according to the protocol of Merck Biosciences AG, Novabiochem Peptide Resin Loading Protocols (based on a protocol of M. Gude *et al.*).^[59,60] For this purpose, the dry resin was swollen in a solution of DMF containing 2% DBU (2 mL) for 30 min with gentle shaking. The resulting solution was diluted to 10 mL with CH_3CN . 2 mL of this mixture were diluted to a volume of 25 mL with CH_3CN . A blank was prepared in the same way without the solution coming into contact with resin. The UV-absorbance of the solutions was measured at 304 nm in triplicate. Equation (1) was used to determine the loading density in mmol/g.

$$\text{mmol/g} = (\text{Abs}_{\text{sample}} - \text{Abs}_{\text{ref}}) \times 16.4 / (\text{mg of resin}) \quad (1)$$

The loading density was determined to be 0.69 mmol/g.

O-Benzyl Protected ipDFO* (**18b**, Synthesis with Wang Resin)

Fmoc- β -alanine loaded Wang resin (714 mg, loading density: 0.69 mmol/g, synthesis scale: 0.5 mmol) was treated with CH_2Cl_2 (10 mL) for 30 min. The resin was then rinsed with DMF (3x10 mL). The subsequent Fmoc deprotection was carried out twice, each time with a fresh solution of 20% piperidine in DMF (15 mL, 1st: 3 min, 80 °C; 2nd: 0.5 min, 80 °C), with rinsing steps between and after the deprotection steps with DMF (3x10 mL). For the subsequent coupling, three stock solutions were prepared: monomer **10b** (5.17 g **10b** in 24 mL DMF), DIPEA (3.49 mL DIPEA in 24 mL DMF) and coupling agent (3.81 g HATU and 1.36 g HOBt in 24 mL DMF). Solution of monomer **10b** (5 eq. based on the loading density of the resin, 6 mL) was mixed with DIPEA solution (10 eq. based on the loading density of the resin, 6 mL) and coupling agent solution (5 eq. based on the loading density of the resin, 6 mL) and gently stirred for 5 min at room temperature to form the active ester *in situ*. The active ester solution was then added to the resin and the microwave assisted coupling step (20 min, 80 °C) was performed. The resin was rinsed with DMF (3x10 mL) after the coupling. Three more coupling and deprotection cycles were performed to obtain the *O*-benzyl protected ipDFO* **18b** bound to the solid phase. After completion of the solid phase synthesis, the resin was washed with DMF (3x10 mL) and CH_2Cl_2 (3x10 mL) and stored in a desiccator under vacuum.

To cleave the products from the Wang resin, the dry resin was placed in a TFA/TIPS/ CH_2Cl_2 solution (90:5:5, 10 mL) cooled to 0 °C and was gently shaken for 2 h at room temperature. The solvent and volatiles were removed under reduced pressure. The residue was coevaporated twice with each 5 mL CH_2Cl_2 . The crude product was purified by chromatography on RP silica gel (column: Macherey Nagel, VP 250/10 Nucleodur C18 HTec, 5 μ m; gradient: $\text{H}_2\text{O}/\text{CH}_3\text{CN}$ 75:25 + 0.1% HCO_2H to 30:70 + 0.1% HCO_2H v/v). The product ipDFO* **18b** (55 mg, 45 μ mol, 9% based on the synthesis scale of 0.5 mmol) was obtained as a slightly yellowish, highly viscous oil. ^1H -NMR (400 MHz, CDCl_3): δ [ppm] = 7.99–7.83 (m, 20H, 14-H, 15-H, 16-H, 28-H, 29-H, 30-H, 42-H, 43-H, 44-H, 56-H, 57-H, 58-H), 5.42–5.27 (m, 8H, 12-H, 26-H, 40-H, 54-H), 4.12–4.24 (m, 8H, 11-H, 25-H, 39-H, 53-H), 3.81–3.88 (m, 8H, 4-H, 19-H, 33-H, 47-H), 3.65 (t, 3J = 6.2 Hz, 2H, 61-H), 3.36 (t, 3J = 5.8 Hz, 2H, 60-H), 3.11 (m, 6H, 18-H, 32-H, 46-H), 2.91 (t, 3J = 6.9 Hz, 2H, 3-H), 2.69–2.60 (m, 8H, 7-H, 22-H, 36-H, 50-H), 2.53–2.50 (m, 1H, 61-H), 2.15–1.94 (m, 16H, 8-H, 10-H, 23-H, 24-H, 37-H, 38-H, 51-H, 52-H). ^{13}C -NMR (100 MHz, CDCl_3): δ [ppm] = 174.6 (C17, C31, C45, C59), 173.0 (C6, C19, C32, C45), 171.7 (C2), 133.9 (C13, C27, C41, C55), 129.4 (C15, C29, C43, C57), 128.9 (C-15, C30, C44, C58), 128.5 (C14, C28, C42, C56), 75.6 (C12, C26, C40, C54), 44.0 (C11, C25, C39, C53), 35.4 (C61), 34.9 (C19, C33, C47), 34.8 (C4), 34.8 (C3), 34.6 (C7, C22, C36, C50), 31.4 (C18, C32, C46), 28.6 (C60), 25.5 (C10, C24, C38, C52), 22.2 (C8, C23, C37, C51). HRMS (ESI): m/z [M+H]⁺ calc. for $\text{C}_{63}\text{H}_{87}\text{N}_9\text{O}_{14}$: 1194.6445, found: 1194.6431.

O-Benzyl Protected ipDFO* (**18b**, Synthesis with CTC Resin)

The synthesis was performed with Fmoc- β -alanine loaded CTC resin on 1 mmol scale according to the same protocol mentioned above but with 3 eq. of the monomer **10b**, DIPEA and HCTU as a coupling reagent. Cleavage from the resin was performed with 1% TFA in CH_2Cl_2 . The resulting crude product had a purity of >70% according to HPLC analysis and was purified by chromatography on RP-silica gel to give **18b** (0.76 g, 64% yield).

O-Benzyl Protected KUE-IpDFO* 24

Fmoc-(tBuO)-glutamic acid loaded CTC resin (149 mg, loading density: 0.67 mmol/g, synthesis scale: 0.1 mmol) was treated with CH_2Cl_2 (10 mL) for 30 min. The resin was then rinsed with DMF (3x10 mL). Fmoc deprotection was carried out twice, each time with a fresh solution of 20% piperidine in DMF (15 mL, 1st: 5 min, rt; 2nd: 3 min, rt), with rinsing steps between and after the deprotection steps with DMF (3x10 mL). The synthesis of the KUE targeting vector was achieved by addition of **22** (5 eq., 0.26 g, 0.5 mmol) and DIEA (10 eq., 0.17 mL, 1 mmol) in 3 mL of DMF to the resin at room temperature while gently agitating for 45 min. Afterwards the resin was rinsed with 3 x 10 mL DMF and Fmoc deprotection was carried out as described above. Fmoc-6-amino-hexanoic acid (5 eq., 177 mg, 0.5 mmol), HCTU (5 eq., 207 mg, 0.5 mmol) and DIEA (10 eq., 0.17 mL, 1 mmol) were dissolved in 3 mL DMF. After 5 minutes, the solution was added to the resin. Coupling was performed for 20 minutes with gentle agitation. Subsequent Fmoc deprotection and rinsing steps were followed by preparation of three stock solutions: monomer **10b** (620 mg **10b** in 2.4 mL DMF), DIEA (0.69 mL DIEA in 2.4 mL DMF) and coupling agent (496 mg HCTU in 2.4 mL DMF). Solution of monomer **10b** (3 eq. based on the loading density of the resin, 0.6 mL) was mixed with DIEA solution (10 eq. based on the loading density of the resin, 0.6 mL) and coupling agent solution (3 eq. based on the loading density of the resin, 0.6 mL) and gently stirred for 5 min at room temperature to form the active ester *in situ*. The active ester solution was then added to the resin and coupling was continued for 20 minutes at room temperature. The resin was rinsed with DMF (3x10 mL) after the coupling. Three more coupling and deprotection cycles were performed to obtain the O-benzyl protected KUE-IpDFO* bound to the solid phase. After completion of the solid phase synthesis, the resin was washed with DMF (3x10 mL) and CH_2Cl_2 (3x10 mL) and stored in a desiccator under vacuum.

To cleave the products from the CTC resin, the dry resin was placed in a TFA/TIPS/ CH_2Cl_2 solution (90:5:5, 10 mL) cooled to 0 °C and was gently shaken for 2 h at room temperature. The solvent and volatiles were removed under reduced pressure. The residue was coevaporated twice with each 5 mL CH_2Cl_2 . The crude product was purified by chromatography on RP silica gel (column: Macherey Nagel, VP 250/10 Nucleodur C18 HTec, 5 μm ; gradient: $\text{H}_2\text{O}/\text{CH}_3\text{CN}$ 75:25 + 0.1% HCO_2H to 30:70 + 0.1% HCO_2H v/v). The product KUE-IpDFO* **25** (129 mg, 84 μmol , 84% based on the synthesis scale of 0.1 mmol) was obtained as a slightly yellowish, highly viscous oil. LC-MS (ESI): m/z $[\text{M} + \text{H}]^+$ calc. for $\text{C}_{78}\text{H}_{112}\text{N}_{12}\text{O}_{20}$: 1536.81, found: 1537.82.

O-Benzyl Protected IpDFO* (18c)

Fmoc- β -alanine loaded Wang resin (714 mg, loading density: 0.69 mmol/g, synthesis scale: 0.5 mmol) was treated with CH_2Cl_2 (10 mL) for 30 min. The resin was then rinsed with DMF (3x10 mL). The subsequent Fmoc deprotection was carried out twice, each time with a fresh solution of 20% piperidine in DMF (15 mL, 1st: 3 min, 80 °C; 2nd: 0.5 min, 80 °C), with rinsing steps between and after the deprotection steps with DMF (3 x 10 mL). For the subsequent coupling, three stock solutions were prepared: monomer **10c** (5.30 g **10c** in 24 mL DMF), DIPEA (3.49 mL DIPEA in 24 mL DMF) and coupling agent (3.81 g HATU and 1.36 g HOBT in 24 mL DMF). Solution of monomer **10c** (5 eq. based on the loading density of the resin, 6 mL) was mixed with DIPEA solution (10 eq. based on the loading density of the resin, 6 mL) and coupling agent solution (5 eq. based on the loading density of the resin, 6 mL) and gently stirred for 5 min at room temperature to form the active ester *in situ*. The active ester solution was then added to the resin and the microwave assisted coupling step (20 min, 80 °C) was

performed. The resin was rinsed with DMF (3x10 mL) after the coupling. Three more coupling and deprotection cycles were performed to obtain the O-benzyl protected IpDFO* **18c** bound to the solid phase. After completion of the solid phase synthesis, the resin was washed with DMF (3x10 mL) and CH_2Cl_2 (3x10 mL) and stored in a desiccator under vacuum.

To cleave the products from the Wang resin, the dry resin was placed in a TFA/TIPS/ CH_2Cl_2 solution (90:5:5, 10 mL) cooled to 0 °C and was gently shaken for 2 h at room temperature. The solvent and volatiles were removed under reduced pressure. The residue was coevaporated twice with each 5 mL CH_2Cl_2 . The crude product was purified by chromatography on RP silica gel (column: Macherey Nagel, VP 250/10 Nucleodur C18 HTec, 5 μm ; gradient: $\text{H}_2\text{O}/\text{CH}_3\text{CN}$ 75:25 + 0.1% HCO_2H to 30:70 + 0.1% HCO_2H v/v). The product IpDFO* **18c** (65 mg, 55 μmol , 11% based on the synthesis scale of 0.5 mmol) was obtained as a slightly yellowish, highly viscous oil. ^1H -NMR (400 MHz, CDCl_3): δ [ppm] = 7.96–7.82 (m, 20H, 14-H, 15-H, 16-H, 29-H, 30-H, 31-H, 44-H, 45-H, 46-H, 59-H, 60-H, 61-H), 5.37–5.24 (m, 8H, 12-H, 27-H, 42-H, 57-H), 4.21–4.04 (m, 8H, 11-H, 26-H, 41-H, 56-H), 3.90–3.75 (m, 8H, 4-H, 19-H, 34-H, 49-H), 3.68–3.58 (m, 2H, 64-H), 3.42–3.27 (m, 2H, 63-H), 3.16–3.04 (m, 6H, 18-H, 33-H, 48-H), 2.96–2.87 (m, 2H, 3-H), 2.66–2.55 (m, 8H, 7, 22-H, 37-H, 52-H), 2.55–2.46 (m, 2H, 65-H), 2.13–1.90 (m, 16H, 8-H, 10-H, 23-H, 25-H, 38-H, 40-H, 53-H, 55-H), 1.80–1.63 (m, 8H, 9-H, 24-H, 39-H, 54-H). ^{13}C -NMR (100 MHz, CDCl_3): δ [ppm] = 176.2 (C62), 175.0 (C6), 174.8 (C17, C32, C47), 172.9 (C21, C36, C51), 171.6 (C2), 134.0 (C13, C28, C43), 133.9 (C58), 129.4 (C14, C29, C44, C59), 128.8 (C16, C31, C46, C61), 128.5 (C15, C30, C45, C60), 75.7 (C12, C27, C42, C57), 44.3 (C11, C26, C41, C56), 35.4 (C65), 35.3 (C19, C34, C49), 34.9 (C4), 34.6 (C3), 34.5 (C7, C22, C37, C52), 31.5 (C18, C33, C48), 28.7 (C63), 25.8 (C10, C25, C40, C55), 25.4 (C8, C23, C38, C53), 24.8 (C9, C24, C39, C54). HRMS (ESI): m/z $[\text{M} + \text{H}]^+$ calc. for $\text{C}_{67}\text{H}_{95}\text{N}_9\text{O}_{14}$: 1250.7071, found: 1250.7074.

O-Benzyl Protected OEGDFO* with Following Benzyl-Deprotection (4)

Fmoc- β -alanine loaded Wang resin (250 mg, loading density: 0.40 mmol/g, synthesis scale: 0.1 mmol) was treated with CH_2Cl_2 (10 mL) for 30 min. The resin was then rinsed with DMF (3x10 mL). The subsequent Fmoc deprotection was carried out twice, each time with a fresh solution of 20% piperidine in DMF (15 mL, 1st: 3 min, 80 °C; 2nd: 0.5 min, 80 °C), with rinsing steps between and after the deprotection steps with DMF (3x10 mL). For the subsequent coupling, three stock solutions were prepared containing: monomer (0.95 g **14** in 24 mL DMF), DIPEA solution (1.26 mL DIPEA in 42 mL DMF) and coupling agent solution (1.58 g PyOxim in 36 mL DMF). Monomer **14** solution (4.85 eq. based on the loading density of the resin, 6 mL) was mixed with DIPEA solution (10 eq. based on the loading density of the resin, 6 mL) and coupling agent solution (5 eq. based on the loading density of the resin, 6 mL) and gently stirred for 5 min at room temperature to form the active ester *in situ*. The active ester solution was then added to the resin and the microwave assisted coupling step (10 min, 80 °C) was performed. The resin was rinsed with DMF (3 x 10 mL) after the coupling. Three more coupling and deprotection cycles were performed to obtain the O-benzyl protected OEGDFO* bound to the solid phase. After completion of the solid phase synthesis, the resin was washed with DMF (3x10 mL) and CH_2Cl_2 (3x10 mL) and stored in a desiccator under vacuum.

To cleave the products from the Wang resin, the dry resin was placed in a TFA/TIPS/ CH_2Cl_2 solution (90:5:5, 10 mL) cooled to 0 °C and was gently shaken for 2 h at room temperature. The solvent and volatiles were removed under reduced pressure. The residue was coevaporated twice with each 5 mL CH_2Cl_2 . The crude product

was purified by chromatography on RP silica gel (column: Macherey Nagel, VP 250/10 Nucleodur C18 HTec, 5 μ m; gradient: H₂O/CH₃CN 75:25 + 0.1% HCO₂H to 30:70 + 0.1% HCO₂H v/v). The product O-benzyl protected OEGDFO* (3.5 mg, 3 μ mol, 3% based on the synthesis scale of 0.1 mmol) was obtained as a slightly yellowish, highly viscous oil. HRMS (ESI): m/z [M+H]⁺ calc. for C₃₈H₈₀N₆O₁₉: 1165.5551, found: 1165.5562.

O-benzyl protected OEGDFO* (1 eq., 3.5 mg) was dissolved in MeOH (665 μ L), dem. H₂O (140 μ L) and mixed with formic acid (8 μ L) and palladium on activated carbon (Pd/C, 10%, 0.25 mg). The solvent was degassed *in vacuo*. The reaction vessel was then flooded with hydrogen. This procedure was repeated twice. The reaction mixture was stirred under H₂ atmosphere for 2–3 h at room temperature. The reaction process was monitored *via* LC/MS. The reaction solution was then filtered, the volatile components were removed under reduced pressure and the residue was dissolved in 20 mL CH₃CN/dem. H₂O (1:1) and freeze-dried. After column chromatography on RP silica gel (column: Macherey Nagel, VP 250/10 Nucleodur C18 HTec, 5 μ m; gradient: H₂O/CH₃CN 75:25 + 0.1% HCO₂H to 30:70 + 0.1% HCO₂H v/v), the desired product OEGDFO* 4 (3.1 mg) was obtained. HRMS (ESI): m/z [M+H]⁺ calc. for C₃₀H₅₆N₆O₁₉: 805.3673, found: 805.3692.

IpDFO* (3b)

O-benzyl protected ipDFO* 18b (1 eq., 2.4 mg) was dissolved in MeOH (570 μ L), dem. H₂O (120 μ L) and mixed with formic acid (6.5 μ L) and palladium on activated carbon (Pd/C, 10%, 0.210 mg). The solvent was degassed *in vacuo*. The reaction vessel was then flooded with hydrogen. This procedure was repeated twice. The reaction mixture was stirred under H₂ atmosphere for 2–3 h at room temperature. The reaction process was monitored *via* LC/MS. The reaction solution was then filtered, the volatile components were removed under reduced pressure and the residue was dissolved in 10 mL CH₃CN/dem. H₂O (1:1) and freeze-dried. After column chromatography on RP silica gel (column: Macherey Nagel, VP 250/10 Nucleodur C18 HTec, 5 μ m; gradient: H₂O/CH₃CN 75:25 + 0.1% HCO₂H to 30:70 + 0.1% HCO₂H v/v), the desired product 3b (1.7 mg, 94%) was obtained. ¹H-NMR (400 MHz, CDCl₃): δ [ppm] = 3.97–3.89 (m, 8H, 10-H, 20-H, 30-H, 40-H), 3.74 (t, ³J = 6.4 Hz, 6H, 14-H, 24-H, 34-H), 3.69 (t, 2H, 4-H), 3.55 (m, 2H, 44-H), 3.23 (t, ³J = 5.9 Hz, 2H, 43-H), 3.03 (t, ³J = 6.4 Hz, 6H, 13-H, 23-H, 33-H), 2.72 (t, ³J = 5.9 Hz, 2H, 3-H), 2.55 (t, ³J = 6.6 Hz, 8H, 7-H, 17-H, 27-H, 37-H), 2.37 (m, 1H, 45-H), 1.97–1.84 (m, 16H, 8-H, 9-H, 18-H, 19-H, 28-H, 29-H, 38-H, 39-H). ¹³C-NMR (100 MHz, CDCl₃): δ [ppm] = 175.2 (C12, C22, C32, C42), 172.4 (C6, C16, C26, C36), 47.0 (C10, C20, C30, C40), 35.8 (C44), 35.5 (C3), 34.9 (C14, C24, C34), 34.6 (C7, C17, C27, C37), 31.3 (C13, C23, C33), 28.5 (C43), 25.0 (C9, C19, C29, C39), 22.0 (C8, C18, C28, C38). HRMS (ESI): m/z [M+H]⁺ calc. for C₃₅H₆₃N₉O₁₄: 834.4567, found: 834.4557.

IpDFO* (3c)

O-benzyl protected ipDFO* 18c (1 eq., 1.8 mg) was dissolved in MeOH (357 μ L), dem. H₂O (75 μ L) and mixed with formic acid (4 μ L) and palladium on activated carbon (Pd/C, 10%, 0.13 mg). The solvent was degassed *in vacuo*. The reaction vessel was then flooded with hydrogen. This procedure was repeated twice. The reaction mixture was stirred under H₂ atmosphere for 2–3 h at room temperature. The reaction process was monitored *via* LC/MS. The reaction solution was then filtered, the volatile components were removed under reduced pressure and the residue was dissolved in 10 mL CH₃CN/dem. H₂O (1:1) and freeze-dried. After column chromatography on RP silica gel (column: Macherey Nagel, VP 250/10 Nucleodur C18 HTec, 5 μ m; gradient: H₂O/CH₃CN 75:25

+ 0.1% HCO₂H to 30:70 + 0.1% HCO₂H v/v), the desired product 3c (1.2 mg, 94%) was obtained. ¹H-NMR (400 MHz, CDCl₃): δ [ppm] = 3.69–3.59 (m, 8H, 11-H, 22-H, 33-H, 44-H), 3.47 (t, ³J = 6.5 Hz, 6H, 15-H, 26-H, 37-H), 3.41 (t, ³J = 6.8 Hz, 2H, 4-H), 3.28 (t, ³J = 6.6 Hz, 2H, 48-H), 2.95 (t, 2H, 47-H), 2.75 (t, ³J = 6.5 Hz, 6H, 14-H, 25-H, 36-H), 2.44 (t, ³J = 6.8 Hz, 2H, 3-H), 2.25 (t, ³J = 7.1 Hz, 8H, 7-H, 18-H, 29-H, 40-H), 1.75–1.56 (m, 16 m, 8-H, 10-H, 19-H, 21-H, 30-H, 32-H, 41-H, 43-H), 1.38–1.25 (m, 8H, 9-H, 20-H, 31-H, 42-H). HRMS (ESI): m/z [M+H]⁺ calc. for C₃₉H₇₁N₉O₁₄: 890.5193, found: 890.5192.

RadioTLC Protocol

The sample was pipetted to the radioTLC plates. After the solvent was dried, the TLC plate was placed in a TLC chamber with an aqueous EDTA solution (50 mM, pH 5.5) as eluent.

[⁸⁹Zr]Zr-3a

A stock solution (1 mM) was prepared by dissolving ipDFO* 3a (0.69 mg, 0.89 μ mol) in dem. H₂O with 1% DMSO (885 μ L). This stock solution (25 μ L) was mixed with HEPES buffer (250 μ L) and [⁸⁹Zr]Zr⁴⁺ (5 MBq in 5 μ L) was added. The solution was gently shaken at 40 °C. The complexation was monitored *via* radioTLC.

[⁸⁹Zr]Zr-3b

A stock solution (1 mM) was prepared by dissolving ipDFO* 3b (0.86 mg, 1.07 μ mol) in dem. H₂O with 1% DMSO (1066 μ L). This stock solution (25 μ L) was mixed with HEPES buffer (250 μ L) and [⁸⁹Zr]Zr⁴⁺ (5 MBq in 5 μ L) was added. The solution was gently shaken at 40 °C. The complexation was monitored *via* radioTLC.

[⁸⁹Zr]Zr-3c

A stock solution (1 mM) was prepared by dissolving ipDFO* 3c (1.00 mg, 1.12 μ mol) in dem. H₂O with 1% DMSO (1124 μ L). This stock solution (25 μ L) was mixed with HEPES buffer (250 μ L) and [⁸⁹Zr]Zr⁴⁺ (5 MBq in 5 μ L) was added. The solution was gently shaken at 40 °C. The complexation was monitored *via* radioTLC.

[⁸⁹Zr]Zr-4

A stock solution (1 mM) was prepared by dissolving OEGDFO* 4 (3.1 mg, 3.85 μ mol) in dem. H₂O with 1% DMSO (3830 μ L). This stock solution (25 μ L) was mixed with HEPES buffer (250 μ L) and [⁸⁹Zr]Zr⁴⁺ (5 MBq in 5 μ L) was added. The solution was gently shaken at 40 °C. The complexation was monitored *via* radioTLC.

[⁸⁹Zr]Zr-1

A stock solution (1 mM) was prepared by solving commercially purchased DFOB mesylate (0.81 mg, 1.23 μ mol) in dem. H₂O with 1% DMSO (1230 μ L). For the complexation the stock solution (25 μ L) was mixed with HEPES buffer (250 μ L) and [⁸⁹Zr]Zr⁴⁺ (5 MBq in 5 μ L) was added. The solution was gently shaken at 40 °C. A complete complexation was checked *via* radioTLC.

[⁸⁹Zr]Zr-Complex Stability in Human Serum

An aliquot of the stock solution (1 mM Chelator in dem. H₂O + 1% DMSO, 25 μ L) was added to HEPES buffer (1 M, pH 7, 250 μ L). [⁸⁹Zr]Zr⁴⁺ (5 MBq in 5 μ L) was added and the solution was gently shaken at 40 °C for 20 min. The complex solution (11 μ L) was added

to human serum (100 μ L) and was incubated for seven days at 37 °C. Triplicate samples were analyzed daily by adding a mix of ice-cold ethanol (75 μ L) and acetonitrile (300 μ L). After centrifugation (13000 rpm for 10 min) the supernatant was decanted and analyzed via radioTLC.

Radioactive Competitions Studies Against 1000 fold Excess of EDTA Via RadioTLC

An aliquot of the stock solution (1 mM chelator in dem. H₂O + 1% DMSO, 40 μ L) was added to HEPES buffer (1 M, pH 7, 400 μ L). [⁸⁹Zr]Zr⁴⁺ (10 MBq in 15 μ L) was added and the solution was gently shaken at 40 °C for 20 min. The complex solution (10 μ L with approx. 0.1 MBq) was added to an EDTA solution (10 mM, 100 μ L) and was incubated for seven days at 37 °C. Triplicate samples were analyzed daily via radioTLC.

Zr-3 c: ipDFO* 3 c (1 eq., 1.20 mg, 1.35 μ mol) was dissolved in HEPES Puffer (2 mM, pH 7, 1 mL) and Zr(acac)₄ (3 eq., 4.5 μ mol, 4 mL HEPES (2 mM, pH 7)) was added. After stirring over night at room temperature, the complete transfer of ipDFO* 3 c to Zr-ipDFO* was confirmed by LC/MS. The HEPES-solution containing the Zr-complex was used without further purification for the complex stability tests. HRMS (ESI): m/z [M+H]⁺ calc. for C₃₉H₆₇N₉O₁₄Zr: 976.3927, found: 976.3954.

Non-Radioactive Competitions Studies Against 1000 fold Excess of EDTA or 300 fold Excess of DFOB Via HPLC-MS

A solution of Zr-3 c (1.35 μ mol in 5 mL HEPES buffer (2 mM, pH 7)) was diluted with HEPES buffer (2 mM, pH 7, 130 mL) to create a stock solution (135 mL, 10 μ M). An aliquot of this solution (1 mL with 0.01 μ mol Zr-3 c) was added to an EDTA solution (0.5 mL with 10 μ mol EDTA in HEPES buffer (2 mM, pH 7)) or to a DFOB solution (0.5 mL with 3 μ mol DFOB in HEPES buffer (2 mM, pH 7)). Triplicate samples were analyzed twice a day via HPLC-MS over a period of three days. The integral of the EIC was used to quantify the complexes in the samples.

Acknowledgements

We acknowledge financial support from the Open Access Publication Fund of Universität Hamburg. Open Access funding enabled and organized by Projekt DEAL.

Conflict of Interests

The authors declare no conflict of interest.

Data Availability Statement

The data that support the findings of this study are available in the supplementary material of this article.

Keywords: Siderophor • Zirconium-89 • DFOB • Complexes • Solid phase synthesis

- [1] G. Crisan, N. S. Moldoveanu-Cioroiu, D. G. Timaru, G. Andries, C. Cainap, V. Chis, *Int. J. Mol. Sci.* **2022**, *23*, 5023–5075.
- [2] P. W. Miller, N. J. Long, R. Vilar, A. D. Gee, *Angew. Chem. Int. Ed. Engl.* **2008**, *47*, 8998–9033.
- [3] J. K. Yoon, B. N. Park, E. K. Ryu, Y. S. An, S. J. Lee, *Int. J. Mol. Sci.* **2020**, *21*, 4309–4327.
- [4] W. Wei, Z. T. Rosenkrans, J. Liu, G. Huang, Q. Y. Luo, W. Cai, *Chem Rev* **2020**, *120*, 3787–3851.
- [5] R. P. Baum, A. Singh, M. Benesova, C. Vermeulen, S. Gnesin, U. Koster, K. Johnston, D. Muller, S. Senftleben, H. R. Kulkarni, A. Turler, R. Schibli, J. O. Prior, N. P. van der Meulen, C. Muller, *Dalton Trans.* **2017**, *46*, 14638–14646.
- [6] B. M. Prive, Y. H. W. Derks, F. Rosar, G. M. Franssen, S. M. B. Peters, F. Khreish, M. Bartholoma, S. Maus, M. Gotthardt, P. Laverman, M. W. Konijnenberg, S. Ezziddin, J. Nagarajah, S. Heskamp, *Eur. J. Nucl. Med. Mol. Imaging* **2022**, *49*, 2064–2076.
- [7] I. Verel, G. W. M. Visser, R. S. W. Boellaard, M. G. B. Snow, G. A. M. S. van Dongen, *J. Nucl. Med.* **2003**, *44*, 1271.
- [8] E. T. Sarcan, M. Silindir-Gunay, A. Y. Ozer, N. Hartman, *J. Radioanal. Nucl. Chem.* **2021**, *330*, 15–28.
- [9] A. Wooten, E. Madrid, G. Schweitzer, L. Lawrence, E. Mebrahtu, B. Lewis, S. Lapi, *Appl. Sci.* **2013**, *3*, 593–613.
- [10] M. W. den Hollander, F. Bensch, A. W. Glaudemans, T. H. Oude Munnink, R. H. Enting, W. F. den Dunnen, M. A. Heesters, F. A. Kruij, M. N. Lub-de Hooge, J. Cees de Groot, J. Pearlberg, J. A. Gietema, E. G. de Vries, A. M. Walenkamp, *J. Nucl. Med.* **2015**, *56*, 1310–1314.
- [11] J. P. Holland, Y. Sheh, J. S. Lewis, *Nucl. Med. Biol.* **2009**, *36*, 729–739.
- [12] S. Heskamp, R. Raavé, O. Boerman, M. Rijpkema, V. Goncalves, F. Denat, *Bioconjug. Chem.* **2017**, *28*, 2211–2223.
- [13] D. Bellotti, M. Remelli, *Molecules* **2021**, *26*, 3255–3276.
- [14] M. Hofmann, G. Retamal-Morales, D. Tischler, *Nat. Prod. Rep.* **2020**, *37*, 1262–1283.
- [15] R. Codd, *Coord. Chem. Rev.* **2008**, *252*, 1387–1408.
- [16] G. Fischer, U. Selbold, R. Schirrmacher, B. Wängler, C. Wängler, *Molecules* **2013**, *18*, 6469–6490.
- [17] J. P. Holland, *Inorg. Chem.* **2020**, *59*, 2070–2082.
- [18] P. J. Blower, R. Cusnir, A. Darwesh, N. J. Long, M. T. Ma, B. E. Osborne, T. W. Price, J. Pellico, G. Reid, R. Southworth, G. J. Stasiuk, S. Y. A. Terry, R. T. M. de Rosales, *Chapter One - Gallium: New developments and applications in radiopharmaceuticals in Advances in Inorganic Chemistry*, (Eds.: C. D. Hubbard, R. van Eldik), Academic Press, **2021**, *78*, pp. 1–35; <https://doi.org/10.1016/bs.adioch.2021.04.002>.
- [19] B. V. Marquez, O. F. Ikotun, A. Zheleznyak, B. Wright, A. Hari-Raj, R. A. Pierce, S. E. Lapi, *Mol. Pharm.* **2014**, *11*, 3988–3995.
- [20] G. A. Ulaner, S. K. Lyashchenko, C. Riedl, S. Ruan, P. B. Zanzonico, D. Lake, K. Jhaveri, B. Zeglis, J. S. Lewis, J. A. O'Donoghue, *J. Nucl. Med.* **2018**, *59*, 900–906.
- [21] S. B. Gaykema, A. H. Brouwers, M. N. Lub-de Hooge, R. G. Pleijhuis, H. Timmer-Bosscha, L. Pot, G. M. van Dam, S. B. van der Meulen, J. R. de Jong, J. Bart, J. de Vries, L. Jansen, E. G. de Vries, C. P. Schroder, *J. Nucl. Med.* **2013**, *54*, 1014–1018.
- [22] S. F. Oosting, S. J. van Asselt, A. H. Brouwers, A. H. Bongaerts, J. D. Steinberg, J. R. de Jong, M. N. Lub-de Hooge, A. N. van der Horst-Schrivers, A. M. Walenkamp, E. W. Hoving, W. J. Sluiter, B. A. Zonnenberg, E. G. de Vries, T. P. Links, *J. Nucl. Med.* **2016**, *57*, 1244–1250.
- [23] M. H. Jansen, S. E. M. Veldhuijzen van Zanten, D. G. van Vuurden, M. C. Huisman, D. J. Vugts, O. S. Hoekstra, G. A. van Dongen, G. L. Kaspers, *J. Nucl. Med.* **2017**, *58*, 711–716.
- [24] L. R. Perk, O. J. Visser, M. Stigter-van Walsum, M. J. Vosjan, G. W. Visser, J. M. Zijlstra, P. C. Huijgens, G. A. van Dongen, *Eur. J. Nucl. Med. Mol. Imaging* **2006**, *33*, 1337–1345.
- [25] A. Ruggiero, J. P. Holland, T. Hudolin, L. Shenker, A. Koulova, N. H. Bander, J. S. Lewis, J. Grimm, *J. Nucl. Med.* **2011**, *52*, 1608–1615.
- [26] N. Pandit-Taskar, J. A. O'Donoghue, J. C. Durack, S. K. Lyashchenko, S. M. Cheal, V. Beylergil, R. A. Lefkowitz, J. A. Carrasquilla, D. F. Martinez, A. M. Fung, S. B. Solomon, M. Gonen, G. Heller, M. Loda, D. M. Nanus, S. T. Tagawa, J. L. Feldman, J. R. Osborne, J. S. Lewis, V. E. Reuter, W. A. Weber, N. H. Bander, H. I. Scher, S. M. Larson, M. J. Morris, *Clin. Cancer Res.* **2015**, *21*, 5277–5285.
- [27] J. P. Holland, V. Divilov, N. H. Bander, P. M. Smith-Jones, S. M. Larson, J. S. Lewis, *J. Nucl. Med.* **2010**, *51*, 1293–1300.
- [28] D. S. Abou, T. Ku, P. M. Smith-Jones, *Nucl. Med. Biol.* **2011**, *38*, 675–681.
- [29] T. K. Nayak, K. Garmestani, D. E. Milenic, M. W. Brechbiel, *J. Nucl. Med.* **2012**, *53*, 113–120.

- [30] M. A. Deri, B. M. Zeglis, L. C. Francesconi, J. S. Lewis, *Nucl. Med. Biol.* **2013**, *40*, 3–14.
- [31] M. A. Deri, S. Ponnala, P. Kozlowski, B. P. Burton-Pye, H. T. Cicek, C. Hu, J. S. Lewis, L. C. Francesconi, *Bioconjug. Chem.* **2015**, *26*, 2579–2591.
- [32] P. Laverman, T. van der Geest, S. Y. Terry, D. Gerrits, B. Walgreen, M. M. Helsen, T. K. Nayak, A. Freimoser-Grundschober, I. Waldhauer, R. J. Hosse, E. Moessner, P. Umana, C. Klein, W. J. Oyen, M. I. Koenders, O. C. Boerman, *J. Nucl. Med.* **2015**, *56*, 778–783.
- [33] W. E. Meijls, H. J. Haisma, R. P. Klok, F. B. van Gog, E. Kievit, H. M. Pinedo, J. D. Herscheid, *J. Nucl. Med.* **1997**, *38*, 112–118.
- [34] G. Sormani, A. Korde, A. Rodriguez, M. Denecke, A. Hassanali, *ACS Omega* **2023**, *8*, 36032–36042.
- [35] N. B. Bhatt, D. N. Pandya, T. J. Wadas, *Molecules* **2018**, *23*, 638–661.
- [36] V. B. Bubenshchikov, A. A. Larenkov, *Russ. J. Coord. Chem.* **2022**, *48*, 675–695.
- [37] C. J. M. Brown, M. P. Gotsbacher, R. Codd, *Aust. J. Chem.* **2020**, *73*, 969–978.
- [38] C. J. Adams, J. J. Wilson, E. Boros, *Mol. Pharm.* **2017**, *14*, 2831–2842.
- [39] L. Allott, C. Da Pieve, J. Meyers, T. Spinks, D. M. Ciobota, G. Kramer-Marek, G. Smith, *Chem. Commun.* **2017**, *53*, 8529–8532.
- [40] D. L. White, P. W. Durbin, N. Jeung, K. N. Raymond, *J. Med. Chem.* **1988**, *31*, 11–18.
- [41] R. Raavé, G. Sandker, P. Adumeau, C. B. Jacobsen, F. Mangin, M. Meyer, M. Moreau, C. Bernhard, L. Da Costa, A. Dubois, V. Goncalves, M. Gustafsson, M. Rijpkema, O. Boerman, J.-C. Chambron, S. Heskamp, F. Denat, *Eur. J. Nucl. Med. Mol. Imaging* **2019**, *46*, 1966–1977.
- [42] E. K. Sarbisheh, A. K. Salih, S. J. Raheem, J. S. Lewis, E. W. Price, *Inorg. Chem.* **2020**, *59*, 11715–11727.
- [43] E. Khozeimeh Sarbisheh, K. L. Summers, A. K. Salih, J. J. H. Cotelesage, A. Zimmerling, I. J. Pickering, G. N. George, E. W. Price, *Inorg. Chem.* **2023**, *62*, 2637–2651.
- [44] A. K. Salih, S. J. Raheem, M. D. Garcia, W. K. Ahiaonu, E. W. Price, *Inorg. Chem.* **2022**, *61*, 20964–20976.
- [45] A. K. Salih, M. Dominguez Garcia, S. J. Raheem, W. K. Ahiaonu, E. W. Price, *Inorg. Chem.* **2023**, *62*, 20806–20819.
- [46] M. Briand, M. L. Aulsebrook, T. L. Mindt, G. Gasser, *Dalton Trans.* **2017**, *46*, 16387–16389.
- [47] T. Richardson-Sanchez, W. Tieu, M. P. Gotsbacher, T. J. Telfer, R. Codd, *Org. Biomol. Chem.* **2017**, *15*, 5719–5730.
- [48] S. E. Rudd, P. Roselt, C. Cullinane, R. J. Hicks, P. S. Donnelly, *Chem. Commun.* **2016**, *52*, 11889–11892.
- [49] U. Seibold, B. Wängler, C. Wängler, *ChemMedChem* **2017**, *12*, 1555–1571.
- [50] F. Guerard, Y. S. Lee, M. W. Brechbiel, *Chem. Eur. J.* **2014**, *20*, 5584–5591.
- [51] W. Tieu, T. Lifa, A. Katsifis, R. Codd, *Inorg. Chem.* **2017**, *56*, 3719–3728.
- [52] M. Patra, A. Bauman, C. Mari, C. A. Fischer, O. Blacque, D. Haussinger, G. Gasser, T. L. Mindt, *Chem. Commun.* **2014**, *50*, 11523–11525.
- [53] M. Chomet, M. Schreurs, M. J. Bolijn, M. Verlaan, W. Beaino, K. Brown, A. J. Poot, A. D. Windhorst, H. Gill, J. Marik, S. Williams, J. Cowell, G. Gasser, T. L. Mindt, G. van Dongen, D. J. Vugts, *Eur. J. Nucl. Med. Mol. Imaging* **2021**, *48*, 694–707.
- [54] L. Outzen, M. Munzmay, J. V. Frangioni, W. Maison, *ChemMedChem* **2023**, *18*, e202300112.
- [55] L. Outzen, H. D. Nguyen, D. Ludolfs, W. Maison, *Eur. J. Org. Chem.* **2024**, *27*, e202400266.
- [56] A. R. Poreddy, O. F. Schall, T. A. Osiek, J. R. Wheatley, D. D. Beusen, G. R. Marshall, U. Slomczynska, *J. Comb. Chem.* **2004**, *6*, 239–254.
- [57] M. El Fakiri, N. M. Geis, N. Ayada, M. Eder, A. C. Eder, *Cancers (Basel)* **2021**, *13*, 3967–3997.
- [58] Inventor: F. Andrae, Applicant: Novartis AG, Synthesis of Prostate Specific Membrane Antigen (PSMA) Ligands (WO2022106633A1, priority 11/19/2020), **2022**.
- [59] Website: SigmaAldrich.com, *Peptide Resin Loading Protocols*, <https://www.sigmaaldrich.com/DE/de/technical-documents/technical-article/chemistry-and-synthesis/peptide-synthesis/peptide-resin-loading> **2024**, last access: 14.08.2024.
- [60] M. Gude, J. Ryf, P. D. White, *Lett. Pept. Sci.* **2002**, *9*, 203–206.

Manuscript received: November 7, 2024

Revised manuscript received: December 9, 2024

Accepted manuscript online: December 10, 2024

Version of record online: December 23, 2024

6. Critical summary and Outlook

By implementing both solution-phase and solid-phase synthetic strategies, this work provides access to a versatile class of modular molecules that hold significant potential as chelators for radiometals. In particular, the SPPS approach demonstrated herein stands out due to its rapid, resource-efficient execution, yielding structurally complex chelators with high purity. While the achievements of this work - presented across the three associated publications - are substantial, a critical evaluation of certain aspects is warranted and will be addressed in this section.

First, the sometimes moderate yields obtained via SPPS are considered, along with the potential recovery and reuse of monomers, which were employed in five-fold excess during the synthesis. In addition, limitations encountered in the HPLC-MS-based non-radioactive assay are discussed. Furthermore, the observed discrepancies in Zr complex stabilities, which appear to correlate with the spacing between hydroxamic acid units, are critically examined.

Although this work focused specifically on the design of highly functionalizable chelators for ^{89}Zr , the modular framework presented here can be adapted for use with other hard, oxophilic cations relevant to PET or SPECT imaging. Beyond medical imaging, potential applications for these chelators may extend into other fields. For example, they could be immobilized on solid-phase matrices and deployed as cross-linked beads in wastewater systems, functioning as molecular sponges for the selective removal of valuable cations. While originally proposed in a light-hearted context, this concept illustrates the broader utility and adaptability of these tailor-made chelators.

6.1 Solid Phase Peptide Synthesis

When evaluating the yields obtained via solid-phase peptide synthesis (SPPS), it becomes apparent that they remain relatively low, ranging from 9% to 26%. The exact reasons for this limited efficiency could not be conclusively identified. Initially, the low yield was attributed to the demanding coupling step between *O*-benzyl-protected hydroxylamine and the activated carboxylic acid on the solid support, which was considered a major bottleneck. To investigate this hypothesis, a modified solution-phase coupling strategy was explored using acid chloride **49** and *O*-benzyl-protected hydroxylamine **48**, as described in Section 5.2. Figure 18 illustrates this approach, tracing the synthesis from coupling through to the final monomer to provide an overview of the process.

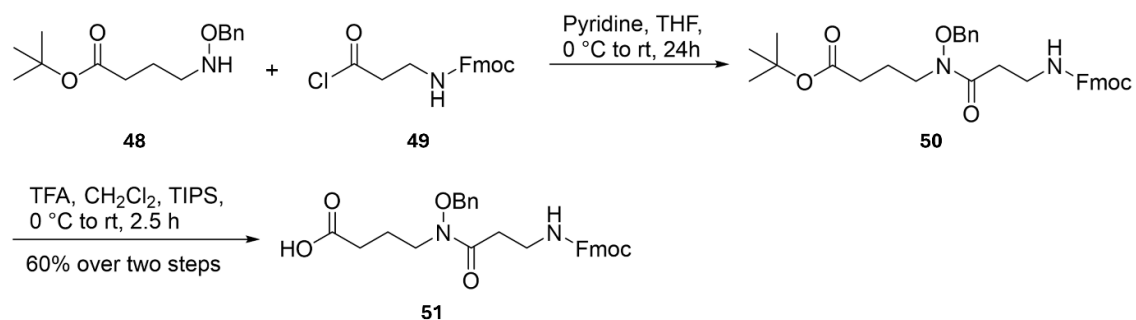


Figure 18: Reaction of an O-benzyl-protected hydroxylamine with an acid chloride with subsequent deprotection of the tert-butyl ester.

This alternative strategy shown in Figure 18 avoided the challenging on-resin hydroxamate coupling by introducing pre-formed monomers, allowing the subsequent SPPS to proceed via conventional peptide couplings between amines and carboxylic acids. Nevertheless, even this streamlined approach - comprising only four standard double coupling steps - resulted in post-purification yields of merely 9% to 13%. These findings suggest that additional issues, possibly related to synthetic conditions or purification inefficiencies, are contributing to the overall low yield and merit further investigation.

To further explore this issue and simultaneously demonstrate the scalability of the synthesis, an SPPS was conducted (Section 5.2) using 2-chlorotrityl chloride (CTC) resin in place of Wang resin. As outlined in Section 3.2, the CTC linker exhibits significantly higher acid lability compared to the Wang resin, allowing cleavage with 1 – 5 % TFA in CH₂Cl₂ for 1 minute, instead of the standard 90 – 95 % TFA in CH₂Cl₂ for 1 – 2 hours using TIPS as scavenger. This modified cleavage protocol resulted in a yield of 64 % after purification via semipreparative HPLC. These results indicate that the high TFA concentration and prolonged exposure times during cleavage from Wang resin likely cause partial degradation of the synthesized structures.

Furthermore, as shown in the reaction scheme, monomers such as **50** - prepared via acid chloride coupling - contain a *tert*-butyl ester that was subsequently cleaved using 50 % TFA in CH₂Cl₂ for 2.5 hours, yielding the corresponding free acid **51**. While no intermediate purification was carried out between coupling and deprotection, overall yields of 60 – 65 % were obtained over the two steps. This yield is relatively low. Taken together, these findings strongly suggest that the improved yield observed with CTC resin is directly related to the milder cleavage conditions, and that the harsh TFA-based cleavage employed with Wang resin may lead to product degradation.

Although the initial choice of Wang resin was based on the intention to perform harsh on-resin deprotection reactions, future experiments should carefully align the resin and linker selection

with the specific synthetic goals. Optimizing this choice will be essential to improve yield and reproducibility in upcoming studies.

In the SPPS conducted in this work, each coupling step typically involved the use of five equivalents of both the monomer and the coupling reagent. This stoichiometry results in exceptionally poor atom economy, raising concerns about the overall sustainability and efficiency of the synthetic process. To partially address this limitation, a series of experiments were undertaken to recover and potentially reuse the excess monomers. Successful recovery would enable their reapplication in subsequent syntheses, thereby improving the atom economy and reducing material waste.

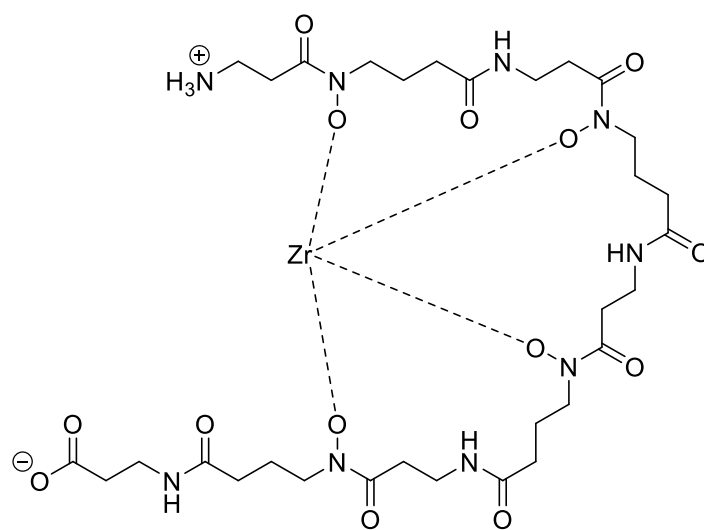
Most of the coupling reactions employed PyOxim® **43** as the activating agent. For the monomer recovery process, the dimethylformamide (DMF) used in the reaction mixture was first removed under reduced pressure. The resulting residue was then redissolved in dichloromethane (CH_2Cl_2), and the organic phase was washed with 1 M hydrochloric acid. This washing step aimed to remove excess DIPEA, hydrolyze any remaining active esters or unused coupling reagent, and ensure protonation of the unreacted carboxylic acids to retain them in the organic phase. The organic solvents were subsequently evaporated under reduced pressure.

Attempts to purify the crude residue by silica gel chromatography were unsuccessful. All collected fractions contained a high proportion of phosphoric acid amides, the by-product when using **43**, which significantly hindered isolation of the desired monomer. To circumvent this challenge, several hydrolysis strategies were explored to cleave the phosphoric acid amide into pyrrolidinium and phosphate under acidic conditions. One such strategy employed a biphasic system of CH_2Cl_2 and 1 M HCl with vigorous stirring. However, even at elevated HCl concentrations, no conversion was observed. Similarly, an attempt using acetonitrile (CH_3CN) with para-toluenesulfonic acid (PTSA) and a small amount of demineralized water also failed to produce any discernible conversion. Reaction progress was monitored via ^{31}P -NMR spectroscopy, confirming the lack of successful hydrolysis.

Despite the lack of success in these preliminary attempts, the concept of monomer recovery remains a promising avenue for improving the sustainability and cost-effectiveness of SPPS-based syntheses. Future investigations should continue to pursue this goal by optimizing both chemical and physical conditions to enable the efficient recovery and reuse of valuable building blocks.

6.2 Non-radiocactive Stability Assay

Several challenges arose during the implementation of the HPLC-MS-based stability assay. During complexation with Zr^{4+} , an ion exchange takes place in which four protons (H^+) are displaced, resulting in an increase in the pH of the reaction medium. Potential transmetallation processes involving ipDFO* and competing chelators such as EDTA or DFOB further influence the solution's pH. These pH shifts were considered in the assay design and mitigated through the use of HEPES buffer, with all buffered solutions adjusted to pH 7 to simulate physiologically relevant conditions. Figure 19 illustrates the structure of an ipDFO* chelator with a seven-atom linker between hydroxamic acid units under these conditions.



Zr-ipDFO* complex **52**

Figure 19: Zr- ipDFO* complex with a spacing of seven atoms between the hydroxamates.

Molecular structure **52** does not provide straightforward sites for simple protonation. The solvents used in the HPLC-MS analysis were 0.1 % formic acid in demineralized water and 0.1 % formic acid in acetonitrile, yielding a pH of approximately 2.8 in the aqueous phase. In order to generate sufficient signal intensity in electrospray ionization mass spectrometry (ESI-MS), a net molecular charge other than zero is required. To enable detection as $[\text{M}+\text{H}]^+$ ions, carboxylic acid groups can be protonated. The β -alanine moiety has a pK_a of 3.55; however, in structure **52**, the nitrogen is present as an amide rather than a free amine. Due to the electron-withdrawing nature of the amide, it is likely that the effective pK_a is somewhat elevated. Taking these factors into account, the assay was designed to ensure detection of the complexes as $[\text{M}+\text{H}]^+$ ions.

Nonetheless, very low signal intensities were occasionally observed. The analyte showed retention on the C_{18} -column used, suggesting that the buffered environment at pH 7 was

entirely displaced during elution. A key factor in these experiments was the use of a 1000-fold excess of EDTA. Although EDTA exhibited negligible retention on the column, it produced significant peak tailing. Furthermore, the EDTA concentration approached the upper limit of the detector's tolerance, with total ion chromatogram (TIC) intensities in the range of 10^9 . This was necessary because the target analyte had to be detected at concentrations three orders of magnitude lower, corresponding to TIC intensities of 10^4 – 10^5 , far below optimal sensitivity. As the analyte signal often coincided with the EDTA tailing, ion suppression due to ESI-MS cannot be entirely excluded. Despite these limitations, the measurements exhibited reasonable consistency, permitting their use in data evaluation.

As an alternative to the HPLC-MS-based non-radioactive stability assay, a UHPLC approach using a high-performance diode-array detector (DAD) was explored. Previous experiments indicated that the ipDFO* chelators exhibit a UV absorption maximum near 225 nm, attributable to the hydroxamate functional groups. While signals corresponding to Zr-ipDFO* complexes were successfully detected, no signal was observed for Zr-DFOB complexes. This may be attributed to the ability of the Zr-DFOB complex to adopt a range of configurations at pH 7, which likely results in variable and inconsistent retention behavior on the hydrophilic interaction chromatography (HILIC) phase.^[192] This signal blurring is further exacerbated by dynamic equilibrium processes, ultimately preventing detectable signals. Figure 20 supports this hypothesis with an illustration from the literature depicting Zr-DFOB speciation across different pH values.

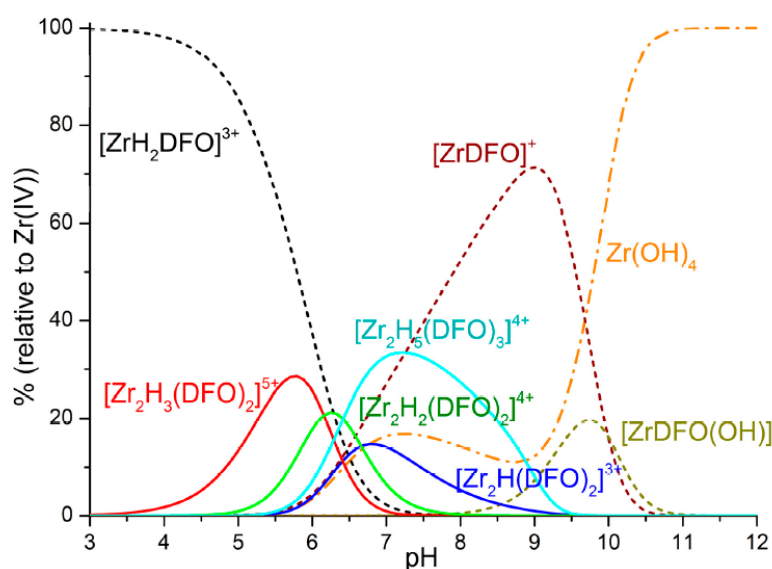


Figure 20: Distribution of individual species of Zr-DFOB-Complexes. Solid lines: binuclear species. Dashed lines: mononuclear species. Dash-dot lines: Zr^{4+} hydroxo species.^[192]

Unfortunately, the UHPLC-UV/Vis approach did not yield reliable results. Signal intensities decreased rapidly over the course of the assay, compromising analytical reliability. As with the HPLC-MS method, EDTA peak tailing remained problematic. In addition, quantification via signal integration was hampered by baseline instability, resulting in data discrepancies. Nonetheless, the method shows promise. With careful optimization - including solvent selection, gradient adjustment, and choice of a column capable of achieving better signal separation - the UHPLC-based assay could serve as a viable alternative to the HPLC-MS method. A major advantage of this technique is that detectors in UV/Vis-based systems are not as easily overwhelmed by high concentrations, thereby allowing for increased analyte concentrations as long as no adverse chemical interactions occur.

6.3 Comparability of stability assays in the literature

In order to contextualize the results of the complex stability assays within the existing literature, a detailed analysis of previously reported assays was conducted. Sixteen publications were identified that investigated the complex stability of DFO **7**, DFO* **8**, and their analogs using competitive assays.^[152, 154-156, 158-162, 165-166, 174, 193-196] Table 5 summarizes the analytical methods employed and the experimental parameters selected.

Tabelle 5: Overview of the methods and parameters of the competition experiments found in the literature regarding the complex stabilities of DFOB and DFO* analogs. Colored areas are comparable experiments within this evaluation due to similar parameters.

Publication	Method	Chelator Concentration	Competitive Chelator	Ratio Chelator to competitive Chelator	Temperature [°C]	pH	Intact DFOB-complex
Allott 2017 ^[156]	iTLC	10 mM	EDTA	100	37 °C	7	66 % (7 d)
Sarbisheh 2020 ^[160]	iTLC	0.02 mM	EDTA	100	37 °C	5 – 8 (0.5 steps)	16 % (7 d)
Sarbisheh 2023 ^[161]	iTLC	0.02 µM	EDTA	100	37 °C	6.5 and 7.0	76 % (7 d)
Salih 2022 ^[162]	iTLC	0.022 mM	EDTA	1000	37 °C	7	35 % (7 d)
Raavé 2019 ^[158]	iTLC	0.1 mM	EDTA	1000	37 °C	/	50 % (7 d)
Outzen 2025 ^[194]	iTLC	0.5 µM	EDTA	1000	37 °C	7	55 % (7 d)
Guerard 2014 ^[174]	iTLC	0.028 mM	EDTA	1750	37 °C	7.4	50 % (7 d)
Guerard 2017 ^[195]	iTLC	0.8 mM	EDTA	2000	rt	6 - 8	/
Brandt 2020 ^[196]	iTLC	0.5 µM	DTPA	10 000 100 000	rt	6	/
Rudd 2016 ^[159]	iTLC	0.1 mM 0.96 mM	EDTA	500	50 °C	7	/
Patra 2014 ^[152]	Radio-HPLC	0.28 µM	DFOB	300 and 3000	rt	7.3	/
Seibold 2017 ^[165]	Radio-HPLC	0.01 mM	EDTA	100, 1000, 9000	rt	7	
Brown 2020 ^[154]	HPLC-MS	0.06 mM	EDTA	160 and 1600	rt	7.4	/
Outzen 2023 ^[193]	HPLC-MS	0.04 µM	EDTA	1000	rt	7	/
Tieu 2017 ^[166]	HPLC-MS	/	EDTA	1800	/	7	/
Adams 2017 ^[155]	/	/	EDTA	1000	/	/	/

Various analytical methods were employed across these publications, including radiochemical iTLC, radio-HPLC, and HPLC-MS. The concentration of the chelator under investigation ranged from 10 mM to 0.02 μ M in the iTLC assays, and from 0.01 mM to 0.04 μ M in the HPLC-based assays. In most assays, EDTA was used as the competing chelator; however, in one case DFOB and in another DTPA was employed. The ratio of the chelator under investigation to the competing chelator varied between 100 and 100,000. Of the 16 experiments conducted, 7 were performed at 37 °C, while the others were carried out at room temperature or, in one instance, at 50 °C. Most experiments were conducted at a pH of 7.

In assessing the suitability of the methodologies with regard to comparability, only two comparable groups could be identified (highlighted in blue and green in Table 5). Beside of the used chelator concentration, both groups used DFOB **7** as a reference chelator under investigation, employed iTLC as the analytical method, utilized EDTA as the competing chelator, and conducted the experiments at 37 °C and pH 7. The only difference between the two groups lies in the ratio of DFOB **7** to EDTA: 1:100 and 1:1000. Nevertheless, significant discrepancies in the results are evident. For the group using a 100-fold excess of EDTA, the percentage of intact ^{89}Zr -DFOB complexes remaining after seven days was reported as 16%, 66%, and 76%. Similarly, for the group using 1000-fold excess of EDTA, values of 35%, 50%, and 55% were observed. No correlation with the applied DFOB **7** concentration could be identified.

This analysis clearly demonstrates that comparisons between the different publications must be approached with great caution. Given the extent of variation observed for a single compound (DFOB), it is hardly possible to draw meaningful conclusions regarding the comparability of different compounds. Ultimately, these experiments only allow for a relative assessment of DFOB or DFO* analogs within the context of a single assay, using a reference compound such as DFOB as a benchmark—absolute comparisons across studies are not supported by the data.

6.4 Structural and conceptual discussion of discrepancies in stability results

Finally, the initially contradictory results from the paper in section 5.1 and the paper in section 5.3 should be addressed. In the first publication, a non-radioactive HPLC-MS stability assay was used to show that increased complex stability occurs with a smaller spacing between the hydroxamic acids. In the results from the third paper in section 5.3, the exact opposite was shown in a radioactive stability assay.

Considering the structures **53** and **54** that were used, there are some obvious structural differences that could have contributed to these different results. As a comparison, Figure 21 shows the corresponding compounds with eight atoms between the hydroxamic acids.

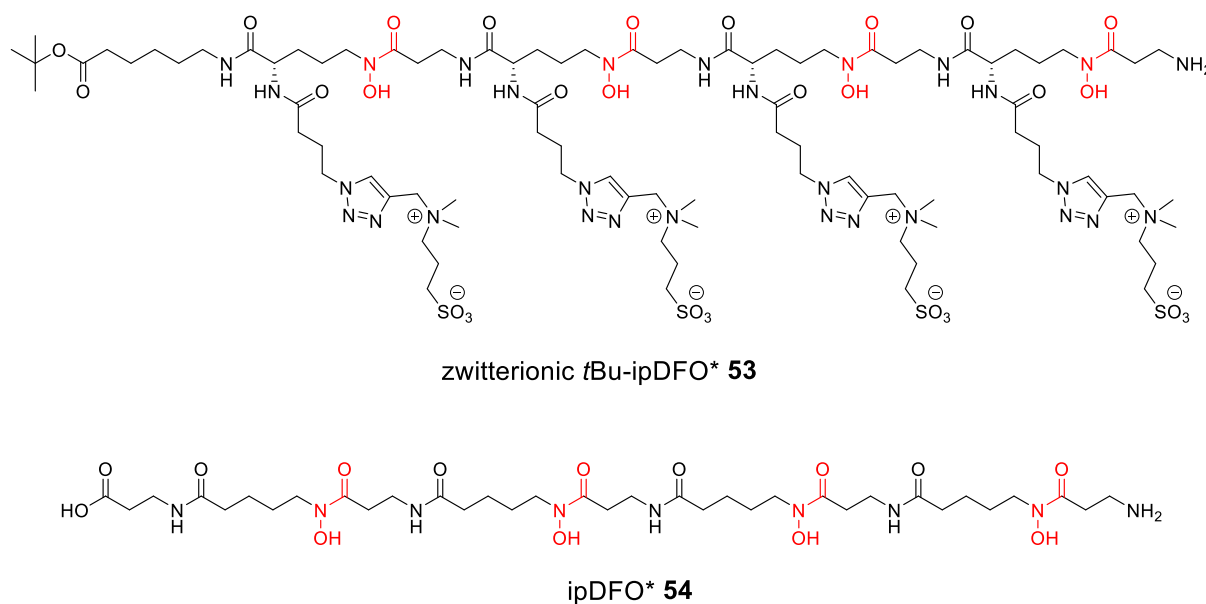


Figure 21: Zwitterionically modified tBu-ipDFO* chelator **53** and isopeptide ipDFO* chelator **54**, both with a spacing of eight atoms between the hydroxamic acids.

The most striking structural difference is the zwitterionic side chains in **53**, which are not present in **54**. These could have a protecting effect, whereby interactions with the solvent or the competing reagent in **53** could be reduced. A second difference is the free terminal carboxylic acid in **54**. In **53**, the C-terminus is still protected by a *tert*-butyl ester. The free acid could serve as an additional complexation site in energetically unfavored states. Whether or not this is conducive to Zr complexation overall, however, would have to be investigated in experiments. It should also be noted at this point that a complete turnaround of the above-mentioned stability results is difficult to explain based on structural differences. This would mean that the structural differences lead to an effect that ensures that the previously more unstable spacing becomes the more stable spacing.

In addition to the structural differences, the concept of the assay is also different. The non-radioactive assay is based on quantitative complexation of the chelators with zirconium. The addition of excess EDTA therefore results in an exactly 1000-fold higher concentration of the competing chelator compared to the Zr complex present. The situation is different for the radioactive assay. For practical reasons, all chelator molecules present are never quantitatively complexed with ^{89}Zr . Only a very small proportion of the chelators are present as ^{89}Zr complexes next to a very large proportion of still free chelators. The molecular number of ^{89}Zr introduced cannot be determined due to the nature of radioactive decay. The design of the

experiments is based solely on radioactive activity. However, the number of competing agents to be added is still determined by the total amount of chelator analyte. As a result of this procedure, EDTA is present in a 1000-fold excess to the ipDFO* chelators, but in a much higher excess of corresponding ^{89}Zr -ipDFO* complexes. It cannot be assumed that the shift in transmetallation at the beginning is the same when the competing chelator is added, because the free analyte chelators now compete with the competing chelator for the ^{89}Zr . From this point of view, it is already a state at the beginning of the radioactive assay that is only reached later in the non-radioactive assay under the assumption that the EDTA is so much in excess that the proportion that is then present in a Zr complex is negligibly small. Depending on the actual number of ^{89}Zr , this state would be in a range in which transmetallation would take place much slower than at the beginning of the non-radioactive assay anyway.

Whether the structural differences of the molecules used or the conceptual differences of the assays carried out or a combination of both lead to the inverse results cannot be conclusively clarified at this point and further experiments must be carried out to clarify this.

6.5 Outlook

In summary, this work has enabled access to a new class of molecules with significant potential for clinical diagnostics, particularly in targeted PET imaging and immunoPET, exemplified by the KuE-ipDFO* construct described in Section 5.2. The newly developed solid-phase synthesis (SPPS) strategy markedly reduces manual workload and facilitates the generation of “clickable” derivatives for targeted conjugation. The synthetic approach presented in this thesis demonstrates strong potential for full automation and exhibits robustness under conditions amenable to scale-up. The chelators introduced herein possess high flexibility for adaption to a variety of novel applications. Furthermore, the studies conducted have shown that Zr^{4+} complexation can be fine-tuned to improve the stability of these chelators for future clinical applications. Ideally, this enhanced stability may beneficially avoid the *in vivo* release of radioactive ^{89}Zr during patient imaging.

One recurring issue in the synthesis workflow was the hydrogenolytic deprotection of O-benzyl-protected hydroxamic acids. This was performed under a hydrogen atmosphere using palladium on activated carbon (Pd/C 10%) as a heterogeneous catalyst. If the reaction proceeded for too long, a partial reduction of hydroxamic acids to amides was observed, necessitating strict monitoring of the reaction’s progression. Notably, the reaction kinetics were varied significantly across experiments, with some trials showing no detectable conversion. This was particularly evident for AZA derivatives and zwitterionic ipDFO* analogues, which posed considerable challenges in achieving complete conversion. Additionally, when an

excessive amount of Pd/C was used (e.g., ~1.5 mg Pd/C per 10 mg substrate), no recoverable product or starting material could be obtained.

Literature reports suggest that certain functional groups or structural motifs - especially non-polar or aromatic moieties - tend to adsorb strongly onto carbon-based supports.^[197-199] Even positively charged species such as protonated anilines at low pH have been shown to undergo significant adsorption under such conditions. Given these findings, it is plausible that the DFOB and DFO* analogues synthesized in this study may also exhibit adsorption to the catalyst surface, thereby impeding reaction efficiency. In addition, possible interactions between free hydroxamic acids and palladium ions must be considered. Although no definitive conclusions could be drawn from the experimental work conducted thus far, further investigation into alternative catalytic systems is warranted. Suitable candidates for such future studies may include Pd/Al₂O₃, Pd/SiO₂, and PtO₂.

From a basic research perspective, crystallographic analysis of Zr complexes formed with these chelators represents a promising avenue. To date, no crystal structures of Zr-DFOB, Zr-DFO*, or their analogues have been reported. Successful implementation would require stable complexes with limited conformational flexibility to enable uniform crystal formation. This reinforces the relevance of further structural optimization of the chelators not only for practical applications, but also to facilitate fundamental insights into Zr coordination chemistry.

From an application-oriented point of view, the development of a fully solid-phase synthesized PET tracer would represent a compelling future goal. The strategy outlined in Section 5.2 for the synthesis of a KuE-ipDFO* derivative already demonstrates feasibility in this direction, although future applications may involve greater complexity. A plausible objective would be the complete solid-phase synthesis of a more advanced construct such as PSMA-617, equipped with a modular linker and an optimized Zr-chelator featuring functionalizable side chains. Crucially, this would entail performing both the palladium-catalyzed O-benzyl deprotection and the copper-catalyzed azide-alkyne cycloaddition directly on-resin. Such an approach could allow the resin to function simultaneously as a purification scaffold for removing residual heavy metals. This feature would be particularly advantageous in a GMP-compliant synthesis for clinical-grade radiopharmaceuticals.

7. Literature

- [1] G. Crisan, N. S. Moldovean-Cioroianu, D. G. Timaru, G. Andries, C. Cainap, V. Chis, *Int J Mol Sci* **2022**, *23*.
- [2] M. Unterrainer, C. Eze, H. Ilhan, S. Marschner, O. Roengvoraphoj, N. S. Schmidt-Hegemann, F. Walter, W. G. Kunz, P. M. A. Rosenschold, R. Jeraj, N. L. Albert, A. L. Grosu, M. Niyazi, P. Bartenstein, C. Belka, *Radiat Oncol* **2020**, *15*, 88.
- [3] U. Bashir, A. Mallia, J. Stirling, J. Joemon, J. MacKewn, G. Charles-Edwards, V. Goh, G. J. Cook, *Diagnostics (Basel)* **2015**, *5*, 333-357.
- [4] W. Jiang, Y. Chalich, M. J. Deen, *Sensors (Basel)* **2019**, *19*.
- [5] P. Zanzonico, *Semin Nucl Med* **2004**, *34*, 87-111.
- [6] L. H. C. Braga, L. Gasparini, L. Grant, R. K. Henderson, N. Massari, M. Perenzoni, D. Stoppa, R. Walker, *IEEE Journal of Solid-State Circuits* **2014**, *49*, 301-314.
- [7] A. Rahmim, H. Zaidi, *Nucl Med Commun* **2008**, *29*, 193-207.
- [8] M. L. James, S. S. Gambhir, *Physiol Rev* **2012**, *92*, 897-965.
- [9] X. Chen, J. Song, X. Chen, H. Yang, *Chem Soc Rev* **2019**, *48*, 3073-3101.
- [10] F. Schick, *Radiologe* **2007**, *47 Suppl 1*, S7-23; quiz S24-25.
- [11] C. Riola-Parada, L. García-Cañamaque, V. Pérez-Dueñas, M. Garcerant-Tafur, J. L. Carreras-Delgado, *Revista Española de Medicina Nuclear e Imagen Molecular (English Edition)* **2016**, *35*, 306-312.
- [12] E. C. Ehman, G. B. Johnson, J. E. Villanueva-Meyer, S. Cha, A. P. Leynes, P. E. Z. Larson, T. A. Hope, *J Magn Reson Imaging* **2017**, *46*, 1247-1262.
- [13] D. L. Chen, P. E. Kinahan, *Clin Transl Imaging* **2014**, *2*, 391-401.
- [14] B. F. Hutton, in *Handbook of Particle Detection and Imaging* (Eds.: I. Fleck, M. Titov, C. Grupen, I. Buvat), Springer International Publishing, Cham, **2021**, pp. 1217-1236.
- [15] K. Shibuya, E. Yoshida, F. Nishikido, T. Suzuki, T. Tsuda, N. Inadama, T. Yamaya, H. Murayama, *Phys Med Biol* **2007**, *52*, 5249-5261.
- [16] J. L. Humm, A. Rosenfeld, A. Del Guerra, *Eur J Nucl Med Mol Imaging* **2003**, *30*, 1574-1597.
- [17] N. Demir, Z. N. Kuluöztürk, *Nuclear Engineering and Technology* **2021**, *53*, 3759-3763.
- [18] M. Pagani, S. Stone-Elander, S. A. Larsson, *Eur J Nucl Med* **1997**, *24*, 1301-1327.
- [19] C. C. Martin, B. T. Christian, M. R. Satter, L. H. Nickerson, R. J. Nickles, *IEEE Trans Med Imaging* **1995**, *14*, 681-687.
- [20] M. J. Schueller, T. L. Mulnix, B. T. Christian, M. Jensen, S. Holm, T. R. Oakes, A. D. Roberts, D. W. Dick, C. C. Martin, R. J. Nickles, *IEEE Transactions on Nuclear Science* **2003**, *50*, 50-52.

- [21] P. W. Miller, N. J. Long, R. Vilar, A. D. Gee, *Angew Chem Int Ed Engl* **2008**, *47*, 8998-9033.
- [22] J. Xu, F. Cai, C. Geng, Z. Wang, X. Tang, *Front Cardiovasc Med* **2021**, *8*, 621389.
- [23] W. A. Weber, K. Ott, K. Becker, H. J. Dittler, H. Helmberger, N. E. Avril, G. Meisetschlager, R. Busch, J. R. Siewert, M. Schwaiger, U. Fink, *J Clin Oncol* **2001**, *19*, 3058-3065.
- [24] T. Schepis, O. Gaemperli, V. Treyer, I. Valenta, C. Burger, P. Koepfli, M. Namdar, I. Adachi, H. Alkadhi, P. A. Kaufmann, *J Nucl Med* **2007**, *48*, 1783-1789.
- [25] P. A. Rowley, A. A. Samsonov, T. J. Betthausen, A. Pirasteh, S. C. Johnson, L. B. Eisenmenger, *Semin Ultrasound CT MR* **2020**, *41*, 572-583.
- [26] P. F. Zhang, F. Gao, *J Neurol* **2022**, *269*, 2304-2314.
- [27] B. Weber, C. Burger, M. T. Wyss, G. K. von Schulthess, F. Scheffold, A. Buck, *Eur J Neurosci* **2004**, *20*, 2664-2670.
- [28] M. Conti, L. Eriksson, *EJNMMI Phys* **2016**, *3*, 8.
- [29] V. Pichler, N. Berroteran-Infante, C. Philippe, C. Vraka, E. M. Klebermass, T. Balber, S. Pfaff, L. Nics, M. Mitterhauser, W. Wadsak, *J Nucl Med* **2018**, *59*, 1350-1354.
- [30] I. M. Jackson, S. J. Lee, A. R. Sowa, M. E. Rodnick, L. Bruton, M. Clark, S. Preshlock, J. Rothley, V. E. Rogers, L. E. Botti, B. D. Henderson, B. G. Hockley, J. Torres, D. M. Raffel, A. F. Brooks, K. A. Frey, M. R. Kilbourn, R. A. Koeppe, X. Shao, P. J. H. Scott, *EJNMMI Radiopharm Chem* **2020**, *5*, 24.
- [31] A. Moscoso, J. Silva-Rodriguez, J. M. Aldrey, J. Cortes, J. M. Pias-Peleiteiro, A. Ruibal, P. Aguiar, I. Alzheimer's Disease Neuroimaging, *Eur J Nucl Med Mol Imaging* **2022**, *49*, 1242-1253.
- [32] A. D. Joshi, M. J. Pontecorvo, L. Adler, M. G. Stabin, D. M. Skovronsky, A. P. Carpenter, M. A. Mintun, F. s. i. Florbetapir, *EJNMMI Res* **2014**, *4*, 4.
- [33] L. Evangelista, A. Briganti, S. Fanti, S. Joniau, S. Reske, R. Schiavina, C. Stief, G. N. Thalmann, M. Picchio, *Eur Urol* **2016**, *70*, 161-175.
- [34] F. E. von Eyben, K. Kairemo, *Nucl Med Commun* **2014**, *35*, 221-230.
- [35] C. Lapa, M. Kircher, M. Da Via, M. Schreder, L. Rasche, K. M. Kortüm, H. Einsele, A. K. Buck, H. Hänscheid, S. Samnick, *Clinical Nuclear Medicine* **2019**, *44*, 620-624.
- [36] C. Lapa, S. Knop, M. Schreder, M. Rudelius, M. Knott, G. Jorg, S. Samnick, K. Herrmann, A. K. Buck, H. Einsele, K. Luckerath, *Theranostics* **2016**, *6*, 254-261.
- [37] Y. Nakamoto, *Clin Lymphoma Myeloma Leuk* **2014**, *14*, 10-11.
- [38] A. W. Glaudemans, R. H. Enting, M. A. Heesters, R. A. Dierckx, R. W. van Rheeën, A. M. Walenkamp, R. H. Slart, *Eur J Nucl Med Mol Imaging* **2013**, *40*, 615-635.
- [39] S. R. Miller, P. Li, M. Schipper, L. Junck, M. Piert, T. S. Lawrence, C. Tsien, Y. Cao, M. Kim, *International Journal of Radiation Oncology*Biophysics* **2019**, *105*.

-
- [40] A. Kardan, S. Choi, M. Satter, A. Sloan, R. F. Muzic, in *Handbook of Neuro-Oncology Neuroimaging (Third Edition)* (Ed.: H. B. Newton), Academic Press, **2022**, pp. 439-459.
- [41] T. Yamaki, Y. Higuchi, H. Yokota, Y. Iwadate, T. Matsutani, S. Hirono, H. Sasaki, R. Sasao, M. Toda, S. Onodera, N. Oka, S. Kobayashi, *Clin Imaging* **2022**, *92*, 124-130.
- [42] F. L. Giesel, C. Kratochwil, J. Schlittenhardt, K. Dendl, M. Eiber, F. Staudinger, L. Kessler, W. P. Fendler, T. Lindner, S. A. Koerber, J. Cardinale, D. Sennung, M. Roehrich, J. Debus, M. Sathekge, U. Haberkorn, J. Calais, S. Serfling, A. L. Buck, *Eur J Nucl Med Mol Imaging* **2021**, *48*, 4377-4385.
- [43] M. G. Vander Heiden, L. C. Cantley, C. B. Thompson, *Science* **2009**, *324*, 1029-1033.
- [44] A. Almuhaideb, N. Papathanasiou, J. Bomanji, *Ann Saudi Med* **2011**, *31*, 3-13.
- [45] W. Wei, Z. T. Rosenkrans, J. Liu, G. Huang, Q. Y. Luo, W. Cai, *Chem Rev* **2020**, *120*, 3787-3851.
- [46] S. L. Pimlott, A. Sutherland, *Chem Soc Rev* **2011**, *40*, 149-162.
- [47] C. Perez-Medina, A. J. P. Teunissen, E. Kluza, W. J. M. Mulder, R. van der Meel, *Adv Drug Deliv Rev* **2020**, *154-155*, 123-141.
- [48] M. Brandt, J. Cardinale, M. L. Aulsebrook, G. Gasser, T. L. Mindt, *Journal of Nuclear Medicine* **2018**, *59*, 1500.
- [49] L. Badier, I. Quelven, *Pharmaceutics* **2024**, *16*.
- [50] O. Boutureira, G. J. Bernardes, *Chem Rev* **2015**, *115*, 2174-2195.
- [51] J. M. Baskin, C. R. Bertozzi, *QSAR & Combinatorial Science* **2007**, *26*, 1211-1219.
- [52] U. Brinkmann, R. E. Kontermann, *MAbs* **2017**, *9*, 182-212.
- [53] K. Runcie, D. R. Budman, V. John, N. Seetharamu, *Mol Med* **2018**, *24*, 50.
- [54] Q. Wan, H. Yuan, P. Cai, Y. Liu, T. Yan, L. Wang, Z. Zhou, W. Zhang, N. Liu, *Mol Pharm* **2024**, *21*, 4430-4440.
- [55] Y. Liu, L. Xia, H. Li, P. Cai, S. Tang, Y. Feng, G. Liu, Y. Chen, N. Liu, W. Zhang, Z. Zhou, *EJNMMI Res* **2024**, *14*, 15.
- [56] D. Brickute, C. Chen, M. Braga, C. Barnes, N. Wang, L. Allott, E. O. Aboagye, *RSC Adv* **2022**, *12*, 26372-26381.
- [57] S. Maschauer, R. Haubner, T. Kuwert, O. Prante, *Mol Pharm* **2014**, *11*, 505-515.
- [58] A. Schmidt, M. Wirtz, S. F. Farber, T. Osl, R. Beck, M. Schottelius, M. Schwaiger, H. J. Wester, *ACS Omega* **2018**, *3*, 8278-8287.
- [59] T. Liu, C. Liu, Y. Ren, X. Guo, J. Jiang, Q. Xie, L. Xia, F. Wang, H. Zhu, Z. Yang, *Front Mol Biosci* **2020**, *7*, 585024.
- [60] J. Zhang, L. Lang, Z. Zhu, F. Li, G. Niu, X. Chen, *J Nucl Med* **2015**, *56*, 1609-1614.
-

- [61] H. H. Sibinga Mulder BG, Vugts DJ, Sewing C, Windhorst AD, Stammes M, de Geus-Oei LF, Bordo MW, Mieog JSD, van de Velde CJ, Frangioni JV, Vahrmeijer AL, *Am J Nucl Med Mol Imaging* **2018**, *8*(5), 282-291.
- [62] M. Holzapfel, T. Baldau, S. Kerpa, G. Guadalupi, B. Qi, Y. Liu, W. J. Parak, W. Maison, *European Journal of Inorganic Chemistry* **2022**, 2022.
- [63] J. Schwenck, D. Sonanini, J. M. Cotton, H. G. Rammensee, C. la Fougere, L. Zender, B. J. Pichler, *Nat Rev Cancer* **2023**, *23*, 474-490.
- [64] M. F. Ullah, M. Aatif, *Cancer Treat Rev* **2009**, *35*, 193-200.
- [65] T. A. Hope, J. Z. Goodman, I. E. Allen, J. Calais, W. P. Fendler, P. R. Carroll, *J Nucl Med* **2019**, *60*, 786-793.
- [66] J. R. Mesters, C. Barinka, W. Li, T. Tsukamoto, P. Majer, B. S. Slusher, J. Konvalinka, R. Hilgenfeld, *EMBO J* **2006**, *25*, 1375-1384.
- [67] M. O. Anderson, L. Y. Wu, N. M. Santiago, J. M. Moser, J. A. Rowley, E. S. Bolstad, C. E. Berkman, *Bioorg Med Chem* **2007**, *15*, 6678-6686.
- [68] M. Benesova, M. Schafer, U. Bauder-Wust, A. Afshar-Oromieh, C. Kratochwil, W. Mier, U. Haberkorn, K. Kopka, M. Eder, *J Nucl Med* **2015**, *56*, 914-920.
- [69] R. Seifert, K. Seitzer, K. Herrmann, K. Kessel, M. Schafers, J. Kleesiek, M. Weckesser, M. Boegemann, K. Rahbar, *Theranostics* **2020**, *10*, 7812-7820.
- [70] O. Sartor, J. de Bono, K. N. Chi, K. Fizazi, K. Herrmann, K. Rahbar, S. T. Tagawa, L. T. Nordquist, N. Vaishampayan, G. El-Haddad, C. H. Park, T. M. Beer, A. Armour, W. J. Perez-Contreras, M. DeSilvio, E. Kpamegan, G. Gericke, R. A. Messmann, M. J. Morris, B. J. Krause, V. Investigators, *N Engl J Med* **2021**, *385*, 1091-1103.
- [71] T. Lindner, A. Loktev, A. Altmann, F. Giesel, C. Kratochwil, J. Debus, D. Jager, W. Mier, U. Haberkorn, *J Nucl Med* **2018**, *59*, 1415-1422.
- [72] M. Sollini, M. Kirienko, F. Gelardi, F. Fiz, N. Gozzi, A. Chiti, *Eur J Nucl Med Mol Imaging* **2021**, *48*, 4396-4414.
- [73] H. Chen, Y. Pang, J. Wu, L. Zhao, B. Hao, J. Wu, J. Wei, S. Wu, L. Zhao, Z. Luo, X. Lin, C. Xie, L. Sun, Q. Lin, H. Wu, *Eur J Nucl Med Mol Imaging* **2020**, *47*, 1820-1832.
- [74] Y. Mori, K. Dendl, J. Cardinale, C. Kratochwil, F. L. Giesel, U. Haberkorn, *Radiology* **2023**, *306*, e220749.
- [75] C. Kratochwil, F. L. Giesel, M. Stefanova, M. Benesova, M. Bronzel, A. Afshar-Oromieh, W. Mier, M. Eder, K. Kopka, U. Haberkorn, *J Nucl Med* **2016**, *57*, 1170-1176.
- [76] X. Zhong, J. Guo, X. Han, W. Wu, R. Yang, J. Zhang, G. Shao, *Mol Pharm* **2023**, *20*, 2402-2414.
- [77] Z. Du, C. M. Lovly, *Mol Cancer* **2018**, *17*, 58.
- [78] J. K. Yoon, B. N. Park, E. K. Ryu, Y. S. An, S. J. Lee, *Int J Mol Sci* **2020**, *21*.

-
- [79] J. K. C. Chan, C. S. NG, P. K. Hui, *Histopathology* **1987**, *12*, 461-480.
 - [80] K. Muylle, P. Flamen, D. J. Vugts, T. Guiot, G. Ghanem, N. Meuleman, P. Bourgeois, B. Vanderlinden, G. A. van Dongen, H. Everaert, M. Vaes, D. Bron, *Eur J Nucl Med Mol Imaging* **2015**, *42*, 1304-1314.
 - [81] E. B. Zwick, J.; Ullrich, A., *Trends in Molecular Medicine* **2002**, *8*, 17 - 23.
 - [82] R. A. Farah, B. Clinchy, L. Herrera, E. S. Vitetta, *Crit Rev Eukaryot Gene Expr* **1998**, *8*, 321-356.
 - [83] P. J. Hudson, *Curr Opin Immunol* **1999**, *11*, 548-557.
 - [84] R. Manafi-Farid, B. Ataeinia, S. Ranjbar, Z. Jamshidi Araghi, M. M. Moradi, C. Pirich, M. Beheshti, *Front Med (Lausanne)* **2022**, *9*, 916693.
 - [85] P. Mohr, J. van Sluis, M. N. Lub-de Hooge, A. A. Lammertsma, A. H. Brouwers, C. Tsoumpas, *Front Nucl Med* **2024**, *4*, 1360710.
 - [86] H. W. Schroeder, Jr., L. Cavacini, *J Allergy Clin Immunol* **2010**, *125*, S41-52.
 - [87] A. M. Scott, J. D. Wolchok, L. J. Old, *Nat Rev Cancer* **2012**, *12*, 278-287.
 - [88] E. T. Sarcan, Y. ÖZER, *Fabad Journal of Pharmaceutical Sciences* **2023**.
 - [89] L. Lindenberg, S. Adler, I. B. Turkbey, F. Mertan, A. Ton, K. Do, S. Kummar, E. M. Gonzalez, S. Bhattacharyya, P. M. Jacobs, P. Choyke, *Am J Nucl Med Mol Imaging* **2017**, *7*, 195-203.
 - [90] K. Tamura, H. Kurihara, K. Yonemori, H. Tsuda, J. Suzuki, Y. Kono, N. Honda, M. Kodaira, H. Yamamoto, M. Yunokawa, C. Shimizu, K. Hasegawa, Y. Kanayama, S. Nozaki, T. Kinoshita, Y. Wada, S. Tazawa, K. Takahashi, Y. Watanabe, Y. Fujiwara, *J Nucl Med* **2013**, *54*, 1869-1875.
 - [91] C. Lohrmann, E. M. O'Reilly, J. A. O'Donoghue, N. Pandit-Taskar, J. A. Carrasquillo, S. K. Lyashchenko, S. Ruan, R. Teng, W. Scholz, P. W. Maffuid, J. S. Lewis, W. A. Weber, *Clin Cancer Res* **2019**, *25*, 7014-7023.
 - [92] N. Pandit-Taskar, J. A. O'Donoghue, V. Beylergil, S. Lyashchenko, S. Ruan, S. B. Solomon, J. C. Durack, J. A. Carrasquillo, R. A. Lefkowitz, M. Gonen, J. S. Lewis, J. P. Holland, S. M. Cheal, V. E. Reuter, J. R. Osborne, M. F. Loda, P. M. Smith-Jones, W. A. Weber, N. H. Bander, H. I. Scher, M. J. Morris, S. M. Larson, *Eur J Nucl Med Mol Imaging* **2014**, *41*, 2093-2105.
 - [93] M. C. H. Hekman, M. Rijpkema, E. H. Aarntzen, S. F. Mulder, J. F. Langenhuijsen, E. Oosterwijk, O. C. Boerman, W. J. G. Oyen, P. F. A. Mulders, *Eur Urol* **2018**, *74*, 257-260.
 - [94] M. W. den Hollander, F. Bensch, A. W. Glaudemans, T. H. Oude Munnink, R. H. Enting, W. F. den Dunnen, M. A. Heesters, F. A. Kruyt, M. N. Lub-de Hooge, J. Cees de Groot, J. Pearlberg, J. A. Gietema, E. G. de Vries, A. M. Walenkamp, *J Nucl Med* **2015**, *56*, 1310-1314.
-

- [95] A. N. Niemeijer, D. Leung, M. C. Huisman, I. Bahce, O. S. Hoekstra, G. van Dongen, R. Boellaard, S. Du, W. Hayes, R. Smith, A. D. Windhorst, N. H. Hendrikse, A. Poot, D. J. Vugts, E. Thunnissen, P. Morin, D. Lipovsek, D. J. Donnelly, S. J. Bonacorsi, L. M. Velasquez, T. D. de Gruijl, E. F. Smit, A. J. de Langen, *Nat Commun* **2018**, *9*, 4664.
- [96] C. W. Menke-van der Houven van Oordt, E. C. Gootjes, M. C. Huisman, D. J. Vugts, C. Roth, A. M. Luik, E. R. Mulder, R. C. Schuit, R. Boellaard, O. S. Hoekstra, G. A. van Dongen, H. M. Verheul, *Oncotarget* **2015**, *6*, 30384-30393.
- [97] A. C. Lockhart, Y. Liu, F. Dehdashti, R. Laforest, J. Picus, J. Frye, L. Trull, S. Belanger, M. Desai, S. Mahmood, J. Mendell, M. J. Welch, B. A. Siegel, *Mol Imaging Biol* **2016**, *18*, 446-453.
- [98] C. W. Menke-van der Houven van Oordt, C. Gomez-Roca, C. van Herpen, A. L. Coveler, D. Mahalingam, H. M. Verheul, W. T. van der Graaf, R. Christen, D. Ruttinger, S. Weigand, M. A. Cannarile, F. Heil, M. Brewster, A. C. Walz, T. K. Nayak, E. Guarin, V. Meresse, C. Le Tourneau, *Oncotarget* **2016**, *7*, 80046-80058.
- [99] N. Pandit-Taskar, M. A. Postow, M. D. Hellmann, J. J. Harding, C. A. Barker, J. A. O'Donoghue, M. Ziolkowska, S. Ruan, S. K. Lyashchenko, F. Tsai, M. Farwell, T. C. Mitchell, R. Korn, W. Le, J. S. Lewis, W. A. Weber, D. Behera, I. Wilson, M. Gordon, A. M. Wu, J. D. Wolchok, *J Nucl Med* **2020**, *61*, 512-519.
- [100] S. M. Knowles, A. M. Wu, *J Clin Oncol* **2012**, *30*, 3884-3892.
- [101] F. Bensch, M. M. Smeenk, S. C. van Es, J. R. de Jong, C. P. Schroder, S. F. Oosting, M. N. Lub-de Hooge, C. W. Menke-van der Houven van Oordt, A. H. Brouwers, R. Boellaard, E. G. E. de Vries, *Theranostics* **2018**, *8*, 4295-4304.
- [102] E. C. Dijkers, T. H. Oude Munnink, J. G. Kosterink, A. H. Brouwers, P. L. Jager, J. R. de Jong, G. A. van Dongen, C. P. Schroder, M. N. Lub-de Hooge, E. G. de Vries, *Clin Pharmacol Ther* **2010**, *87*, 586-592.
- [103] K. D. Orcutt, G. P. Adams, A. M. Wu, M. D. Silva, C. Harwell, J. Hoppin, M. Matsumura, M. Kotsuma, J. Greenberg, A. M. Scott, R. A. Beckman, *Mol Imaging Biol* **2017**, *19*, 656-664.
- [104] R. Fu, L. Carroll, G. Yahioğlu, E. O. Aboagye, P. W. Miller, *ChemMedChem* **2018**, *13*, 2466-2478.
- [105] N. E. Weisser, J. C. Hall, *Biotechnol Adv* **2009**, *27*, 502-520.
- [106] P. Holliger, P. J. Hudson, *Nat Biotechnol* **2005**, *23*, 1126-1136.
- [107] M. Rashidian, L. Wang, J. G. Edens, J. T. Jacobsen, I. Hossain, Q. Wang, G. D. Vitoria, N. Vasdev, H. Ploegh, S. H. Liang, *Angew Chem Int Ed Engl* **2016**, *55*, 528-533.

-
- [108] D. Schumacher, J. Helma, A. F. L. Schneider, H. Leonhardt, C. P. R. Hackenberger, *Angew Chem Int Ed Engl* **2018**, *57*, 2314-2333.
- [109] B. M. Tijink, T. Laeremans, M. Budde, M. Stigter-van Walsum, T. Dreier, H. J. de Haard, C. R. Leemans, G. A. van Dongen, *Mol Cancer Ther* **2008**, *7*, 2288-2297.
- [110] Y. Vugmeyster, C. A. Entrican, A. P. Joyce, R. F. Lawrence-Henderson, B. A. Leary, C. S. Mahoney, H. K. Patel, S. W. Raso, S. H. Olland, M. Hegen, X. Xu, *Bioconjug Chem* **2012**, *23*, 1452-1462.
- [111] M. Lubberink, H. Herzog, *Eur J Nucl Med Mol Imaging* **2011**, *38 Suppl 1*, S10-18.
- [112] W. Bambynek, H. Behrens, M. H. Chen, B. Crasemann, M. L. Fitzpatrick, K. W. D. Ledingham, H. Genz, M. Mutterer, R. L. Intemann, *Reviews of Modern Physics* **1977**, *49*, 77-221.
- [113] M. N. Amiot, M. M. Bé, T. Branger, P. Cassette, M. C. Lépy, Y. Ménesguen, I. Da Silva, *Nuclear Instruments and Methods in Physics Research Section A: Accelerators, Spectrometers, Detectors and Associated Equipment* **2012**, *684*, 97-104.
- [114] W. M. van Wyngaardt, M. L. Smith, T. W. Jackson, B. Howe, S. M. Tobin, M. I. Reinhard, *Appl Radiat Isot* **2018**, *134*, 79-84.
- [115] E. T. Sarcan, M. Silindir-Gunay, A. Y. Ozer, N. Hartman, *Journal of Radioanalytical and Nuclear Chemistry* **2021**, *330*, 15-28.
- [116] O. Keinanen, K. Fung, J. M. Brennan, N. Zia, M. Harris, E. van Dam, C. Biggin, A. Hedt, J. Stoner, P. S. Donnelly, J. S. Lewis, B. M. Zeglis, *Proc Natl Acad Sci U S A* **2020**, *117*, 28316-28327.
- [117] S. Ghosh, N. L. Fletcher, P. Huda, Z. H. Houston, C. B. Howard, M. E. Lund, Y. Lu, D. H. Campbell, B. J. Walsh, K. J. Thurecht, *Mol Pharm* **2023**, *20*, 1549-1563.
- [118] K. A. Zettlitz, R. Tavaré, S. M. Knowles, K. K. Steward, J. M. Timmerman, A. M. Wu, *Clin Cancer Res* **2017**, *23*, 7242-7252.
- [119] M. A. Deri, B. M. Zeglis, L. C. Francesconi, J. S. Lewis, *Nuclear Medicine and Biology* **2013**, *40*, 3-14.
- [120] I. Verel, G. W. M. Visser, R. Boellaard, M. S.-v. Walsum, G. B. Snow, G. A. M. S. v. Dongen, *Journal of Nuclear Medicine* **2003**, *44*, 1271-1281.
- [121] A. Wooten, E. Madrid, G. Schweitzer, L. Lawrence, E. Mebrahtu, B. Lewis, S. Lapi, *Appl Sci-Basel* **2013**, *3*, 593-613.
- [122] I. Persson, *Pure and Applied Chemistry* **2010**, *82*, 1901-1917.
- [123] P. L. Brown, E. Curti, B. Grambow, C. Ekberg, *Chemical Thermodynamics of Zirconium*, Vol. 8, 1 ed., Elsevier Science, **2005**.
- [124] N. Wiberg, *Holleman Wiberg Lehrbuch der Anorganischen Chemie*, 102 ed., Walter de Gruyter, Berlin, **2007**.
-

- [125] R. H. Crabtree, *The Organometallic Chemistry of the Transition Metals*, 6 ed., John Wiley & Sons, Hoboken, New Jersey, **2014**.
- [126] M. Hofmann, G. Retamal-Morales, D. Tischler, *Nat Prod Rep* **2020**, *37*, 1262-1283.
- [127] R. Codd, *Coordination chemistry Reviews* **2008**, *252*, 1387 - 1408.
- [128] R. Codd, T. Richardson-Sanchez, T. J. Telfer, M. P. Gotsbacher, *ACS Chem Biol* **2018**, *13*, 11-25.
- [129] W. E. Meijs, H. J. Haisma, R. P. Klok, F. B. van Gog, E. Kievit, H. M. Pinedo, J. D. Herscheid, *J Nucl Med* **1997**, *38*, 112-118.
- [130] S. Heskamp, R. Raavé, O. Boerman, M. Rijpkema, V. Goncalves, F. Denat, *Bioconjugate chemistry* **2017**, *28*, 2211-2223.
- [131] H. Bickel, G. E. Hall, W. Keller-Schierlein, V. Prelog, E. Vischer, A. Wettstein, *Helvetica Chimica Acta* **2004**, *43*, 2129-2138.
- [132] R. C. Hider, X. Kong, *Nat Prod Rep* **2010**, *27*, 637-657.
- [133] D. Bellotti, M. Remelli, *Molecules* **2021**, *26*.
- [134] Z. D. Liu, R. C. Hider, *Med Res Rev* **2002**, *22*, 26-64.
- [135] A. E. Fazary, *Journal of Chemical & Engineering Data* **2005**, *50*, 888-895.
- [136] S. Dhungana, C. Ratledge, A. L. Crumbliss, *Inorg Chem* **2004**, *43*, 6274-6283.
- [137] P. J. Blower, R. Cusnir, A. Darwesh, N. J. Long, M. T. Ma, B. E. Osborne, T. W. Price, J. Pellico, G. Reid, R. Southworth, G. J. Stasiuk, S. Y. A. Terry, R. T. M. de Rosales, in *Advances in Inorganic Chemistry*, Vol. 78 (Eds.: C. D. Hubbard, R. van Eldik), Academic Press, **2021**, pp. 1-35.
- [138] G. Fischer, U. Seibold, R. Schirmacher, B. Wängler, C. Wängler, *Molecules* **2013**, *18*, 6469-6490.
- [139] J. P. Holland, V. Divilov, N. H. Bander, P. M. Smith-Jones, S. M. Larson, J. S. Lewis, *J Nucl Med* **2010**, *51*, 1293-1300.
- [140] B. V. Marquez, O. F. Ikotun, A. Zheleznyak, B. Wright, A. Hari-Raj, R. A. Pierce, S. E. Lapi, *Mol Pharm* **2014**, *11*, 3988-3995.
- [141] G. A. Ulaner, S. K. Lyashchenko, C. Riedl, S. Ruan, P. B. Zanzonico, D. Lake, K. Jhaveri, B. Zeglis, J. S. Lewis, J. A. O'Donoghue, *J Nucl Med* **2018**, *59*, 900-906.
- [142] S. B. Gaykema, A. H. Brouwers, M. N. Lub-de Hooge, R. G. Pleijhuis, H. Timmer-Bosscha, L. Pot, G. M. van Dam, S. B. van der Meulen, J. R. de Jong, J. Bart, J. de Vries, L. Jansen, E. G. de Vries, C. P. Schroder, *J Nucl Med* **2013**, *54*, 1014-1018.
- [143] S. F. Oosting, S. J. van Asselt, A. H. Brouwers, A. H. Bongaerts, J. D. Steinberg, J. R. de Jong, M. N. Lub-de Hooge, A. N. van der Horst-Schrivers, A. M. Walenkamp, E. W. Hoving, W. J. Sluiter, B. A. Zonnenberg, E. G. de Vries, T. P. Links, *J Nucl Med* **2016**, *57*, 1244-1250.

-
- [144] M. H. Jansen, S. E. M. Veldhuijzen van Zanten, D. G. van Vuurden, M. C. Huisman, D. J. Vugts, O. S. Hoekstra, G. A. van Dongen, G. L. Kaspers, *J Nucl Med* **2017**, *58*, 711-716.
- [145] L. R. Perk, O. J. Visser, M. Stigter-van Walsum, M. J. Vosjan, G. W. Visser, J. M. Zijlstra, P. C. Huijgens, G. A. van Dongen, *Eur J Nucl Med Mol Imaging* **2006**, *33*, 1337-1345.
- [146] A. Ruggiero, J. P. Holland, T. Hudolin, L. Shenker, A. Koulova, N. H. Bander, J. S. Lewis, J. Grimm, *J Nucl Med* **2011**, *52*, 1608-1615.
- [147] N. Pandit-Taskar, J. A. O'Donoghue, J. C. Durack, S. K. Lyashchenko, S. M. Cheal, V. Beylertgil, R. A. Lefkowitz, J. A. Carrasquillo, D. F. Martinez, A. M. Fung, S. B. Solomon, M. Gonen, G. Heller, M. Loda, D. M. Nanus, S. T. Tagawa, J. L. Feldman, J. R. Osborne, J. S. Lewis, V. E. Reuter, W. A. Weber, N. H. Bander, H. I. Scher, S. M. Larson, M. J. Morris, *Clin Cancer Res* **2015**, *21*, 5277-5285.
- [148] D. S. Abou, T. Ku, P. M. Smith-Jones, *Nucl Med Biol* **2011**, *38*, 675-681.
- [149] T. K. Nayak, K. Garmestani, D. E. Milenic, M. W. Brechbiel, *J Nucl Med* **2012**, *53*, 113-120.
- [150] M. A. Deri, S. Ponnala, P. Kozlowski, B. P. Burton-Pye, H. T. Cicek, C. Hu, J. S. Lewis, L. C. Francesconi, *Bioconjug Chem* **2015**, *26*, 2579-2591.
- [151] P. Laverman, T. van der Geest, S. Y. Terry, D. Gerrits, B. Walgreen, M. M. Helsen, T. K. Nayak, A. Freimoser-Grundschober, I. Waldhauer, R. J. Hosse, E. Moessner, P. Umana, C. Klein, W. J. Oyen, M. I. Koenders, O. C. Boerman, *J Nucl Med* **2015**, *56*, 778-783.
- [152] M. Patra, A. Bauman, C. Mari, C. A. Fischer, O. Blacque, D. Haussinger, G. Gasser, T. L. Mindt, *Chem Commun (Camb)* **2014**, *50*, 11523-11525.
- [153] M. Chomet, M. Schreurs, M. J. Bolijn, M. Verlaan, W. Beaino, K. Brown, A. J. Poot, A. D. Windhorst, H. Gill, J. Marik, S. Williams, J. Cowell, G. Gasser, T. L. Mindt, G. van Dongen, D. J. Vugts, *Eur J Nucl Med Mol Imaging* **2021**, *48*, 694-707.
- [154] C. J. M. Brown, M. P. Gotsbacher, R. Codd, *Australian Journal of Chemistry* **2020**.
- [155] C. J. Adams, J. J. Wilson, E. Boros, *Mol Pharm* **2017**, *14*, 2831-2842.
- [156] L. Allott, C. Da Pieve, J. Meyers, T. Spinks, D. M. Ciobota, G. Kramer-Marek, G. Smith, *Chem Commun (Camb)* **2017**, *53*, 8529-8532.
- [157] D. L. White, P. W. Durbin, N. Jeung, K. N. Raymond, *J Med Chem* **1988**, *31*, 11-18.
- [158] R. Raavé, G. Sandker, P. Adumeau, C. B. Jacobsen, F. Mangin, M. Meyer, M. Moreau, C. Bernhard, L. Da Costa, A. Dubois, V. Goncalves, M. Gustafsson, M. Rijpkema, O. Boerman, J.-C. Chambron, S. Heskamp, F. Denat, *European Journal of Nuclear Medicine and Molecular Imaging* **2019**, *46*, 1966-1977.
-

- [159] S. E. Rudd, P. Roselt, C. Cullinane, R. J. Hicks, P. S. Donnelly, *Chem Commun (Camb)* **2016**, 52, 11889-11892.
- [160] E. K. Sarbisheh, A. K. Salih, S. J. Raheem, J. S. Lewis, E. W. Price, *Inorg Chem* **2020**, 59, 11715-11727.
- [161] E. Khozeimeh Sarbisheh, K. L. Summers, A. K. Salih, J. J. H. Cotelesage, A. Zimmerling, I. J. Pickering, G. N. George, E. W. Price, *Inorg Chem* **2023**, 62, 2637-2651.
- [162] A. K. Salih, S. J. Raheem, M. D. Garcia, W. K. Ahiahonu, E. W. Price, *Inorg Chem* **2022**, 61, 20964-20976.
- [163] A. K. Salih, M. Dominguez Garcia, S. J. Raheem, W. K. Ahiahonu, E. W. Price, *Inorg Chem* **2023**, 62, 20806-20819.
- [164] M. Briand, M. L. Aulsebrook, T. L. Mindt, G. Gasser, *Dalton Trans* **2017**, 46, 16387-16389.
- [165] U. Seibold, B. Wängler, C. Wängler, *ChemMedChem* **2017**, 12, 1555-1571.
- [166] W. Tieu, T. Lifa, A. Katsifis, R. Codd, *Inorg Chem* **2017**, 56, 3719-3728.
- [167] M. A. Deri, S. Ponnala, B. M. Zeglis, G. Pohl, J. J. Dannenberg, J. S. Lewis, L. C. Francesconi, *Journal of Medicinal Chemistry* **2014**, 57, 4849-4860.
- [168] H. Damerow, X. Cheng, V. von Kiedrowski, R. Schirmacher, B. Wangler, G. Fricker, C. Wangler, *Pharmaceutics* **2022**, 14.
- [169] D. J. Vugts, C. Klaver, C. Sewing, A. J. Poot, K. Adamzek, S. Huegli, C. Mari, G. W. M. Visser, I. E. Valverde, G. Gasser, T. L. Mindt, G. van Dongen, *Eur J Nucl Med Mol Imaging* **2017**, 44, 286-295.
- [170] M. Chomet, G. van Dongen, D. J. Vugts, *Bioconjug Chem* **2021**, 32, 1315-1330.
- [171] T. J., D. N. Pandya, S. L. Pailloux, A. Ogasawara, A. N. Vanderbilt, H. S. Gill, S. P. Williams, T. J. Wadas, D. Magda, J. Marik, *Theranostics* **2016**, 6, 511-521.
- [172] S. D. Domagal-Goldman, K. W. Paul, D. L. Sparks, J. D. Kubicki, *Geochimica et Cosmochimica Acta* **2009**, 73, 1-12.
- [173] C. Hagfeldt, V. Kessler, I. Persson, *Dalton Trans* **2004**, 2142-2151.
- [174] F. Guérard, Y.-S. Lee, M. W. Brechbiel, *Chemistry – A European Journal* **2014**, 20, 5584-5591.
- [175] J. P. Holland, *Inorg Chem* **2020**, 59, 2070-2082.
- [176] B. Merrifield, *British Polymer Journal* **1984**, 16, 173-178.
- [177] J. M. Palomo, *RSC Adv.* **2014**, 4, 32658-32672.
- [178] C. O. Kappe, D. Dallinger, *Nat Rev Drug Discov* **2006**, 5, 51-63.
- [179] S. S. Wang, *J Am Chem Soc* **1973**, 95, 1328-1333.
- [180] H. Rink, *Tetrahedron Letters* **1987**, 28, 3787-3790.

-
- [181] K. B. O. Chatzi, D. Gatos, G. Stavropoulos, *International Journal of Peptide and Protein Research* **1991**, 37, 513-520.
- [182] E. Atherton, E. Brown, R. C. Sheppard, A. Rosevear, *Journal of the Chemical Society, Chemical Communications* **1981**.
- [183] R. Behrendt, P. White, J. Offer, *J Pept Sci* **2016**, 22, 4-27.
- [184] M. Gude, J. Ryf, P. D. White, *Letters in Peptide Science* **2002**, 9, 203-206.
- [185] M. Á. A. Isidro-Llobet, F. Albericio, *Chem. Rev.* **2009**, 109, 2455-2504.
- [186] E. Valeur, M. Bradley, *Chem Soc Rev* **2009**, 38, 606-631.
- [187] A. El-Faham, F. Albericio, *Chem Rev* **2011**, 111, 6557-6602.
- [188] W. König, R. Geiger, *Chem Ber* **1970**, 103, 788-798.
- [189] L. A. Carpino, *Journal of the American Chemical Society* **1993**, 115, 4397-4398.
- [190] R. Subirós-Funosas, R. Prohens, R. Barbas, A. El-Faham, F. Albericio, *Chemistry – A European Journal* **2009**, 15, 9394-9403.
- [191] A. R. Poreddy, O. F. Schall, T. A. Osiek, J. R. Wheatley, D. D. Beusen, G. R. Marshall, U. Slomczynska, *Journal of Combinatorial Chemistry* **2004**, 6, 239-254.
- [192] M. Savastano, C. Bazzicalupi, G. Ferraro, E. Fratini, P. Gratteri, A. Bianchi, *Molecules* **2019**, 24.
- [193] L. Outzen, M. Munzmay, J. V. Frangioni, W. Maison, *ChemMedChem* **2023**, 18, e202300112.
- [194] L. Outzen, D. Ludolfs, M. Irl, S. Kossatz, W. Maison, *ChemMedChem* **2025**, 20, e202400890.
- [195] F. Guérard, Y.-S. Lee, R. Tripier, L. P. Szajek, J. R. Deschamps, M. W. Brechbiel, *Chemical Communications* **2013**, 49, 1002-1004.
- [196] M. Brandt, J. Cowell, M. L. Aulsebrook, G. Gasser, T. L. Mindt, *J Biol Inorg Chem* **2020**, 25, 789-796.
- [197] M. Wasilewska, A. Derylo-Marczewska, A. W. Marczewski, *Molecules* **2024**, 29.
- [198] F. Haghseresht, J. J. Finnerty, S. Nouri, G. Q. Lu, *Langmuir* **2002**, 18, 6193-6200.
- [199] F. Villacanas, M. F. Pereira, J. J. Orfao, J. L. Figueiredo, *J Colloid Interface Sci* **2006**, 293, 128-136.

8. Appendix

8.1 Supplementary Materials

8.1.1 Synthesis of Modular Desferrioxamine Analogues and Evaluation of Zwitterionic Derivatives for Zirconium Complexation

ChemMedChem

Supporting Information

Synthesis of Modular Desferrioxamine Analogues and Evaluation of Zwitterionic Derivatives for Zirconium Complexation

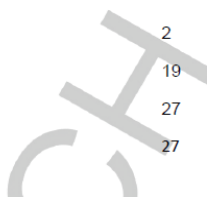
Lasse Outzen, Moritz Münzmay, John V. Frangioni, and Wolfgang Maison*

WILEY-VCH

FULL PAPER

TABLE OF CONTENT

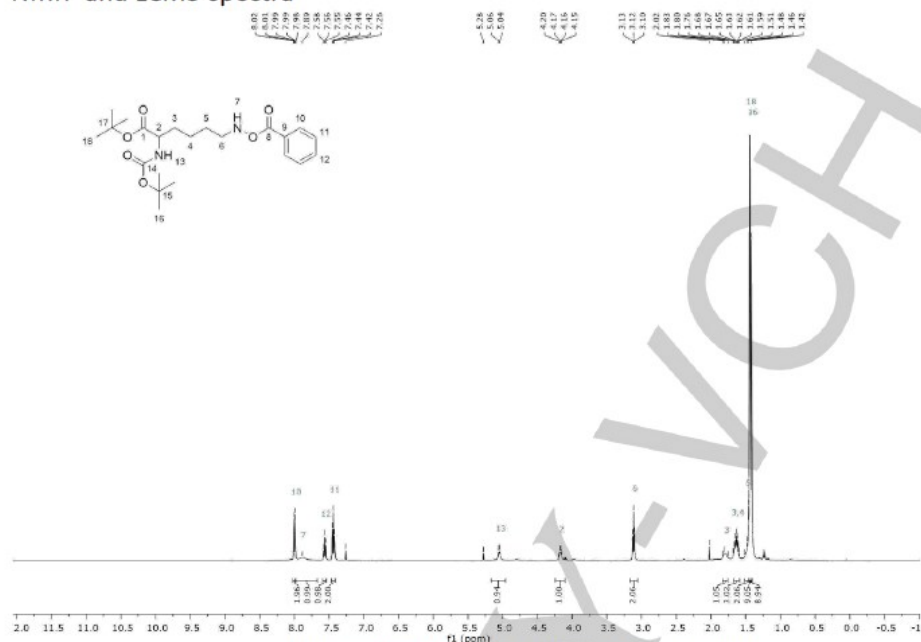
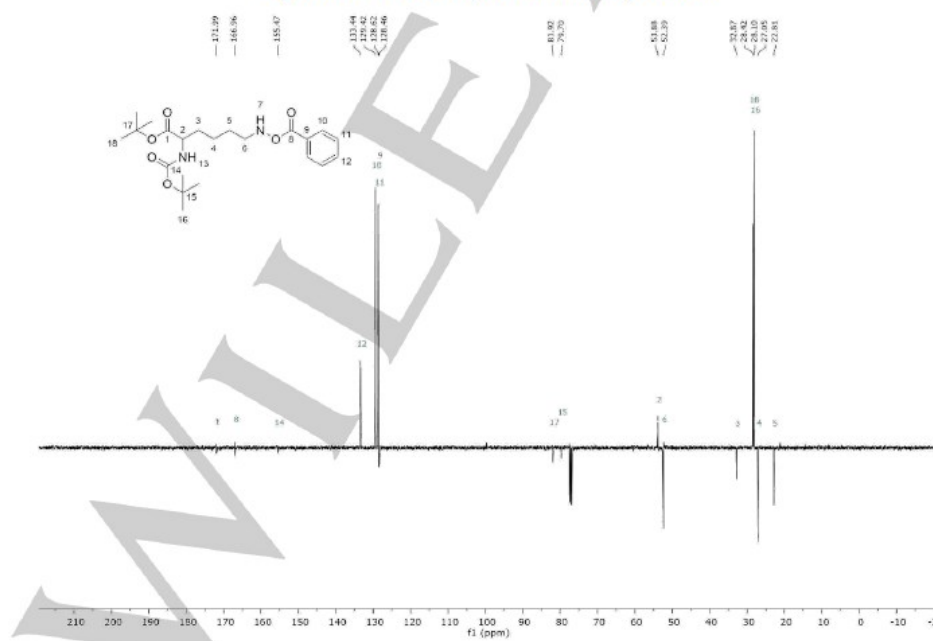
NMR- and LCMS-spectra	2
LC/MS data for unprotected zwitterionic chelators	19
Evaluation of Zr-complexes	27
Exemplary transchelation assay	27



WILEY-VCH

FULL PAPER

NMR- and LCMS-spectra

Figure S1. ^1H -NMR spectrum of compound 4.Figure S2. ^{13}C -NMR spectrum of compound 4.

Chemical structure of the compound is shown above the spectrum. The structure is a complex molecule with multiple functional groups, including amide, ester, and amine groups, and is labeled with numbers 1 through 27. The spectrum displays chemical shifts in ppm (r1 (ppm)) on the x-axis, ranging from 20 to -10. Key peaks are labeled with their corresponding chemical shift values:

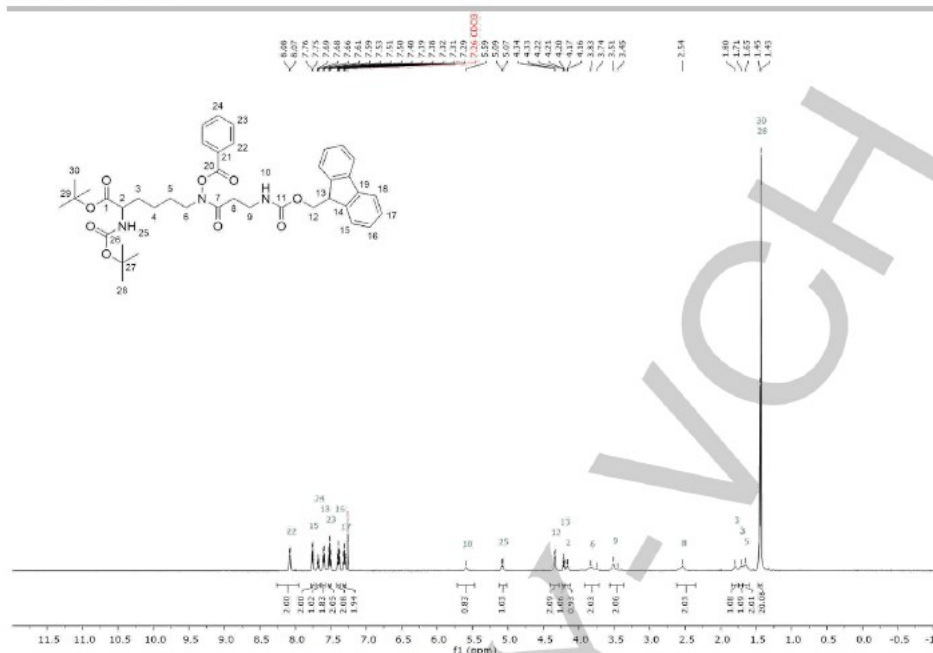
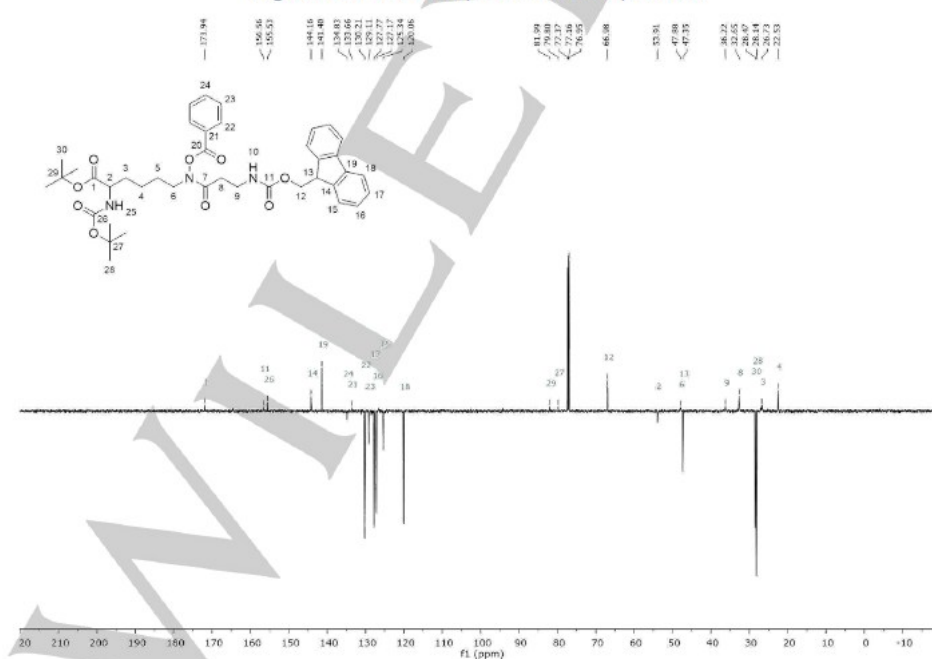
- 164.62
- 154.15
- 153.54
- 152.53
- 144.15
- 138.97
- 138.97
- 138.11
- 137.11
- 136.97
- 136.97
- 82.21
- 79.83
- 77.31
- 77.15
- 76.15
- 66.58
- 53.73
- 47.82
- 47.25
- 32.71
- 32.71
- 30.49
- 29.63
- 29.63
- 22.15

The spectrum shows a series of peaks corresponding to these chemical shifts, with the most prominent peaks occurring between 130 and 165 ppm, and a cluster of peaks between 20 and 40 ppm.

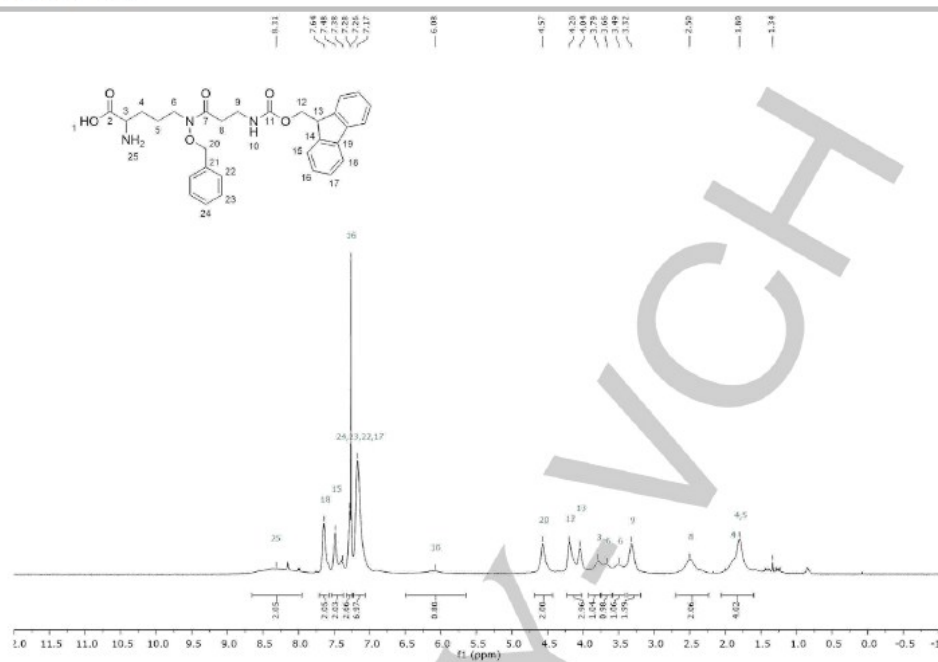
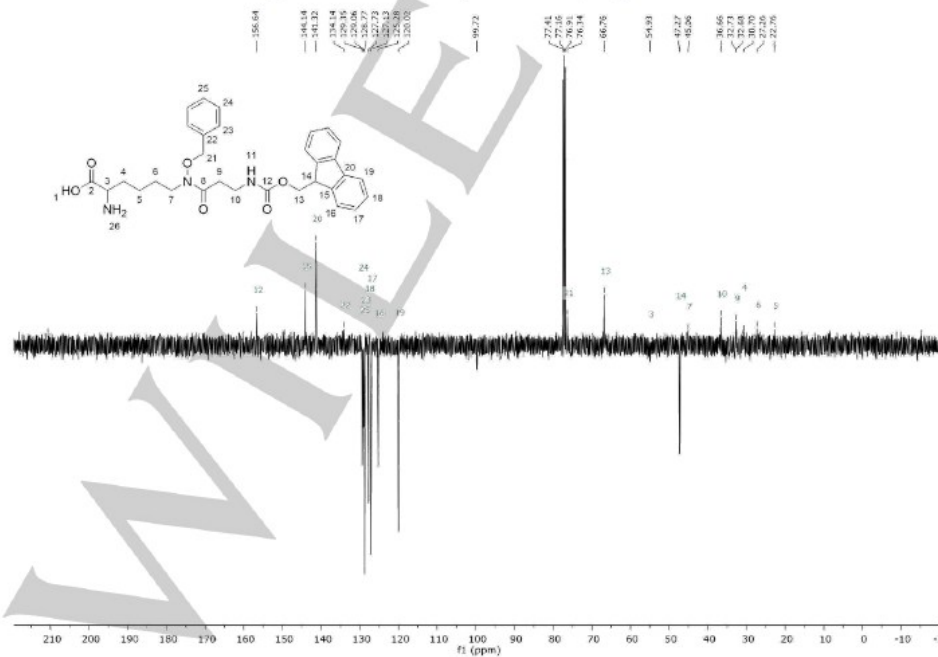
Figure S4. ^{13}C -NMR spectrum of compound **5**.

WILEY-VCH

FULL PAPER

Figure S5. ^1H -NMR spectrum of compound 6.Figure S6. ^{13}C -NMR spectrum of compound 6.

FULL PAPER

Figure S7. ^1H -NMR spectrum of compound 7.

WILEY-VCH

FULL PAPER

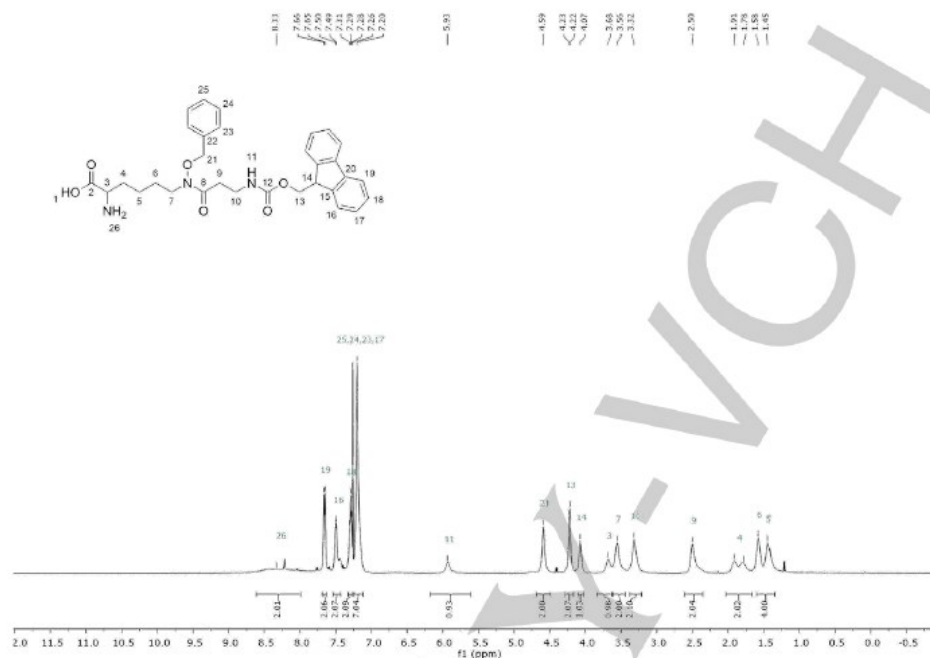
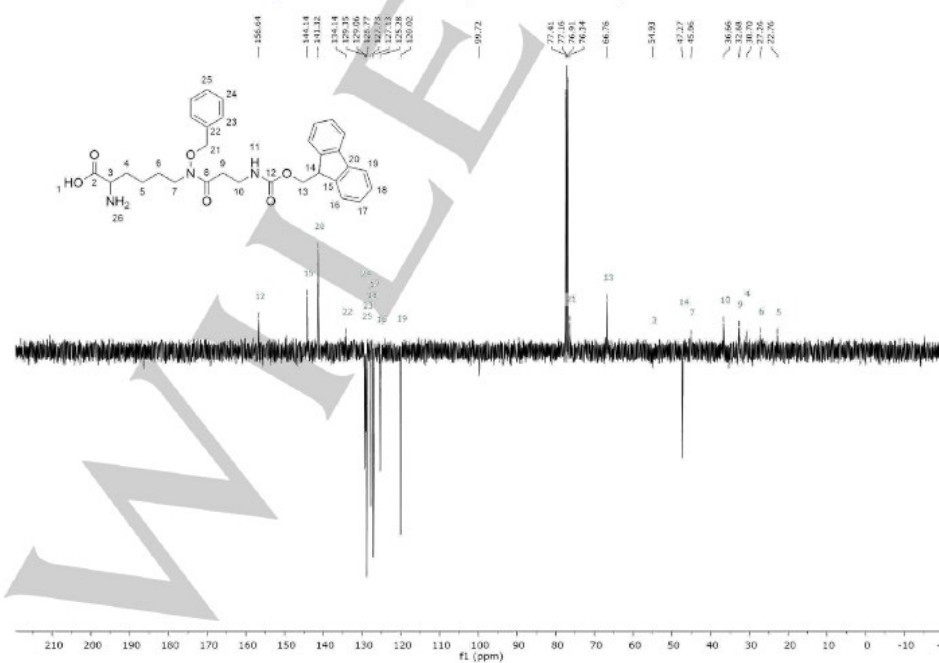
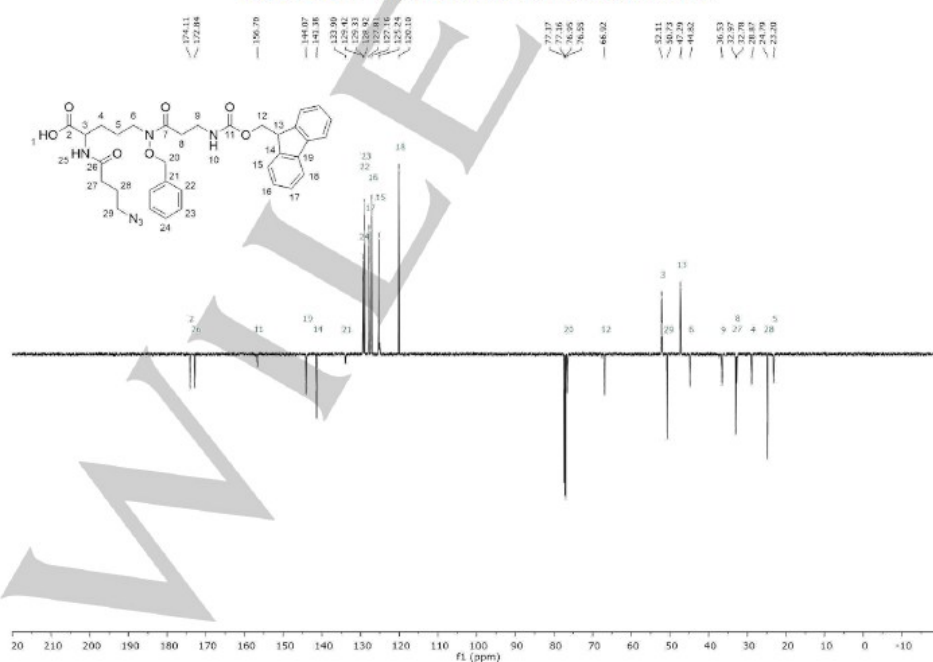
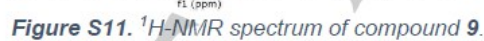
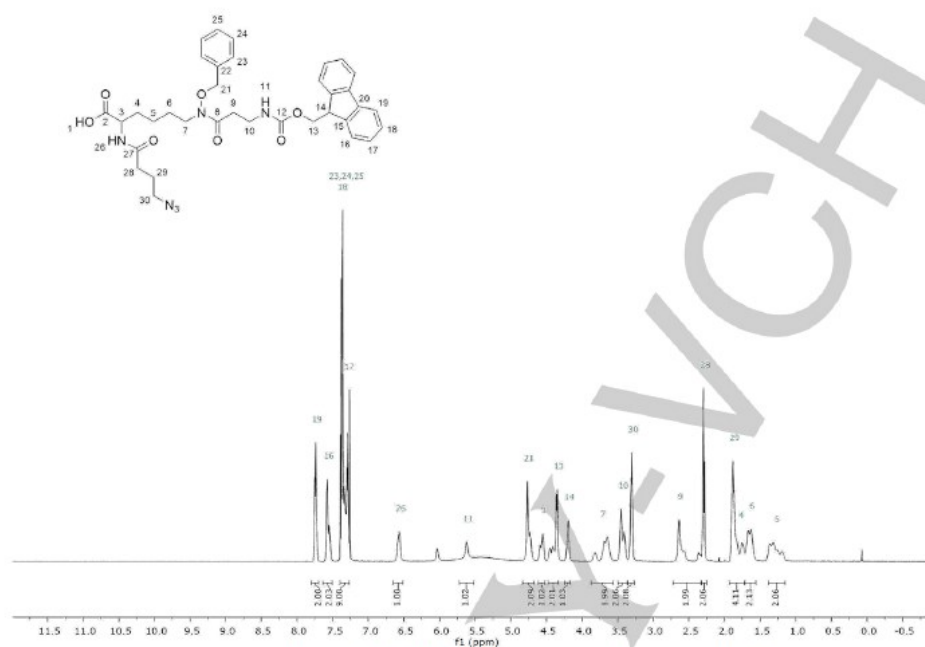
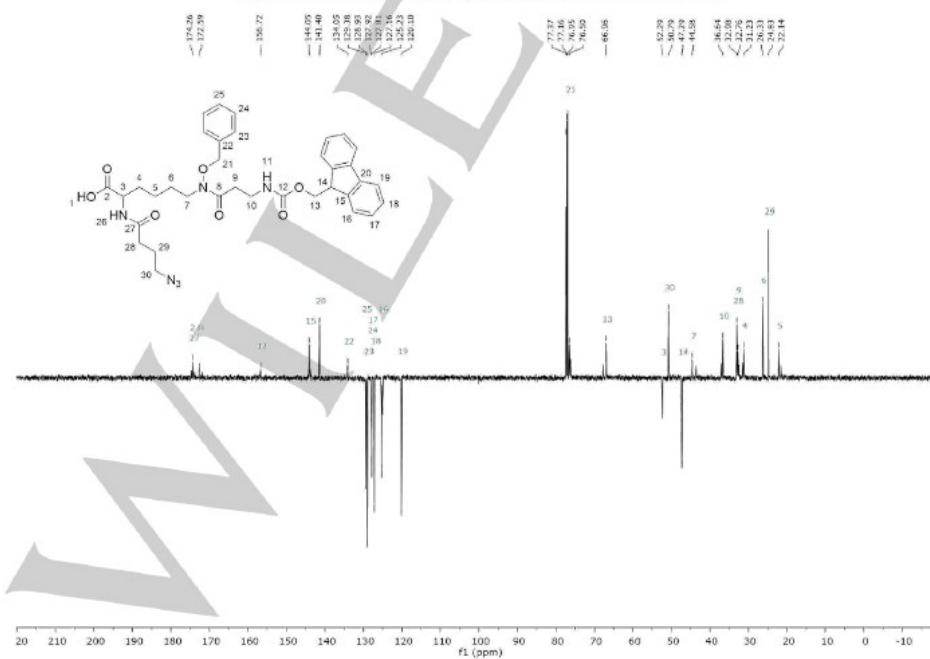
Figure S8. ^{13}C -NMR spectrum of compound 7.Figure S9. ^1H -NMR spectrum of compound 8.

Figure S10. ^{13}C -NMR spectrum of compound **8**.

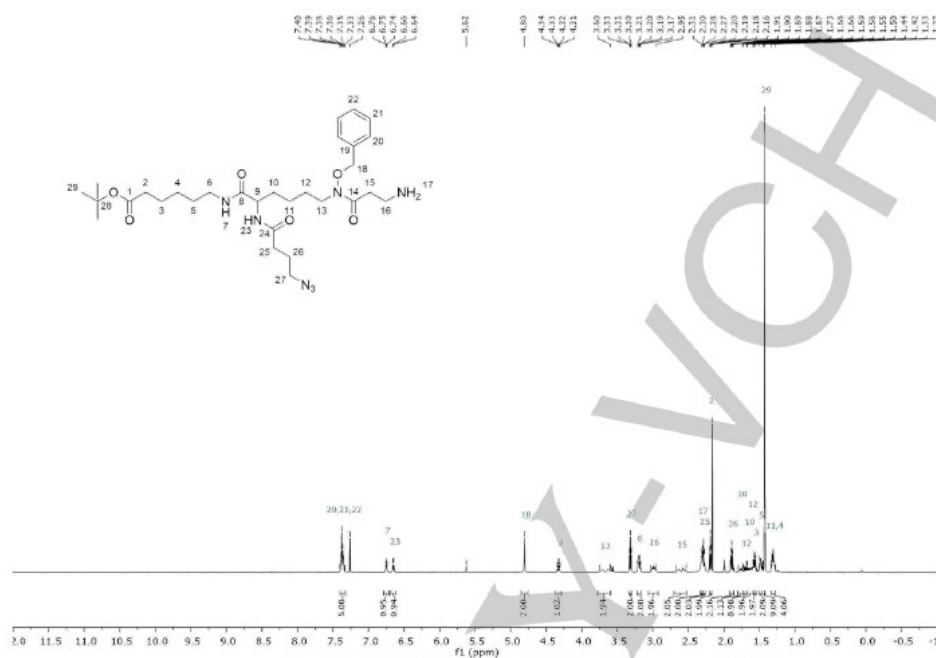
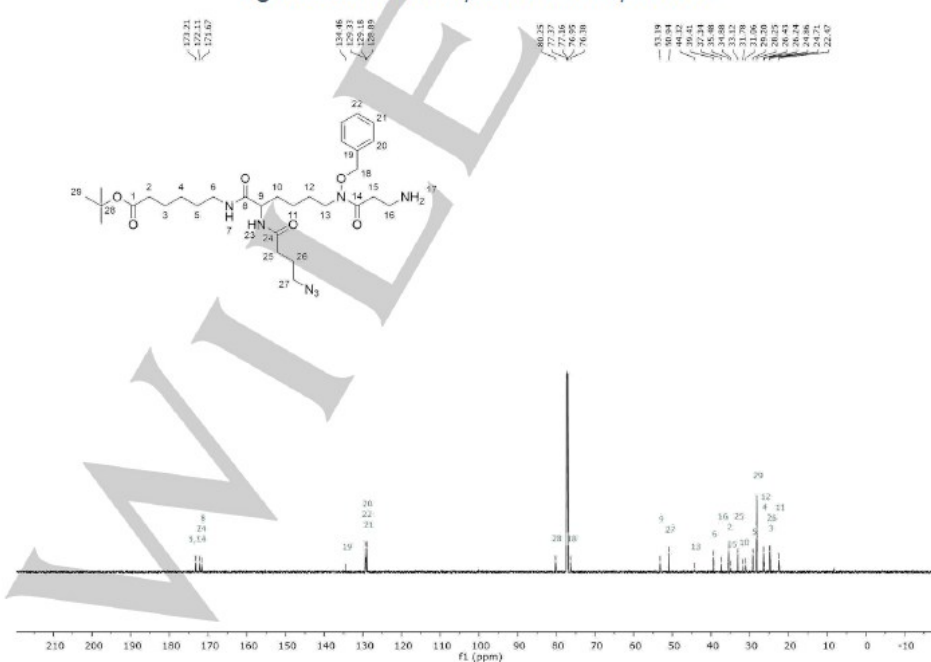


WILEY-VCH

FULL PAPER

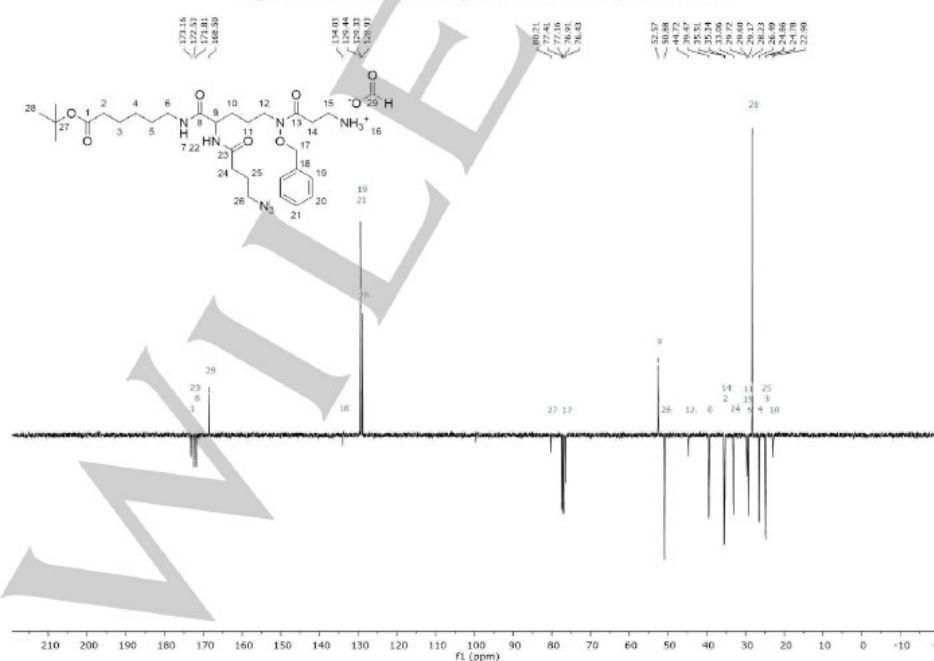
Figure S12. ^{13}C -NMR spectrum of compound 9.Figure S13. ^1H -NMR spectrum of compound 10.

FULL PAPER

Figure S14. ^{13}C -NMR spectrum of compound 10.Figure S15. ^1H -NMR spectrum of compound 12.

WILEY-VCH

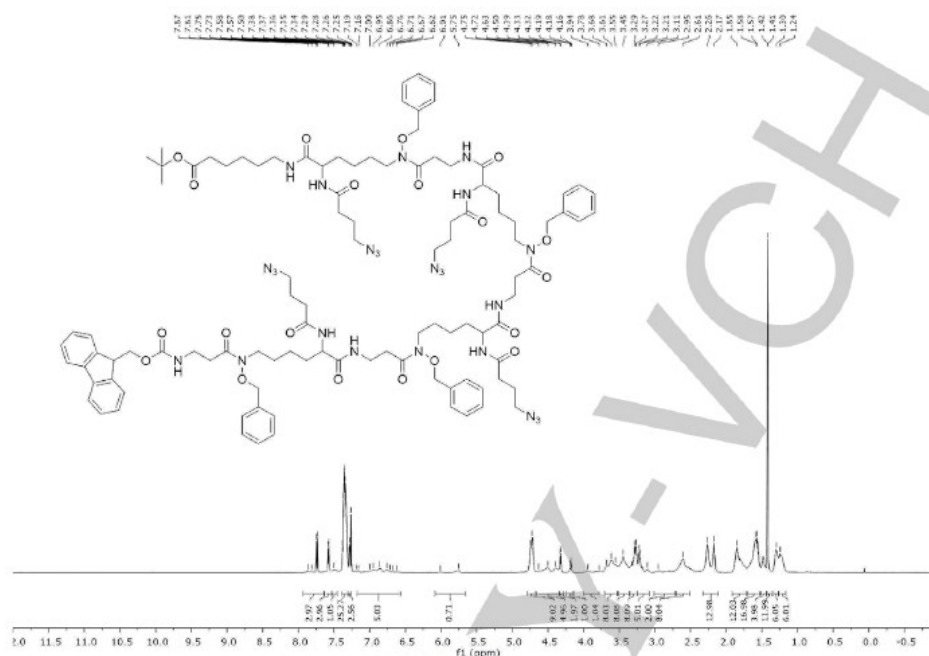
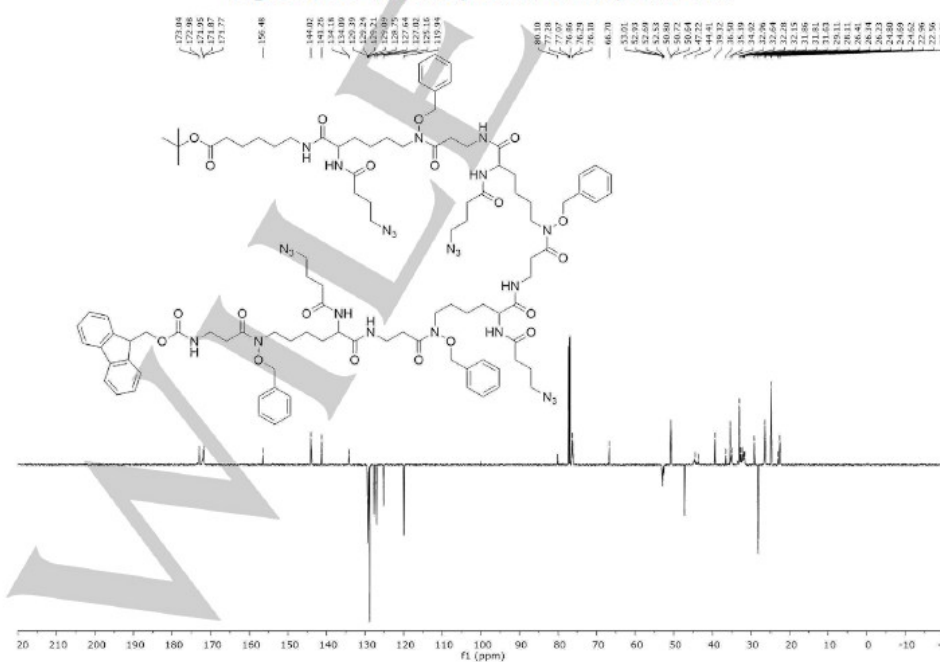
FULL PAPER

Figure S16. ^{13}C -NMR spectrum of compound 12.Figure S18. ^1H -NMR spectrum of compound 13.



WILEY-VCH

FULL PAPER

Figure S22. ^{13}C -NMR spectrum of compound **14a**.Figure S23. ^1H -NMR spectrum of compound **15a**.

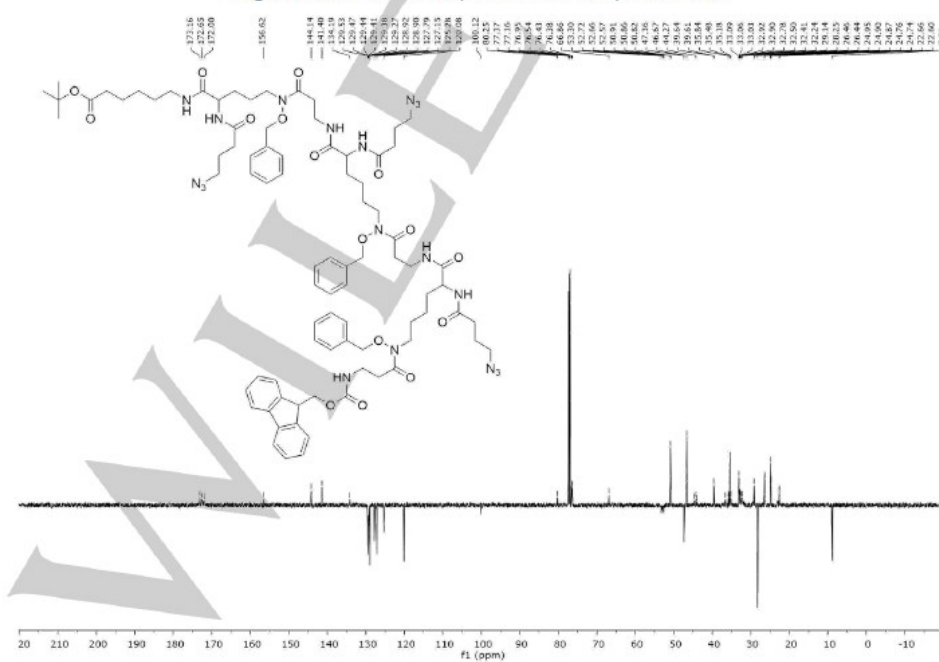


Figure 26. ^{13}C -NMR spectrum of compound **14b**.

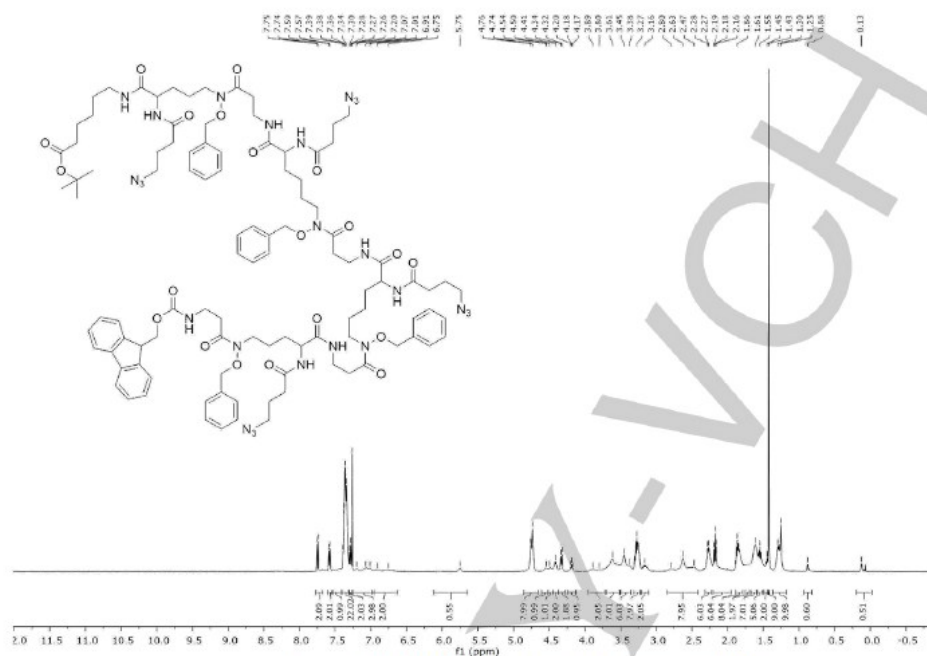
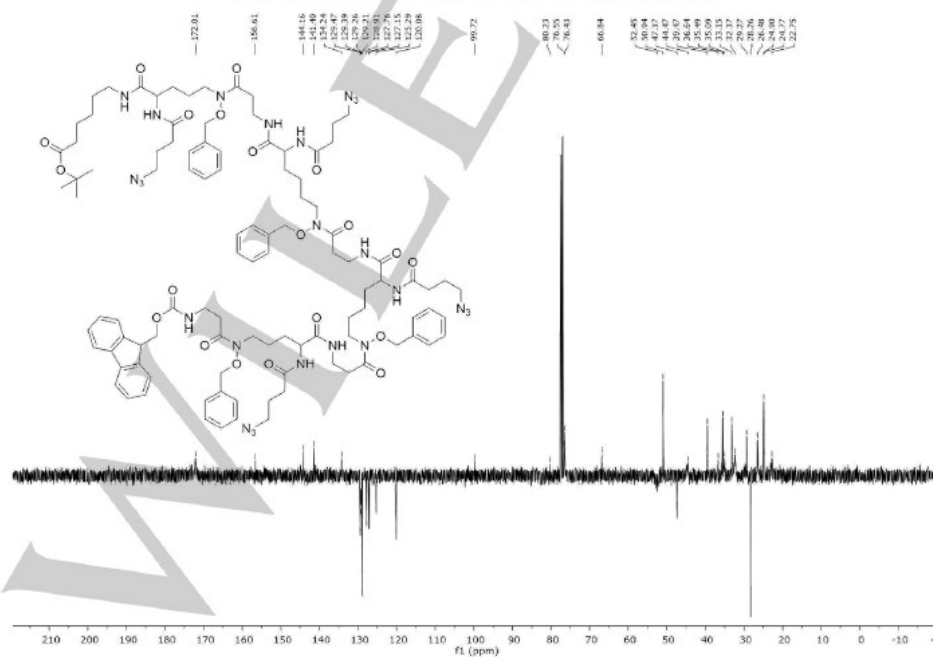
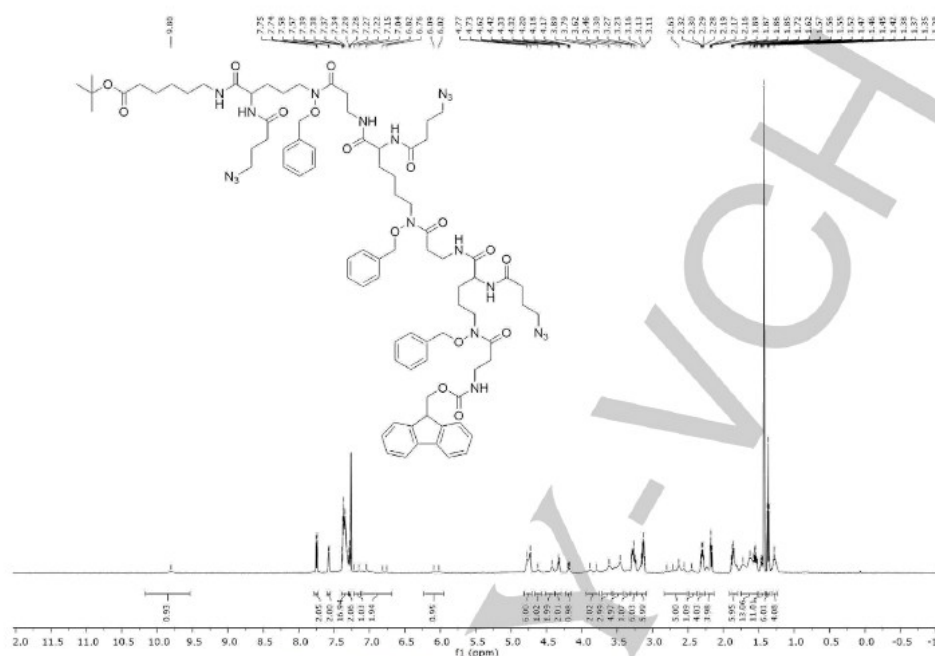
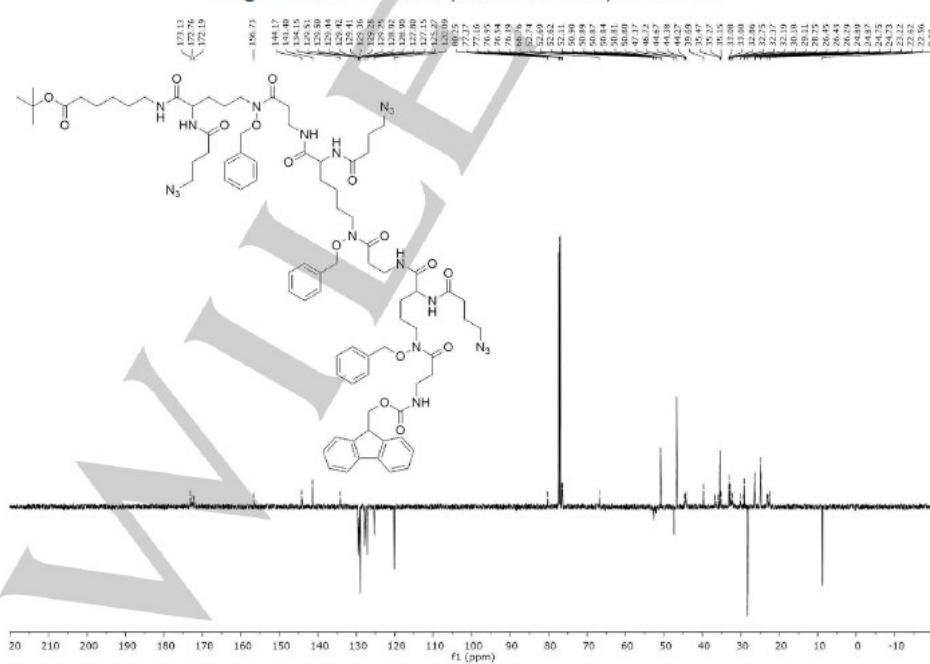
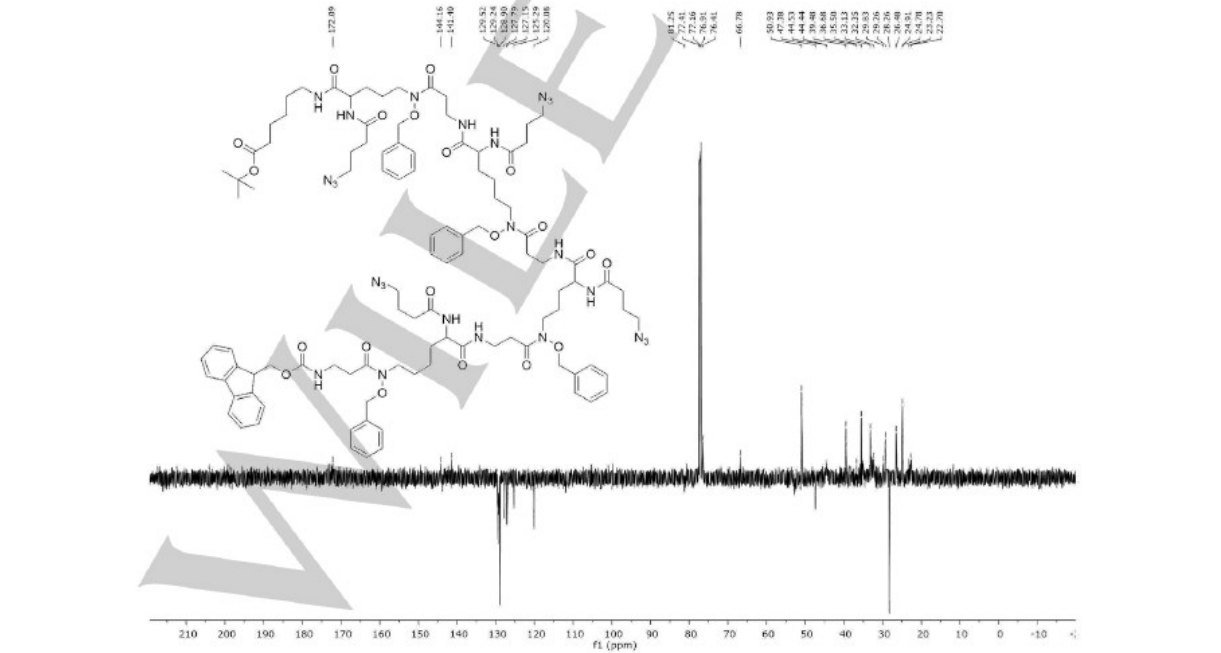
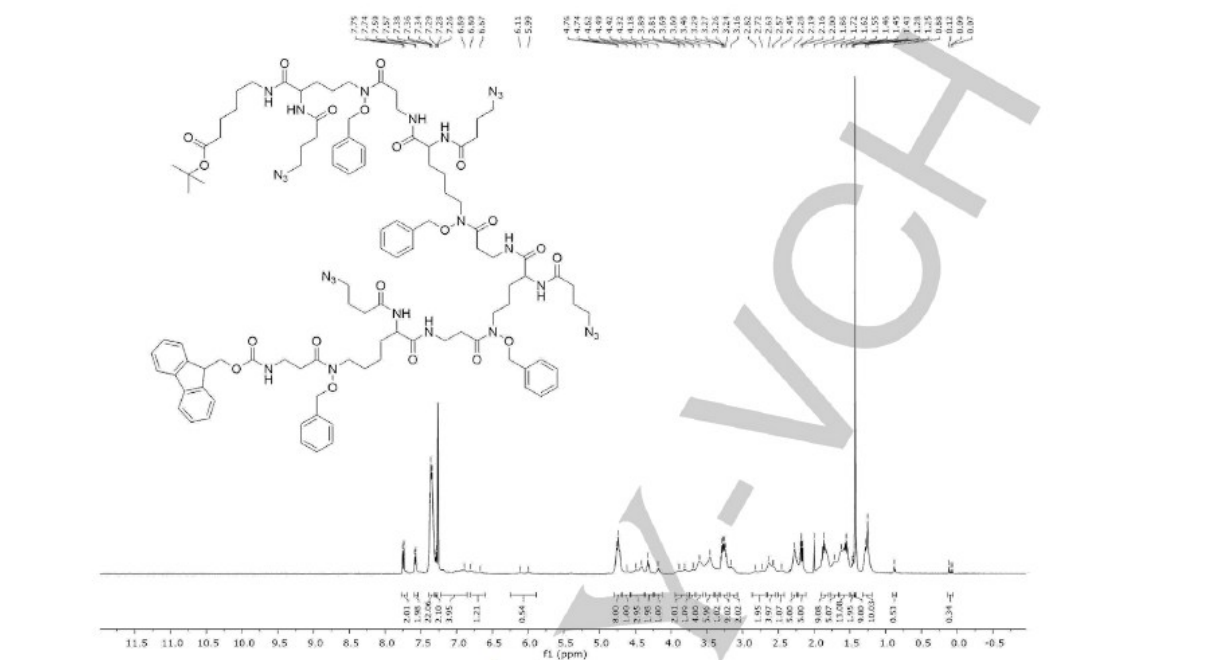


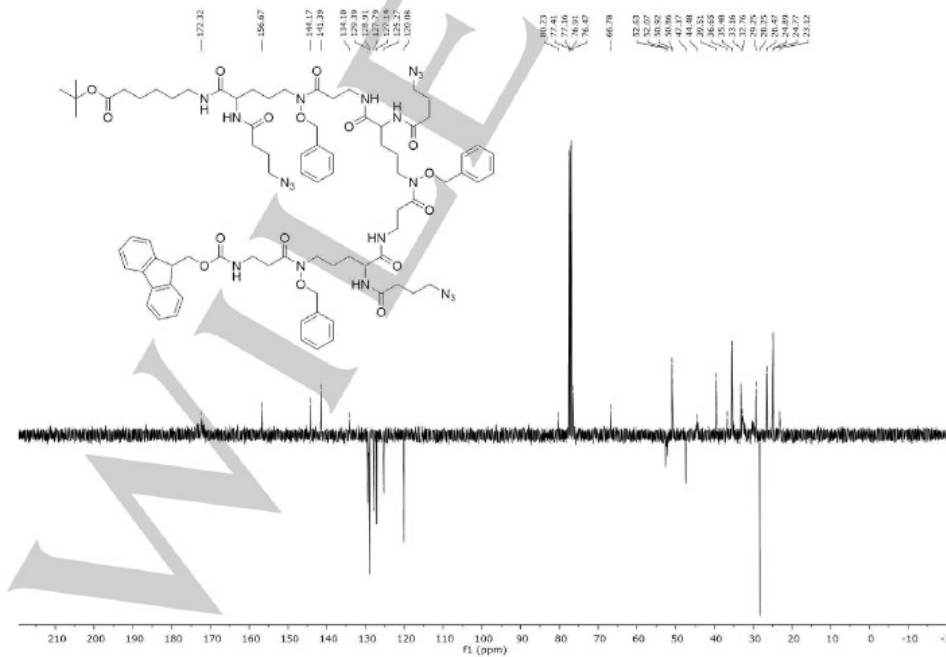
Figure 27. ^1H -NMR spectrum of compound **15b**.



FULL PAPER

Figure S28. ^{13}C -NMR spectrum of compound 15b.Figure S29. ^1H -NMR spectrum of compound 14c.





WILEY-VCH

FULL PAPER

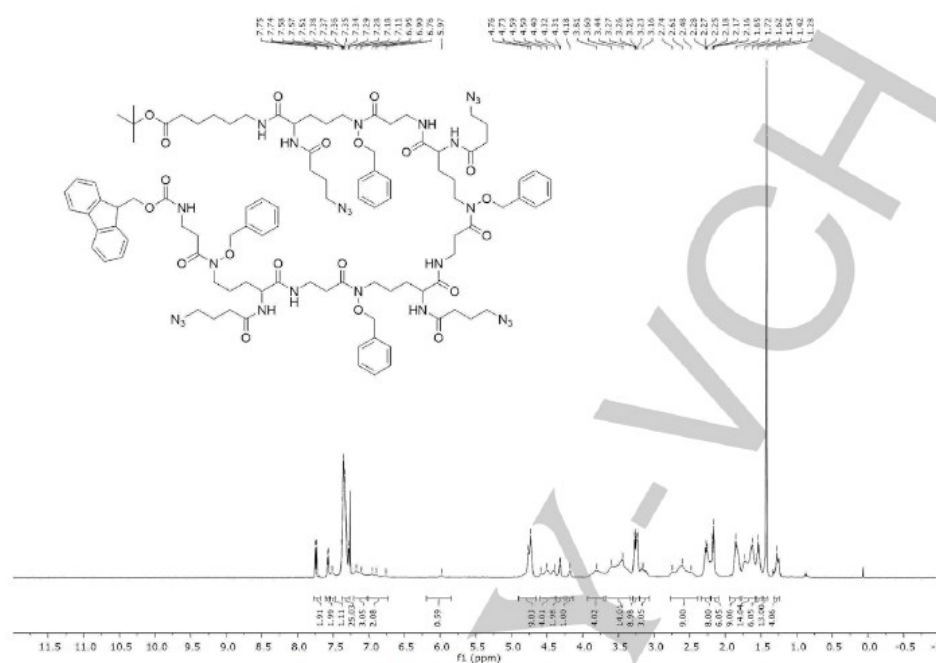
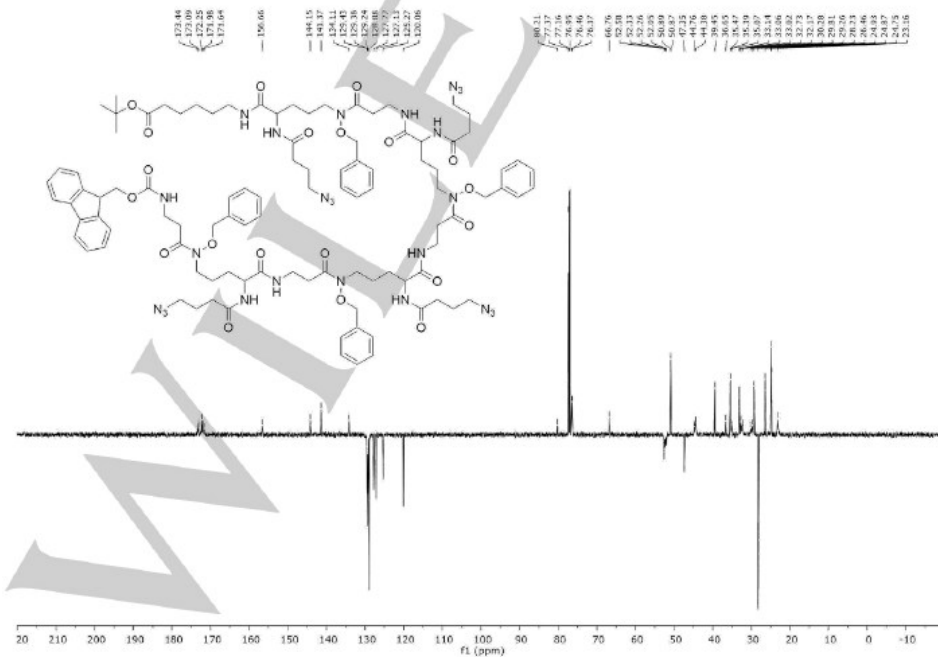
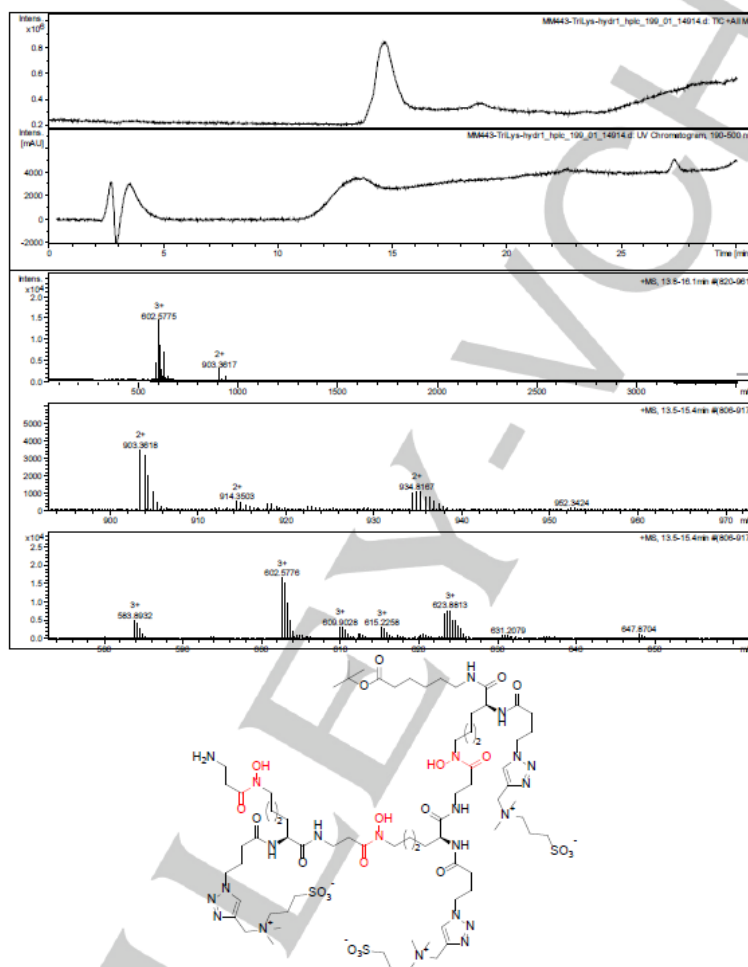
Figure S34. ^{13}C -NMR spectrum of compound 14d.Figure S35. ^1H -NMR spectrum of compound 15d.

Figure S36. ^{13}C -NMR spectrum of compound **15d**.

LC/MS data for unprotected zwitterionic chelators

**Figure S37.** HPLC-chromatogram (Anal. HPLC: Nucleodur C₁₈ HTec EC, 150 x 10 mm ID, 5 μm , $\text{H}_2\text{O}/\text{CH}_3\text{CN}$ 98:2 + 0.05% HCO_2H \rightarrow 5:95 + 0.05% HCO_2H , 15 min, 0.2 mL/min; t_{R} = 14.6 min) and MS(ESI)-spectra of **16c**.

WILEY-VCH

FULL PAPER

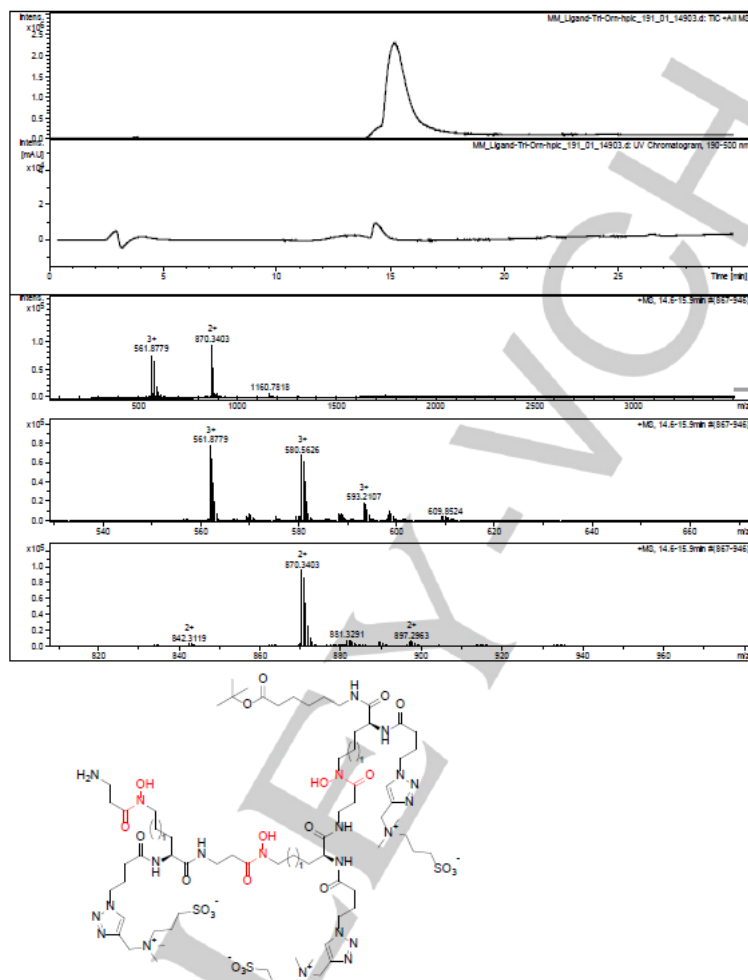


Figure S38. HPLC-chromatogram (Anal. HPLC: Nucleodur C₁₈ HTec EC, 150 x 10 mm ID, 5 μ m, H₂O/CH₃CN 98:2 + 0.05% HCO₂H \rightarrow 5:95 + 0.05% HCO₂H, 15 min, 0.2 mL/min; t_R = 15.3 min) and MS(ESI)-spectra of **16a**.

FULL PAPER

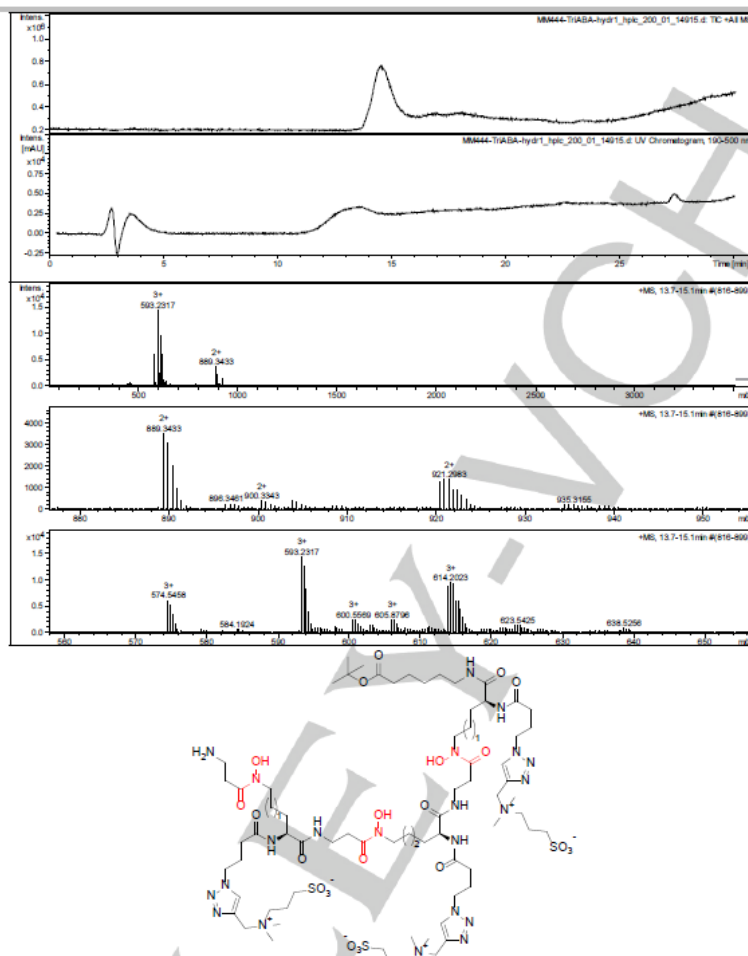


Figure S39. HPLC-chromatogram (Anal. HPLC: Nucleodur C₁₈ HTec EC, 150 x 10 mm ID, 5 μm, H₂O/CH₃CN 98:2 + 0.05% HCO₂H → 5:95 + 0.05% HCO₂H, 15 min, 0.2 mL/min; t_R = 14.6 min) and MS(ESI)-spectra of **16e**.

WILEY-VCH

FULL PAPER

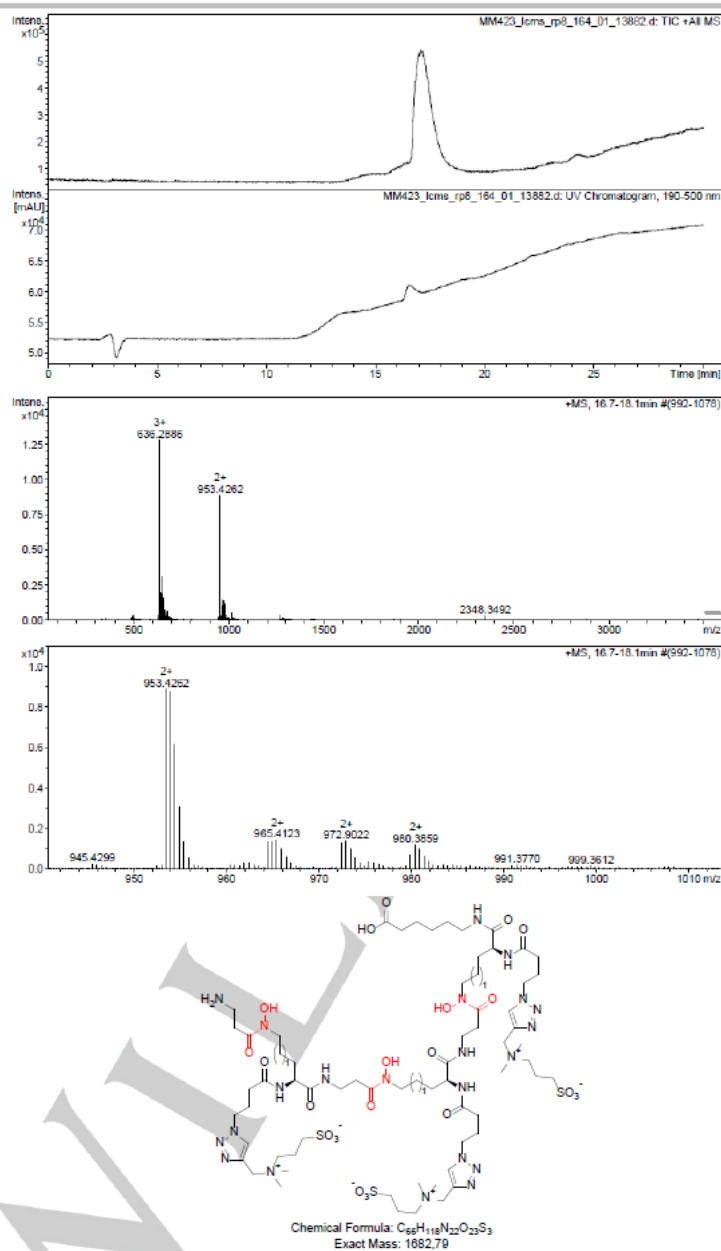


Figure S40. HPLC-chromatogram (Anal. HPLC: Nucleodur C_{18} HTec EC, 150 x 10 mm ID, 5 μ m, H_2O/CH_3CN 98:2 + 0.05% $HCO_2H \rightarrow$ 5:95 + 0.05% HCO_2H , 15 min, 0.2 mL/min; t_R = 17.1 min) and MS(ESI)-spectra of **16b**.

FULL PAPER

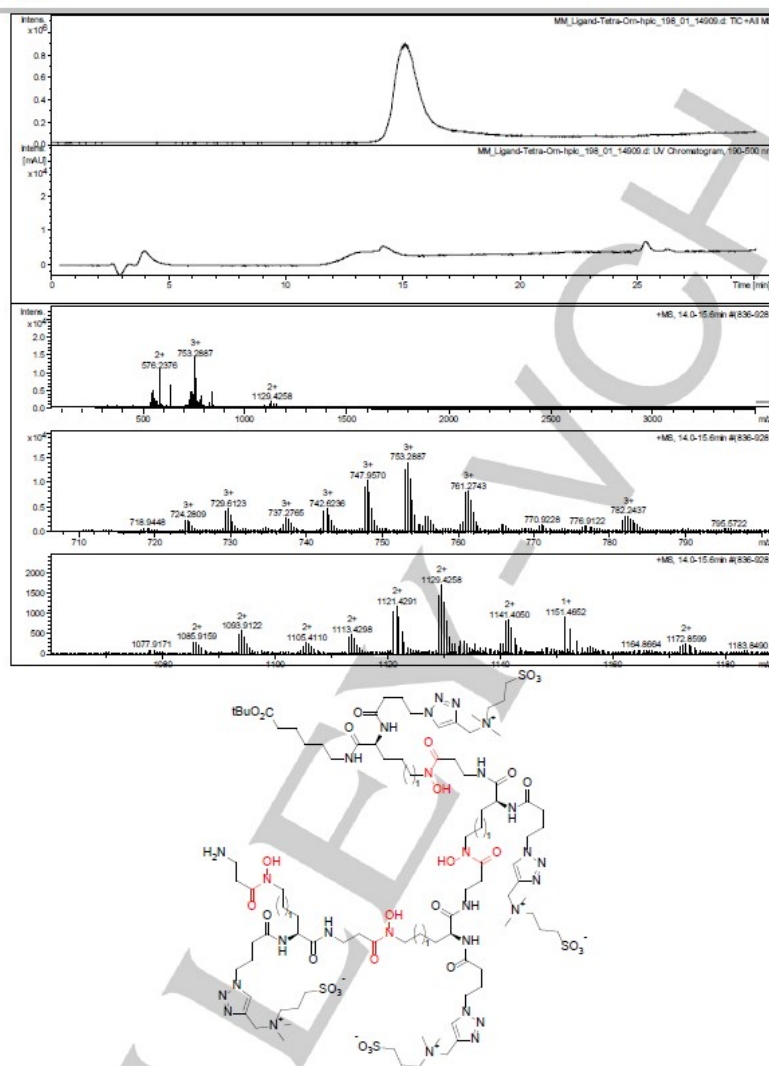


Figure S41. HPLC-chromatogram (Anal. HPLC: Nucleodur C₁₈ HTec EC, 150 x 10 mm ID, 5 μ m, H₂O/CH₃CN 98:2 + 0.05% HCO₂H \rightarrow 5:95 + 0.05% HCO₂H, 15 min, 0.2 mL/min; t_R = 14.1 min) and MS(ESI)-spectra of **17a**.

WILEY-VCH

FULL PAPER

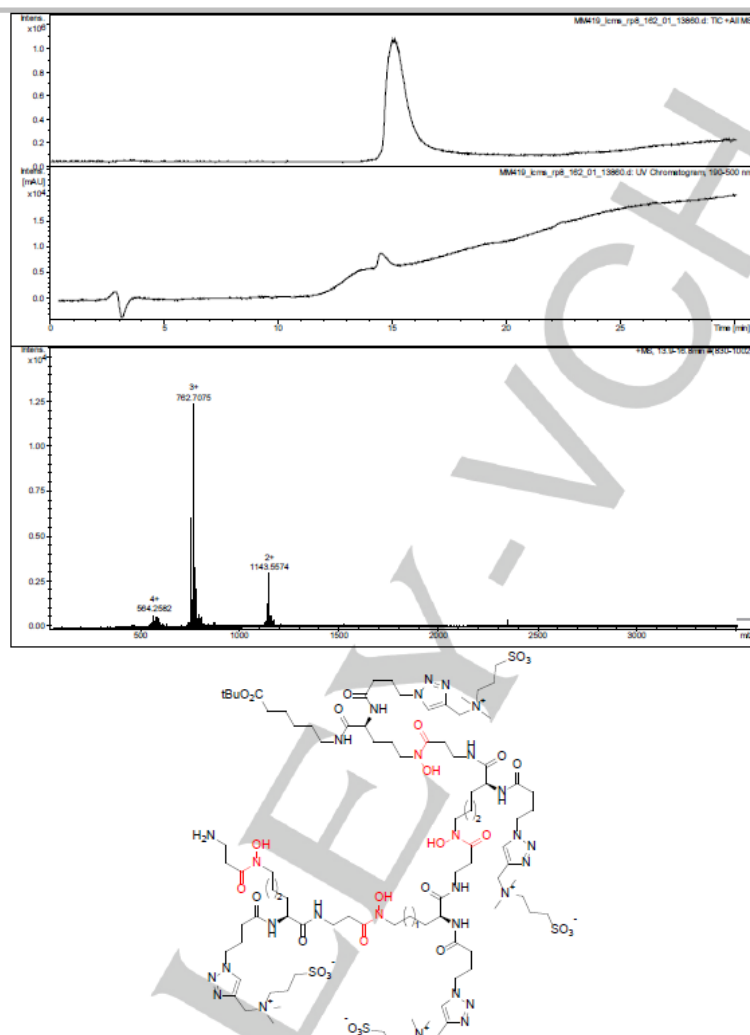


Figure S42. HPLC-chromatogram (Anal. HPLC: Nucleodur C₈ HTec EC, 150 x 10 mm ID, 5 μ m, H₂O/CH₃CN 98:2 + 0.05% HCO₂H \rightarrow 5:95 + 0.05% HCO₂H, 15 min, 0.2 mL/min; t_R = 14.9 min) and MS(ESI)-spectra of **17b**.

FULL PAPER

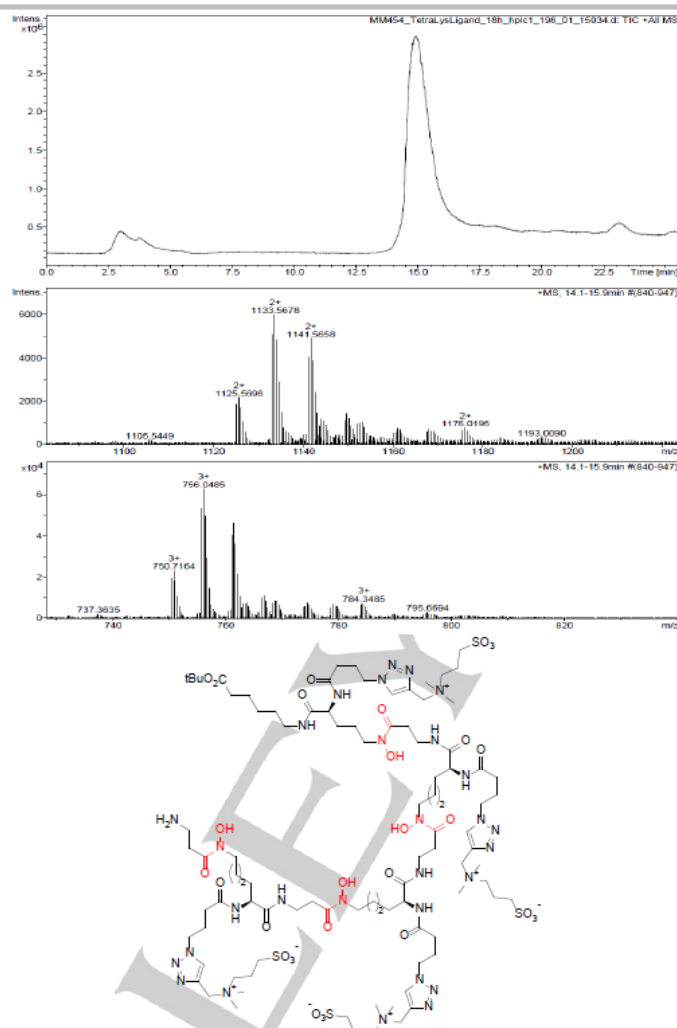


Figure S43. HPLC-chromatogram (Anal. HPLC: Nucleodur C₁₈ HTec EC, 150 x 10 mm ID, 5 μ m, H₂O/CH₃CN 98:2 + 0.05% HCO₂H \rightarrow 5:95 + 0.05% HCO₂H, 15 min, 0.2 mL/min; t_R = 14.1 min) and MS(ESI)-spectra of **17c**.

WILEY-VCH

FULL PAPER

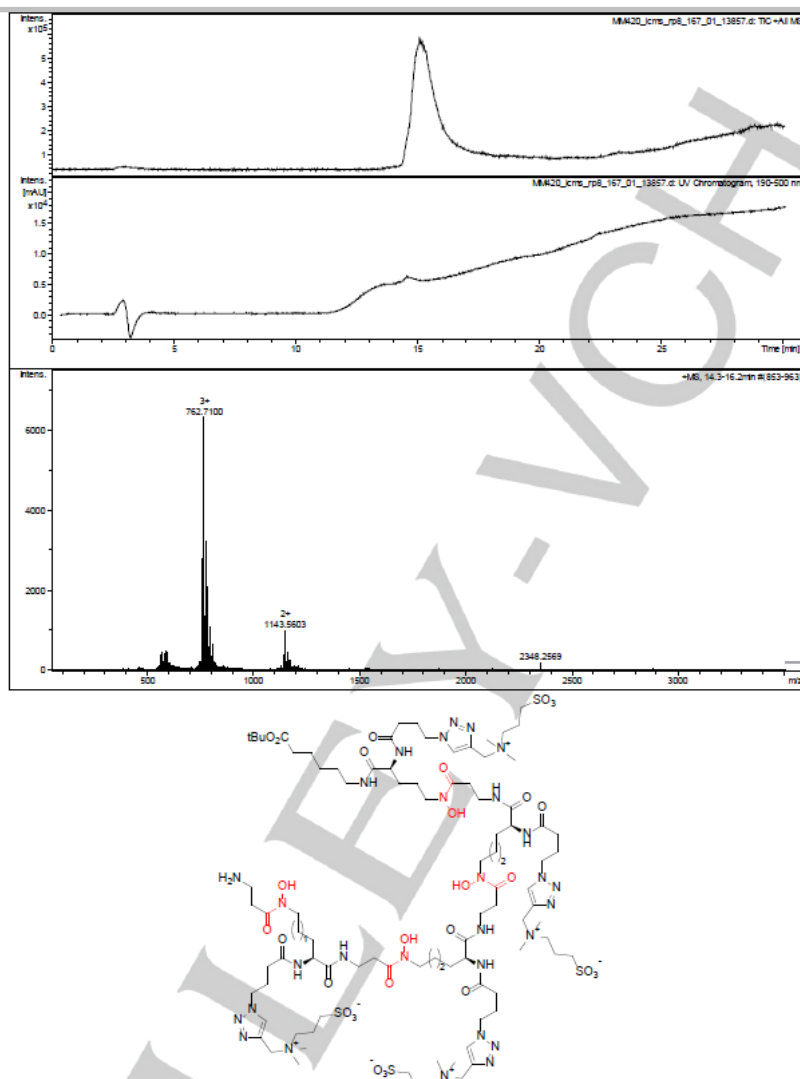


Figure S44. HPLC-chromatogram (Anal. HPLC: Nucleodur C₈ HTec EC, 150 x 10 mm ID, 5 μ m, H₂O/CH₃CN 98:2 + 0.05% HCO₂H \rightarrow 5:95 + 0.05% HCO₂H, 15 min, 0.2 mL/min; t_R = 15.0 min) and MS(ESI)-spectra of **17d**.

FULL PAPER

Evaluation of Zr-complexes

Exemplary transchelation assay of Zr-17a with 1000 fold excess of EDTA: The complex **Zr-17a** was dissolved in Milli-Q water (500 μ L). EDTA solution (100 μ L, 1000-fold excess, 0.0432 mM) was added. The pH of the solution was adjusted to pH = 7 by adding HCl(aq) (0.05 M) and the solution was stored at room temperature. After 0 h, 2 h, 8 h and 24 h, 15 μ L of the solution were analyzed by HPLC-MS (ESI, positive mode). The amount of intact Zr complex was determined by integration of peaks in the EIC (extracted ion chromatogram) for $[M + 3H]^{3+}$, $[M + 2H + Na]^{3+}$ and $[M + 2H]^{3+}$. HPLC: NUCLEODUR C₁₈ HTec EC, 150 x 10 mm ID, 5 μ m particles, H₂O/CH₃CN 98:2 + 0.05% HCO₂H \rightarrow 5:95 + 0.05% HCO₂H, 15 min, 0.2 mL/min.

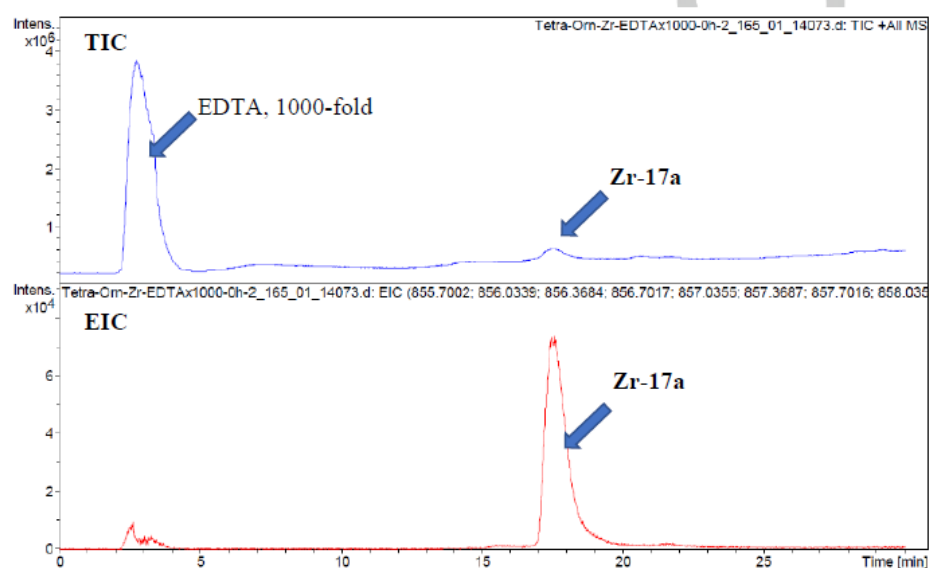


Figure S45. Total ion chromatogram (TIC, blue) and extracted ion chromatogram (EIC, red) for the transchelation assay of **Zr-17a** challenged with a 1000-fold excess of EDTA at pH 7. EIC using the most abundant Zr-isotope peaks of **Zr-17a** (855.7002; 856.0339; 856.3684; 856.7017; 857.0355; 857.3687; 857.7016; 858.0355; 1283.0415; 1283.5427; 1284.0447; 1284.5447; 1285.0435; 1285.5450; 1286.0455; 1286.5444; ± 0.01).

WILEY-VCH

FULL PAPER

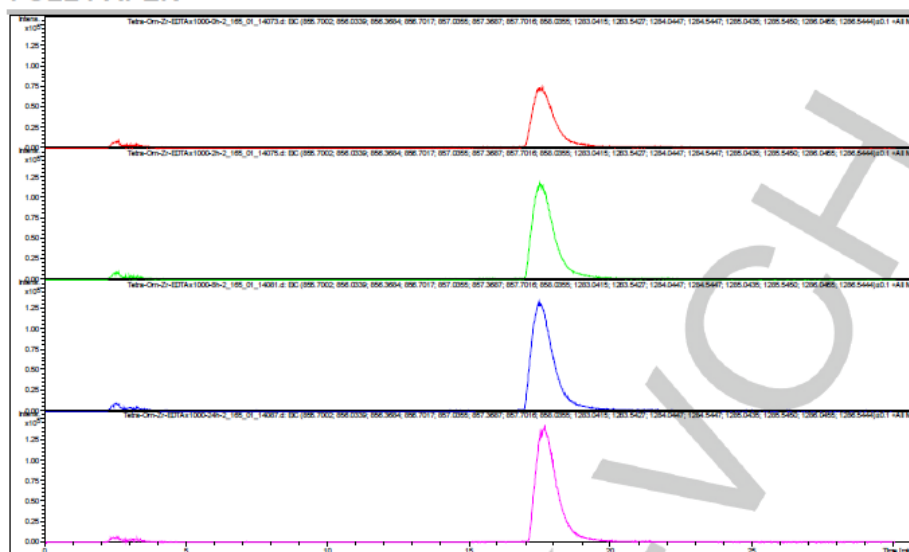


Figure S46. Extracted ion chromatograms for the transchelation assay of Zr-17a challenged with a 1000-fold excess of EDTA at pH 7. Aliquots were taken after 0 h (red), 2 h (green), 8 h (blue) and 24 h (pink). EIC using the most abundant Zr-isotope peaks of Zr-17a (855.7002; 856.0339; 856.3684; 856.7017; 857.0355; 857.3687; 857.7016; 858.0355; 1283.0415; 1283.5427; 1284.0447; 1284.5447; 1285.0435; 1285.5450; 1286.0455; 1286.5444; ± 0.01).

FULL PAPER

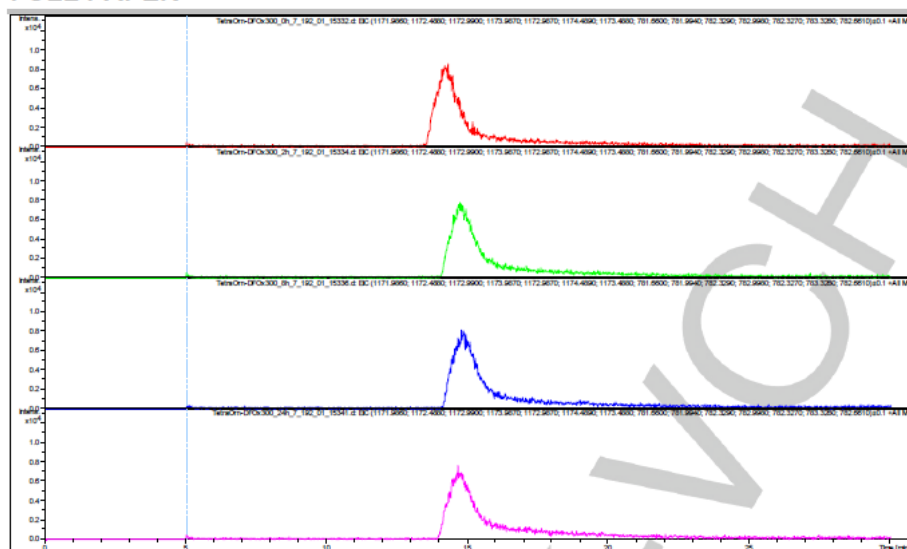


Figure S47. Extracted ion chromatograms for the transchelation assay of **Zr-17a** challenged with a 300-fold excess of DFOB at pH 7. Aliquots were taken after 0 h (red), 2 h (green), 8 h (blue) and 24 h (pink). EIC using the most abundant Zr-isotope peaks of **Zr-17a** (855.7002; 856.0339; 856.3684; 856.7017; 857.0355; 857.3687; 857.7016; 858.0355; 1283.0415; 1283.5427; 1284.0447; 1284.5447; 1285.0435; 1285.5450; 1286.0455; 1286.5444; ± 0.01).

8.1.2 Mixed Liquid and Solid Phase Synthesis of Isopeptidic Desferrioxamine Analogues for Complexation of Zirconium

European Journal of Organic Chemistry

Supporting Information

Mixed Liquid and Solid Phase Synthesis of Isopeptidic Desferrioxamine Analogues for Complexation of Zirconium

Lasse Outzen, Hoang Duc Nguyen, Darius Ludolfs and Wolfgang Maison*

Supporting Information

General Information	2
Experimental Procedures	3
Solid Phase Synthesis.....	12
NMR spectra	21
HPLC-MS spectra	32
References	38

General Information

All reagents and solvents were obtained commercially in required grades and used without further purification. Dem. H₂O was obtained through purification by PURELAB Classic from ELGA LabWater. Atmospheric oxygen or moisture sensitive reactions were performed under a protective gas atmosphere (N₂ or Ar). The progress of reactions were monitored by TLC performed on silica gel ALUGRAM Xtra SIL G/UV254 (normal phase) from Macherey-Nagel. The detection was achieved by UV (λ = 254 nm and 364 nm) or by dipping in ninhydrin solution (1.5 wt% ninhydrin and 3% v/v glacial acetic acid in *n*-butanol) and potassium permanganate solution (KMnO₄ (3 g), K₂CO₃ (20 g), aq. NaOH (5%, 5 mL) in dem. H₂O (300 mL)) followed by heating. The ozonolysis reaction was performed on the 500AF ozone generator by enaly and on the Laboratory Ozonizer 301.7 by Erwin Sander. Reactions with microwave conditions were performed by Initiator+ from Biotage with a Robot Sixty autosampler from Biotage. Silicagel for column chromatography carried out by hand was POLYGOPREP 60–80 from Macherey-Nagel for normal phase. Purifications with automated column chromatography were performed on the Isolera Prime from the company Biotage with self-packed cartridges from Macherey-Nagel filled with POLYGOPREP 60-80 silicagel. Separation on reversed-phase were performed on the puriFlash450 from Interchim with the cartridges CHROMABOND Flash RS 15, CHROMABOND Flash RS 25 or CHROMABOND Flash RS 80 from the company Macherey-Nagel. Compound were freeze dried in water/CH₃CN using the ALPHA 2-4 LDplus system from Martin Christ. The purification via preparative HPLC was performed on the Pure C-850 FlashPrep system from the company Büchi with Nucleodur HTec, 5 μ m, 250x10 mm from Macherey-Nagel. HRMS-ESI-MS measurements were performed using 6224 ESI-TOF spectrometer coupled with HPLC 1200 series from Agilent Technologies with a Agilent Zorbax Extend C18, 2.1 x 50 mm. Non-HRMS-ESI-MS measurements were performed using a Agilent HPLC coupled to the ion trap amaZon SL from Bruker Daltonic with Macherey-Nagel EC Nucleodur C18 Gravity-SB, 5 μ m, 150x4 mm and Macherey-Nagel Nucleodur C18 HTec, 3 μ m, 150x4,6 mm. NMR spectra were measured with Avance III 600 MHz, an Avance I 500 MHz, a DRX 500 MHz, an Avance III HD 400 MHz, an Avance II 400 MHz, an Avance I 400 MHz or a FourierHD 300 MHz from Bruker Daltonics.

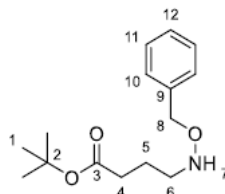
The following molecules were synthesized according to literature procedures:

2,5-Dioxopyrrolidine-1-yl-4-azidobutanoate **17**: [30] and [31].

Fmoc- β -Ala-COCl **11**: [32].

Experimental Procedures

tert-Butyl 4-(benzyloxy)aminobutanoate **2**



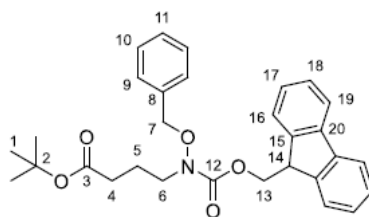
The *tert*-butyl 4-bromobutanoate **1** (1 eq., 7.00 g, 31.0 mmol) was dissolved with *O*-benzyl hydroxylamine (3 eq., 11.6 g, 94.0 mmol, 10.9 mL) and K_2CO_3 (3 eq., 13.0 g, 94.0 mmol) in DMF (120 mL) and stirred for 3 h at 80 °C. The reaction mixture was then mixed with dem. water (200 mL) and extracted with EtOAc (3 x 150 mL). The combined organic phases were washed with sat. aq. NaCl (2 x 150 mL) and dried over $MgSO_4$. The solvent was removed under reduced pressure and the remaining *O*-benzyl hydroxylamine was removed by distillation at 75 °C. The product **2** (7.8 g, 29.4 mmol, 95%) was obtained as a colorless oil.

¹H-NMR (300 MHz, $CDCl_3$): δ [ppm] = 7.38 – 7.27 (m, 5H, 10-C, 11-C, 12-C), 4.70 (s, 2H, 8-C), 2.95 (t, 3J = 6.9 Hz, 2H, 6-C), 2.27 (t, 3J = 7.4 Hz, 2H, 4-C), 1.81 (p, 3J = 7.2 Hz, 2H, 5-C), 1.44 (s, 9H, 1-C).

¹³C-NMR (75 MHz, $CDCl_3$): δ [ppm] = 173.2 (C3), 138.4 (C9), 128.9 (C11), 128.8 (C12), 128.8 (C10), 80.6 (C2), 76.7 (C9), 51.7 (C6), 33.6 (C4), 28.5 (C1), 23.4 (C5).

HRMS (ESI): m/z [$M+H-tBu$]⁺ calc. for $C_{15}H_{23}NO_3$: 210.1125, found: 210.1130.

tert-Butyl 4-(Fmoc)(benzyloxy)aminobutanoate **3**



The *tert*-butyl 4-(benzyloxy)aminobutanoate **2** (1 eq., 7.80 g, 29.4 mmol) was dissolved in CH_2Cl_2 (210 mL), treated with DIPEA (2 eq., 7.60 g, 58.8 mmol, 9.99 mL) and cooled to 0 °C. FmocCl (1.1 eq., 8.36 g, 32.3 mmol) was dissolved in CH_2Cl_2 , cooled to 0 °C and added slowly to the first solution. The resulting reaction mixture was stirred at 0 °C for 3 h, then washed with HCl (1 M, 3 x 120 mL) and sat. aq. NaCl (2 x 120 mL) and dried over $MgSO_4$. The solvent was

S3

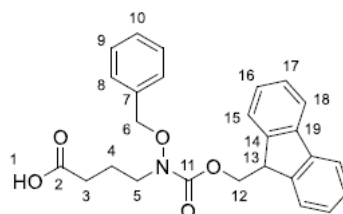
removed under reduced pressure to give the title compound **3** (15.5 g) as a colorless oil. The crude product was used without further purification.

¹H-NMR (500 MHz, CDCl₃): δ [ppm] = 7.75 (d, 3J = 7.6 Hz, 2H, 19-H), 7.63 (d, 3J = 7.6 Hz, 2H, 2H, 16-H), 7.42 – 7.28 (m, 9H, 9-H, 10-H, 11-H, 17-H, 18-H), 4.71 (s, 2H, 7-H), 4.61 (d, 3J = 6.3 Hz, 2H, 13-H), 4.27 (t, 3J = 6.3 Hz, 1H, 14-H), 3.43 (t, 3J = 7.1 Hz, 2H, 6-H), 2.18 (t, 3J = 7.5 Hz, 2H, 4-H), 1.82 (p, 3J = 7.3 Hz, 2H, 5-H), 1.43 (s, 9H, 1-H).

¹³C-NMR (126 MHz, CDCl₃): δ [ppm] = 172.4 (C3), 157.3 (C12), 143.9 (C15), 141.5 (C20), 135.4 (C8), 129.4 (C10), 128.7 (C11), 128.6 (C9), 127.9 (C18), 127.3 (C19), 125.1 (C17), 120.1 (C16), 80.4 (C2), 77.1 (C7), 67.4 (C13), 49.2 (C6), 47.5 (C14), 32.8 (C4), 28.2 (C1), 22.7 (C5).

HRMS (ESI): m/z [M+Na]⁺ calc. for C₃₀H₃₃NO₅: 510.2251, found: 510.2250.

4-Fmoc-(Benzyloxy)aminobutanoate **4**

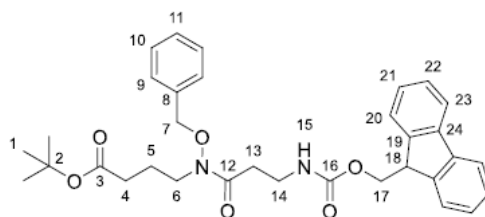


tert-Butyl 4-(Fmoc)(benzyloxy)aminobutanoate **3** was dissolved with TIPS (5 eq., 24.36 g, 153.8 mmol, 33.46 mL) in CH₂Cl₂ (90 mL). Afterwards TFA (90 mL) was added at 0 °C. The reaction mixture was stirred for 3 h at room temperature. CH₂Cl₂ and TFA were removed under reduced pressure and the resulting residue was coevaporated three times with CH₂Cl₂ (3 x 20 mL). After column chromatography on silica gel (2% methanol in CH₂Cl₂), the product **4** (9.6 g, 22.25 mmol, 69% over two steps) was obtained as a slightly yellowish oil.

¹H-NMR (600 MHz, CDCl₃): δ [ppm] = 7.75 (d, 3J = 7.5 Hz, 2H, 18-C), 7.62 (d, 3J = 7.5 Hz, 2H, 15-C), 7.40 (t, 3J = 7.5 Hz, 2H, 17-C), 7.36 – 7.22 (m, 7H, 8-C, 9-C, 10-C, 16-C), 4.69 (s, 2H, 6-C), 4.63 (d, 3J = 6.2 Hz, 2H, 12-C), 4.26 (t, 3J = 6.2 Hz, 1H, 13-C), 3.42 (t, 3J = 6.9 Hz, 2H, 5-C), 2.28 (t, 3J = 7.4 Hz, 2H, 3-C), 1.81 (p, 3J = 7.1 Hz, 2H, 4-C).

¹³C-NMR (151 MHz, CDCl₃): δ [ppm] = 178.4 (C2), 157.2 (C11), 143.7 (C14), 141.4 (C19), 135.2 (C7), 129.3 (C9), 128.6 (C10), 128.5 (C8), 127.8 (C17), 127.2 (C18), 125.0 (C16), 120.0 (C15), 77.0 (C6), 67.3 (C12), 48.8 (C5), 47.3 (C13), 30.9 (C3), 22.1 (C4).

HRMS (ESI): m/z [M+H]⁺ calc. for C₂₆H₂₅NO₅: 432.1806, found: 432.1816.

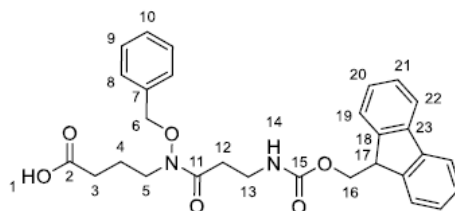
tert*-Butyl 4-(benzyloxy)(3-(Fmoc)- β -alanine)aminobutanoate **12*

For the formation of the acid chloride **11** Fmoc- β -alanine (1.52 eq, 6.97 g, 22.4 mmol) was dissolved und nitrogen atmosphere in abs. CH_2Cl_2 (330 mL), cooled to 0 °C and catalytic amounts of DMF (2 – 3 drops) were added. Ice cold thionyl chloride (7.6 eq., 13.32 g, 118.9 mmol, 8.12 mL) was added over a period of 10 min and the solution was stirred for 3 h at room temperature. The volatile components were removed under reduced pressure. The residue was coevaporated twice with CH_2Cl_2 . The slightly yellow residue was dissolved under nitrogen atmosphere in abs. THF (35 mL) and was cooled to 0 °C. *tert*-Butyl 4-(benzyloxy)aminobutanoate **2** (1 eq., 3.91 g, 14.8 mmol) was dissolved in abs. THF (45 mL), mixed with abs. pyridine (3 eq., 3.50 g, 44.3 mmol, 3.57 mL) and cooled to 0 °C. The solution with the acid chloride was slowly dripped to the solution with the *O*-benzyl hydroxylamine derivative. The reaction mixture was stirred for 24 h at room temperature. Subsequently, the solvent was removed under reduced pressure and the resulting brown oil was dissolved in EtOAc (200 mL). Afterwards, the solution was washed with HCl (1 M, 3 x 80 mL), sat. aq. NaHCO_3 (3 x 80 mL) and sat. aq. NaCl (3 x 80 mL) and dried over Na_2SO_4 . The title compound (9.78 g) was obtained by removing the solvent under reduced pressure as a slightly yellowish oil. The crude product was used without further purification.

$^1\text{H-NMR}$ (400 MHz, CDCl_3): δ [ppm] = 7.76 (d, 3J = 7.5 Hz, 2H, 23-C), 7.60 (d, 3J = 7.4 Hz, 2H, 20-C), 7.43 – 7.26 (m, 9H, 9-C, 10-C, 11-C, 21-C, 22-C), 5.56 (t, 3J = 7.1 Hz, 1H, 15-N), 4.79 (s, 2H, 7-C), 4.35 (d, 3J = 7.2 Hz, 2H, 17-C), 4.20 (t, 3J = 7.2 Hz, 2H, 18-C), 3.72 (t, 3J = 7.1 Hz, 2H, 6-C), 3.48 (t, 3J = 5.9 Hz, 2H, 14-C), 2.63 (t, 3J = 5.6 Hz, 2H, 13-C), 2.26 (t, 3J = 7.2 Hz, 2H, 4-C), 1.93 (m, 2H, 5-C), 1.44 (s, 9H, 1-C).

$^{13}\text{C-NMR}$ (101 MHz, CDCl_3): δ [ppm] = 172.3 (C3), 156.5 (C12), 144.1 (C19), 141.4 (C24), 129.6 (C16), 129.4 (C10), 129.2 (C8), 128.9 (C9), 127.8 (C23), 127.1 (C21), 125.3 (C11), 120.1 (C20), 80.6 (C2), 76.4 (C7), 66.8 (C17), 47.3 (C18), 44.7 (C6), 36.4 (C14), 32.8 (C4), 32.7 (C13), 28.2 (C1), 22.5 (C5).

HRMS (ESI): m/z $[\text{M}+\text{H}]^+$ calc. for $\text{C}_{33}\text{H}_{38}\text{N}_2\text{O}_6$: 559.2803, found: 559.2819.

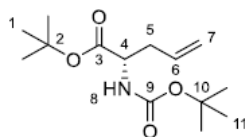
4-(Benzyloxy)(3-(Fmoc)- β -alanine)aminobutanoate **13**

tert-Butyl 4-(benzyloxy)(3-(Fmoc)- β -alanine)aminobutanoate **12** (1 eq., 9.54 g, 17.1 mmol) was dissolved with TIPS (3 eq., 8.12 g, 51.2 mmol, 11.2 mL) in CH_2Cl_2 (50 mL). Afterwards TFA (50 mL) was added at 0 °C. The reaction mixture was stirred for 3 h at room temperature. The CH_2Cl_2 and TFA were removed under reduced pressure and the resulting residue was coevaporated two times with CH_2Cl_2 (2 x 10 mL). After column chromatography on silica gel (5% to 95% EtOAc in pentane), the product **13** (5.19 g, 10.3 mmol, 70% over two steps) was obtained as a slightly yellow oil.

$^1\text{H-NMR}$ (400 MHz, CDCl_3): δ [ppm] = 7.75 (d, $^3J = 7.4$ Hz, 2H, 22-C), 7.59 (d, $^3J = 7.5$ Hz, 2H, 19-C), 7.41 – 7.25 (m, 9H, 8-C, 9-C, 10-C, 20-C, 21-C), 5.61 (t, $^3J = 6.5$ Hz, 1H, 14-N), 4.78 (s, 2H, 6-C), 4.34 (d, $^3J = 7.2$ Hz, 2H, 16-C), 4.19 (t, $^3J = 7.1$ Hz, 1H, 17-C), 3.74 (q, $^3J = 6.9$ Hz, 2H, 5-C), 3.46 (t, $^3J = 5.9$ Hz, 1H, 13-C), 2.64 (t, $^3J = 5.7$ Hz, 2H, 12-C), 2.38 (t, $^3J = 7.0$ Hz, 2H, 3-C), 1.97 (m, 2H, 4-C).

$^{13}\text{C-NMR}$ (101 MHz, CDCl_3): δ [ppm] = 176.7 (C2), 155.5 (C11), 144.1 (C18), 140.0 (C23), 129.4 (C15), 129.3 (C9), 128.9 (C7), 127.8 (C8), 127.8 (C22), 127.2 (C20), 125.3 (C10), 120.1 (C19), 76.5 (C6), 66.9 (C16), 47.3 (C17), 44.4 (C5), 36.4 (C13), 32.8 (C3), 31.0 (C12), 22.1 (C4).

HRMS (ESI): m/z $[\text{M}+\text{H}]^+$ calc. for $\text{C}_{29}\text{H}_{30}\text{N}_2\text{O}_6$: 503.2177, found: 503.2188.

tert*-Butyl *N*-Boc-allylglycine ester **21*

A solution of Boc-*L*-allylglycine **14** (1.0 eq., 10.0 g, 46.5 mmol) and *t*BuOH (5.0 eq., 232 mmol, 22 mL) in dry CH_2Cl_2 (50 mL) was cooled to 0 °C. Subsequently, DCC (1.1 eq., 10.5 g, 51.1 mmol) and DMAP (0.1 eq., 568 mg, 4.65 mmol) were added in portions and the solution was stirred to room temperature for 14 h. The colorless precipitate was filtered and the solvent

S6

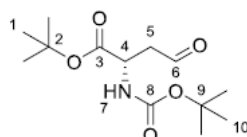
was removed under reduced pressure. After purification by column chromatography on silica gel (n-pentane/EtOAc, 3:2 v/v), the product **21** (11.0 g, 40.4 mmol, 87%) was obtained as a yellow oil.

¹H-NMR (500 MHz, CDCl₃): δ [ppm] = 5.70 (ddt, 3J = 16.4 Hz, 3J = 10.7 Hz, 3J = 7.2 Hz, 1H, 6-C), 5.12 (m, 2H, 7-C), 5.04 (d, 3J = 8.2 Hz, 1H, 8-N), 4.25 (dt, 3J = 8.2 Hz, 3J = 5.7 Hz, 1H, 4-C), 2.49 (m, 2H, 5-C), 1.45 (s, 9H, 1-C), 1.43 (s, 9H, 11-C).

¹³C-NMR (101 MHz, CDCl₃): δ [ppm] = 132.7 (C6), 118.9 (C7), 53.5 (C4), 37.2 (C5) 28.5 (C11), 28.2 (C1).

HRMS (ESI): m/z [M+Na]⁺ calc. for C₁₄H₂₅NO₄: 294.1676, found: 294.1670.

tert-Butyl 2-(N-Boc)-4-oxobutanoate 15

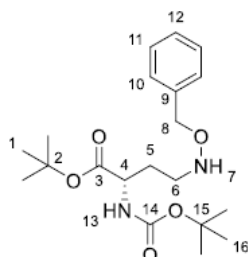


tert-Butyl *N*-Boc allylglycine ester (1.0 eq., 10.9 g, 40.0 mmol) was dissolved in CH₂Cl₂ (100 mL) and the solution was cooled to -78 °C. Gaseous ozone was then passed through the solution as a reactant. After complete consumption of the starting material (detected by TLC), oxygen was passed through the solution for 30 min to remove excess ozone. Triphenylphosphine (1.2 eq., 12.7 g, 48.4 mmol) was then added in portions and the reaction mixture was stirred at room temperature for 18 h. The volatiles were removed under reduced pressure and the resulting triphenylphosphine oxide was precipitated in a mixture of cold *n*-hexane/diethyl ether (20 mL, 1:1 v/v). The precipitate was filtered and the solvent was removed under reduced pressure. After column chromatographic purification on silica gel (n-pentane/EtOAc, 9:1 v/v), the product **15** (5.52 g, 10.2 mmol, 51%) was obtained as a colorless oil.

¹H-NMR (500 MHz, CDCl₃): δ [ppm] = 9.73 (s, 1H, 6-C), 5.36 (d, 3J = 8.1 Hz, 1H, 7-N), 4.47 (m, 1H, 4-C), 2.97 (qd, 3J = 18.0 Hz, 3J = 5.2 Hz, 2H, 5-C), 1.44 (s, 9H, 1-C), 1.43 (s, 9H, 10-C).

¹³C-NMR (131 MHz, CDCl₃): δ [ppm] = 199.6 (C6), 170.1 (C3), 155.5 (C8), 82.3 (C2), 80.2 (C9), 49.4 (C4), 46.5 (C5), 28.4 (C1), 28.0 (C10).

HRMS (ESI): m/z [M+Na]⁺ calc. for C₁₃H₂₃NO₅: 296.1468, found: 296.1457.

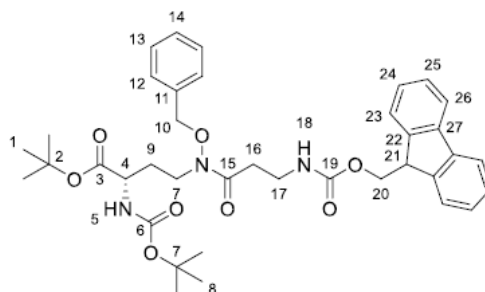
tert*-Butyl 2-(*N*-Boc)-4-(benzyloxy)aminobutanoate **16*

The starting compound *tert*-butyl 2-(*N*-Boc)-4-oxobutanoate **15** (1.0 eq., 5.40 g, 19.8 mmol) was dissolved in dry MeOH (40 mL) and *O*-benzyl hydroxylamine (1.2 eq., 2.8 mL, 24 mmol), dissolved in dry MeOH (10 mL), was added dropwise. After complete consumption of the starting material (detected by TLC), the reaction solution was cooled to 0 °C. A NaCNBH₃ solution in THF (2.0 eq., 40 mL, 1.0 M, 40 mmol) was added and the pH was adjusted below a value of 3 with conc. hydrochloric acid for 30 min while stirring at room temperature. After further 30 min, the volatiles were removed under reduced pressure, the white residue was suspended in H₂O (50 mL) and a pH of 9 was adjusted by adding an aq. KOH solution (0.5 M). The aqueous phase was extracted with CH₂Cl₂ (3 x 50 mL), the combined organic phases were washed with H₂O (75 mL) and sat. NaCl solution (75 mL) and dried over anhydrous Na₂SO₄. After filtration, the solvent was removed under reduced pressure and the product was dried under high vacuum. The product **16** was obtained as a colorless oil (7.43 g, 19.5 mmol, 99%).

¹H-NMR (600 MHz, CDCl₃): δ [ppm] = 7.34 (m, 5H, 10-C, 11-C, 12-C), 5.67 (s, 1H, N-7), 5.36 (d, 3J = 8.1 Hz, 1H, N-13), 4.71 (s, 2H, 5-C), 4.25 (td, 3J = 8.2 Hz, 3J = 4.7 Hz, 1H, 4-C), 3.00 (m, 2H, 5-C), 2.08 (m, 1H, 6-C), 1.78 (m, 1H, 6-C), 1.46 (s, 9H, 1-C), 1.44 (s, 9H, 16-C).

¹³C-NMR (151 MHz, CDCl₃): δ [ppm] = 171.9 (C2), 155.7 (C14), 138.0 (C9), 128.6 (C11), 128.5 (C10), 128.0 (C12), 82.0 (C2), 79.8 (C15), 76.4 (C8), 52.6 (C4), 48.5 (C6), 30.4 (C5), 28.5 (C1), 28.1 (C16).

HRMS (ESI): *m/z* [M+Na]⁺ calc. for C₂₀H₃₂N₂O₅: 403.2203, found: 403.2202.

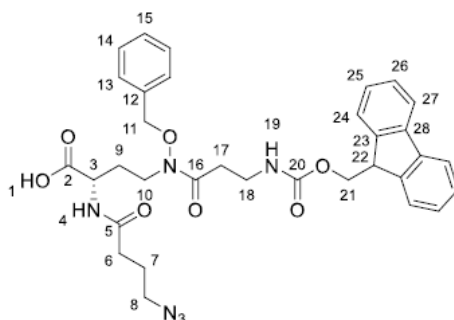
tert*-Butyl 2-(*N*-Boc)-4-(benzyloxy)(3-(Fmoc)- β -alanine)aminobutanoate **22*

tert-Butyl 2-(*N*-Boc)-4-(benzyloxy)aminobutanoate **16** (1.0 eq., 7.30 g, 19.2 mmol) was dissolved in dry THF (50 mL) and dry pyridine (3.0 eq., 4.64 mL, 57.6 mmol) was added at 0 °C. The acid chloride **11** was synthesized as described in the synthesis for **12**. **11** (1.5 eq., 9.50 g, 28.8 mmol) in dry THF (40 mL) was added dropwise to the reaction solution of **16** and stirred for 17 h at room temperature. The solvent was removed under reduced pressure and the brown residue was suspended in EtOAc (100 mL). The organic phase was purified with aq. HCl (1 M, 2 x 75 mL), sat. NaHCO₃ (2 x 75 mL) and washed with sat. NaCl solution (50 mL). The organic phase was dried over anhydrous Na₂SO₄, filtered and the solvent was removed under reduced pressure. After column chromatography on silica gel (n-pentane/EtOAc, 9:1 v/v), the product **22** (9.98 g, 14.8 mmol, 77%) was obtained as an orange solid.

¹H-NMR (400 MHz, CDCl₃): δ [ppm] = 7.75 (d, 3J = 7.4 Hz, 2H, 26-C), 7.59 (d, 3J = 7.5 Hz, 2H, 26-C), 7.36 (m, 9H, 12-C, 13-C, 14-C, 24-C, 25-C), 5.64 (sbr, 1H, 5-N), 5.19 (d, 3J = 8.4 Hz, 1H, 18-N), 4.49 (s, 2H, 10-C), 4.34 (m, 2H, 20-C), 4.21 (m, 1H, 4-C), 4.21 (m, 1H, 21-C), 3.75 (sbr, 2H, 17-C), 3.48 (m, 2H, 16-C), 2.61 (m, 2H, 9-C), 2.15 (m, 1H, 7-C), 1.93 (m, 1H, 7-C), 1.45 (s, 9H, 1-C), 1.44 (s, 9H, 8-C).

¹³C-NMR (101 MHz, CDCl₃): δ [ppm] = 173.8 (C15), 173.6 (C3), 156.6 (C19), 155.6 (C6), 144.2 (C22), 141.4 (C27), 134.0 (C11), 129.4 (C13), 129.3 (C14), 128.9 (C12), 127.8 (C25), 127.2 (C26), 125.3 (C24), 120.1 (C23), 82.4 (C10), 80.0 (C2), 76.5 (C7), 66.9 (C10), 59.6 (C20), 52.1 (C21), 47.4 (C4), 41.8 (C7), 36.4 (C17), 32.9 (C16), 29.8 (C9), 28.5 (C1), 28.1 (C8).

HRMS (ESI): m/z [M+Na]⁺ calc. for C₃₈H₄₇N₃O₈: 696.3255, found: 696.3273.

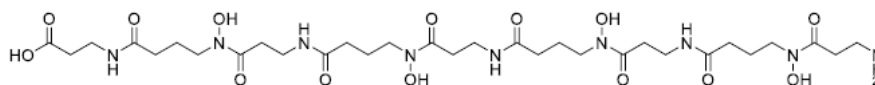
2-(N-(4-Azidobutyric acid))-4-(benzyloxy)(3-(Fmoc)-β-alanine)aminobutanoate 18

tert-Butyl 2-(*N*-Boc)-4-(benzyloxy)(3-(Fmoc)-β-alanine)aminobutanoate (1 eq., 107 mg, 0.16 mmol) was dissolved in a mixture of TFA/CH₂Cl₂ (2 mL, 1:1 v/v), then TIPS (2.0 eq., 0.07 mL, 0.32 mmol) was added and stirred for 3 h at room temperature. The volatiles were removed under reduced pressure. The residue was suspended in CH₂Cl₂ (10 mL) and again removed under reduced pressure. This procedure was repeated three times to obtain a mixture of deprotected **22** and the corresponding *tert*-butyl ester as a colorless solid. The mixture (163 mg) was dissolved in dry CH₂Cl₂ (2 mL) and dry DIPEA (0.08 mL, 0.48 mmol) was added. The active ester **17** (1.2 eq. calculated from the starting compound used, 45 mg, 0.2 mmol) was added to the reaction solution. After stirring for 1 h at room temperature, the volatiles were removed under reduced pressure and the residue was coevaporated three times in CH₂Cl₂ (5 mL). After column chromatography on RP silica gel (RP C18, H₂O/MeCN 95:5 + 0.1% HCO₂H to 5:95 + 0.1% HCO₂H v/v), the product **18** (38 mg, 0.06 mmol, 38%) was obtained as a colorless solid after freeze-drying.

¹H-NMR (400 MHz, CDCl₃): δ [ppm] = 7.75 (d, 3J = 7.4 Hz, 2H, 27-C), 7.57 (d, 3J = 7.6 Hz, 2H, 24-C), 7.32 (m, 9H, 13-C, 14-C, 15-C, 25-C, 26-C), 6.79 (d, 3J = 7.5 Hz 1H, 4-N), 5.78 (t, 3J = 6.3 Hz, 1H, 19-N), 4.80 (s, 2H, 11-C), 4.60 (q, 3J = 6.9 Hz, 1H, 3-C), 4.31 (m, 2H, 21-C), 4.16 (t, 3J = 7.2 Hz 1H, 22-C), 3.89 (m, 1H, 18-C), 3.62 (m, 1H, 18-C), 3.46 (m, 2H, 6-C), 3.30 (t, 3J = 6.7 Hz, 2H, 17-C), 2.68 (m, 1H, 10-C), 2.56 (m, 1H, 10-C), 2.31 (t, 3J = 7.3 Hz, 2H, 9-C), 2.22 (m, 1H, 8-C), 2.08 (m, 1H, 8-C) 1.89 (m, 2H, 7-C).

¹³C-NMR (101 MHz, CDCl₃): δ [ppm] = 174.6 (C2), 173.2 (C5), 172.6 (C16), 156.8 (C20), 144.1 (C23), 141.4 (C28), 133.8 (C12), 129.5 (C15), 129.4 (C14), 129.0 (C13), 127.8 (C26), 127.2 (C27), 125.2 (C25), 120.1 (C24), 76.5 (C11), 66.9 (C21), 50.8 (C8), 50.1 (C3), 47.3 (C22), 42.1 (C10), 36.7 (C18), 33.1 (C6), 32.8 (C17), 29.7 (C7), 24.7 (C9).

HRMS (ESI): *m/z* [M+Na]⁺ calc. for C₃₃H₃₆N₆O₇: 651.2538, found: 651.2579.

ipDFO* 10

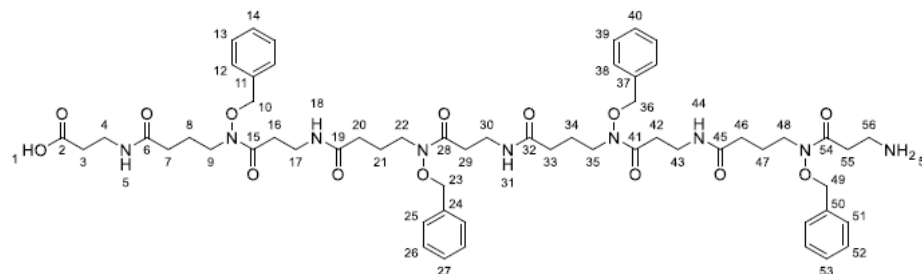
To remove the benzyl protecting groups, **9** (1 eq., 10 mg, 8.8 μmol) were dissolved in methanol (1.9 mL) and dem. Water (0.4 mL) and mixed with formic acid (22 μL) and palladium on activated carbon (Pd/C, 10%, 0.7 mg). The solvent was brought to reflux under reduced pressure. The reaction vessel was then flooded with hydrogen. This procedure was repeated twice. The reaction mixture was stirred under H_2 atmosphere for 3 h at room temperature. The reaction solution was then filtered, the volatile components were removed under reduced pressure and the residue was dissolved in $\text{CH}_3\text{CN}/\text{dem. H}_2\text{O}$ (1:1 v/v) and freeze-dried. After freeze-drying, the product **10** (6.1 mg, 7.9 μmol , 90 %) was obtained as a colorless solid.

HRMS (ESI): m/z $[\text{M}+\text{H}]^+$ calc. for $\text{C}_{31}\text{H}_{59}\text{N}_9\text{O}_{14}$: 778.3941, found: 778.3948.

Anal. HPLC (Agilent Zorbax Extend C18, 2.1 x 50 mm, $\text{H}_2\text{O}/\text{CH}_3\text{CN}$ 5:95 + 0.1% HCO_2H to 95:5 + 0.1% HCO_2H , 14 min, 0.3 ml/min): t_R = 2.8 min.

Solid Phase Synthesis

O-Benzyl-protected ipDFO* 9



Synthesis for the formation of ipDFO* 9 using 4 and Fmoc-β-alanine (Scheme 1B):

The unloaded Wang resin (1.00 g, maximum loading density according to the manufacturer: 1.00 mmol/g) was allowed to swell in CH₂Cl₂ (6 mL) on a shaker for 30 min. It was then rinsed three times with DMF (3 x 6 mL). Fmoc-β-Alanine (4 eq., 1.25 g, 4.00 mmol) was dissolved in DMF (10 mL), mixed with 1-hydroxybenzotriazole (HOBt, 3 eq., 0.46 g, 3.00 mmol) and cooled to 0 °C. DCC (4 eq., 0.83 g, 4.00 mmol) was added and the solution was stirred for 15 min at room temperature. The solution with the HOBt-activated Fmoc-β-alanine was transferred to the resin and allowed to react overnight at room temperature by gentle shaking. The reaction solution was then separated from the Wang resin which was washed three times with CH₂Cl₂ (3 x 6 mL), three times with 2-propanol (3 x 6 mL), three times with CH₂Cl₂ (3 x 6 mL), three times with 2-propanol (3 x 6 mL) and three times with methanol (3 x 6 mL). The resin was stored in a desiccator until constant mass was reached.

The loading density of the initial Fmoc-β-alanine on the resin was determined with a few milligrams of the dry resin according to the protocol of Merck Biosciences AG, Novabiochem Peptide Resin Loading Protocols (based on M. Gude et al., *Lett. Pept. Sci.*, **2002**, 9, 203).^[33] For this purpose, the dry resin was swollen in a solution of DMF with 2% DBU for 30 min with gentle shaking. The resulting solution was diluted to 10 mL with CH₃CN. Of this, 2 mL was diluted to 25 mL with CH₃CN. A blank was prepared in the same way without the solution coming into contact with resin. The absorbance of the solutions was measured at 304 nm. A triple determination was carried out. Equation (1) was used to determine the loading density in mmol/g.

$$\frac{\text{mmol}}{\text{g}} = \frac{(\text{Abs}_{\text{sample}} - \text{Abs}_{\text{control}}) \cdot 16.4}{\text{mg of resin}} \quad (1)$$

The loading density was determined to be 0.48 mmol/g.

The synthesis on the solid phase was carried out in repeating cycles. One cycle consists of the cleavage of the Fmoc protecting group of the amine or *O*-benzyl hydroxylamine of the amino acid bound to the solid phase. Subsequently, the coupling of an active ester of the subsequent amino acid to the released amine or *O*-benzyl hydroxylamine takes place. The Fmoc deprotection steps, the coupling steps and the masking of unreacted *O*-benzyl hydroxylamines with an acetic anhydride solution during the solid phase synthesis took place under microwave conditions. The liquid phase of each step was separated from the resin *via* filtration before the subsequent step.

The Wang resin initially loaded with Fmoc- β -alanine (200 mg, loading density: 0.48 mmol/g, synthesis scale: 0.1 mmol) was initially swelled in CH_2Cl_2 (6 mL) for 30 min. The resin was then rinsed with DMF (3 x 10 mL). The subsequent Fmoc deprotection was carried out twice, each time with a fresh solution of 20% piperidine in DMF (5 mL, 1st: 3 min, 80 °C; 2nd: 0.5 min, 80 °C), with rinsing steps between and after the deprotection steps with DMF (3 x 10 mL). For the subsequent coupling, **4** (5 eq. based on the loading density of the resin, 2 mL (from 2.16 g **4** in DMF (20 mL))) was mixed with DIPEA (10 eq. based on the loading density of the resin, 2 mL (from 3.5 mL DIPEA in DMF (40 mL))) and PyOxim (5 eq. based on the loading density of the resin, 2 mL (from 5.27 g PyOxim in DMF (40 mL))) and gently stirred for 5 min at room temperature to form the active ester *in situ*. The active ester solution was then added to the resin and two consecutive coupling steps (1.: 20 min, 80 °C; 2.: 10 min, 80 °C) were carried out, each with fresh solutions. Here also, rinsing steps with DMF (3 x 10 mL) were carried out between and after the couplings. After these steps, the first cycle to extend the amino acid sequence by one monomer was complete. The second cycle is similar to the first except for the exchange of **4** to Fmoc- β -alanine. Scale of the coupling steps with Fmoc- β -alanine: Fmoc- β -alanine (5 eq. based on the loading density of the resin, 2 mL (from 1.49 g Fmoc- β -alanine in DMF (20 mL))). After the second coupling of Fmoc- β -alanine, the unreacted *O*-benzyl hydroxylamines were acetylated with an acetic anhydride solution (1.18 mL acetic anhydride, 0.55 mL DIPEA, 0.057 g HOBt in DMF (25 mL)) at 65 °C for 3 min under microwave conditions. The two cycles described were each repeated three more times to obtain the ipDFO* **8** bound to the solid phase. After completion of the solid phase synthesis, the resin was washed with DMF (3 x 10 mL) and CH_2Cl_2 (3 x 10 mL) and stored in a desiccator under vacuum.

To separate the products obtained during the solid phase synthesis from the Wang resin, the dry resin was placed in an ice cold TFA/TIPS/ CH_2Cl_2 solution (90:5:5, 10 mL) for 2 h and gently shaken at room temperature. The solvent and volatiles were removed under reduced pressure. The residue was taken up in CH_2Cl_2 and again removed under reduced pressure. This was repeated twice to obtain the crude product. Then, the residue was taken up in CH_3CN /dem.

H₂O (1:1) and freeze-dried. The crude product was subsequently obtained as a slightly yellowish oil (146 mg). After column chromatographic purification on RP silica gel (column: Macherey Nagel, VP 250/10 Nucleodur C18 HTec, 5 µm; gradient: H₂O/CH₃CN 25:75 + 0.1% HCO₂H to 70:30 + 0.1% HCO₂H v/v), the ipDFO* **9** (30 mg, 26 µmol, 26% based on the synthesis batch of 0.1 mmol) was obtained as a slightly yellowish, highly viscous oil.

Synthesis for the formation of ipDFO **9** using O-benzyl-protected hydroxamic acid-bearing monomer **13** (Scheme 2B):*

The unloaded Wang resin (2.00 g, maximum loading density according to the manufacturer: 1.00 mmol/g) was allowed to swell in CH₂Cl₂ (12 mL) on a shaker for 30 min. It was then rinsed three times with DMF (3 x 6 mL). The Fmoc-β-alanine (4 eq., 2.50 g, 8.00 mmol) was dissolved in DMF (10 mL), mixed with 1-hydroxybenzotriazole (HOBt, 4 eq., 1.23 g, 8.00 mmol) and cooled to 0 °C. The DCC (4 eq., 1.60 g, 8.00 mmol) was added and the solution was stirred for 15 min at room temperature. The solution with the HOBt-activated Fmoc-β-alanine was transferred to the resin and allowed to react overnight at room temperature by gentle shaking. The reaction solution was then separated from the Wang resin by filtration and was washed three times with CH₂Cl₂ (3 x 6 mL), three times with 2-propanol (3 x 6 mL), three times with CH₂Cl₂ (3 x 6 mL), three times with 2-propanol (3 x 6 mL) and three times with methanol (3 x 6 mL). The resin was stored in a desiccator until constant mass was reached.

The loading density was determined as described above to be 0.69 mmol/g.

The synthesis on the solid phase was carried out in repeating cycles. One cycle consists of the cleavage of the Fmoc protecting group of the amine or O-benzyl hydroxylamine of the amino acid bound to the solid phase. Subsequently, the coupling of an active ester of the subsequent amino acid to the released amine or O-benzyl hydroxylamine takes place. The Fmoc deprotection steps, the coupling steps and the masking of unreacted O-benzyl hydroxylamines with an acetic anhydride solution during the solid phase synthesis took place under microwave conditions. The liquid phase of each step was separated from the resin via a frit before the subsequent step.

The Wang resin (714 mg, loading density: 0.69 mmol/g, synthesis scale: 0.5 mmol) initially loaded with Fmoc-β-alanine was initially swelled in CH₂Cl₂ (10 mL) for 30 min. The resin was then rinsed with DMF (3 x 10 mL). The subsequent Fmoc deprotection was carried out twice, each time with a fresh solution of 20% piperidine in DMF (15 mL, 1st: 3 min, 80 °C; 2nd: 0.5 min, 80 °C), with rinsing steps between and after the deprotection steps with DMF (3 x 10 mL). For the subsequent coupling, **13** (5 eq. based on the loading density of the resin, 6 mL (from

S14

5.03 g **12** in DMF (24 mL))) was mixed with DIPEA (10 eq. based on the loading density of the resin, 6 mL (from 3.49 mL DIPEA in DMF (24 mL))) and HATU/HOBt (5 eq. each based on the loading density of the resin, 6 mL (from 3.81 g HATU and 1.36 g HOBt in DMF (24 mL))) and gently stirred for 5 min at room temperature to form the active ester *in situ*. The active ester solution was then added to the resin and two consecutive coupling steps (1.: 20 min, 80 °C; 2.: 10 min, 80 °C) were carried out, each with fresh solutions. Here too, rinsing steps with DMF (3 x 10 mL) were carried out between and after the coupling. After this step, the first cycle to extend the amino acid sequence by one monomer was completed. Three more cycles were performed to obtain the ipDFO* **8** bound to the solid phase. After completion of the solid phase synthesis, the resin was washed with DMF (3 x 10 mL) and CH₂Cl₂ (3 x 10 mL) and stored in a desiccator under vacuum.

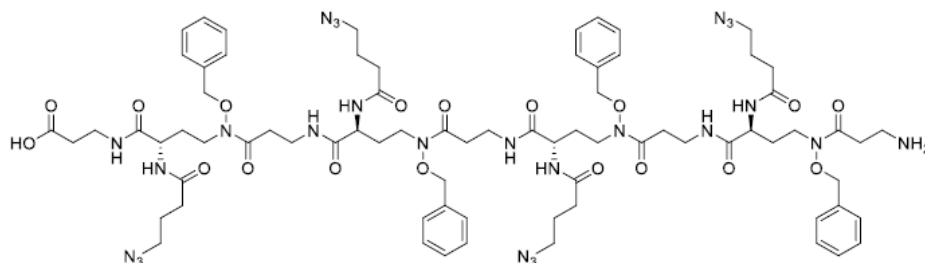
To separate the products obtained during the solid phase synthesis from the Wang resin, the dry resin was placed in a TFA/TIPS/CH₂Cl₂ solution (90:5:5, 10 mL) cooled to 0 °C for 2 h and gently shaken at room temperature. The solvent and volatiles were removed under reduced pressure. The residue was taken up in CH₂Cl₂ and again removed under reduced pressure. This was repeated twice to obtain the crude product (691 mg). After column chromatographic purification on RP silica gel (column: Macherey Nagel, VP 250/10 Nucleodur C18 HTec, 5 µm; gradient: H₂O/CH₃CN 25:75 + 0.1% HCO₂H to 70:30 + 0.1% HCO₂H v/v) and subsequent freeze-drying, the product ipDFO* **9** (71 mg, 62 µmol, 13% based on the synthesis scale of 0.5 mmol) was obtained as a slightly yellowish, highly viscous oil.

¹H-NMR (600 MHz, CH₃CN + D₂O): δ [ppm] = 8.06 – 7.90 (m, 20H, 12-C, 13-C, 14-C, 25-C, 26-C, 27-C, 38-C, 39-C, 40-C, 51-C, 52-C, 53-C.), 5.47 – 5.34 (m, 8H, 10-C, 23-C, 36-C, 49-C.), 4.24 (q, ³J = 9.7, 8.4 Hz, 8H, 9-C, 22-C, 35-C, 48-C), 3.91 (q, ³J = 11.3, 6.3 Hz, 8H, 4-C, 17-C, 30-C, 43-C.), 3.72 (t, ³J = 6.2 Hz, 2H, 56-C.), 3.42 (d, ³J = 6.5 Hz, 2H, 55-C.), 3.19 (t, ³J = 6.9 Hz, 6H, 16-C, 29-C, 42-C.), 2.92 (t, ³J = 7.6, 2H, 3-C.), 2.72 (p, ³J = 7.4 Hz, 8H, 7-C, 20-C, 33-C, 46-C.), 2.58 (p, ³J = 2.5 Hz, 1H), 2.48 – 2.34 (m, 8H, 8-C, 21-C, 34-C, 47-C.).

¹³C-NMR (151 MHz, CH₃CN + D₂O): δ [ppm] = 175.0 (C15, C28, C41, C54), 174.3 (C6, C19, C32, C45), 173.0 (C2), 135.1 (C11, C24, C37, C50), 130.6 (C13, C26, C39, C52), 130.0 (C14, C27, C40, C53), 129.7 (C12, C25, C38, C51), 76.8 (C10, C23, C36, C49), 45.0 (C9, C22, C35, C48), 37.2 (C17, C30, C43), 37.0 (C56), 36.1 (C3), 35.8 (C4), 33.7 (C7, C20, C33, C46), 32.7 (C16, C29, C42), 29.9 (C55), 23.7 (C8, C21, C34, C47).

HRMS (ESI): m/z [M+H]⁺ calc. for C₅₉H₇₉N₉O₁₄: 1138.5819, found: 1138.5807.

Anal. HPLC (Agilent Zorbax Extend C18, 2.1 x 50 mm, H₂O/CH₃CN 5:95 + 0.1% HCO₂H to 95:5 + 0.1% HCO₂H, 25 min, 0.3 ml/min): t_R = 14.7 min.

O-Benzyl-protected AZA-ipDFO* 20

The unloaded Wang resin (500 mg, maximum loading density according to the manufacturer: 1.00 mmol/g) was allowed to swell in CH_2Cl_2 (6 mL) on a shaker for 30 min. It was then rinsed three times with DMF (3 x 6 mL). The Fmoc- β -alanine (4 eq., 663 mg, 2.00 mmol) was dissolved in DMF (6 mL), mixed with 1-hydroxybenzotriazole (HOBt, 4 eq., 306 mg, 2.00 mmol) and was added to the resin after cooled to 0 °C. The DCC (4 eq., 413 mg, 2.00 mmol) and 4-DMAP (0.1 eq., 6 mg, 0.05 mmol) was added and allowed to react overnight at room temperature by gentle shaking. After washing with DMF (3 x 6 mL) a capping solution (acetic anhydride (2.0 eq., 0.1 mL, 1.0 mmol) and DIPEA (2.0 eq., 1.7 mL, 1.0 mmol) in CH_2Cl_2 (6 mL)) was added to the resin to cap the unreacted and thus free hydroxyl groups on the resin. After 30 min the resin was separated from the solution by filtration and was washed with DMF (3 x 8 mL), DMF/ CH_2Cl_2 (3 x 8 mL, 1:1 v/v) and CH_2Cl_2 (3 x 8 mL). The resin was stored in a desiccator until constant mass was reached.

The loading density was determined as described above to be 0.41 mmol/g.

The synthesis on the solid phase was carried out in repeating cycles. One cycle consists of the cleavage of the Fmoc protecting group of the amine or O-benzyl hydroxylamine of the amino acid bound to the solid phase. Subsequently, the coupling of an active ester of the subsequent amino acid to the released amine or O-benzyl hydroxylamine takes place. The Fmoc deprotection steps, the coupling steps and the masking of unreacted O-benzyl hydroxylamines with an acetic anhydride solution during the solid phase synthesis took place under microwave conditions. The liquid phase of each step was separated from the resin *via* filtration before the subsequent step.

The Wang resin (116 mg, loading density: 0.41 mmol/g, synthesis scale: 0.5 mmol) initially loaded with Fmoc- β -alanine was initially swollen in CH_2Cl_2 (10 mL) for 30 min. The resin was then rinsed with DMF (3 x 10 mL). The subsequent Fmoc deprotection was carried out twice, each time with a fresh solution of 20% piperidine in DMF (4 mL, 1st: 3 min, 80 °C; 2nd: 0.5 min, 80 °C), with rinsing steps between and after the deprotection steps with DMF (3 x 6 mL). For the subsequent coupling, **18** (4 eq. based on the loading density of the resin, 1 mL (from

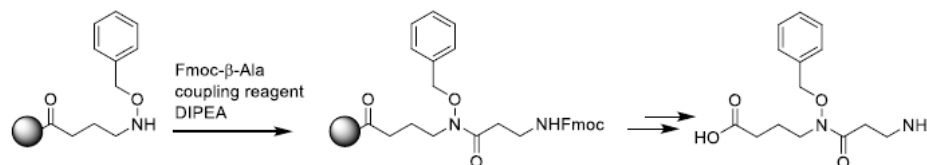
479 mg **18** in DMF (4 mL))) was mixed with DIPEA (8 eq. based on the loading density of the resin, 1 mL (from 0.27 mL DIPEA in DMF (4 mL))) and HATU/HOBt (4 eq. each based on the loading density of the resin, 1 mL (from 290 mg HATU and 117 mg HOBt in DMF (4 mL))) and gently stirred for 5 min at room temperature to form the active ester *in situ*. The active ester solution was then added to the resin and one coupling steps (20 min, 80 °C) were carried out. Here too, rinsing steps with DMF (3 x 6 mL) were carried out after the coupling. After this step, the first cycle to extend the amino acid sequence by one monomer was completed. Three more cycles were performed to obtain the AZA-ipDFO* **19** bound to the solid phase.

To separate the products obtained during the solid phase synthesis from the Wang resin, the dry resin was placed in a TFA/TIPS/CH₂Cl₂ solution (90:5:5, 10 mL) for 2 h and gently shaken at room temperature. The solution was separated from the resin by filtration and the resin was repeatedly washed with CH₂Cl₂. The solvent and volatiles were removed under reduced pressure. The residue was taken up in CH₂Cl₂ and again removed under reduced pressure. This was repeated twice to obtain the crude product. After column chromatographic purification on RP silica gel (column: Macherey Nagel, VP 250/10 Nucleodur C18 HTec, 5 µm; gradient: H₂O/CH₃CN 70:30 + 0.1% HCO₂H to 2:98 + 0.1% HCO₂H v/v) and subsequent freeze-drying, the product **20** (12 mg, 7.3 µmol, 15% based on the synthesis scale of 0.5 mmol) was obtained as a slightly yellowish, highly viscous oil.

HRMS (ESI): *m/z* [M+H]⁺ calc. for C₅₉H₇₉N₉O₁₄: 1642.7986, found: 1642.7937.

Anal. **HPLC** (Agilent Zorbax Extend C18, 2.1 x 50 mm, H₂O/CH₃CN 5:95 + 0.1% HCO₂H to 95:5 + 0.1% HCO₂H, 14 min, 0.3 ml/min): *t_R* = 10.4 min.

Optimization of coupling conditions for the preparation of *O*-benzyl protected hydroxamic acids on the solid phase:



Unloaded Wang resin (1.01 g, maximum loading density according to the manufacturer: 1.00 mmol/g) was allowed to swell in CH_2Cl_2 (40 mL) on a shaker for 30 min. It was then rinsed three times with DMF (3 x 10 mL). Compound **4** (4.64 eq., 2.00 g, 4.64 mmol) was dissolved in DMF (8 mL) and CH_2Cl_2 (5 mL), mixed with 1-hydroxybenzotriazole (HOBt, 3.5 eq., 537 mg, 3.49 mmol) and was added to the resin after cooling to 0 °C. DCC (4 eq., 954 mg, 4.62 mmol) was added and allowed to react overnight at room temperature by gentle shaking. After washing three times with CH_2Cl_2 (3 x 6 mL), three times with 2-propanol (3 x 6 mL), three times with CH_2Cl_2 (3 x 6 mL), three times with 2-propanol (3 x 6 mL) and three times with methanol (3 x 6 mL), the resin was dried *in vacuo*. The loading density was determined as described above to be 0.52 mmol/g.

The Wang resin (96 mg, loading density: 0.52 mmol/g, synthesis scale: 0.05 mmol) loaded with compound **4** was swelled in CH_2Cl_2 (10 mL) for 30 min. The resin was then rinsed with DMF (3 x 10 mL). The subsequent Fmoc deprotection was carried out twice, each time with a fresh solution of 20% piperidine in DMF (4 mL, 1st: 3 min, 80 °C; 2nd: 0.5 min, 80 °C), with rinsing steps between and after the deprotection steps with DMF (3 x 6 mL). For the subsequent coupling, Fmoc- β -alanine (equivalents see table S1) was mixed with DIPEA (equivalents see table S1) and coupling reagent (equivalents see table S1) and gently stirred for 5 min at room temperature. The solution was then added to the resin and coupling was performed under the conditions specified in table S1. The resin was washed with DMF (3 x 6 mL) after the coupling. The Fmoc-protecting group was cleaved by 20% piperidine in DMF (4 mL, 1st: 3 min, 80 °C; 2nd: 0.5 min, 80 °C) as described before, with rinsing steps between and after the deprotection steps with DMF (3 x 6 mL). After washing with CH_2Cl_2 (3 x 10 mL), the resin was dried *in vacuo*. Swollen resin (15 min in CH_2Cl_2) was then placed in a TFA/TIPS/ CH_2Cl_2 solution (90:5:5, 10 mL) for 2 h and gently shaken at room temperature. The solution was separated from the resin by filtration and the resin was repeatedly washed with CH_2Cl_2 . The solvent and volatiles were removed under reduced pressure. The residue was dissolved in CH_2Cl_2 and the solvent was again removed under reduced pressure. This was repeated twice. The residue was dissolved in water and CH_3CN was added until a clear solution was observed. The crude

products were analyzed by quantitative NMR after spiking with a specific amount of fumaric acid (5 mg, 0.043 mmol).

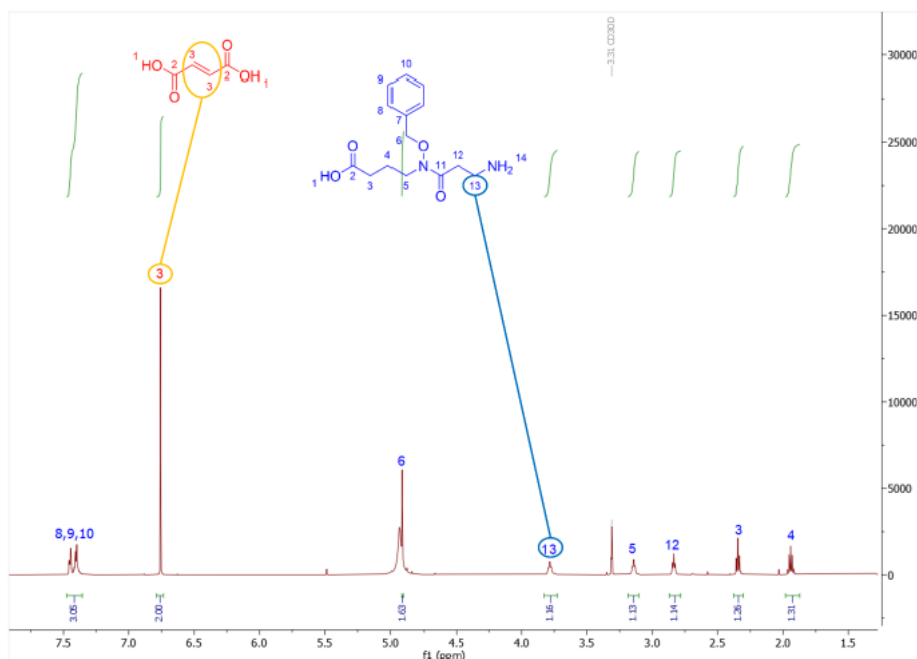
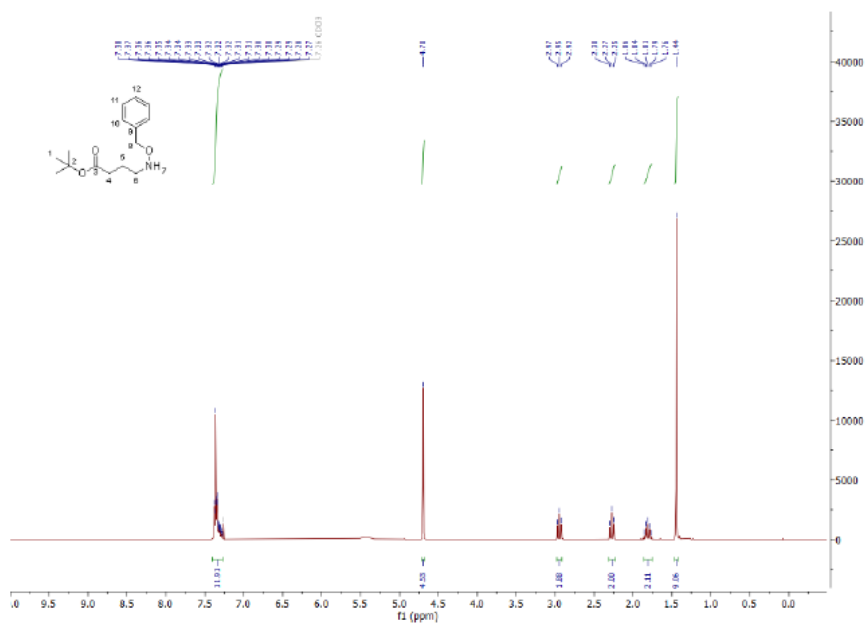
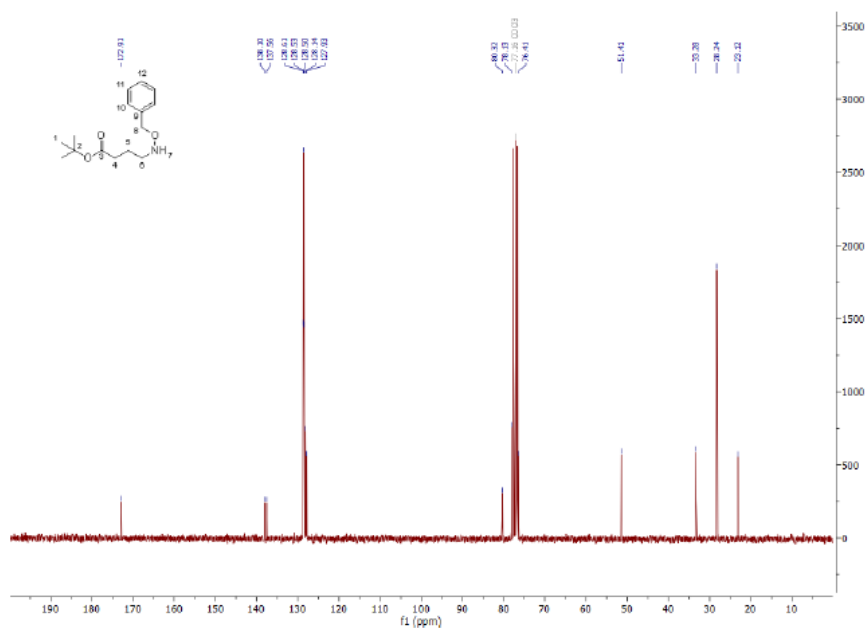


Figure S1: Example for the quantification of a crude coupling product spiked with fumaric acid via qNMR. Shown is the qNMR-spectrum obtained following entry 5 in table S1. This reaction was performed with PyOxim as coupling agent with 5 eq., at 80 °C for 20 min under microwave conditions. The yield was calculated based on resin loading.

Table S1: Different coupling conditions for SPS couplings of a O-benzyl protected hydroxylamine and Fmoc- β -Ala. Yields were obtained by qNMR and calculated based on resin loading.

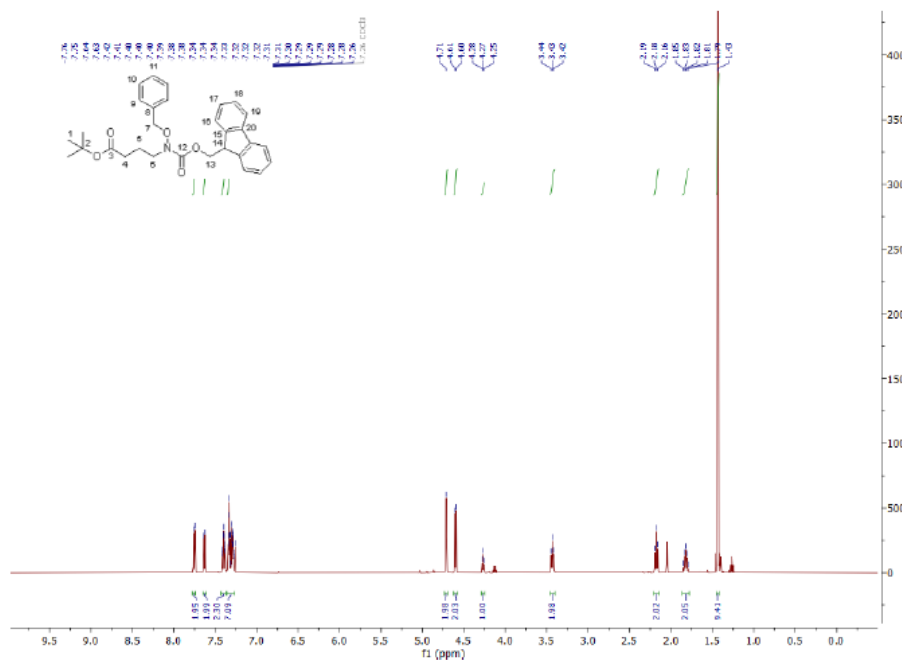
Experiment	Coupling reagent	eq. (coupling reagent and Fmoc- β -Ala)	Time t [min]	Temperature T [°C]	n(Product) [μ mol]	Yield [%]
1	DIC/HOBt	5	20	80	8.6	20
2	HBTU/HOBt	5	20	80	1.3	3
3	HATU/HOAt	5	20	80	10.8	25
4	PyBOP	5	20	80	8.2	19
5	PyOxim	5	20	80	24.1	56
6	BTFFH	5	20	80	no product	/
7	Acid chloride	5	20	80	no product	/

NMR spectra

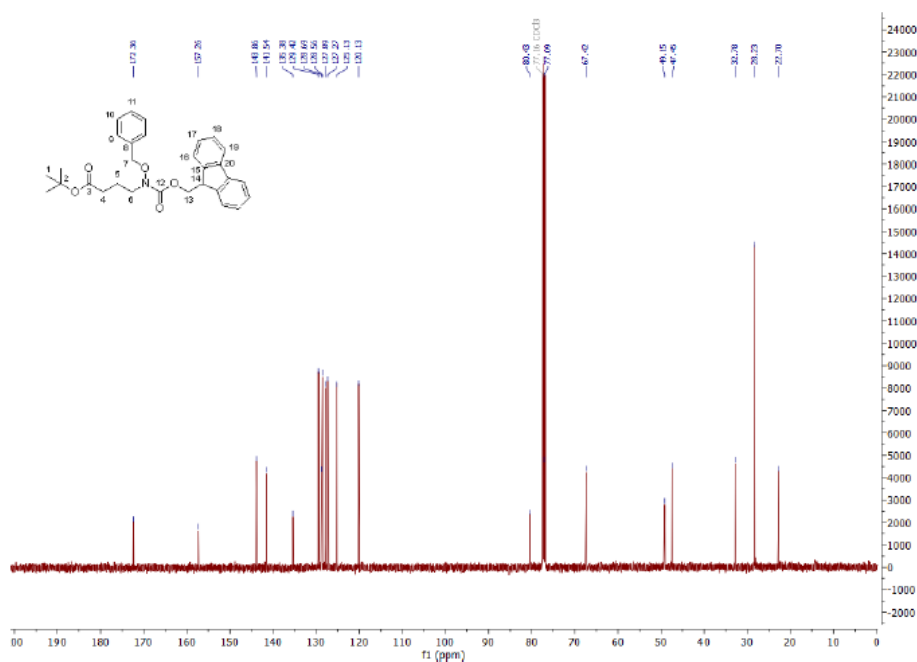
¹H NMR of compound 2 (300 MHz, CDCl₃):¹³C NMR of compound 2 (75 MHz, CDCl₃):

S21

¹H NMR of compound 3 (500 MHz, CDCl₃):



¹³C NMR of compound 3 (126 MHz, CDCl₃):



S22

Chemical Structure of 1: OC(=O)CC(C)C(=O)Oc1ccc(C)cc1

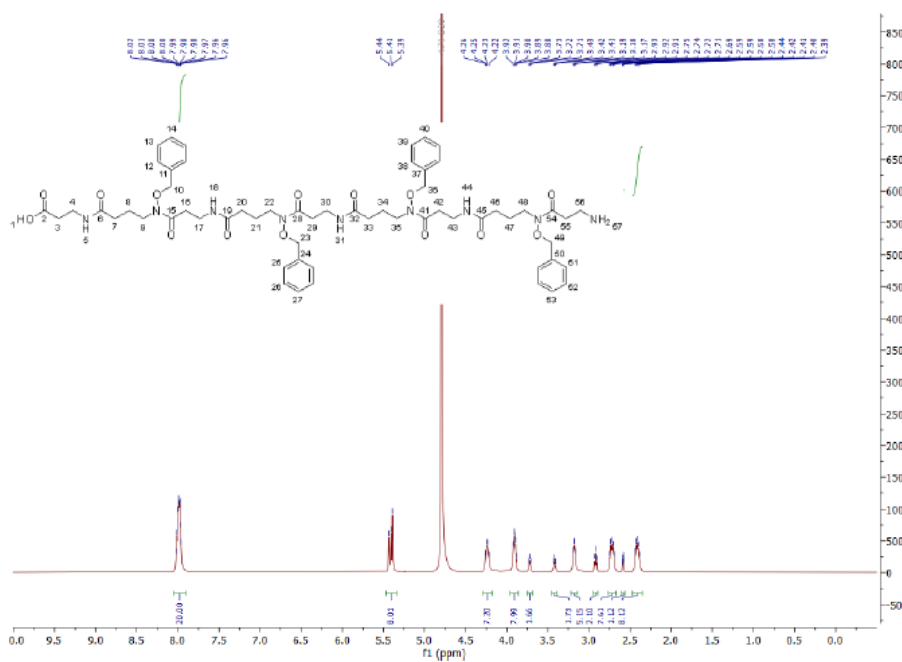
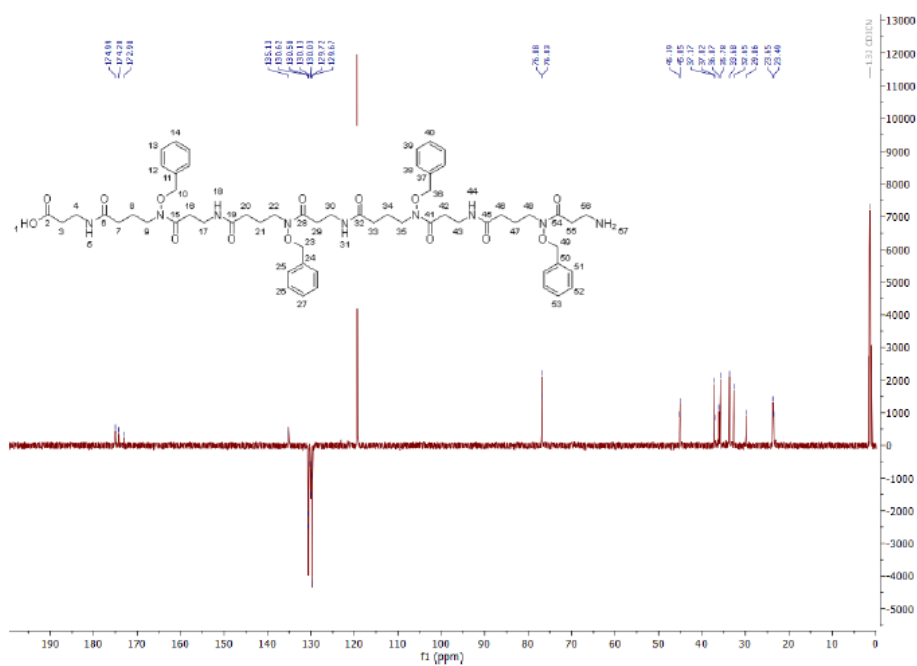
¹H NMR Data (CDCl₃):

Chemical Shift (ppm)	Integration
11.26 (s, 1H)	1.00
7.75 (d, 2H)	2.00
7.64 (d, 2H)	2.00
7.62 (d, 2H)	2.00
7.40 (d, 2H)	2.00
7.39 (d, 2H)	2.00
7.34 (d, 2H)	2.00
7.33 (d, 2H)	2.00
7.33 (d, 2H)	2.00
7.32 (d, 2H)	2.00
7.31 (d, 2H)	2.00
7.30 (d, 2H)	2.00
7.29 (d, 2H)	2.00
7.27 (d, 2H)	2.00
4.65 (s, 1H)	1.00
3.84 (s, 3H)	3.00
2.29 (s, 3H)	3.00
2.27 (s, 3H)	3.00
1.84 (s, 3H)	3.00
1.82 (s, 3H)	3.00
1.81 (s, 3H)	3.00
1.80 (s, 3H)	3.00

Chemical structure of compound 10: O=C1C=CC(=O)N1

¹H NMR spectrum (CDCl₃) of compound 10. The x-axis represents the chemical shift (δ) in ppm, ranging from 0 to 20. The y-axis represents the intensity. The spectrum shows several peaks, with the most prominent one at approximately 7.7 ppm. The chemical structure of compound 10 is shown in the top right corner.

S23

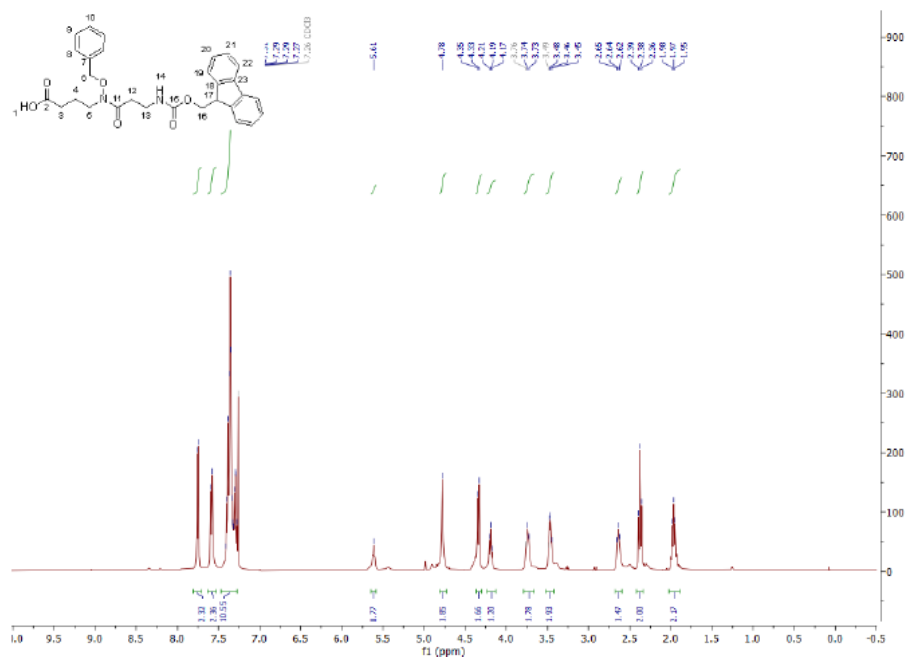
¹H NMR of compound 9 (600 MHz, CH₃CN + D₂O):**¹³C NMR of compound 9 (151 MHz, CH₃CN + D₂O):**

S24

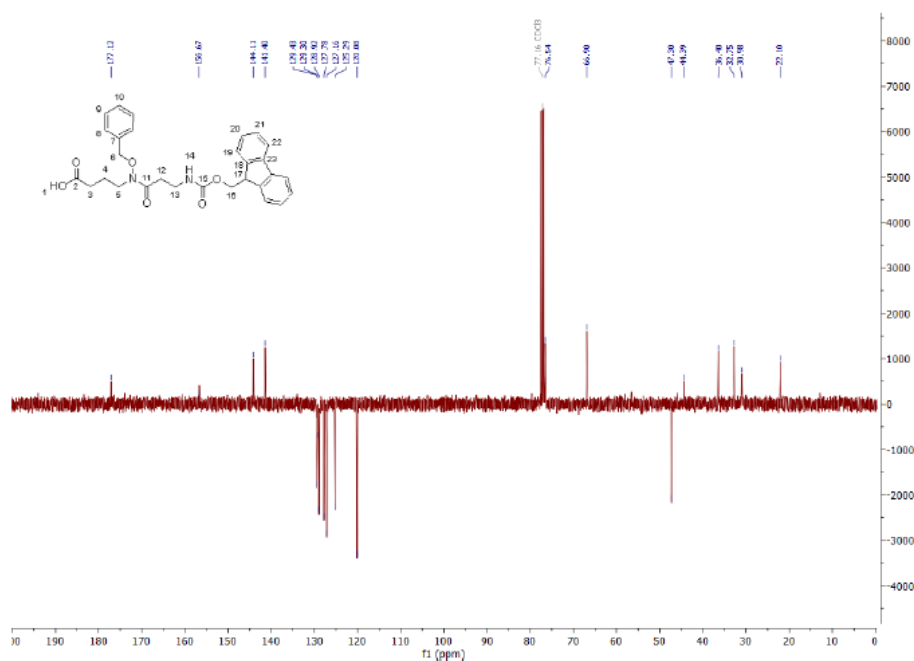
[illegible]

S25

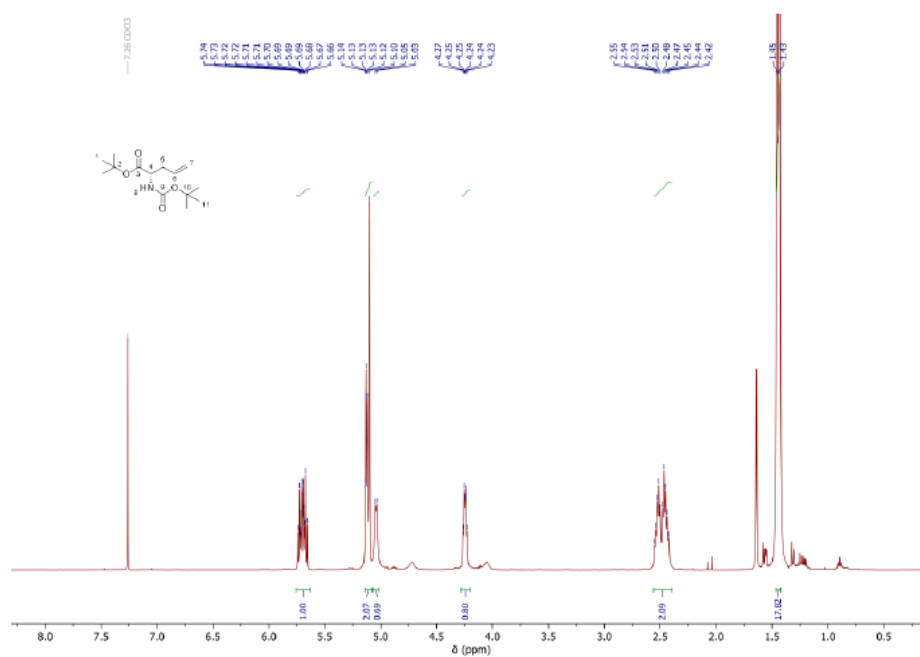
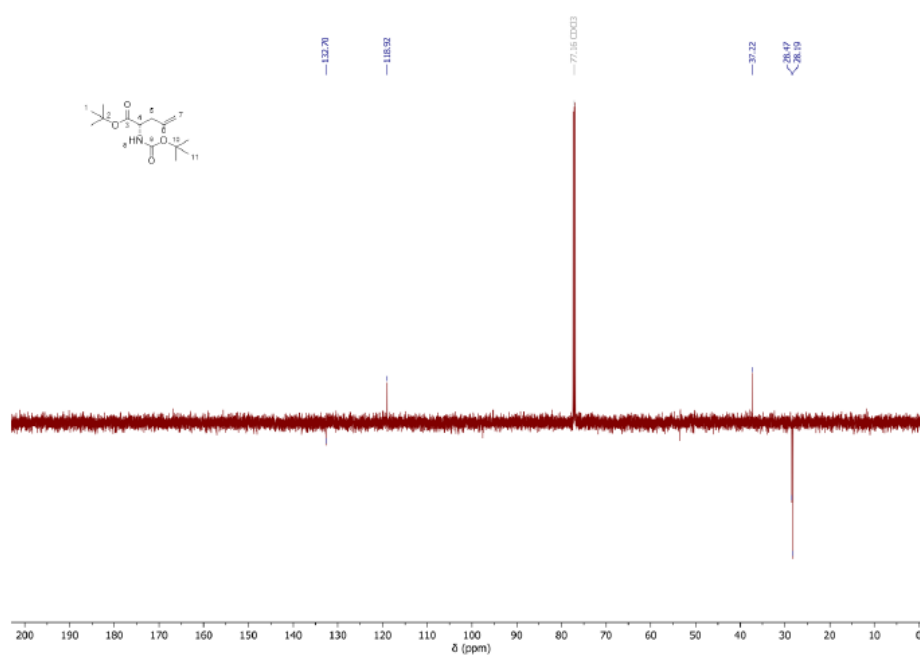
¹H NMR of compound 13 (400 MHz, CDCl₃):



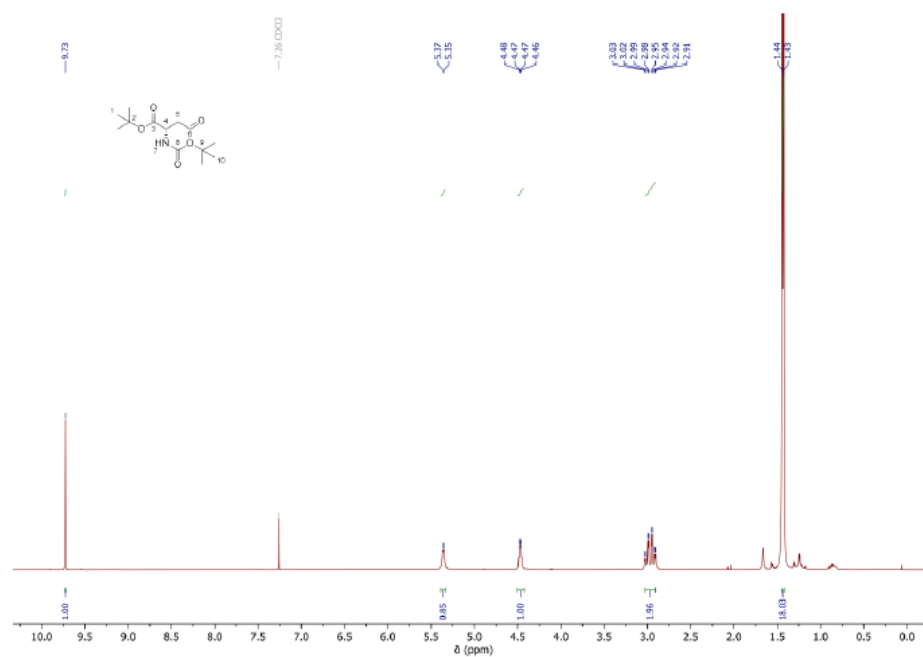
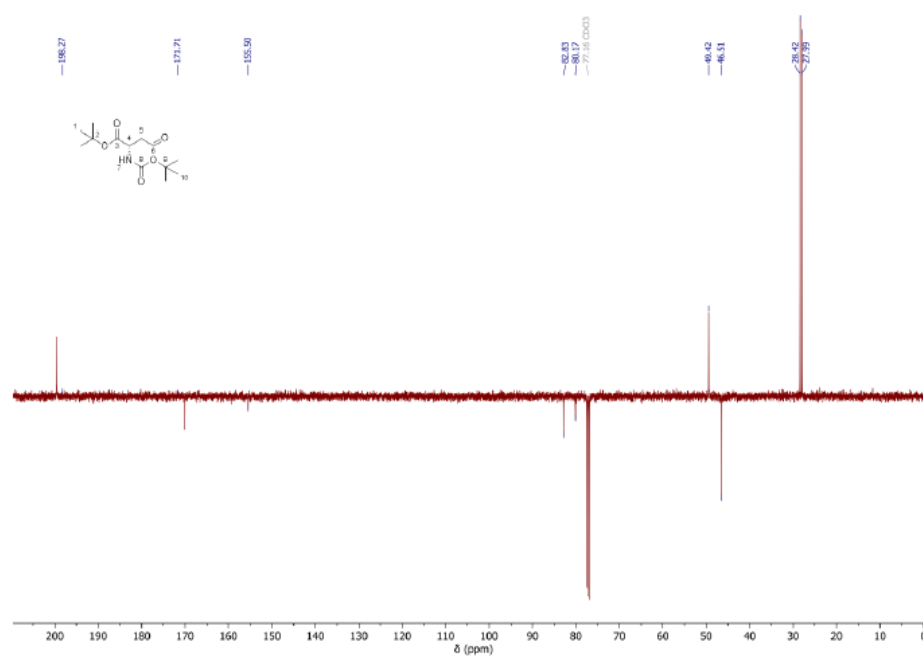
¹³C NMR of compound 13 (101 MHz, CDCl₃):



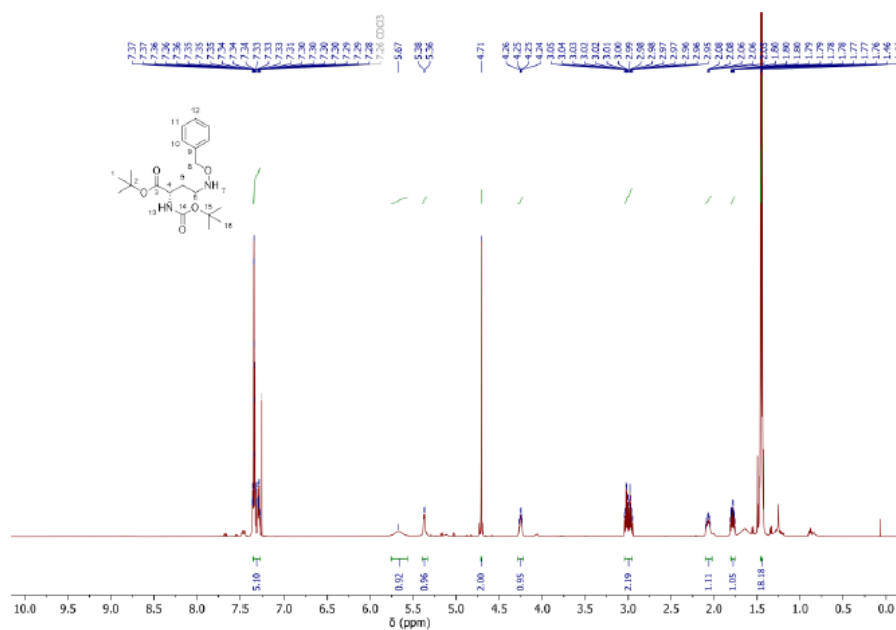
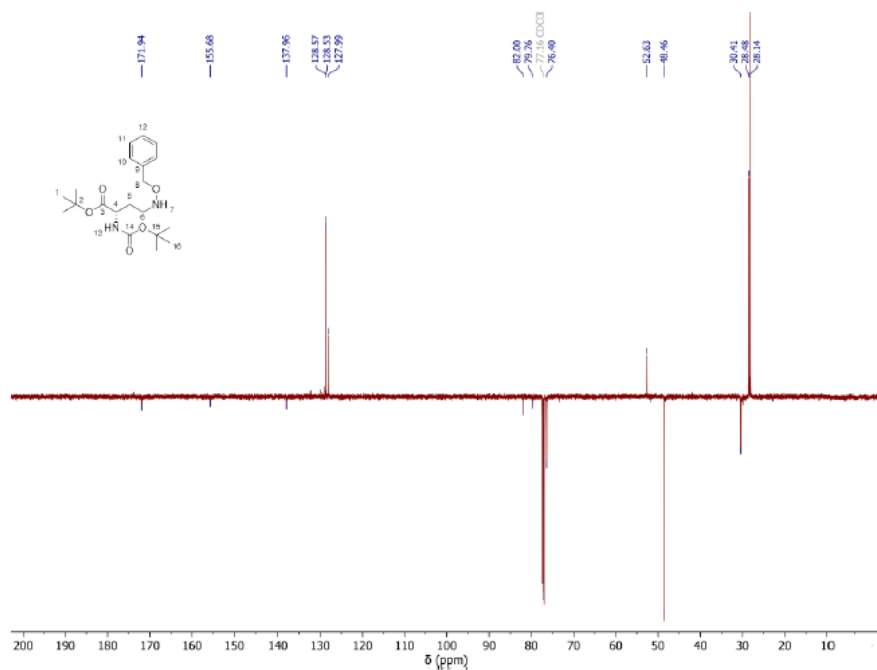
S26

¹H NMR of compound 21 (500 MHz, CDCl₃):**¹³C NMR of compound 21 (101 MHz, CDCl₃):**

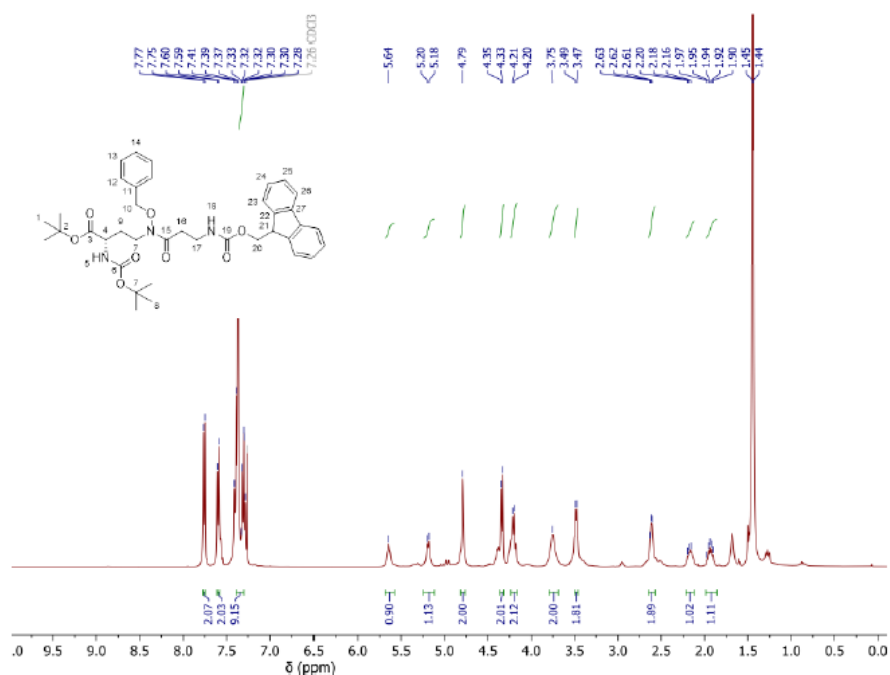
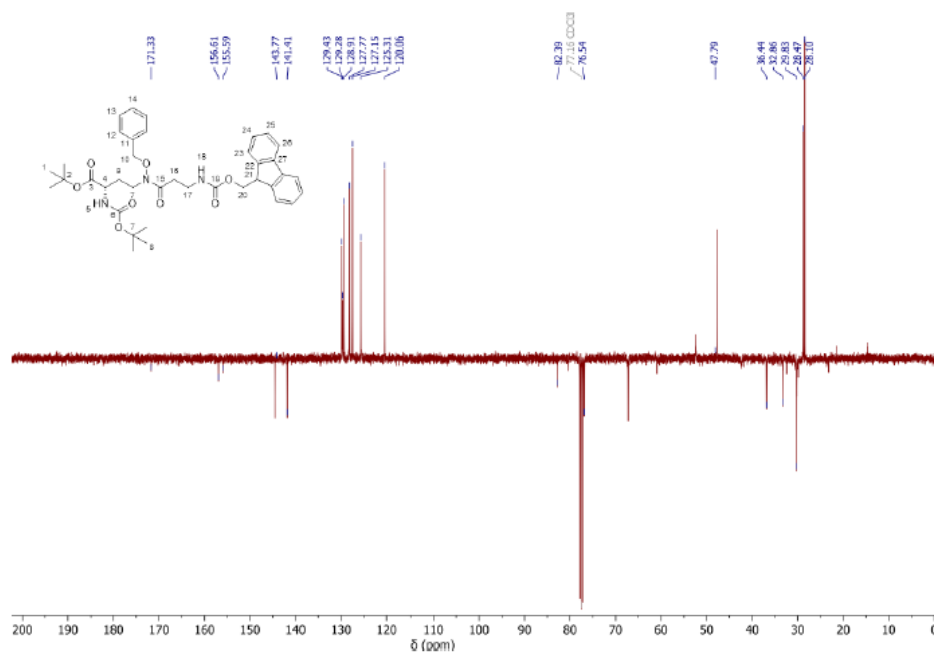
S27

¹H NMR of compound 15 (500 MHz, CDCl₃):**¹³C NMR of compound 15 (131 MHz, CDCl₃):**

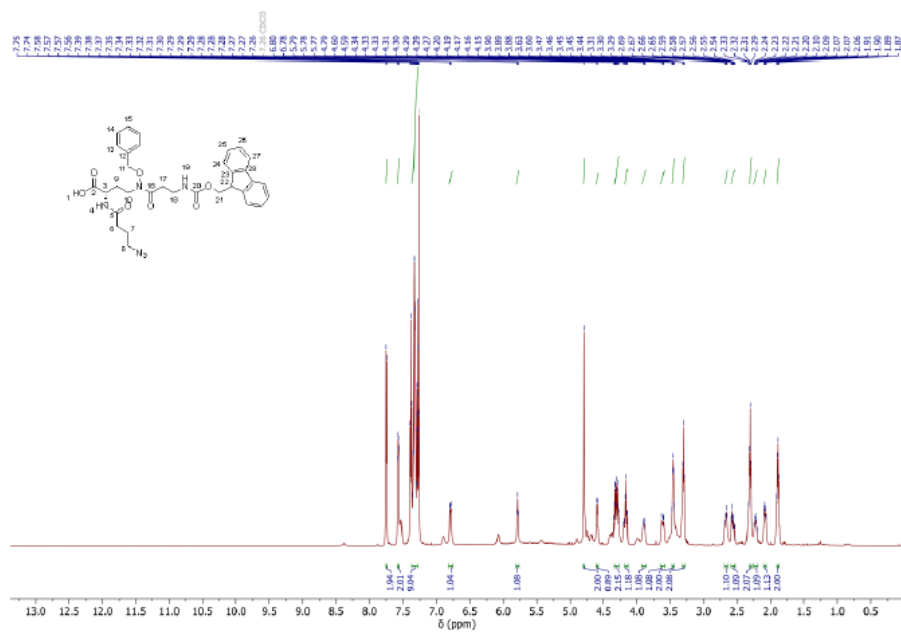
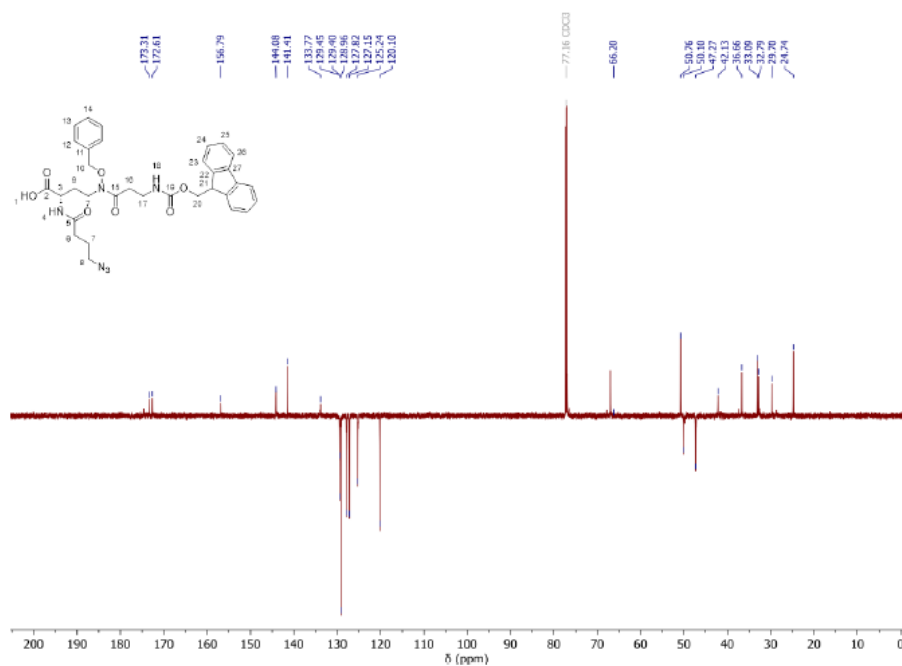
S28

¹H NMR of compound 16 (600 MHz, CDCl₃):**¹³C NMR of compound 16 (151 MHz, CDCl₃):**

S29

¹H NMR of compound 22 (400 MHz, CDCl₃):**¹³C NMR of compound 22 (101 MHz, CDCl₃):**

S30

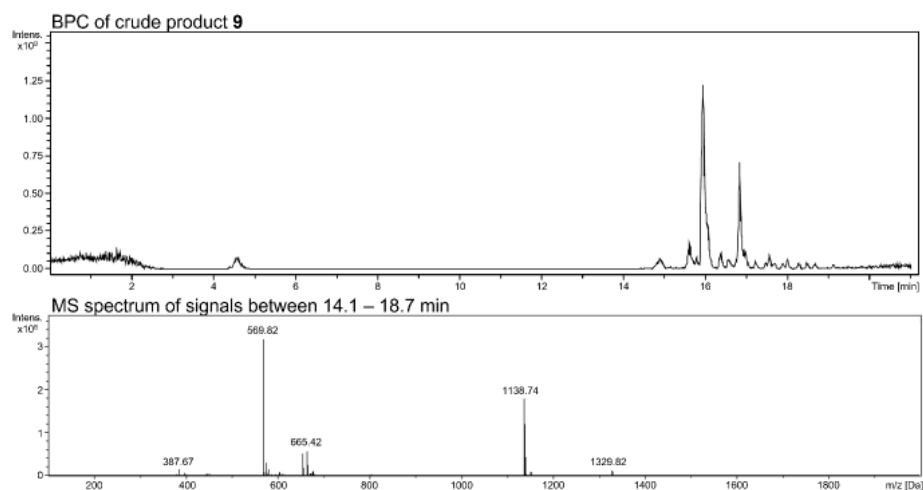
¹H NMR of compound 18 (400 MHz, CDCl₃):**¹³C NMR of compound 18 (101 MHz, CDCl₃):**

S31

HPLC-MS spectra

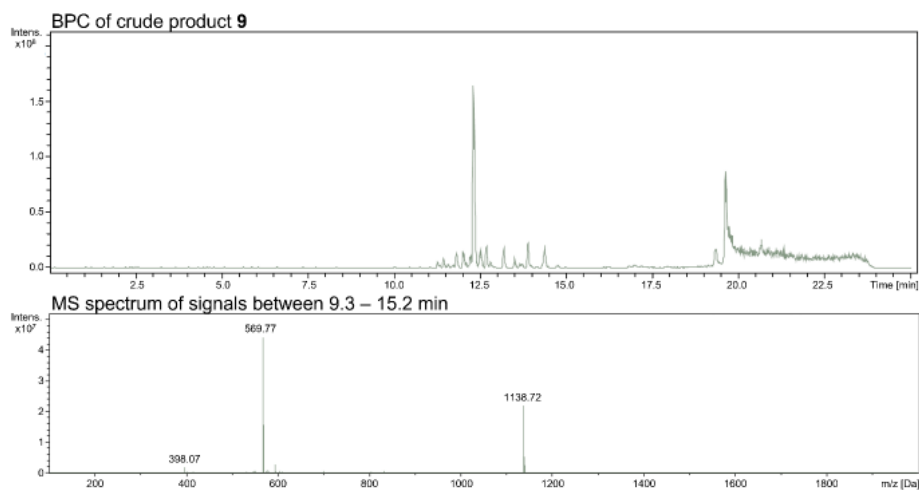
HPLC-ESI-MS chromatogram and spectrum of crude product **9** synthesized via SPS (Scheme 1B)

Anal. HPLC (Macherey-Nagel EC Nucleodur C18 HTec, 3 μ m, 150x4 mm, H₂O/CH₃CN 95:5 + 0.1% HCO₂H to 5:95 + 0.1% HCO₂H, 15 min, 0.3 ml/min): t_R = 16.0 min.



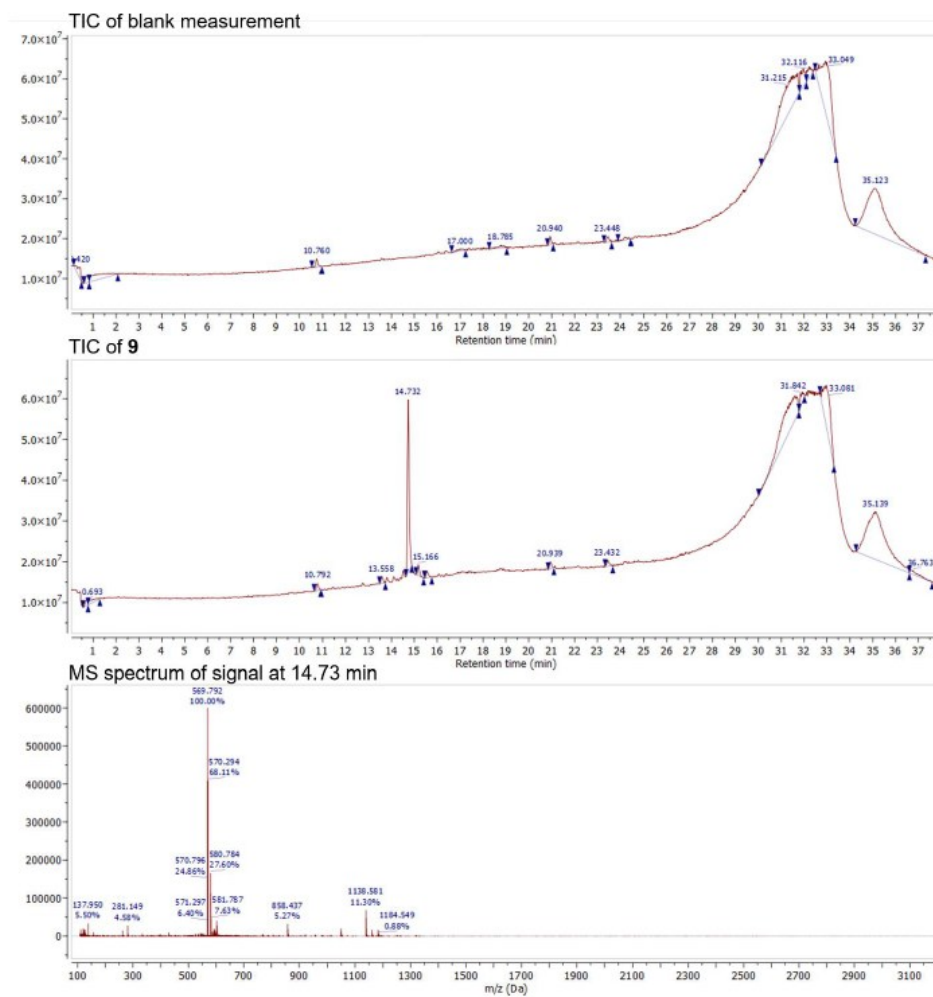
HPLC-ESI-MS chromatogram and spectrum of crude product 9 synthesized via SPS (Scheme 2B)

Anal. HPLC (Macherey-Nagel EC Nucleodur C18 Gravity-SB, 5 μ m, 150x4 mm, H₂O/CH₃CN 98:2 + 0.1% HCO₂H to 2:98 + 0.1% HCO₂H, 12 min, 0.3 ml/min): t_R = 12.3 min.



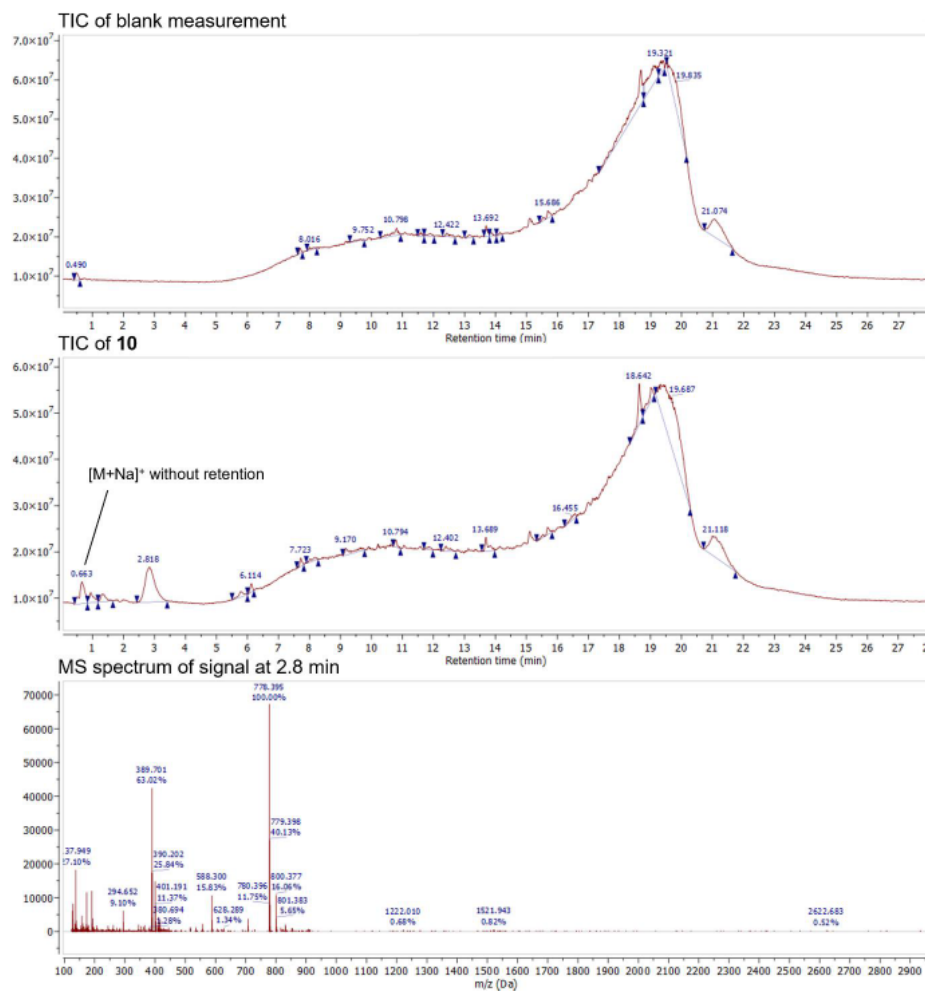
HPLC-ESI-MS chromatogram and spectrum of compound 9

Anal. HPLC (Agilent Zorbax Extend C18, 2.1 x 50 mm, H₂O/CH₃CN 5:95 + 0.1% HCO₂H to 95:5 + 0.1% HCO₂H, 25 min, 0.3 ml/min): t_R = 14.7 min.



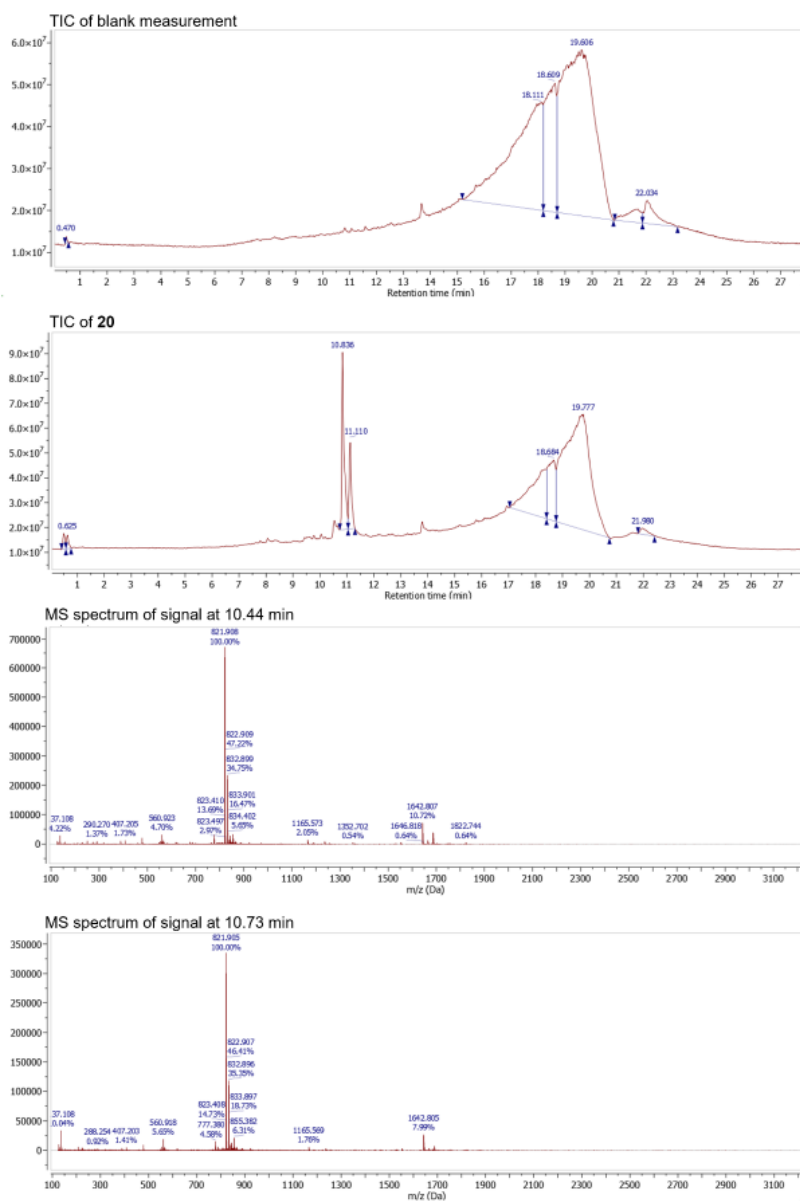
HPLC-ESI-MS chromatogram and spectrum of compound 10

Anal. HPLC (Agilent Zorbax Extend C18, 2.1 x 50 mm, H₂O/CH₃CN 5:95 + 0.1% HCO₂H to 95:5 + 0.1% HCO₂H, 14 min, 0.3 ml/min): t_R = 2.8 min.



HPLC-ESI-MS chromatogram and spectra of compound 20

Anal. HPLC (Agilent Zorbax Extend C18, 2.1 x 50 mm, H₂O/CH₃CN 5:95 + 0.1% HCO₂H to 95:5 + 0.1% HCO₂H, 14 min, 0.3 ml/min): t_R = 10.4 min and 11.77 min.



The observed double peak at 10.44 and 10.77 min retention is most likely due to a problem with our injector system and does not indicate an impurity. We have checked that both peaks have the same mass spectrum as can be seen from the spectra above. A double peak is also observed for the injection peak, which is an additional hint to an injection problem.

References

- [30] H. Sun, X. Peng, *Bioconjug. Chem.*, **2013**, 24, 1226-1234.
- [31] C. A. DeForest, D. A. Tirrell, *Nat. Mater.*, **2015**, 14, 523-531.
- [32] J. L. Suh, B. Watts, J. I. Stuckey, J. L. Norris-Drouin, S. H. Cholensky, B. M. Dickson, Y. An, S. Mathea, E. Salah, S. Knapp, A. Khan, A. T. Adams, B. D. Strahl, C. A. Sagum, M. T. Bedford, L. I. James, D. B. Kireev, S. V. Frye, *Biochemistry*, **2018**, 57, 2140-2149.
- [33] M. Gude, J. Ryf, P. D. White, *Lett. Pept. Sci.*, **2002**, 9, 203-206.

8.1.3 Isopeptidic Desferrioxamine Analogues: The Role of Hydroxamate Spacing for Chelation of Zr^{4+}

ChemMedChem

Supporting Information

Isopeptidic Desferrioxamine Analogues: The Role of Hydroxamate Spacing for Chelation of Zr^{4+}

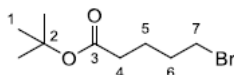
Lasse Outzen, Darius Ludolfs, Maximilian Irl, Susanne Kossatz, and Wolfgang Maison*

TABLE OF CONTENT

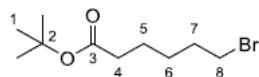
Synthesis of precursors	3
NMR-spectra	14
HPLC-MS spectra	29
RadioTLC	37
Stability in human serum	38
Synthesis of 18b on CTC-Resin	39

Synthesis of precursors

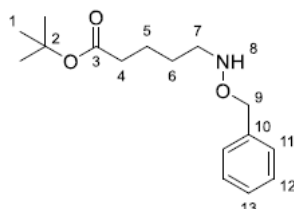
tert-butyl 5-bromopentanoate (**6b**):



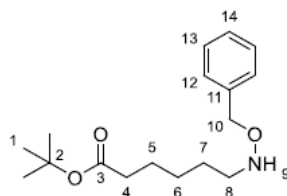
***tert*-butyl 5-bromopentanoate (**6b**):** The ω -bromopentanoic acid **5b** (1 eq., 4.01 g, 22.2 mmol) was dissolved in CH_2Cl_2 (20 mL) and cooled to 0 °C under a nitrogen atmosphere. Subsequently, *tert*-butanol (5 eq., 110 mmol, 8.19 g, 10.5 mL), DMAP (0.1 eq., 0.27 g, 2.21 mmol) and DCC (1.1 eq., 5.03 g, 24.4 mmol) were added and the solution was allowed to warm to room temperature while stirring. The reaction mixture was stirred overnight and the colorless solid was then filtered and washed with CH_2Cl_2 . The solvent was removed under reduced pressure. The product **6b** (4.10 g, 17.3 mmol, 78%) was obtained as a colorless oil after column chromatography on silica gel (n-pentane/EtOAc 9:1). $^1\text{H-NMR}$ (600 MHz, CDCl_3): δ [ppm] = 3.41 (t, 3J = 6.7 Hz, 2H, 7-H), 2.25 (t, 3J = 7.3 Hz, 2H, 4-H), 1.89 (p, 3J = 6.7 Hz, 2H, 6-H), 1.73 (p, 3J = 7.3 Hz, 2H, 5-H), 1.44 (s, 9H, 1-H). $^{13}\text{C-NMR}$ (125 MHz, CDCl_3): δ [ppm] = 172.7 (C3), 80.5 (C2), 34.7 (C7), 33.3 (C4), 32.2 (C6), 28.3 (C1), 23.8 (C5).

***tert*-butyl 6-bromohexanoate (**6c**):**

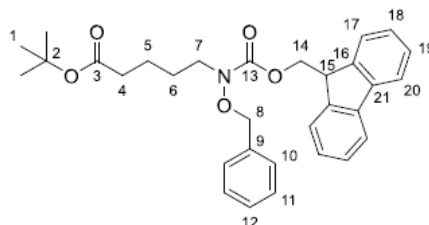
The ω -bromohexanoic acid **5c** (1 eq., 5.00 g, 25.6 mmol) was dissolved in CH_2Cl_2 (20 mL) and cooled to 0 °C under a nitrogen atmosphere. Subsequently, *tert*-butanol (5 eq., 9.50 g, 128 mmol, 12.0 mL), DMAP (0.1 eq., 0.31 g, 2.56 mmol) and DCC (1.1 eq., 5.82 g, 28.3 mmol) were added and the solution was allowed to warm to room temperature while stirring. The reaction mixture was stirred overnight and the colorless solid was filtered and washed with 20 mL CH_2Cl_2 . The solvent was removed under reduced pressure. The product **6c** (5.17 g, 20.6 mmol, 80%) was obtained as a colorless oil after column chromatography on silica gel (n-pentane/EtOAc 9:1). $^1\text{H-NMR}$ (300 MHz, CDCl_3): δ [ppm] = 3.40 (t, 3J = 6.8 Hz, 2H, 8-H), 2.22 (t, 3J = 7.4 Hz, 2H, 4-H), 1.86 (m, 2H, 7-H), 1.60 (m, 2H, 5-H), 1.47 (m, 2H, 6-H), 1.43 (s, 9H, 1-H). $^{13}\text{C-NMR}$ (75 MHz, CDCl_3): δ [ppm] = 173.0 (C3), 80.3 (C2), 35.4 (C8), 33.7 (C4), 32.6 (C7), 28.2 (C1), 27.7 (C6), 24.3 (C5).

***tert*-butyl 5-(benzyloxy)aminopentanoate (**7b**):**

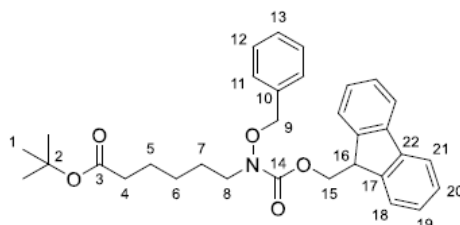
The *tert*-butyl 5-bromopentanoate **6b** (1 eq., 4.10 g, 17.3 mmol), *O*-benzyl hydroxylamine (3 eq., 6.06 g, 49.2 mmol, 5.70 mL) and K_2CO_3 (3 eq., 6.83 g, 49.4 mmol) were dissolved in DMF (66 mL) and stirred for 3 h at 80 °C. The reaction mixture was then mixed with dem. H_2O (200 mL) and extracted with EtOAc (3 x 100 mL). The combined organic phases were washed with sat. NaCl solution (2 x 100 mL) and dried over $MgSO_4$. The solvent was removed under reduced pressure and the remaining *O*-benzyl hydroxylamine was removed by distillation at 75 °C under vacuum. The product **7b** (4.3 g, 15.4 mmol, 89%) was obtained as a colorless oil. 1H -NMR (600 MHz, $CDCl_3$): δ [ppm] = 7.38 – 7.27 (m, 5H, 11-H, 12-H, 13-H), 4.72 (s, 2H, 9-H), 2.94 (t, 3J = 7.0 Hz, 2H, 7-H), 2.22 (t, 3J = 7.3 Hz, 2H, 4-H), 1.67 – 1.51 (m, 4H, 5-H, 6-H), 1.44 (s, 9H, 1-H). ^{13}C -NMR (100 MHz, $CDCl_3$): δ [ppm] = 173.0 (C3), 138.0 (C10), 128.5 (C13), 128.5 (C12), 128.0 (C11), 80.2 (C2), 76.4 (C9), 51.8 (C7), 35.5 (C4), 28.2 (C1), 26.9 (C6), 22.8 (C5). HRMS (ESI): m/z $[M+H-tBu]^+$ calc. for $C_{16}H_{25}NO_3$: 224.1281, found: 224.1268.

tert-butyl 6-(benzyloxy)aminohexanoate (7c):

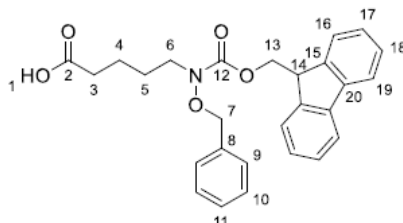
Tert-Butyl 6-bromohexanoate **6c** (1 eq., 5.00 g, 20.0 mmol), *O*-benzyl hydroxylamine (3 eq., 7.39 g, 60.0 mmol, 6.95 mL) and K_2CO_3 (3 eq., 8.29 g, 60.0 mmol) were dissolved in DMF (80 mL) and stirred for 3 h at 80 °C. The reaction mixture was then mixed with dem. H_2O (240 mL) and extracted with EtOAc (3 x 80 mL). The combined organic phases were washed with sat. NaCl solution (3 x 80 mL) and dried over $MgSO_4$. The solvent was removed under reduced pressure and the remaining *O*-benzyl hydroxylamine was removed by distillation at 75 °C under vacuum. The product **7c** (4.58 g, 15.6 mmol, 78%) was obtained as a colorless oil. 1H -NMR (600 MHz, $CDCl_3$): δ [ppm] = 7.39 – 7.28 (m, 5H, 12-H, 13-H, 14-H), 4.70 (s, 2H, 10-H), 2.92 (t, 3J = 7.2 Hz, 2H, 8-H), 2.20 (t, 3J = 7.5 Hz, 2H, 4-H), 1.60 (m, 2H, 4-H), 1.56 (m, 2H, 7-H), 1.37 (s, 9H, 1-H), 1.33 (m, 2H, 6-H). ^{13}C -NMR (150 MHz, $CDCl_3$): δ [ppm] = 173.3 (C3), 138.6 (C11), 128.6 (C14), 128.5 (C13), 127.9 (C12), 78.2 (C2), 76.4 (C10), 52.1 (C8), 35.6 (C4), 28.3 (C1), 27.2 (C7), 26.8 (C6), 25.1 (C5). HRMS (ESI): m/z $[M+H-tBu]^+$ calc. for $C_{17}H_{27}NO_3$: 238.1438, found: 238.1428.

***tert*-butyl 5-(benzyloxy)(3-(Fmoc)- β -alanine)aminopentan-oate (**9b**):**

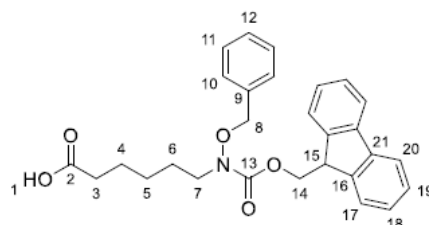
Fmoc- β -alanine (1.03 eq, 3.71 g, 11.9 mmol) was dissolved in CH_2Cl_2 (180 mL), cooled to 0 °C and catalytic amounts of DMF (2 drops) were added. Cold thionyl chloride (5 eq., 7.08 g, 59.5 mmol, 4.32 mL) was added over a period of 10 min and the solution was stirred for 3 h at room temperature. The volatile components were removed under reduced pressure. The residue was coevaporated twice with 20 mL CH_2Cl_2 . The slightly yellowish residue was dissolved in abs. THF (20 mL) and cooled to 0 °C. *tert*-Butyl 5-(benzyloxy)aminopentanoate **7b** (1 eq., 3.20 g, 11.5 mmol) was dissolved in abs. THF (35 mL), mixed with abs. pyridine (3 eq., 2.73 g, 34.5 mmol, 2.78 mL) and cooled to 0 °C. The solution with the acid chloride was slowly added to the solution with the O-benzyl hydroxylamine. The reaction mixture was stirred for 24 h at room temperature. The solvent was removed under reduced pressure and the resulting brown oil was dissolved in 20 mL EtOAc. The solution was then washed with each 20 mL HCl (1 M), sat. NaHCO_3 solution and sat. NaCl solution and dried over Na_2SO_4 . The product **9b** (6.20 g) was obtained after evaporation of the solvent under reduced pressure and was used without further purification. $^1\text{H-NMR}$ (400 MHz, CDCl_3): δ [ppm] = 7.76 (d, 3J = 7.6 Hz, 2H, 24-H), 7.59 (d, 3J = 7.4 Hz, 2H, 21-H), 7.41 – 7.28 (m, 9H, 10-H, 11-H, 12-H, 22-H, 23-H), 5.56 (t, 1H, 16-H), 4.79 (s, 2H, 8-H), 4.34 (d, 3J = 7.2 Hz, 2H, 18-H), 4.20 (t, 3J = 7.2 Hz, 1H, 19-H), 3.67 (t, 2H, 7-H), 3.48 (q, 3J = 5.8 Hz, 2H, 15-H), 2.64 (t, 2H, 14-H), 2.23 (t, 3J = 7.1 Hz, 2H, 4-H), 1.71 – 1.57 (m, 4H, 5-H, 6-H), 1.43 (s, 9H, 1-H). $^{13}\text{C-NMR}$ (100 MHz, CDCl_3): δ [ppm] = 172.8 (C3), 156.5 (C13), 144.1 (C20), 141.4 (C25), 129.4 (C17), 129.2 (C11), 128.9 (C9), 127.8 (C10), 127.2 (C21), 125.3 (C12), 120.1 (C21), 80.4 (C2), 76.5 (C8), 66.8 (C18), 47.3 (C19), 45.2 (C7), 36.5 (C15), 35.1 (C4), 32.8 (C14), 28.2 (C1), 26.4 (C6), 22.4 (C5). HRMS (ESI): m/z [$\text{M}+\text{H}$] $^+$ calc. for $\text{C}_{34}\text{H}_{40}\text{N}_2\text{O}_6$: 573.2959, found: 573.2957.

***tert*-butyl 6-(benzyloxy)(3-(Fmoc)- β -alanine)aminohexanoate (**9c**):**

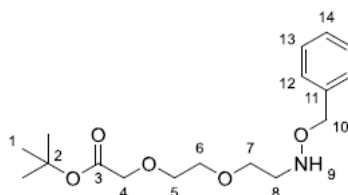
Fmoc- β -alanine (1.1 eq, 5.69 g, 18.3 mmol) was dissolved in CH_2Cl_2 (275 mL), cooled to 0 °C and catalytic amounts of DMF (2 drops) were added. Cold thionyl chloride (5 eq., 10.9 g, 91.4 mmol, 6.64 mL) was added over a period of 10 min and the solution was stirred for 3 h at room temperature. The volatile components were removed under reduced pressure. The residue was coevaporated twice with each 20 mL CH_2Cl_2 . The yellowish residue was dissolved in abs. THF (25 mL) and cooled to 0 °C. The *tert*-butyl 6-(benzyloxy)aminohexanoate **7c** (1 eq., 4.79 g, 16.3 mmol) was dissolved in abs. THF (50 mL), mixed with abs. pyridine (3 eq., 3.87 g, 48.9 mmol, 3.94 mL) and cooled to 0 °C. The solution with the acid chloride was slowly added to the solution with the *O*-benzyl hydroxylamine. The reaction mixture was stirred for 24 h at room temperature. The solvent was removed under reduced pressure and the resulting brown oil was dissolved in 100 mL EtOAc. The solution was then washed with each 50 mL HCl (1 M), sat. NaHCO_3 solution and sat. NaCl solution and dried over Na_2SO_4 . The crude product **9c** (9.70 g) was obtained after evaporation of the solvent under reduced pressure and was used without further purification. $^1\text{H-NMR}$ (400 MHz, CDCl_3): δ [ppm] = 7.77 (d, $^3J = 7.5$ Hz, 2H, 25-H), 7.61 (d, $^3J = 7.5$ Hz, 2H, 22-H), 7.42 – 7.30 (m, 9H, 11-H, 12-H, 13-H, 23-H, 24-H), 5.49 (t, $^3J = 6.1$ Hz, 1H, 17-H), 4.79 (s, 2H, 9-H), 4.38 (d, $^3J = 7.2$ Hz, 2H, 20-H), 4.21 (t, $^3J = 7.2$ Hz, 1H, 19-H), 3.67 (t, $^3J = 7.1$ Hz, 2H, 8-H), 3.50 (q, $^3J = 5.9$ Hz, 2H, 16-H), 2.65 (t, $^3J = 5.8$ Hz, 2H, 15-H), 2.22 (t, $^3J = 7.4$ Hz, 2H, 4-H), 1.72 – 1.46 (m, 4H, 5-H, 7-H), 1.46 (s, 9H, 1-H), 1.38 (m, 2H, 6-H). $^{13}\text{C-NMR}$ (100 MHz, CDCl_3): δ [ppm] = 173.1 (C3), 156.5 (C14), 144.1 (C21), 141.4 (C26), 129.3 (C18), 129.2 (C12), 129.0 (C10), 127.8 (C11), 127.2 (C22), 125.3 (C13), 120.1 (C24), 80.2 (C2), 76.5 (C9), 66.8 (C19), 47.3 (C20), 45.4 (C8), 36.5 (C16), 35.5 (C4), 32.8 (C15), 28.2 (C1), 26.7 (C7), 26.4 (C5), 24.8 (C6). HRMS (ESI): m/z $[\text{M}+\text{H}]^+$ calc. for $\text{C}_{35}\text{H}_{42}\text{N}_2\text{O}_6$: 587.3116, found: 587.3120.

5-(benzyloxy)(3-Fmoc)- β -alanine)aminopentanoic acid (10b**):**

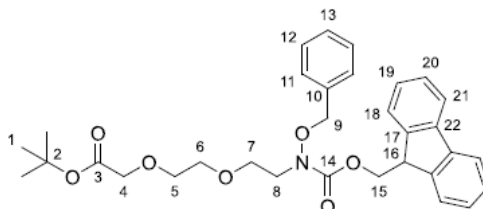
Tert-butyl 5-(benzyloxy)(3-(Fmoc)- β -alanine)aminopentanoate **9b** (1 eq., 6.20 g, 10.8 mmol) was dissolved in CH_2Cl_2 (35 mL) with TIPS (3 eq., 5.13 g, 32.4 mmol, 6.64 mL) and mixed with TFA (35 mL) at 0 °C. The reaction mixture was stirred at room temperature for 3 h. The volatile compounds were removed under reduced pressure and the resulting residue was coevaporated three times with each 20 mL CH_2Cl_2 . After column chromatography on silica gel (5 % to 95 % EtOAc in pentane), the product **10b** (3.55 g, 6.87 mmol, 60% over two steps) was obtained as a slightly yellow oil. $^1\text{H-NMR}$ (400 MHz, CDCl_3): δ [ppm] = 7.75 (d, 3J = 7.6 Hz, 2H, 23-H), 7.58 (d, 3J = 7.5 Hz, 2H, 20-H), 7.40 – 7.28 (m, 9H, 9-H, 10-H, 11-H, 21-H, 22-H), 5.59 (t, 3J = 6.3 Hz, 1H, 15-H), 4.77 (s, 2H, 7-H), 4.34 (d, 3J = 7.2 Hz, 2H, 17-H), 4.19 (t, 3J = 7.2 Hz, 1H, 18-H), 3.67 (d, 3J = 7.1 Hz, 2H, 6-H), 3.47 (q, 3J = 5.8 Hz, 2H, 14-H), 2.64 (t, 3J = 5.6 Hz, 2H, 13-H), 2.35 (t, 3J = 7.0 Hz, 2H, 3-H), 1.71 – 1.58 (m, 4H, 4-C, 5-H). $^{13}\text{C-NMR}$ (100 MHz, CDCl_3): δ [ppm] = 178.2 (C2), 156.6 (C12), 144.1 (C19), 141.4 (C24), 129.4 (C16), 129.3 (C10), 128.9 (C8), 127.8 (C9), 127.2 (C20), 125.3 (C11), 120.1 (C22), 76.5 (C7), 66.9 (C17), 47.3 (C18), 45.0 (C6), 36.5 (C14), 33.4 (C3), 32.8 (C13), 26.3 (C5), 21.9 (C4). HRMS (ESI): m/z [$\text{M}+\text{H}$] $^+$ calc. for $\text{C}_{30}\text{H}_{32}\text{N}_2\text{O}_6$: 517.2333, found: 517.2339.

6-(benzyloxy)(3-(Fmoc)- β -alanine)aminohexanoic acid (10c**):**

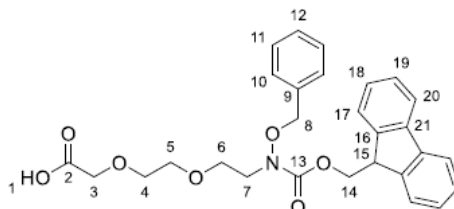
Tert-butyl 6-(benzyloxy)(3-(Fmoc)- β -alanine)aminohexanoate **9c** (1 eq., 9.53 g, 16.2 mmol) was dissolved in CH_2Cl_2 (50 mL) with TIPS (3 eq., 7.70 g, 48.6 mmol, 9.96 mL) and mixed with TFA (50 mL) at 0 °C. The reaction mixture was stirred at room temperature for 3 h. The volatile compounds were removed under reduced pressure and the resulting residue was coevaporated three times with each 10 mL CH_2Cl_2 . After column chromatography on silica gel (5 % to 95 % EtOAc in pentane), the product **10c** (5.54 g, 10.4 mmol, 64% over two steps) was obtained as a slightly yellow oil. $^1\text{H-NMR}$ (400 MHz, CDCl_3): δ [ppm] = 7.75 (d, 3J = 7.4 Hz, 2H, 24-H), 7.58 (d, 3J = 7.5 Hz, 2H, 21-H), 7.40 – 7.28 (m, 9H, 10-H, 11-H, 12-H, 22-H, 23-H), 5.55 (s, 1H, 16-H), 4.77 (s, 2H, 8-H), 4.35 (d, 3J = 7.2 Hz, 2H, 18-H), 4.19 (t, 3J = 7.1 Hz, 1H, 19-H), 3.72 – 3.60 (m, 2H, 7-H), 3.52 – 3.38 (m, 2H, 15-H), 2.62 (t, 3J = 5.7 Hz, 2H, 14-H), 2.33 (t, 3J = 7.3 Hz, 2H, 3-H), 1.72 – 1.56 (m, 4H, 4-H, 6-H), 1.39 – 1.22 (m, 2H, 5-H). $^{13}\text{C-NMR}$ (100 MHz, CDCl_3): δ [ppm] = 144.1 (C20), 141.4 (C25), 129.4 (C17), 129.1 (C11), 128.9 (C9), 127.9 (C10), 127.2 (C21), 125.3 (C12), 120.1 (C23), 76.4 (C8), 66.9 (C18), 47.3 (C19), 45.1 (C7), 36.4 (C15), 33.7 (C3), 32.8 (C14), 26.2 (C6), 24.3 (C4). HRMS (ESI): m/z $[\text{M}+\text{H}]^+$ calc. for $\text{C}_{31}\text{H}_{34}\text{N}_2\text{O}_6$: 531.2490, found: 531.2495.

tert-butyl 8-(benzyloxy)amino-3,6-dioxaoctanoate (12):

Tert-butyl 8-bromoamino-3,6-dioxaoctanoate **11** (1 eq., 2.00 g, 7.06 mmol), *O*-benzyl hydroxylamine (3 eq., 2.61 g, 21.2 mmol, 2.45 mL) and K_2CO_3 (3 eq., 2.93 g, 21.2 mmol) were dissolved in DMF (30 mL) and stirred for 3 h at 80 °C. The reaction mixture was then mixed with dem. H_2O (100 mL) and extracted with EtOAc (3 x 30 mL). The combined organic phases were washed with sat. NaCl solution (3 x 30 mL) and dried over $MgSO_4$. The solvent was removed under reduced pressure and the remaining *O*-benzyl hydroxylamine was removed by distillation at 75 °C under vacuum. The product **12** (2.85 g) was obtained as a colorless oil and was used without further purification. 1H -NMR (600 MHz, $CDCl_3$): δ [ppm] = 7.37 – 7.27 (m, 5H, 12-H, 13-H, 14-H), 4.71 (s, 2H, 10-H), 4.00 (s, 2H, 4-H), 3.71 – 3.61 (m, 8H, 5-H, 6-H, 7-H, 8-H), 1.47 (s, 9H, 1-H). ^{13}C -NMR (150 MHz, $CDCl_3$): δ [ppm] = 169.8 (C3), 138.1 (C11), 128.5 (C13), 128.5 (C12), 127.9 (C14), 76.1 (C2), 70.8 (C10), 70.6 (C5), 69.2 (C6), 67.7 (C4), 51.7 (C7), 30.4 (C8), 28.3 (C1). HRMS (ESI): m/z $[M+H]^+$ calc. for $C_{17}H_{27}NO_5$: 326.1967, found: 326.1967.

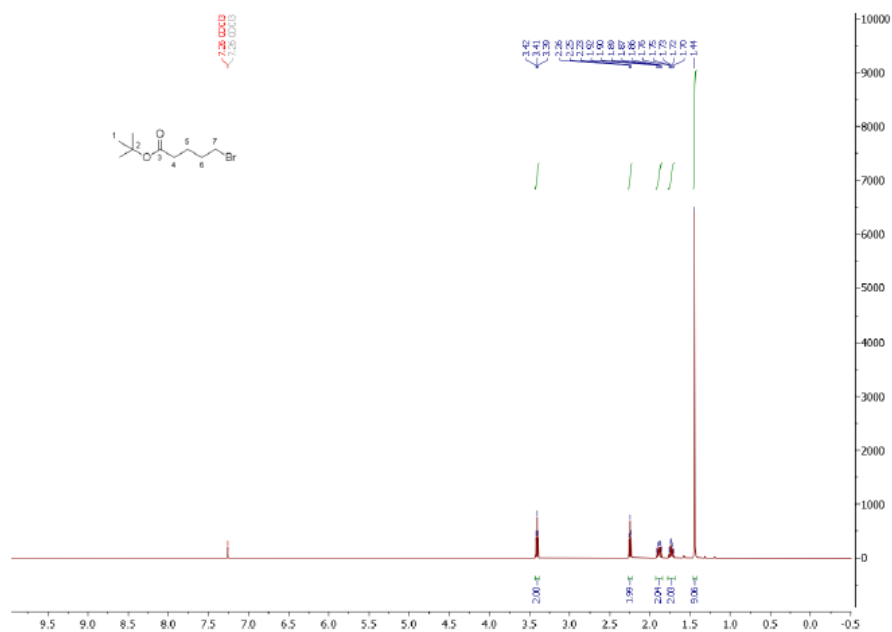
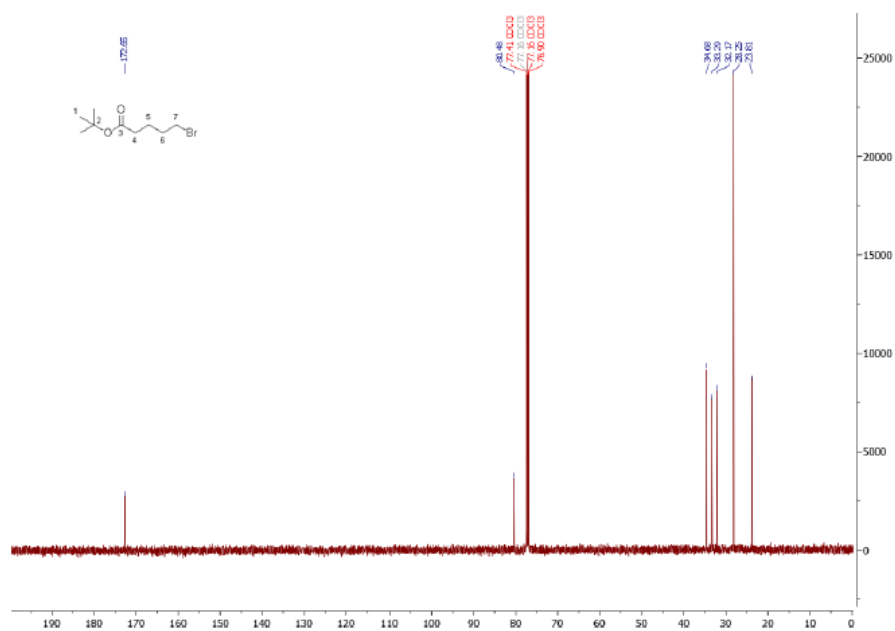
***tert*-butyl 8-(Fmoc)(benzyloxy)amino-3,6-dioxaoctanoate (**13**):**

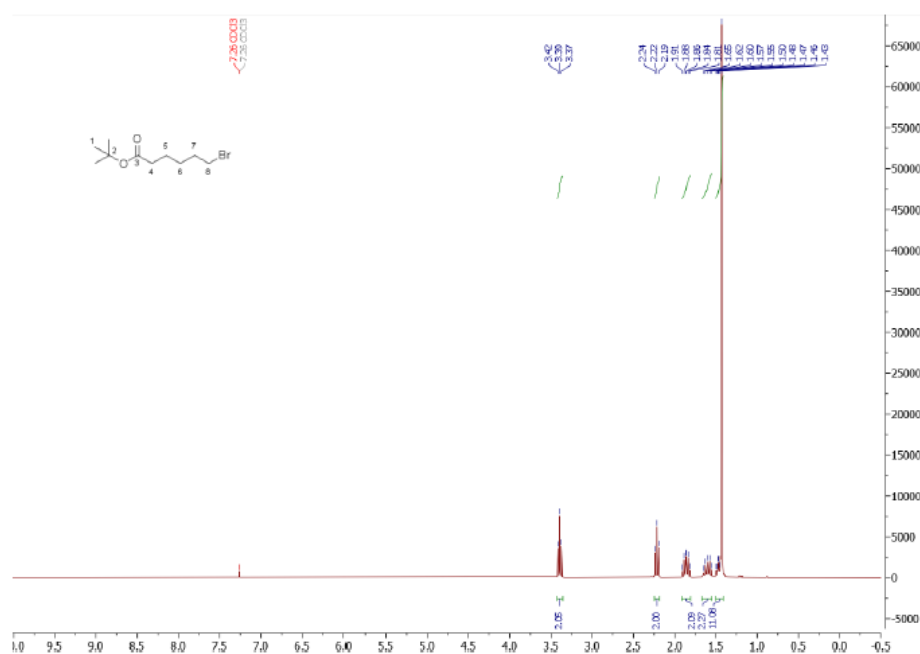
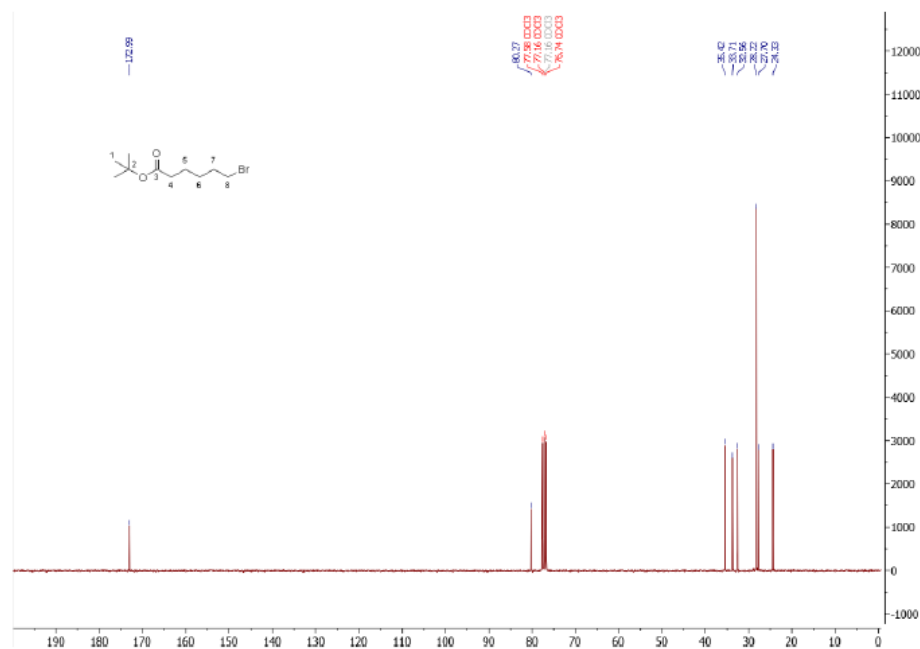
Tert-butyl 8-(benzyloxy)amino-3,6-dioxaoctanoate **12** (1 eq., 2.72 g, 8.36 mmol) was dissolved in CH₂Cl₂ (40 mL), mixed with DIPEA (2 eq., 2.16 g, 16.7 mmol, 2.83 mL) and cooled to 0 °C. FmocCl (1 eq., 2.16 g, 8.36 mmol) was dissolved in CH₂Cl₂ (23 mL), cooled to 0 °C and added slowly to the first solution. The resulting reaction mixture was stirred at 0 °C for 3 h and then washed with HCl (1 M, 4 x 50 mL) and sat. NaCl solution (2 x 50 mL) and dried over MgSO₄. The solvent was removed under reduced pressure. The product **13** (4.78 g) was obtained as a slightly yellow oil and was used without further purification. ¹H-NMR (600 MHz, CDCl₃): δ [ppm] = 7.75 (d, ³J = 7.6 Hz, 2H, 21-H), 7.64 (d, ³J = 7.6 Hz, 2H, 18-H), 7.42 – 7.27 (m, 9H, 11-H, 12-H, 13-H, 19-H, 20-H), 4.78 (s, 2H, 9-H), 4.57 (d, ³J = 6.5 Hz, 2H, 15-H), 4.26 (t, ³J = 6.5 Hz, 1H, 16-H), 3.96 (s, 2H, 4-H), 3.67 – 3.58 (m, 8H, 5-H, 6-H, 7-H, 8-H), 1.45 (s, 9H, 1-H). ¹³C-NMR (150 MHz, CDCl₃): δ [ppm] = 169.7 (C3), 157.5 (C14), 143.9 (C17), 141.5 (C22), 135.5 (C10), 129.5 (C12), 128.7 (C13), 128.6 (C11), 127.9 (C20), 127.3 (C21), 125.2 (C19), 120.1 (C18), 81.5 (C2), 77.2 (C9), 70.8 (C5), 70.5 (C6), 69.2 (C4), 67.6 (C15), 67.5 (C7), 49.8 (C8), 47.4 (C16), 28.2 (C1). HRMS (ESI): *m/z* [M+Na]⁺ calc. for C₃₂H₃₇NO₇: 570.2462, found: 570.2467.

8-(Fmoc)(benzyloxy)amino-3,6-dioxaoctanoate (14):

Tert-butyl 8-(Fmoc)(benzyloxy)amino-3,6-dioxaoctanoate **13** (1 eq., 4.19 g, 8.52 mmol) was dissolved in CH_2Cl_2 (26 mL) with TIPS (5 eq., 6.75 g, 42.6 mmol, 8.73 mL) and mixed with TFA (26 mL) at 0 °C. The reaction mixture was stirred at room temperature for 3 h. The volatile compounds were removed under reduced pressure and the resulting residue was coevaporated three times with each 10 mL CH_2Cl_2 . After column chromatographic purification on silica gel (5 % to 95 % EtOAc in pentane), the product **14** (0.945 g, 1.92 mmol, 27% over three steps) was obtained as a slightly yellow oil. ^1H -NMR (600 MHz, CDCl_3): δ [ppm] = 7.75 (d, 3J = 7.5 Hz, 2H, 20-H), 7.64 (d, 3J = 7.5 Hz, 2H, 17-H), 7.42 – 7.25 (m, 9H, 10-H, 11-H, 12-H, 18-H, 19-H), 4.72 (s, 2H, 8-H), 4.60 (d, 3J = 6.3 Hz, 2H, 14-H), 4.27 (t, 3J = 6.3 Hz, 1H, 15-H), 4.08 (s, 2H, 3-H), 3.68 – 3.57 (m, 8H, 4-H, 5-H, 6-H, 7-H). ^{13}C -NMR (150 MHz, CDCl_3): δ [ppm] = 170.0 (C2), 157.7 (C13), 143.8 (C16), 141.5 (C21), 135.4 (C9), 129.5 (C11), 128.8 (C12), 128.6 (C10), 127.9 (C19), 127.3 (C20), 125.2 (C18), 120.1 (C17), 77.2 (C8), 71.4 (C4), 69.9 (C5), 68.8 (C14), 67.7 (C3), 67.4 (C6), 49.4 (C7), 47.4 (C15). HRMS (ESI): m/z $[\text{M}+\text{H}]^+$ calc. for $\text{C}_{28}\text{H}_{29}\text{NO}_7$: 492.2017, found: 492.2009.

NMR-spectra

Figure S1. ^1H -NMR spectrum of compound **6b**.Figure S2. ^{13}C -NMR spectrum of compound **6b**.

Figure S3. ¹H-NMR spectrum of compound 6c.Figure S4. ¹³C-NMR spectrum of compound 6c.

S15

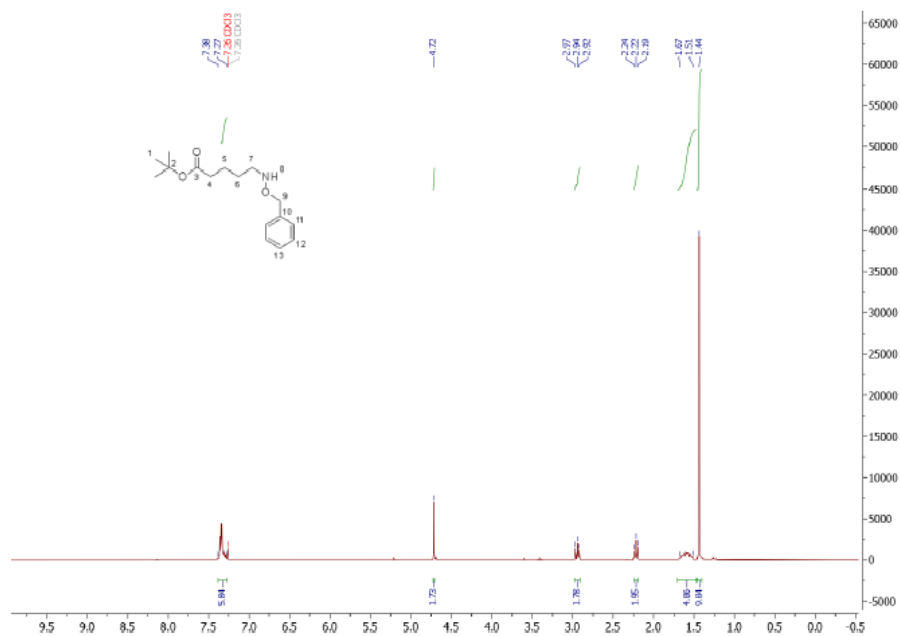


Figure S5. ¹H-NMR spectrum of compound **7b**.

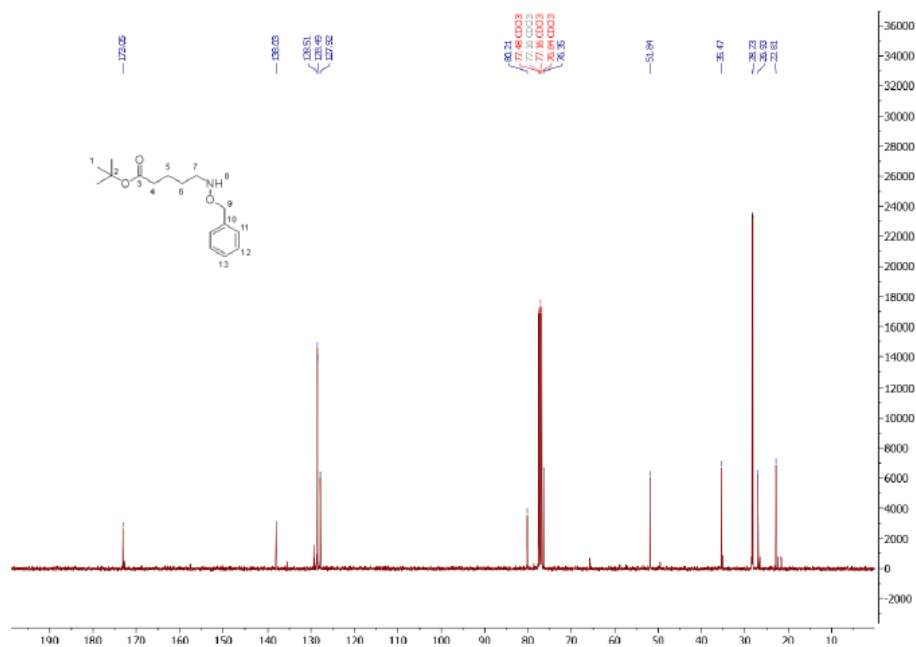
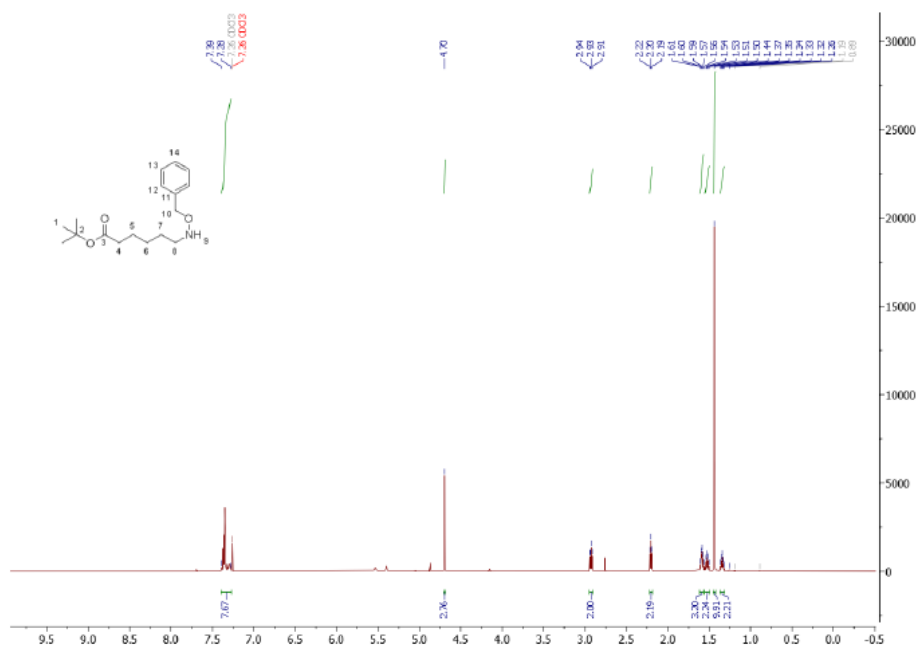
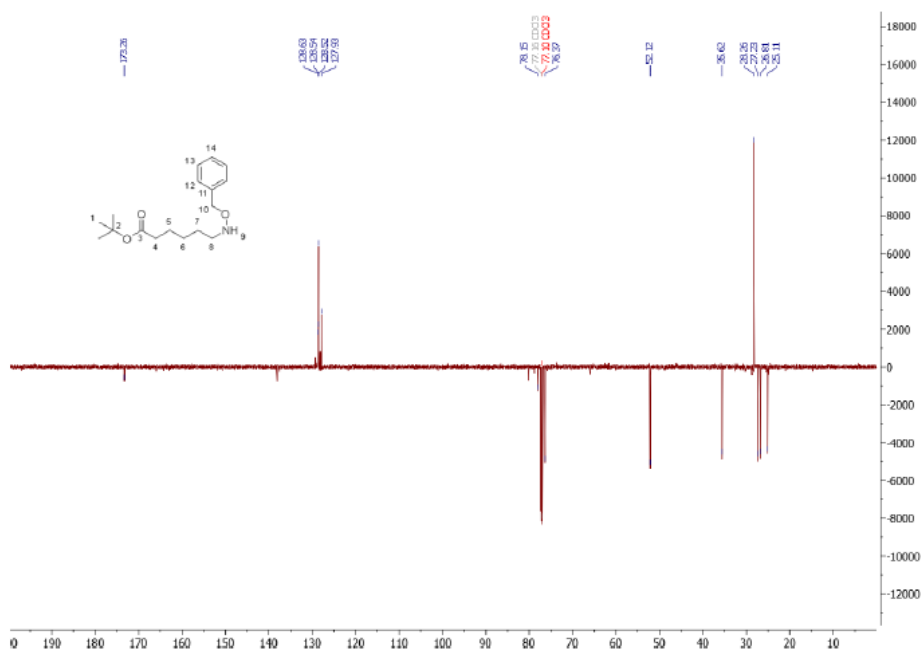
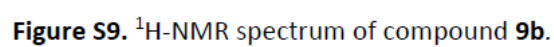
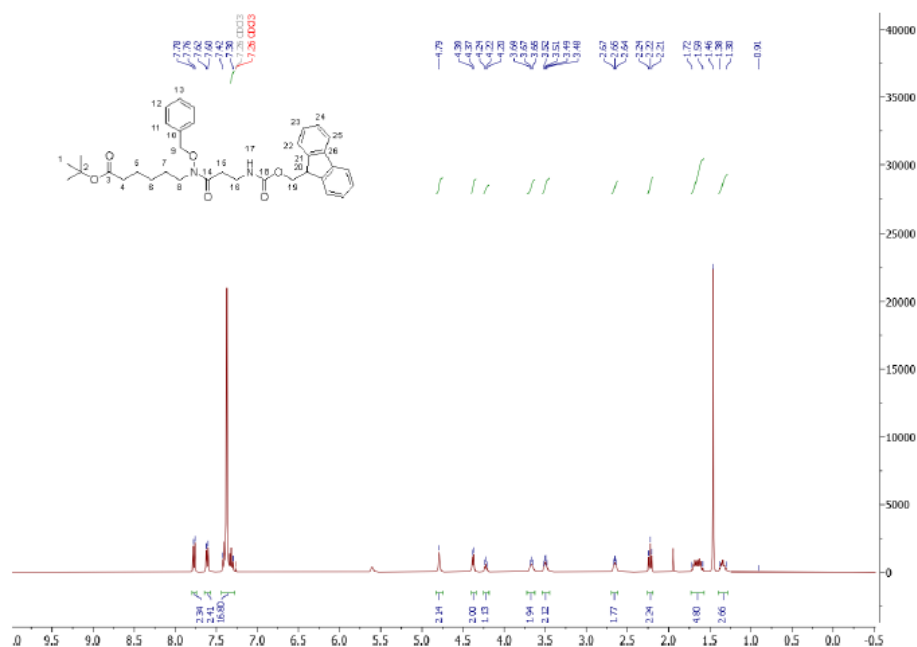
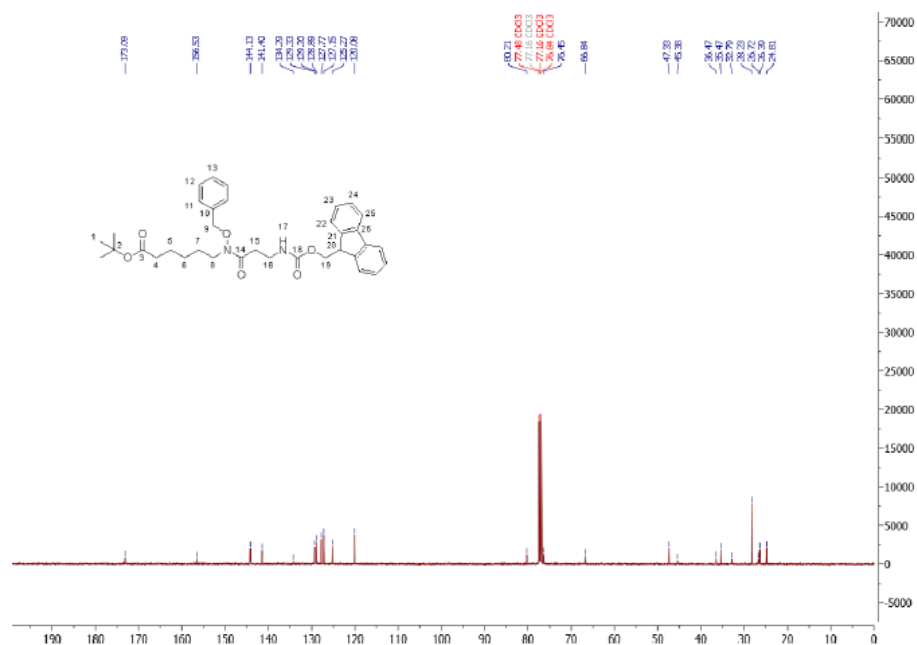


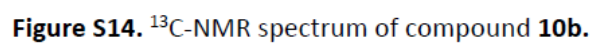
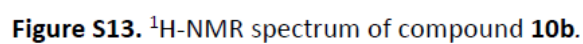
Figure S6. ¹³C-NMR spectrum of compound **7b**.

Figure S7. ¹H-NMR spectrum of compound **7c**.Figure S8. ¹³C-NMR spectrum of compound **7c**.

S17



Figure S11. ^1H -NMR spectrum of compound 9c.



S20

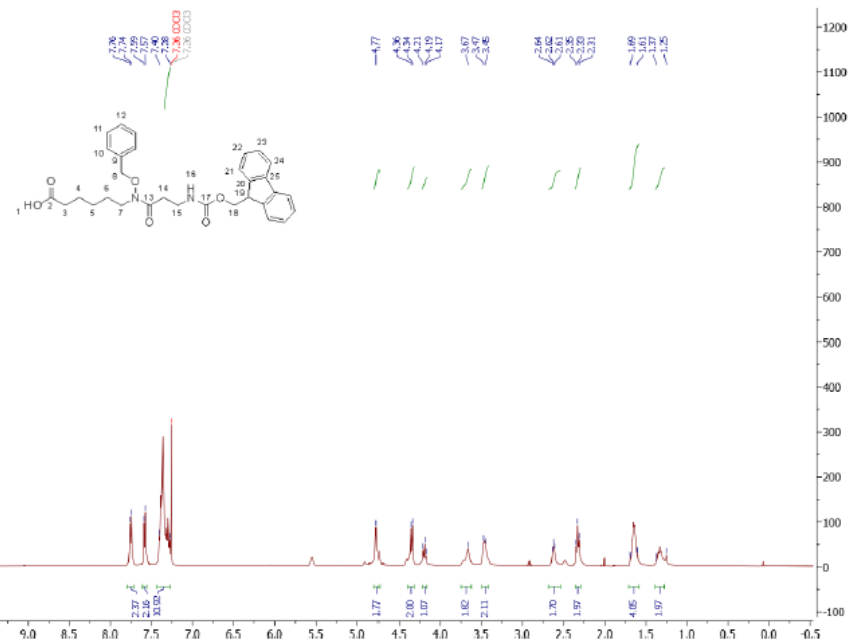


Figure S15. ^1H -NMR spectrum of compound **10c**.

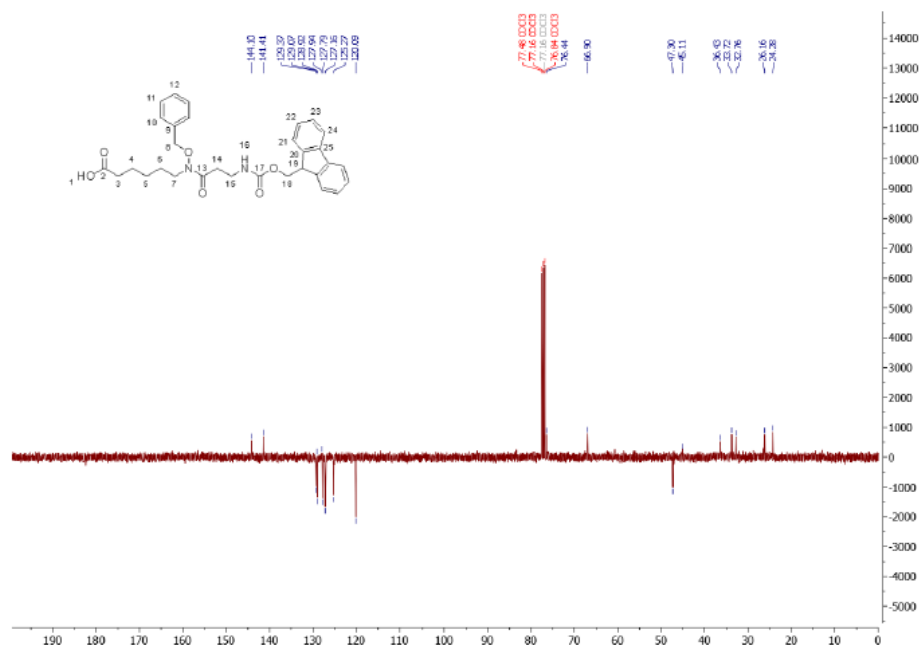


Figure S16. ^{13}C -NMR spectrum of compound **10c**.

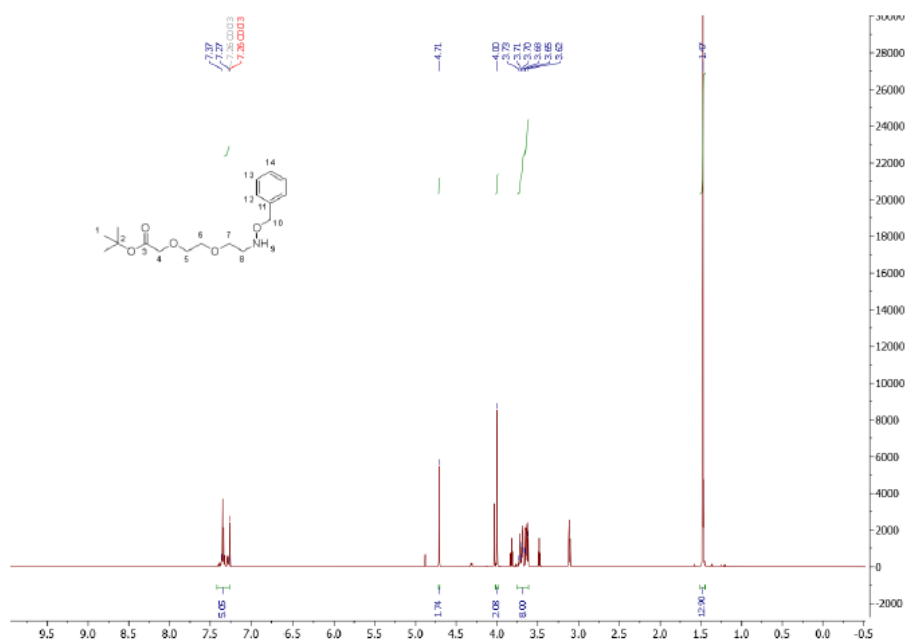


Figure S17. ^1H -NMR spectrum of compound 12.

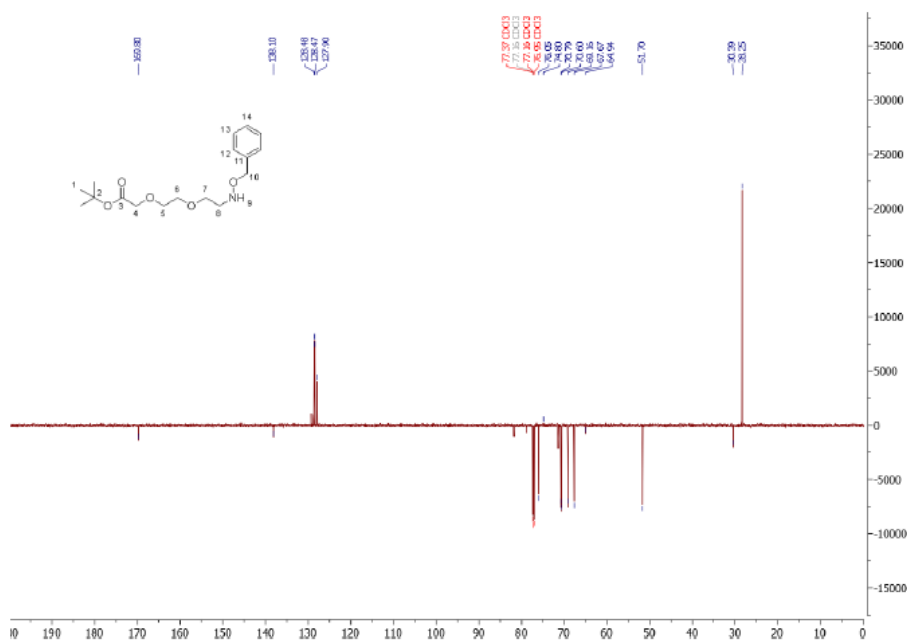


Figure S18. ^{13}C -NMR spectrum of compound 12.

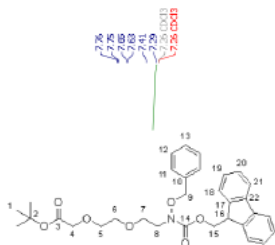


Figure S19. ^1H -NMR spectrum of compound **13**.

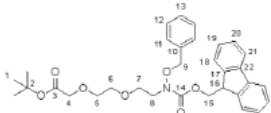
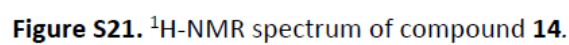
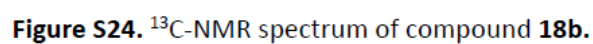
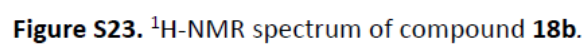
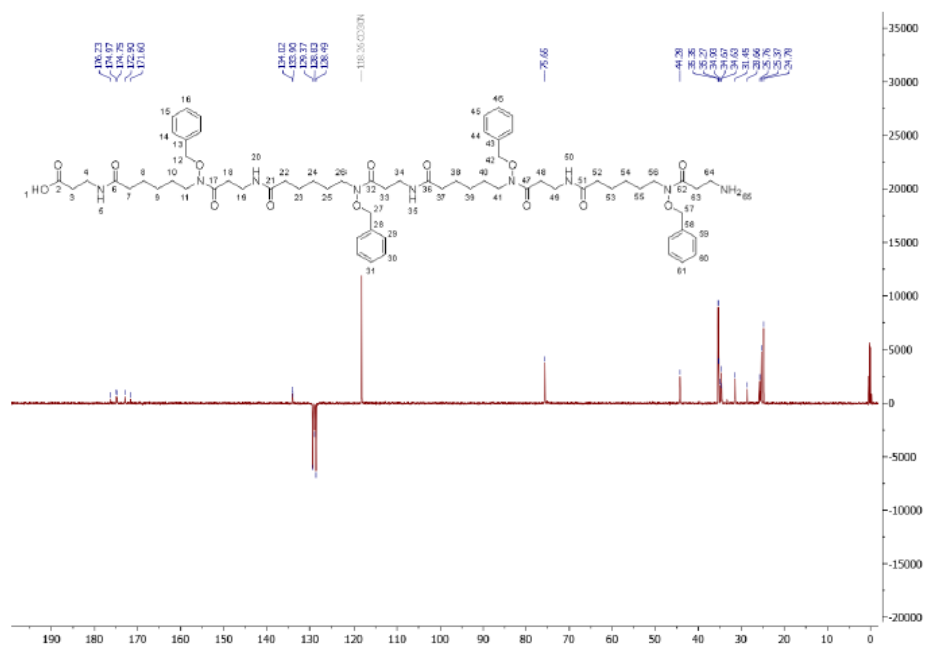
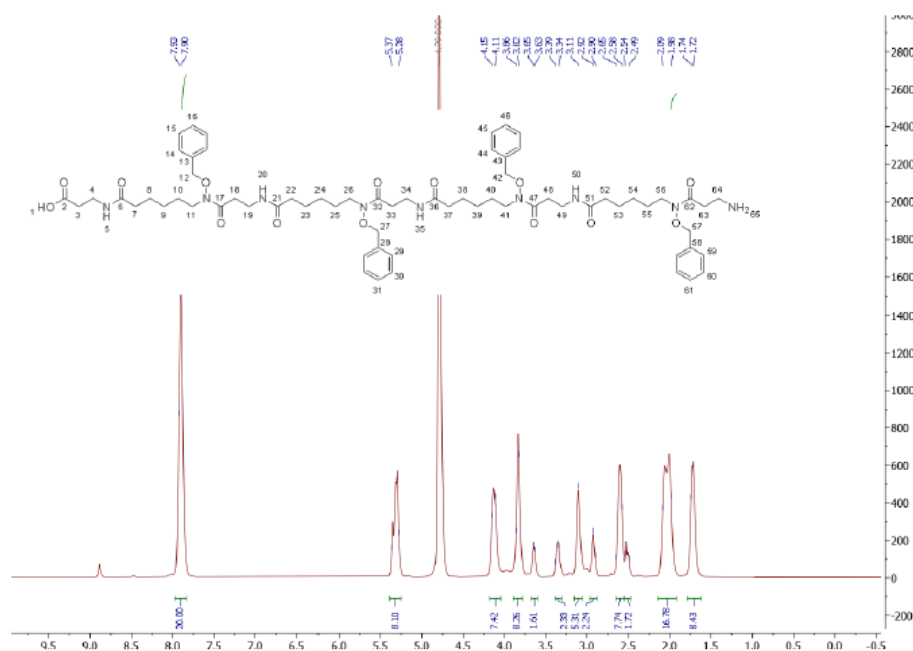


Figure S20. ^{13}C -NMR spectrum of compound **13**.







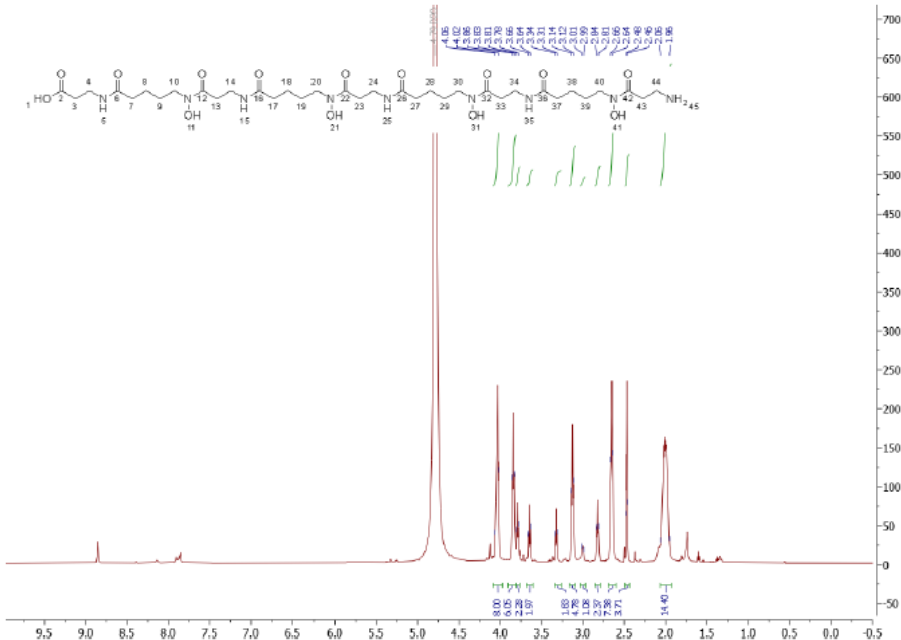


Figure S27. ^1H -NMR spectrum of compound **3b**.

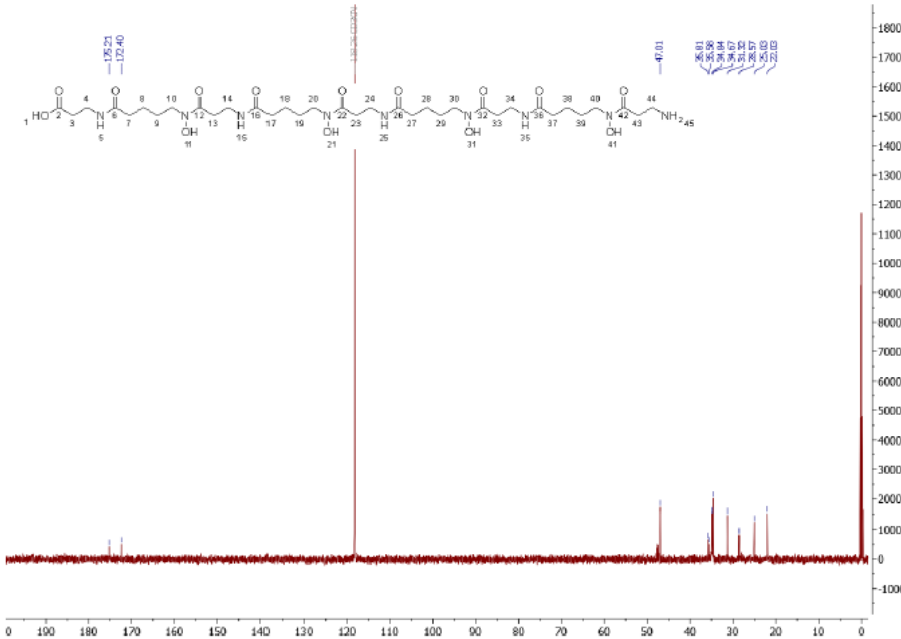
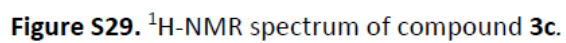


Figure S28. ^{13}C -NMR spectrum of compound **3b**.

S27



HPLC-MS spectra

HPLC-ESI-MS chromatogram and spectrum of compound 18b

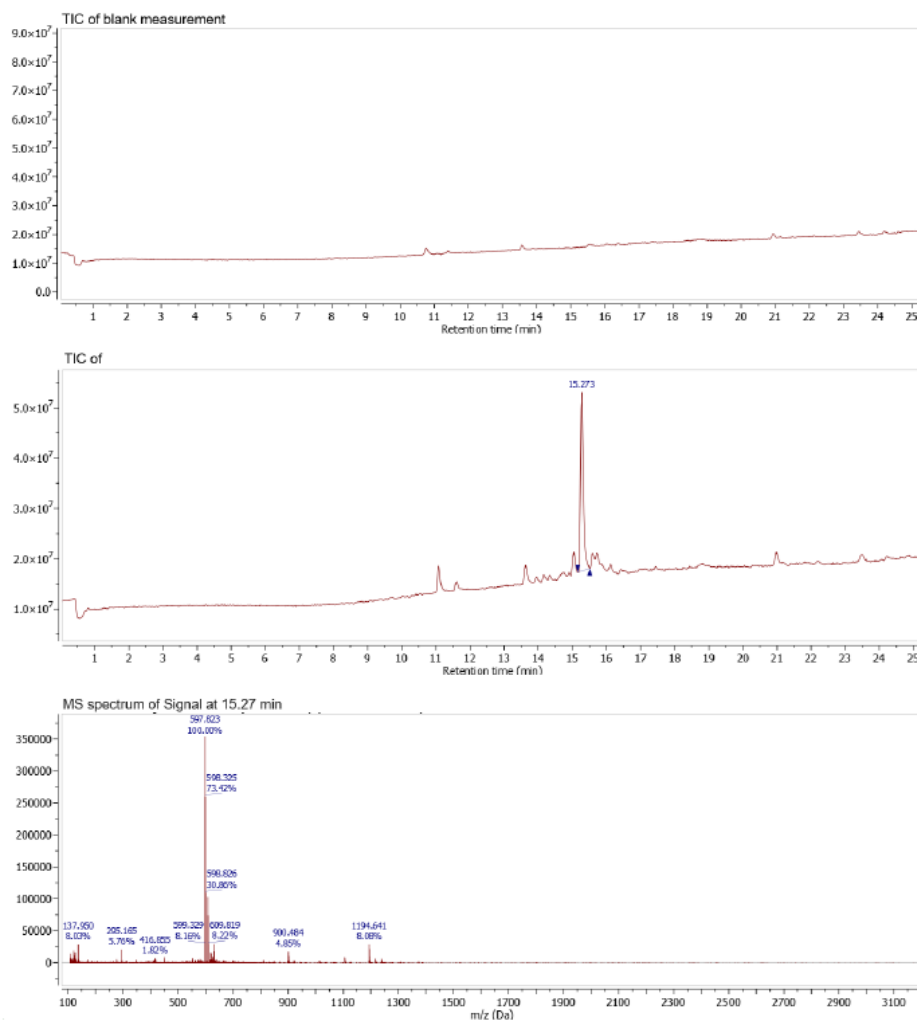


Figure S30. HPLC-chromatogram (Anal. HPLC (Agilent Zorbax Extend C18, 2.1 x 50 mm, H₂O/CH₃CN 5:95 + 0.1% HCO₂H to 95:5 + 0.1% HCO₂H, 25 min, 0.3 ml/min): t_R = 15.3 min.) and MS(ESI)-spectrum of **18b**.

HPLC-ESI-MS chromatogram and spectrum of compound 18c

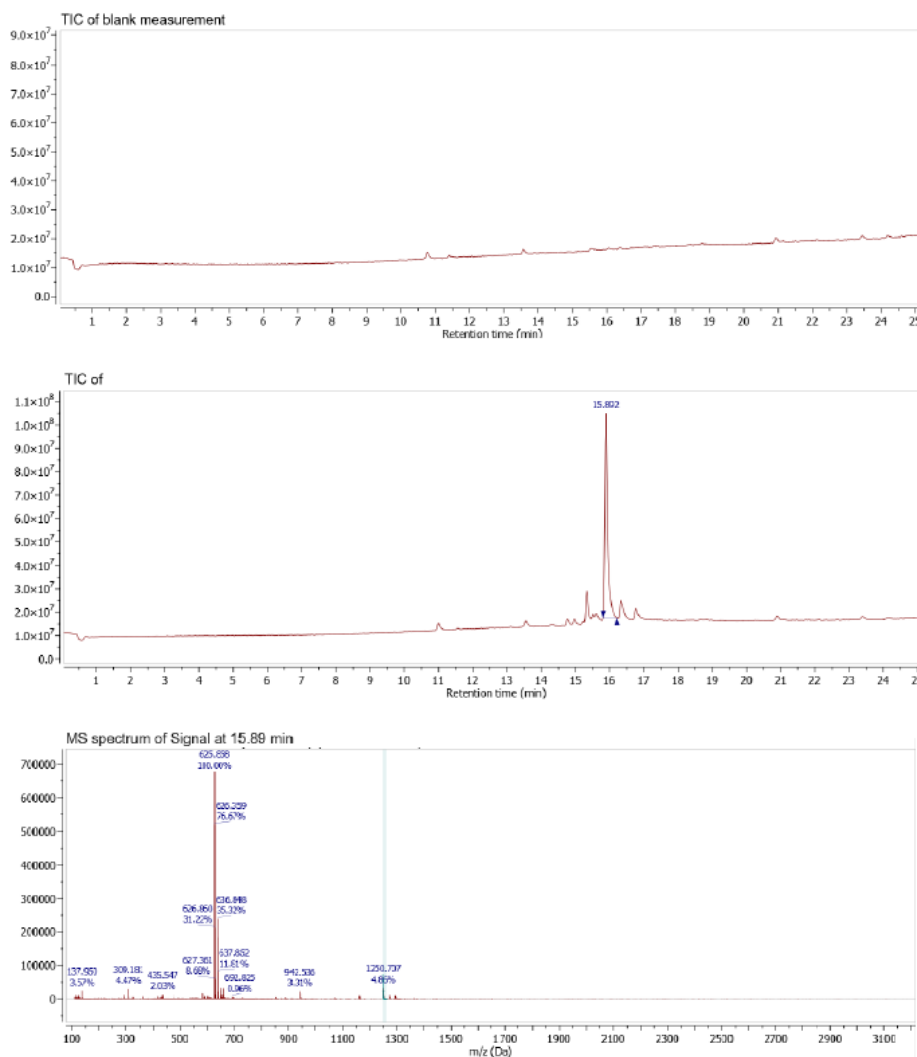


Figure S31. HPLC-chromatogram (Anal. HPLC (Agilent Zorbax Extend C18, 2.1 x 50 mm, H₂O/CH₃CN 5:95 + 0.1% HCO₂H to 95:5 + 0.1% HCO₂H, 25 min, 0.3 ml/min): t_R = 15.9 min.) and MS(ESI)-spectrum of **18c**.

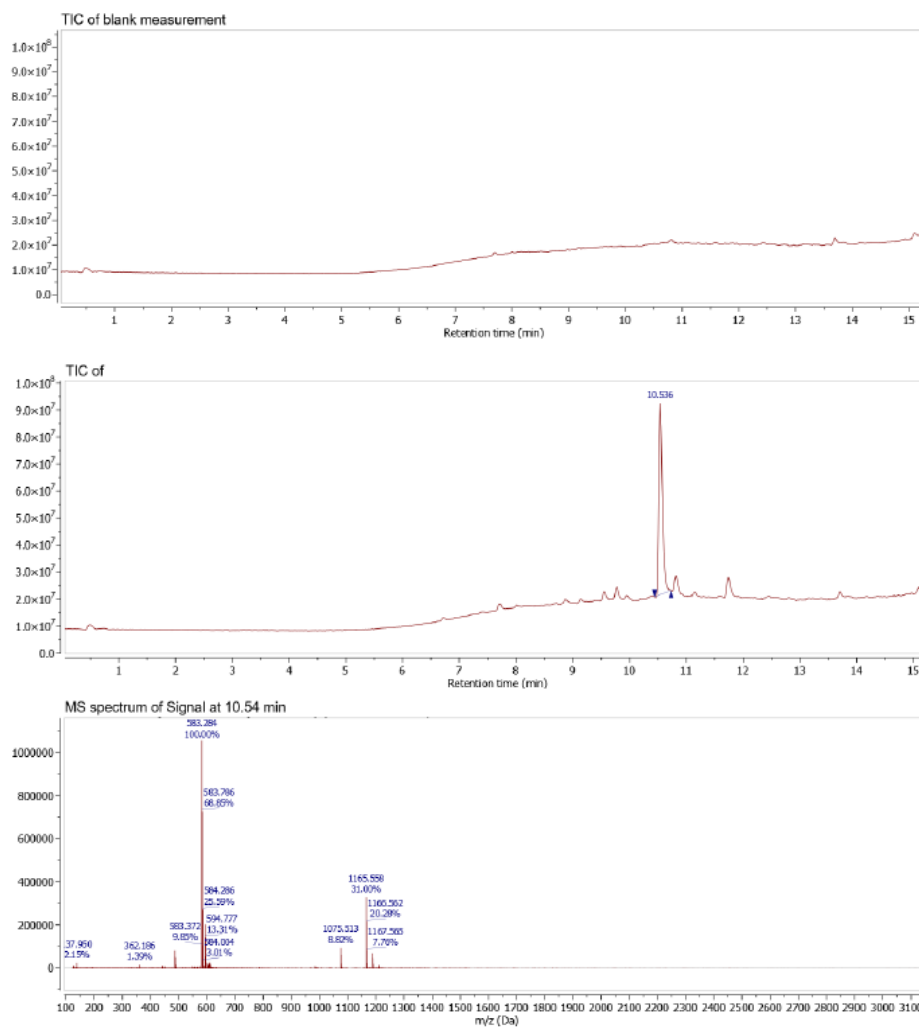
HPLC-ESI-MS chromatogram and spectrum of compound *O*-benzyl protected OEGDFO*

Figure S32. HPLC-chromatogram (Anal. HPLC (Agilent Zorbax Extend C18, 2.1 x 50 mm, H₂O/CH₃CN 5:95 + 0.1% HCO₂H to 95:5 + 0.1% HCO₂H, 15 min, 0.3 ml/min): t_R = 10.5 min.) and MS(ESI)-spectrum of *O*-benzyl protected OEGDFO*.

HPLC-ESI-MS chromatogram and spectrum of compound 3b

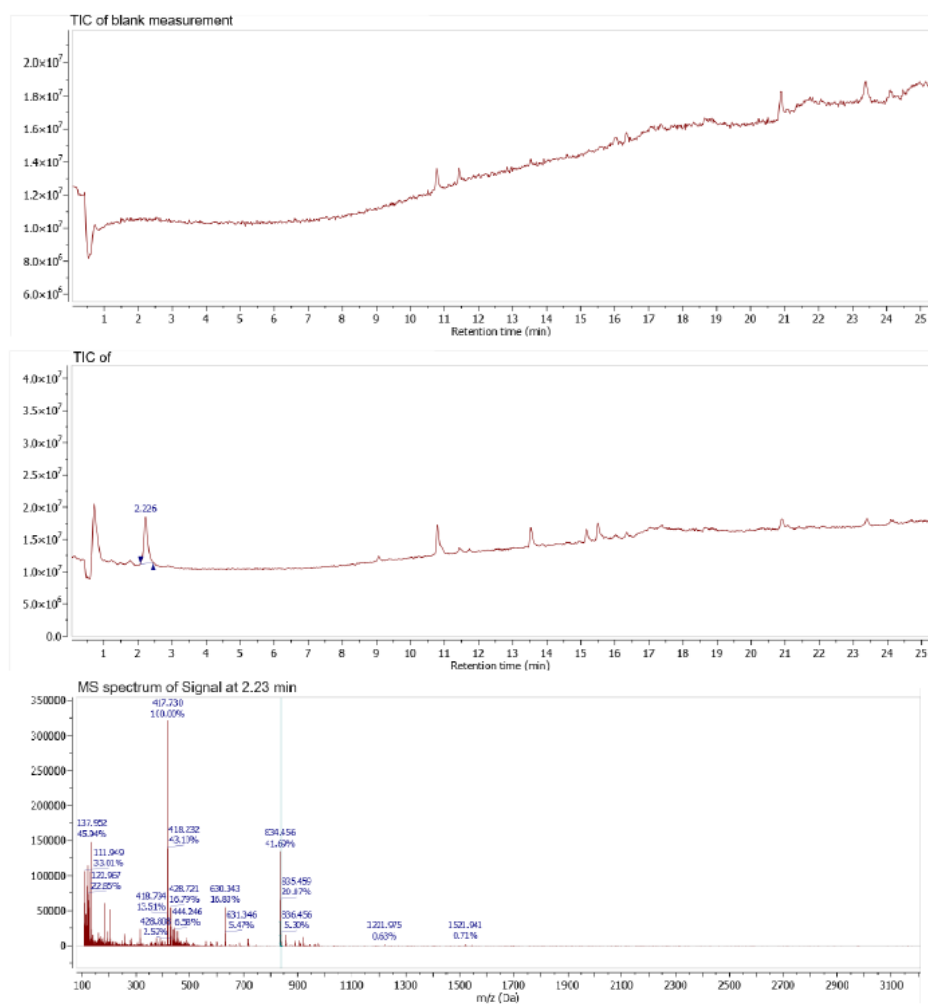


Figure S33. HPLC-chromatogram (Anal. HPLC (Agilent Zorbax Extend C18, 2.1 x 50 mm, H₂O/CH₃CN 5:95 + 0.1% HCO₂H to 95:5 + 0.1% HCO₂H, 25 min, 0.3 ml/min): t_R = 2.2 min.) and MS(ESI)-spectrum of **3b**.

HPLC-ESI-MS chromatogram and spectrum of compound 3c

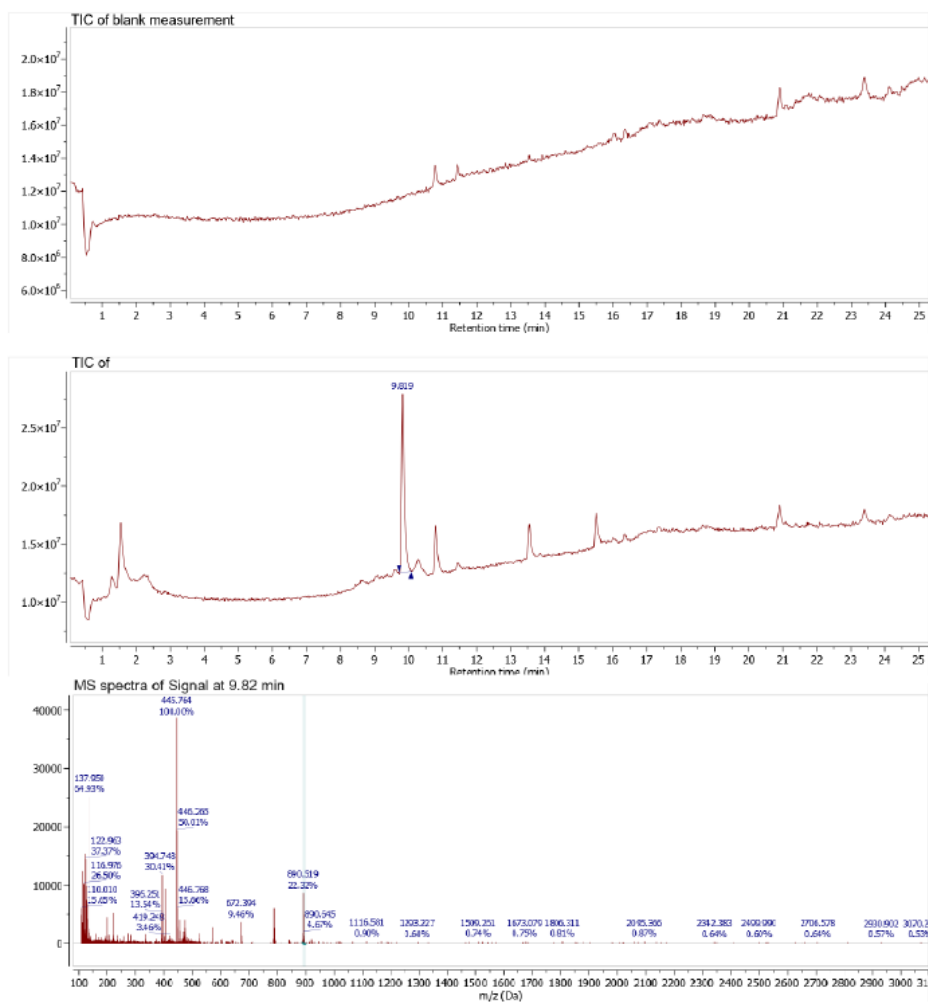


Figure S34. HPLC-chromatogram (Anal. HPLC (Agilent Zorbax Extend C18, 2.1 x 50 mm, H₂O/CH₃CN 5:95 + 0.1% HCO₂H to 95:5 + 0.1% HCO₂H, 25 min, 0.3 ml/min): t_R = 9.8 min.) and MS(ESI)-spectrum of **3c**.

HPLC-ESI-MS chromatogram and spectrum of compound 4

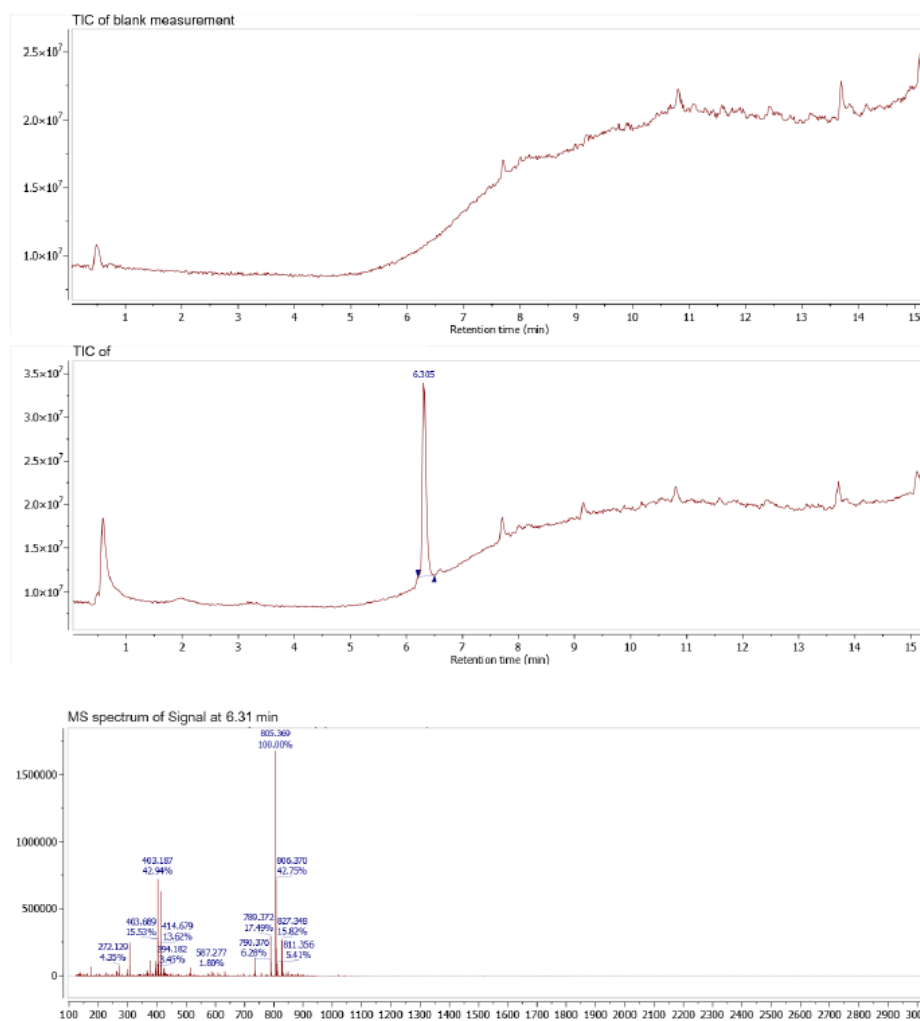


Figure S35. HPLC-chromatogram (Anal. HPLC (Agilent Zorbax Extend C18, 2.1 x 50 mm, H₂O/CH₃CN 5:95 + 0.1% HCO₂H to 95:5 + 0.1% HCO₂H, 15 min, 0.3 ml/min): t_R = 6.3 min.) and MS(ESI)-spectrum of **4**.

HPLC-ESI-MS chromatogram and spectrum of compound Zr-3c

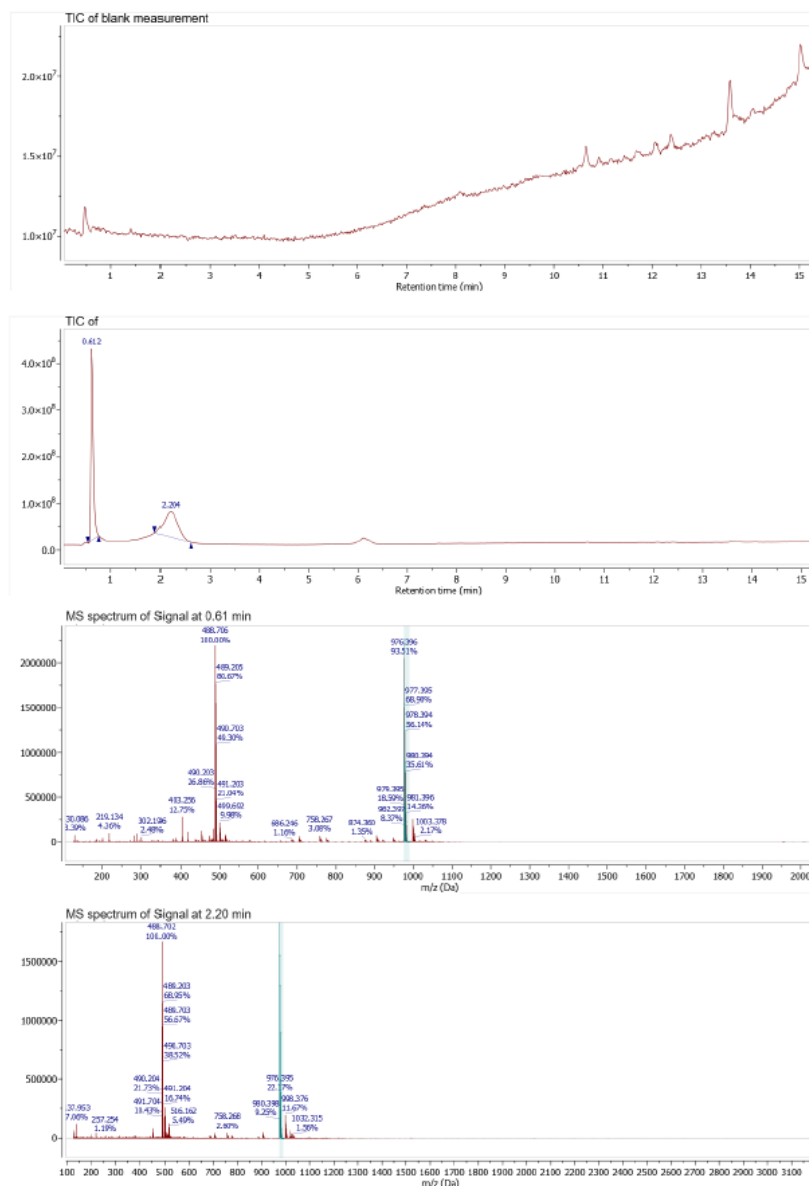


Figure S36. HPLC-chromatogram (Anal. HPLC (Agilent Zorbax Extend C18, 2.1 x 50 mm, H₂O/CH₃CN 5:95 + 0.1% HCO₂H to 95:5 + 0.1% HCO₂H, 15 min, 0.3 ml/min): t_R = 2.2 min.) and MS(ESI)-spectrum of **Zr-3c**.

S35

HPLC-ESI-MS chromatogram and spectrum of compound 24

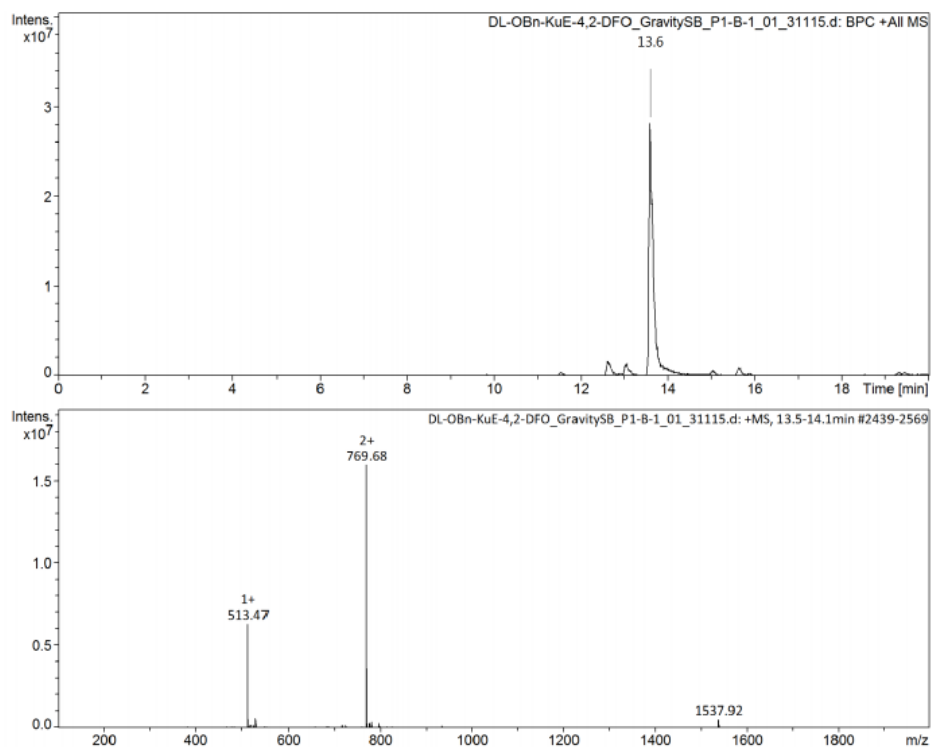
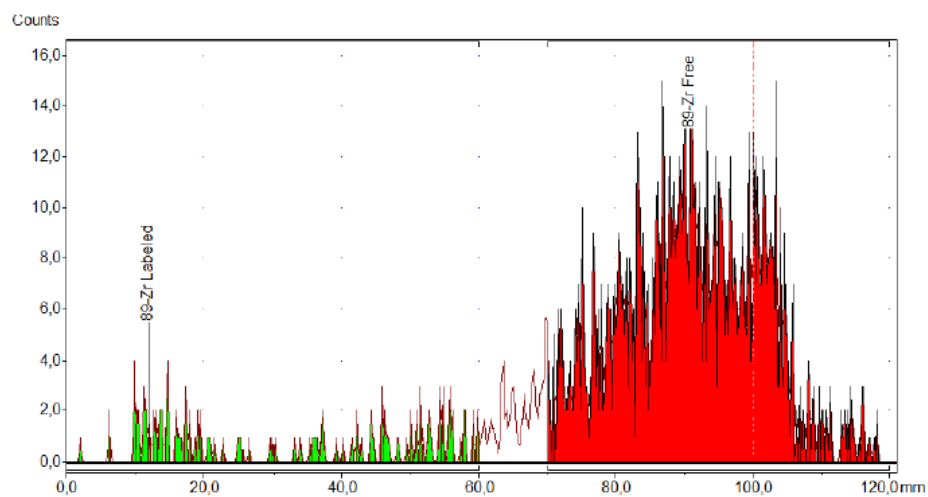
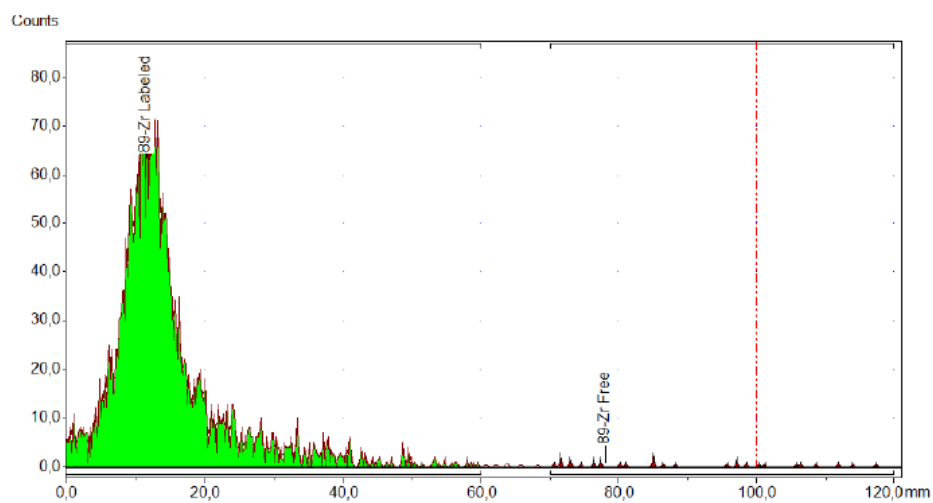


Figure S37. HPLC-chromatogram (Anal. HPLC (Macherey & Nagel Gravity SB C18, 2.1 x 50 mm, H₂O/CH₃CN 5:95 + 0.1% HCO₂H to 95:5 + 0.1% HCO₂H, 15 min, 0.3 ml/min): *t_R* = 2.2 min.) and MS(ESI)-spectrum of **24**.

RadioTLC**Figure S38.** TLC of free $[^{89}\text{Zr}]\text{Zr}^{4+}$ as a control**Figure S39.** Example of TLC of bound $[^{89}\text{Zr}]\text{Zr}^{4+}$.

Stability in human serum

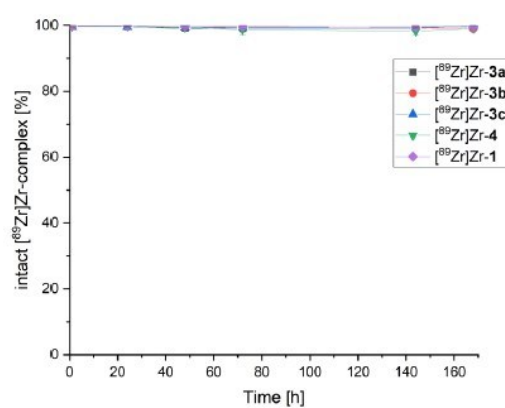


Figure S40. Stability of the [⁸⁹Zr]Zr⁴⁺ complexes of **1**, **3a-c** and **4** in human serum at 37°C.

Synthesis of **18b** on CTC-Resin

The CTC resin was preloaded with Fmoc- β -alanine (scale: 1.00 mmol), which was deprotected with piperidine. The monomer **10b** was used with 3 molar equivalents and couplings were performed with DIPEA (3 eq.) and HCTU (3 eq.) for 1 h at room temperature. Repeated coupling and deprotection cycles gave the resin-bound protected chelator **18b**. Cleavage was performed with 1% TFA in CH_2Cl_2 and the resulting crude product **18b** (1.09 g) had a purity of >70% according to HPLC analysis.

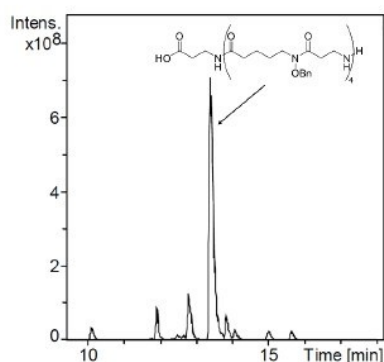































Figure S41. HPLC chromatogram of the raw product of compound **18b** via a solid phase synthesis with CTC resin.






















8.2 Hazardous Materials
























Substance	Pictogram	H-Phrases	P-Phrases
2-Propanol	 	225, 319, 336	210, 233, 240, 241, 242, 305+351+338
5-Bromopentanoic acid		315, 319, 335	261, 264, 271, 280, 302+352, 305+351+338
6-Bromohexanoic acid		314	260, 280, 303+361+353, 304+340+310, 305+351+338, 363
Ammonium Cerium sulfate		315, 319, 335	261, 262, 264, 280, 302+352, 305+351+338, 314, 332+313, 337+313, 362
Benzylbromide (BnBr)		315, 319, 335	261, 264, 271, 280, 302+352, 305+351+338
Benzoyl peroxide (BPO)	   	241, 317, 319, 410	210, 261, 273, 280, 305+351+338, 333+313, 420, 501
BTFFH		315, 319, 335	261, 264, 271, 280, 302+352, 305+351+338
Chloroform	 	302, 315, 319, 331, 336, 351, 361d, 372	202, 301+312, 302+352, 304+340+311, 305+351+338, 308+313

Carbonyldiimidazole (CDI)		302, 314, 360d	260, 280, 303+361+353, 304+340+310, 305+351+338
Dichloromethane		315, 319, 336, 351	201, 302+352, 305+351+338, 308+313
Copper(I)iodide		302, 315, 317, 318, 410	273, 280, 301+312+330, 302+352, 305+351+338+310
1,8- Diazabicyclo[5.4.0]undec- 7-ene (DBU)		290, 301, 314, 412	234, 273, 280, 303+361+353, 304+340+310, 305+351+338
<i>N,N'</i> - Dicyclohexylcarbodiimide (DCC)		302, 311, 317, 318	361, 264, 280, 301+312, 302+352+312, 305+351+338
<i>N,N'</i> - Diisopropylcarbodiimide (DIC)		226, 317, 318, 330, 334	210, 233, 280, 303+361+353, 304+340+310, 305+351+338
Diethylether		224, 302, 336	210, 233, 240, 241, 301+312, 403+233
DIPEA		225, 302, 318, 331, 335, 411	210, 273, 280, 301+312, 304+340+311, 305+351+338

4-Dimethylaminopyridine (DMAP)		301+331, 310, 315, 318, 370, 411	262, 273, 280, 301+310, 302+352+312, 305+351+338
DMF		226, 312, 332, 319, 360d	201, 210, 302+352, 305+351+338, 308+313
EDTA		319, 332, 373	280, 304+340, 312, 305+351+338, 337+313
Acetic acid		226, 314	210, 280, 301+330+331, 303+361+353, 305+351+338, 310
Ethyl acetate		225, 319, 336, 066	210, 233, 240, 305+351+338, 403+235
Ethanol		225, 319	210, 233, 240, 241, 242, 305+351+338
FmocCl		314	260, 280, 303+361+353, 304+341+310, 305+351+338, 363
Formic acid		226, 302, 331, 314	210, 280, 303+361+353, 304+340+310, 305+351+338
H ₂ (gas)		220, 280	210, 377, 381, 403

HBTU		315, 319, 335	210, 240, 241, 261, 264, 271, 280, 302+352, 304+340, 305+351+338, 312, 332+313, 337+313, 362, 370+378, 403+233, 405, 501
Hydrochloric acid		290, 314, 335	234, 261, 271, 280, 303+361+353, 30+351+338
HCTU		317, 261, 272, 280, 302+352, 333+313, 362+364	
HOBt		207, 319, 412	210, 212, 230, 233, 280, 370+380+375, 501
Potassium carbonate (K ₂ CO ₃)		315, 319, 335	261, 264, 271, 280, 302+352, 305+351+338
Potassium permanganate (KMnO ₄)		272, 302, 314, 361d, 373, 410	210, 220, 280, 301+330+331, 303+361+353, 305+351+338, 310
Potassium hydroxide (KOH)		290, 302, 314	234, 260, 280, 301+312, 303+361+353, 305+351+338
Acetonitrile		225, 302, 312, 319, 332	210, 280, 305+351+338

Methanol	  	225, 301+311+331, 370	210, 233, 280, 301+310, 303+361+353, 304+340+311
Sodium cyanoborohydride (NaCNBH ₃)	   	260, 300, 310, 330, 314, 410, 032	273, 280, 301+330+331, 302+352, 304+340, 305+351+338, 402+404
Sodium hydroxide (solid)		290, 314	280, 301+330+331, 305+351+338, 308+310
<i>n</i> -Butanol	  	226, 302, 318, 315, 335, 336	210, 280, 302+352, 305+351+338, 313
Triethylamine	  	225, 301+311+331, 314, 335	210, 280, 301+312, 303+361+353, 304+340+310, 305+351+338+310
<i>n</i> -Hexan	   	225, 304, 361f, 373, 315, 336, 411	210, 240, 271, 301+310, 331, 302+352, 403+235
Ninhydrin		302, 315, 319, 335	261, 264, 270, 271, 280, 301+312, 302+352, 304+340, 305+351+338, 312, 321, 330, 332+313, 337+313, 362, 403+233, 405, 501
<i>N</i> -methylmorpholine	 	228, 361f	202, 210, 240, 241, 280, 308, 313

<i>n</i> -Pentan	   	225, 304, 336, 411, 066	210, 233, 240, 273, 301+310, 331
Ozone (O ₃)	     	270, 314, 330, 335, 341, 361, 370, 410	203, 220, 244, 260, 264+265, 270, 271, 273, 280, 284 ,301+330+331, 302+361+354, 304+340, 305+351+338, 308+316, 362+364, 370+376, 391, 403+233, 405
O-Benzyl hydroxylamine	 	301, 314, 335, 412	261, 273, 280, 303+361+353, 304+340+310, 305+351+338
Oxalic Acid	 	302+312, 318	264, 270, 280, 302+352+312, 305+351+338+310, 501
Phosphomolybdic Acid	 	272, 314	220, 280, 305+351+338, 310
Piperidine	  	225, 302, 311+331, 314	210, 280, 301+312, 303+361+353, 304+340+310, 305+351+338
PyBOP	 	302, 317, 410	261, 264, 273, 280, 301+312, 302+352
Pyridine	 	225, 302+312+332, 315, 319	210, 280, 301+3112, 303+361+353,

			304+340+312, 305+351+338
Silica gel		373	260, 270, 314
<i>t</i> -Butanol		225, 332, 319, 335, 336	210, 240, 305+351+338, 403+233
<i>tert</i> -butyl 4-bromobutanoate		302, 315, 319, 335	261, 305, 338, 351
TFA		290, 331, 314, 412, 071	260, 273, 280, 303+361+353, 305+351+338, 312
THF		225, 302, 319, 335, 351, 019	210, 280, 301+312+330, 305+351+338, 370+378, 403+235
Thionylchloride		302, 331, 314, 335, 014, 029	261, 280, 301+312, 303+361+353, 304+340+310, 305+351+338
Triisopropyl silane (TIPS)		226	210, 233, 240, 241, 242, 243
Triphenylphosphin		302, 317, 318, 372	260, 280, 301+312, 302+352, 305+351+338, 314
Zirconium tetrachloride (ZrCl ₄)		302, 314, 014	280, 301+330+331, 305+351+338, 308+310

9. Declaration

I hereby declare and affirm that this doctoral dissertation is my own work and that I have not used any aids and sources other than those indicated. If electronic resources based on generative artificial intelligence (gAI) were used in the course of writing this dissertation, I confirm that my own work was the main and value-adding contribution and that complete documentation of all resources used is available in accordance with good scientific practice. I am responsible for any erroneous or distorted content, incorrect references, violations of data protection and copyright law or plagiarism that may have been generated by the gAI.

Eidesstaatliche Versicherung

Hiermit versichere ich an Eides statt, die vorliegende Dissertationsschrift selbst verfasst und keine anderen als die angegebenen Quellen und Hilfsmittel benutzt zu haben. Sofern im Zuge der Erstellung der vorliegenden Dissertationsschrift generative Künstliche Intelligenz (gKI) basierte elektronische Hilfsmittel verwendet wurden, versichere ich, dass meine eigene Leistung im Vordergrund stand und dass eine vollständige Dokumentation aller verwendeten Hilfsmittel gemäß der Guten wissenschaftlichen Praxis vorliegt. Ich trage die Verantwortung für eventuell durch die gKI generierte fehlerhafte oder verzerrte Inhalte, fehlerhafte Referenzen, Verstöße gegen das Datenschutz- und Urheberrecht oder Plagiate.

Hamburg, den 25.11.2025



Lasse Outzen